

# Targeted protein degradation of FK506-binding proteins

*Gezielte Protein Degradation von FK506-bindenden Proteinen*

Vom Fachbereich Chemie  
der Technischen Universität Darmstadt



TECHNISCHE  
UNIVERSITÄT  
DARMSTADT

zur Erlangung des Grades  
Doctor rerum naturalium (Dr. rer. nat.)

Dissertation von  
Thomas Maximilian Geiger, M.Sc.


Erstgutachter:

Prof. Dr. Felix Hausch

Zweitgutachter:

Prof. Dr. Harald Kolmar

Darmstadt 2023



---

Geiger, Thomas Maximilian: Targeted protein degradation of FK506-binding proteins

Darmstadt, Technische Universität Darmstadt,


Jahr der Veröffentlichung der Dissertation auf TUpriints: 2024

URN: urn:nbn:de:tuda-tuprints-267571

Tag der mündlichen Prüfung: 04.12.2023

Veröffentlicht unter CC-BY-SA 4.0. International

<https://creativecommons.org/licenses/>



---

Tag der Einreichung: 19. Oktober 2023

Tag der mündlichen Prüfung: 04. Dezember 2023

---

## 1. Erklärung

---

### **§8 Abs. 1 lit. c der Promotionsordnung der TU Darmstadt**

Ich versichere hiermit, dass die elektronische Version meiner Dissertation mit der schriftlichen Version übereinstimmt und für die Durchführung des Promotionsverfahrens vorliegt.

### **§8 Abs. 1 lit. d der Promotionsordnung der TU Darmstadt**

Ich versichere hiermit, dass zu einem vorherigen Zeitpunkt noch keine Promotion versucht wurde und zu keinem früheren Zeitpunkt an einer in- oder ausländischen Hochschule eingereicht wurde. In diesem Fall sind nähere Angaben über Zeitpunkt, Hochschule, Dissertationsthema und Ergebnis dieses Versuchs mitzuteilen.

### **§9 Abs. 1 der Promotionsordnung der TU Darmstadt**

Ich versichere hiermit, dass die vorliegende Dissertation selbstständig und nur unter Verwendung der angegebenen Quellen verfasst wurde.

### **§9 Abs. 2 der Promotionsordnung der TU Darmstadt**

Die Arbeit hat bisher noch nicht zu Prüfungszwecken gedient.

Darmstadt, den .....

-----  
Thomas Geiger

---

---

## Table of contents

---

1.....Erklärung	iv
2.....Abstract	1
2.1. Zusammenfassung	1
2.2. Abstract	4
3.....Introduction	7
3.1. FK506-binding proteins	7
3.1.1. Cellular functions of prominent FKBP	7
3.1.2. Pharmacological FKBP inhibition	11
3.2. Molecular glues	12
3.2.1. Natural Immunophilin-based molecular glues	15
3.2.2. Synthetic degradative molecular glues	17
3.2.3. Screening for molecular glues	23
3.3. Bivalent functional tools	24
3.3.1. PROTACs	25
3.3.2. FKBP PROTACs	27
4.....Results and Discussion	29
4.1. HTRF-binding assay for FKBP ligands	29
4.1.1. HTRF-binding assay development	31
4.2. NanoBRET-based intracellular FKBP ligand target engagement assay	37
4.2.1. Optimization of the FKBP51-engagement assay	38
4.2.2. Development towards a semi-automatic high throughput assay and cost reduction	39
4.2.3. Characterization of FKBP ligands by competitive NanoBRET target-engagement assays	42
4.3. Glucocorticoid receptor reporter gene assays	45
4.4. Development of a fluorescent reporter assay for FKBP51 and FKBP12 level	51
4.5. Development of an HTRF-based FKBP52 quantification assay	56
4.6. FKBP-PROTACs	59
4.6.1. Cellular assessment of PROTAC activity	59
4.6.2. Degradability assessment of FKBP51 and FKBP12 reporter swap mutants	61
4.6.3. Cellular characterization of FKBP12 PROTACs	63
4.6.4. Optimization of first generation PROTACs yields the most selective and highly active FKBP51- PROTAC SelDeg51	67

---

4.6.5.	Cellular characterization of SelDeg51	68
4.6.6.	Cellular effects of FKBP51-degrading PROTACs surpass conventional ligands.	70
4.7.	Cellular discovery of FKBP12-degrading molecular glues	74
4.7.1.	Cellular screening of a FKBP-focused ligand library for FKBP12-degrading molecular glues	75
4.7.2.	SAR and optimization of FKBP12-degrading molecular glues	76
4.7.3.	Mechanistic insights in the mode of action	81
4.7.4.	FKBP12_eGFP degradation is tag-dependent	82
4.7.5.	Elucidation and validation of UBR3 as the relevant E3 ligase	83
5.....	<b>Conclusion and Outlook</b>	88
6.....	<b>Materials and Methods</b>	95
6.1.	Materials	95
6.1.1.	General chemicals	95
6.1.2.	General plastics and materials	96
6.1.3.	Cell culture media and additives	97
6.1.4.	Devices	98
6.1.5.	Tecan Reader	98
6.1.6.	Software	98
6.1.7.	Antibodies	99
6.2.	Biochemical methods	102
6.2.1.	Agarose gel electrophoresis	102
6.2.2.	PCR	102
6.2.3.	Restriction digest	105
6.2.4.	Gibson assembly	105
6.2.5.	T4 ligation	106
6.2.6.	Heat shock transformation	106
6.2.7.	Plasmid isolation	107
6.2.8.	Active-site titrations	107
6.2.9.	Fluorescence polarization binding curves	107
6.2.10.	HTRF binding assays	108
6.2.11.	BCA protein quantification	109
6.2.12.	Expression of recombinant proteins	109

---

6.2.13.	Cell lysis and recombinant protein purification	109
6.3.	Cell culture	110
6.3.1.	Mammalian cell culture	110
6.3.2.	Mammalian cell passaging	111
6.3.3.	Surface coating	111
6.3.4.	Cell counting	111
6.3.5.	FKBP52 siRNA knockdown and transient overexpression	111
6.3.6.	HTRF-based relative FKBP52 quantification assay	112
6.3.7.	Generation of stable cell lines	113
6.3.8.	Fluorescent FKBP-eGFP level reporter assays	113
6.3.9.	SDS page	116
6.3.10.	Coomassie stain analysis	116
6.3.11.	Western blot	116
6.3.12.	FACS	117
6.3.13.	GR reporter gene assays (Hela AZ-GR)	117
6.3.14.	GR reporter gene assays (HEK293T)	118
6.3.15.	NanoBRET assays	118
7.....	<b>References</b>	121
8.....	<b>Supplemental Information</b>	141
9.....	<b>Abbreviations</b>	170
10. ..	<b>Curriculum Vitae</b>	174
11. ..	<b>Fellowships, Key Publications, Prizes, Conference contributions and Co-authorships</b>	175
11.1.	Fellowships	175
11.2.	Key publications	175
11.3.	Congress talks	176
11.4.	Conference and congress posters	176
11.5.	Co-authorships	176
12. ..	<b>Acknowledgment</b>	178

---

## 2. Abstract

---

### 2.1. Zusammenfassung

Die FK506-bindenden Proteine FKBP12, FKBP51 und FKBP52 sind Peptidyl-Prolyl Isomerasen und am besten dafür bekannt, dass sie den Wirkmechanismus der natürlichen molekularen Kleber FK506 und Rapamycin ermöglichen. Innerhalb der FKBP-Familie fungieren die großen Proteine FKBP51 und FKBP52 als Cochaperone in der Hsp90-Maschinerie und als Schlüsselregulatoren des Glucocorticoid Rezeptor Signalwegs. Dabei hemmt FKBP51 die GR-Aktivität und FKBP52 aktiviert diese.

Um die Entwicklung von FKBP-basierten Liganden zu unterstützen, habe ich zunächst verschiedene Testsysteme etabliert, um Aufschluss über biochemische und molekularbiologische Schlüsselaspekte von FKBP zu ermöglichen. (i) Ich habe einen HTRF-Bindungstest für FKBP-Liganden entwickelt, der eine präzise Messung der Bindungsaffinität von ultra-hoch affinen FKBP-Liganden möglich macht. (ii) Anschließend wurde ein NanoBRET-Testsystem zur Charakterisierung von FKBP-Liganden in lebenden Zellen entwickelt, optimiert und semi-automatisiert. Dieses Testsystem ermöglicht eine schnelle Charakterisierung der intrazellulären Bindung von FKBP-Liganden und FKBP. (iii) Des Weiteren habe ich zur Untersuchung der Schlüsselfunktionen von FKBP51 und FKBP52 im GR-Signalweg ein GR Aktivität Reporter-Testsystem etabliert. (iv) Um den Abbau von FKBP zu untersuchen, entwickelte ich darüber hinaus eGFP-fusionsbasierte Reportersysteme zur Bestimmung von zellulären FKBP12- und FKBP51-Spiegeln, sowie einen HTRF-basiertes Reportersystem für die FKBP52-Mengen.

Die Affinität von Liganden ist ein Schlüsselparameter für deren Wirksamkeit. Der HTRF-Bindungstest zeigte, dass FKBP-Liganden biochemisch mit picomolarer Affinität an FKBP binden. Jedoch ist für die Wirksamkeit von Liganden in einem zellulären Umfeld die intrazelluläre Zielproteinbindung entscheidend. Mit dem NanoBRET-Testsystem konnte zum ersten Mal gezeigt werden, dass FKBP-Liganden menschliche FKBP in lebenden Zellen binden. Dabei wurde jedoch eine systematische Diskrepanz zwischen der biochemischen Bindungsstärke und der zellulären Zielproteinbindung deutlich. Darüber hinaus zeigten die Ergebnisse, dass makrocyclische Liganden in ihrer zellulären Potenz gegenüber linearen Liganden der SAFit-Klasse (bei gleichen biochemischen Affinitäten) überlegen sind. Das NanoBRET-Testsystem schließt die Lücke zwischen biochemischer Bindung und zellulären Effekten und wird die Ligandenoptimierung in Richtung zellulärer Potenz weisen.



---

FKBP51 ist im zellulären Kontext ein hemmender Schlüsselregulator des Glucocorticoid Rezeptor Signalwegs, der das funktionelle Bindeglied zu Stress-bedingten Störungen darstellt. Mit dem GR Aktivität Reporter-Testsystem konnte ich zeigen, dass die synthetischen Liganden SAFit2 und 18<sup>(S-Me)</sup> den GR Signalweg nicht reaktivierten und keine funktionellen Effekte zeigten, obwohl das NanoBRET-Testsystem zeigte, dass diese die FK506-Bindetasche blockieren. Dies zeigt, dass FKBP51 den Glucocorticoid Rezeptor durch Gerüstfunktionen reguliert und die Bindetasche dabei entbehrlich ist. Jedoch reaktivierte der immunsuppressive Naturstoff FK506, welcher viel weiter aus der Bindetasche hervorsteht, den Glucocorticoid Rezeptor Signalweg. Dies zeigte, dass FK506, aber nicht kleinere Liganden, regulatorische FKBP51:GR-Kontakte aufheben können.

Die Reporter-Testsysteme zeigen, dass die Gerüstfunktionen von FKBP51 nicht durch synthetische, kleine Liganden aufgehoben werden können. Jedoch können diese Liganden, die eine nicht funktionelle Bindetasche adressieren, zur Entwicklung von PROTACs genutzt werden. PROTACs degradieren das Protein und blockieren damit alle Proteinfunktionen. Da die Entwicklung von PROTACs für FKBP51 deutlich herausfordernder war als erwartet, musste eine große Anzahl an PROTAC-Kandidaten getestet werden. Um 220 FKBP-fokussierte PROTAC-Kandidaten bezüglich des Abbaus der relevantesten FKBP zu testen, habe ich eGFP-fusionsbasierte Proteinmengen-Reportersysteme für FKBP12 und FKBP51, sowie ein HTRF-basiertes Proteinmengen-Reportersystem für FKBP52 etabliert. Überraschenderweise hatten die PROTAC-Kandidaten eine starke Degradationspräferenz für FKBP12 gegenüber den ähnlichen Homologen FKBP51 und FKBP52. Von den Kandidaten war dabei eine Großzahl aktiv für FKBP12, sechs für FKBP51 und keiner für FKBP52. Eine anschließende Analyse von FKBP12-FKBP51<sup>FK1</sup> Tauschmutanten zeigte, dass die FK2- und TPR-Domäne die Abbaubarkeit negativ beeinflussen. Die Linker-basierte Optimierung eines PROTACs der ersten Generation mit begrenzter Selektivität konnte jedoch die negative Abbaupräferenz für FKBP51 überwinden und führte zu dem potenten FKBP51 PROTAC SelDeg51 mit verbesserter zellulärer Aktivität und Selektivität. SelDeg51 baut FKBP51 auf effiziente Weise ab und ist die beste Substanz ihrer Art. Durch Bestätigung des Wirkmechanismus und eine gründliche zelluläre Charakterisierung habe ich SelDeg51 als nützliches funktionelles Werkzeug etabliert. Anschließend konnte ich in einem Reporter-Testsystem zeigen, dass der Abbau von FKBP51, aber nicht die Inhibition, den GR-Signalweg auf potente Weise reaktivierte. Dieses Ergebnis demonstriert eine fundamental neuartige Pharmakologie mit höherer Wirksamkeit gegenüber kleinen funktionell inaktiven synthetischen Liganden.

---

Die Natur hat wiederholt auf FKBP12 als Adapterprotein zurückgegriffen, um die Wirksamkeit von molekularen Klebern zu ermöglichen. Zusammen mit der hohen Abbaubarkeit von FKBP12 deutet dies an, dass FKBP12 ein ideales Modellsystem für die Entdeckung von Proteinabbau-induzierenden molekularen Klebern sein könnte. In geeigneten Fällen können Liganden molekulare Kleber sein, die zusätzlichen Funktionen besitzen. Ich habe in dieser Studie das eGFP-fusionsbasierte Proteinmengen-Reportersystem für FKBP12, genutzt um durch zelluläre Tests aus über 900 hauseigenen FKBP-Liganden Proteinabbau-induzierende molekulare Kleber für FKBP12\_eGFP zu identifizieren. Aus der Struktur-Aktivitätsbeziehung der primären Treffer sowie aus der Struktur von inaktiven Analoga konnte eine rationale Strategie zur Optimierung des vielversprechenden Treffers abgeleitet werden. Die Optimierung führte zur Synthese der Substanz PPU670, welche doppelt so effektiv wie das Ausgangsmolekül war. Anschließende zelluläre Tests zeigten einen FK506-Bindestelle- und Proteasom-abhängigen, aber Neddylierungs-unabhängigen Wirkmechanismus. Letztendlich identifizierte eine CRISPR-basierte Genom-weite Funktionsverlustanalyse die E3 Ligase UBR3 als relevantes Zielprotein. Meine Studie demonstriert, dass Zielprotein-fokussierte Substanzbibliotheken abbauende molekulare Kleber enthalten können und dass sich diese durch zelluläre Testsysteme identifizieren lassen.

Zusammengefasst werden die von mir entwickelten Testsysteme wegweisend in der künftigen Entwicklung von FKBP-Liganden sein. SelDeg51 kann genutzt werden, um alle Proteinfunktionen zu blockieren und um die Frage zu beantworten, ob zelluläre FKBP51-Mengen in einem bestimmten Kontext wichtig sind. Darüber hinaus zeigt meine Arbeit, dass zelluläre Tests von zielgerichteten Bibliotheken ein fruchtbarer Ansatz sein können, um Proteinabbauende molekulare Kleber zu entdecken.

---

## 2.2. Abstract

The FK506-binding proteins FKBP12, FKBP51 and FKBP52 are peptidyl-prolyl isomerases and best known for their ability to enable the natural molecular glues FK506 and Rapamycin. Among them, the large FKBP51 and FKBP52 are co-chaperones in the Hsp90-machinery and key regulators of glucocorticoid receptor signaling, with FKBP51 inhibiting and FKBP52 potentiating GR activity.

To support the development of FKBP-directed drugs, I first established a panel of assays to address key biochemical and molecular biological aspects of FKBP. (i) I developed a HTRF-based binding assay for FKBP ligands. This assay allows precise affinity determination for a new generation of ultra-high affinity FKBP ligands. (ii) Next, a NanoBRET assay for FKBP ligand profiling in living cells was developed, optimized and semi-automated. With this assay, FKBP ligands can be rapidly profiled for intracellular target-engagement. (iii) To assess the key cellular functions of FKBP51 and FKBP52 in glucocorticoid receptor signaling, I established GR activity reporter gene assays. Additionally, I developed (iv) eGFP fusion-based FKBP12- and FKBP51-level reporter assays as well as (v) a HTRF-based FKBP52 level reporter assay to assess the degradation of the respective FKBP.

Ligand affinity is a key parameter for ligand efficacy. The HTRF assay demonstrated that FKBP ligands biochemically bind to FKBP with picomolar affinities. Yet, intracellular target occupation is critical for ligands to act in a cellular environment. The NanoBRET binding assays unambiguously demonstrated for the first time that FKBP ligands occupy human FKBP in living cells. However, a general off-set between biochemical affinity and intracellular target engagement became evident. Additionally, the results showed the superiority in cellular potency of macrocycles compared to linear SAFit-type ligands with similar affinity. The NanoBRET assay bridges the gap between biochemical binding and cellular effects and will thereby further guide ligand optimization towards ligands with cellular potency.

In a cellular context, FKBP51 is a key regulator and inhibitor of glucocorticoid signaling, which constitutes the functional link to stress-related disorders. Using the glucocorticoid signaling reporter gene assays, I was able to demonstrate that the synthetic ligands SAFit2 and 18<sup>(S-Me)</sup> did not reactivate FKBP51-suppressed GR signaling and were functionally silent, albeit they occupied the FK506-binding site as evidenced by the NanoBRET assay. This demonstrates that FKBP51 regulates the GR through scaffolding functions and that the binding pocket is dispensable for GR regulation. However, the immunosuppressive natural product FK506, which

---

protrudes far further from the binding-site reactivated GR signaling. This shows that FK506, but not smaller ligands, can abrogate regulatory FKBP51:GR contacts.

The reporter gene data show that the scaffolding functions of FKBP51 cannot be addressed by synthetic FKBP ligands. But ligands for non-functional binding sites can be used to generate PROTACs that degrade the protein and therefore abolish all protein functions. Since the development of PROTACs for FKBP51 turned out to be much more challenging than expected, a large number of PROTAC candidates needed to be profiled. Towards this aim, I established the eGFP-fusion based FKBP12- and FKBP51-level reporter assays and the HTRF-based FKBP52-level reporter assay to test 220 FKBP-directed PROTAC candidates for degradation of the respective FKBP. Surprisingly, the PROTAC candidates had a strong degradation bias for FKBP12 over the close homologs FKBP51 and FKBP52. Among the candidates, a plethora of PROTACs was active for FKBP12, six for FKBP51 and none for FKBP52. Subsequent, FKBP12-FKBP51<sup>FK1</sup> swap mutant analysis showed that the presence of the FK2 and TPR domain negatively influences the degradability. However, linker-based optimization of a first generation PROTAC with limited selectivity overcame the negative degradation bias for FKBP51 and lead to potent FKBP51 PROTAC SelDeg51 with improved cellular activity and selectivity. Ultimately, SelDeg51 is the best-in-class compound and efficiently depletes FKBP51. I established SelDeg51 as a useful functional tool through thorough cellular characterization and by confirming its mode of action. In subsequent reporter gene assays, I could show that FKBP51 depletion, but not inhibition, potently reactivated GR signaling. This demonstrated a fundamentally different pharmacology with enhanced efficacy compared to the functionally silent synthetic ligands.

Nature repeatedly resorted to FKBP as adapter proteins to enable molecular glues. Taken together with the high degradability of FKBP12 this indicated FKBP12 as ideal model system to discover molecular glue degraders. In favorable cases, ligands can be molecular glues that possess additional gain of function properties. In this work, I used the eGFP-fusion based FKBP12 reporter assays to discover FKBP12\_eGFP degrading molecular glues through cellular testing of >900 in-house FKBP ligands. The structure-activity relationship of the initial screening hits and inactive analogs enabled the rational optimization of the most promising hit into PPU670 with doubled cellular potency. Subsequent cellular analysis revealed a FK506-binding site- and proteasome- but not neddylation-dependent mode of action. Finally, a CRISPR-based genome-wide knockout screen identified UBR3 as the relevant engaged E3 ligase. This work demonstrates that target-focused libraries can contain molecular glue degraders and that the E3 ligase UBR3 is glue-able and can be (re)directed to neo-substrates.

---

Overall, the assays I established will be instrumental to guide future FKBP ligand development. SelDeg51 can be used to target all protein functions and answer the question if cellular FKBP51 levels matter in certain contexts. Finally, my work demonstrates that cellular testing of target-focused libraries can be a fruitful approach to discover molecular glue degraders.

---

## 3. Introduction

---

### 3.1. FK506-binding proteins

FK506-binding proteins (FKBPs) are named after their ability to tightly bind the immunosuppressive drug FK506 and thus belong, next to cyclosporin-binding cyclophilins to the protein family of immunophilins. Many members of these protein families possess catalytic peptidyl-prolyl-isomerase (PPIase) activity and catalyze the transition of peptide-prolyl bonds from cis- to trans-configuration. Most peptide bonds in proteins occupy an energetically more favorable trans-configuration (> 99.9%) due to higher steric hindrance between neighboring amino acids in the cis-configuration. Proline is an exception, where the cis-configuration is populated up to 5% [1]. This cis- trans-conversion increases the structural variety of protein folds and is considered a rate-limiting step in protein folding [1]. FKBPs feature versatile structures but share at least one archetypical PPIase domain which folds into five beta-sheets that curve around an  $\alpha$ -helix. While the localization of FKBPs is diverse the most prominent members FKBP12, 12.6, 51 and 52 reside mainly in the cytoplasm.

#### 3.1.1. Cellular functions of prominent FKBPs

FKBP12 was first described in 1989 and is most prominently known to act as receptor for FK506 and Rapamycin [2–4] enabling their immunosuppressant properties via a gain-of-function mechanism (see 3.2.1). With only 12 kDa FKBP12 the smallest member of the immunophilin family. However, FKBP12.6 features 85% similarity compared to FKBP12 [5]. Both contain only the PPIase core domain (Figure 1A). Strikingly, FKBP12 knockouts in mice are embryonically lethal [6] but pharmacological inhibition of FKBP12 has been demonstrated to be tolerated by the clinical use of FK506 and Rapamycin. It is hypothesized that embryonic lethality can be attributed to severe heart defects caused by FKBP12's regulatory role of ryanodine receptors [6], which are calcium channels and involved in muscle contraction.

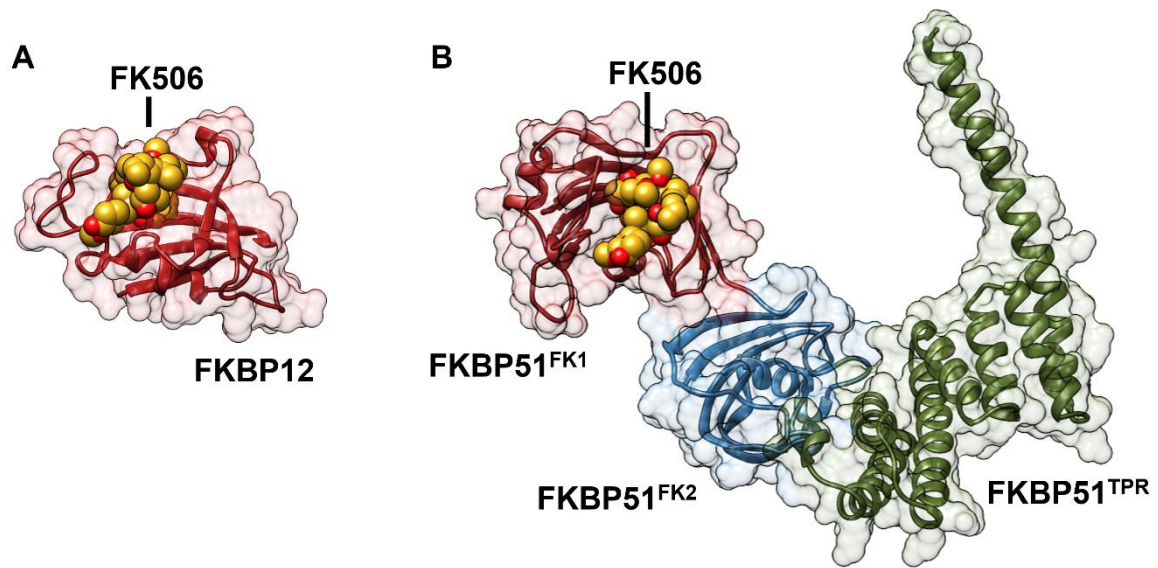


**Figure 1** Structures of FKBP12 and FKBP51. **A** Crystal structure (pdb: 1FKJ) of FKBP12 (red cartoon and transparent surface) in complex with FK506 (shown as spheres). **B** Superimposition of the crystal structures of FKBP51 (pdb: 5OMP, shown as cartoon) in complex with FK506 (golden spheres, superimposed from 3O5R; FKBP51<sup>FK1</sup>: red, FKBP51<sup>FK2</sup>: blue, FKBP51<sup>TPR</sup>: green):

The large FKBP51 and FKBP52, respectively encoded by the *FKBP5* and *FKBP4* genes, consist of three domains: (i) An N-terminal FK1 domain that exhibits PPIase activity and binds FKBP ligands. (ii) An enzymatically inactive FK2 domain that does not bind FKBP ligands but shares a similar fold with the FK1 domain, and (iii) a C-terminal tetratricopeptide repeat (TPR) domain that mediates Heat shock protein 90 (Hsp90) binding (Figure 1B) [7]. FKBP51 and FKBP52 are close homologs (60% identity and 75% similarity) and act as co-chaperons in the Hsp90 machinery (Figure 2).

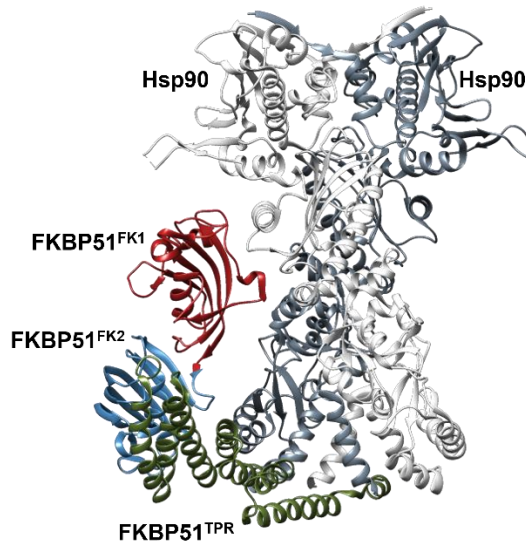


**Figure 2** Cryo-EM structure of the FKBP51:Hsp90<sub>2</sub> complex. (Hsp90 monomers: light and dark grey; FKBP51<sup>FK1</sup>: red; FKBP51<sup>FK2</sup>: blue; FKBP51<sup>TPR</sup>: green; PDB: 7I7I [8])

Hsp90 is involved in the folding and functional maturation of at least 10% of the eukaryotic proteome [9]. While several Hsp90-dependent regulatory roles of FKBP51 are postulated (e. g. CDK4 [10] and Tau [11–13]), FKBP51 and FKBP52 remain best described as co-regulators of the steroid hormone receptors (SHRs) and are thought to fine-tune the maturation thereof. Their physiological importance became evident in transgenic studies of knockout mice. While FKBP52 knockout mice display severely compromised sexual development [14,15], FKBP51 knockout mice were protected from various forms of chronic pain [16,17] and showed enhanced stress coping behavior [18–20] without displaying adverse phenotypes [16,21–23]. In humans, the *FKBP5* gene contains several glucocorticoid responsive elements (GREs) and FKBP51 expression is robustly induced by steroid hormones across various tissues [24]. Additionally, several single nucleotide polymorphisms have been reported and functionally annotated to enhance FKBP51 expression. These have been linked to an increased risk for stress-induced disorders [25]. FKBP51's regulatory role in glucocorticoid receptor (GR) signaling functionally links FKBP51 expression and stress signaling. Thereby, FKBP51 negatively regulates GR activity through an ultra-short negative feedback loop [26]. However, FKBP51 is not the sole regulator of steroid hormone receptors (SHRs) among the FKBP5s but acts in concert with FKBP52. The two immunophilins display a clear antagonizing behavior in the regulation of several members of the SHR family including the glucocorticoid receptor, progesterone receptor (PR) and to a lesser extent of the mineralocorticoid receptor (MR) with FKBP52-potentiating and FKBP51-inhibiting receptor activity [27]. For the androgen receptor (AR) the regulatory role of FKBP51 is more ambiguous and might be cell type-dependent. Here, FKBP51 was repeatedly postulated as an AR potentiator in prostate cancer cell lines [28–30]



---

but showed no or negative AR regulatory effects in other mammalian cell lines [31–33]. The estrogen receptor (ER) was demonstrated to be just modestly influenced by Hsp90 inhibition [32] and thus likely by TPR domain containing proteins as FKBP51 or FKBP52, yet both have been described to be associated with the ER [32].

SHRs undergo a complex Hsp90-dependent maturation cycle to reach their active ligand-bound state. Here, the GR maturation has been investigated as a model system and key intermediate steps were structurally elucidated. The minimal machinery for GR activation includes Hsp90 as well as the co-chaperons Hsp70, Hsp40, HOP and p23 [34]. Initially, the steroid hormone-unbound GR ligand binding domain (apoGR<sup>LBD</sup>) is partially unfolded by Hsp70 and Hsp40 and transferred to Hsp90 with the help of HOP and another Hsp70 that scaffolds HOP and Hsp90 to constitute the ‘Hsp90-client loading complex’ [35]. This complex does not contain p23 [35]. The GR is thereby threaded through the Hsp90 dimer lumen [35]. However, the functional mechanism of this threading is not fully clear, even though it could be of high physiological relevance. It is postulated to play an important role in opening the binding pocket. From there, the GR maturation progresses further to p23 and/or FKBP containing apoGR:(Hsp90)<sub>2</sub> complexes [36]. The p23:(Hsp90)<sub>2</sub>:GR<sup>LBD</sup> complex was recently structurally elucidated by cryo-EM and termed ‘maturation complex’ [37]. An overlay of this structure and the cryo-EM structure of the FKBP51:(Hsp90)<sub>2</sub>:p23 complex [8] indicated that the FKBP51 would clash with the GR<sup>LBD</sup> in this conformation [27]. This further implied that FKBP51 and the GR<sup>LBD</sup> have to undergo substantial conformational changes to accommodate each other [27]. The structural elucidation of the FKBP containing apoGR:(Hsp90)<sub>2</sub> complexes is matter of ongoing research. Ultimately, the ligand bound GR is released from Hsp90 complexes to act as a transcription factor. Yet, the mode of action of how FKBP51 and FKBP52 differentially regulate GR activity is not fully clear.

Next to its role in steroid hormone receptor signaling, FKBP51 has been postulated as a regulator of the Akt and NF-κB pathway. Akt (or protein kinase B (PKB)) is a serine-threonine kinase that acts as a central regulator of cellular pathways. FKBP51 was first suggested to act as a scaffold which recruits the phosphatase PHLPP via the FKBP51<sup>TPR</sup> domain to act on Akt which is recruited via the FKBP51<sup>FK1</sup> domain, thereby negatively regulating AKT phosphorylation and hence activity [38]. Conversely, truncation studies suggested a bimodal model for Akt binding, where the FKBP51<sup>FK1</sup> domain alone interacts with AKT, but binding is also partially mediated via Hsp90 that is bound to the FKBP51<sup>TPR</sup> domain [39]. Notable for the suggested model is that neither the PPIase-dead FKBP51<sup>F67D/D68V</sup> mutant nor FKBP ligands disrupted AKT:FKBP51 association and an increase of Akt phosphorylation was observed upon

---

FKBP51 overexpression. More recently, different models [40–42] for FKBP51-mediated Akt regulation were suggested. However, the precise mode of action is still under discussion.

In NF- $\kappa$ B signaling, FKBP51 is described to be associated with several members of the IKK complex (IKK $\alpha$ , IKK $\beta$ , IKK $\gamma$ ) but the underlying mechanism and outcome of pathway regulation is controversial [7].

### 3.1.2. Pharmacological FKBP inhibition

The first FKBP ligands described were the natural products FK506 and Rapamycin which bind FKBP51 mainly via their pipercolate moiety. Initial ligand development focused on cyclic and acyclic FK506 analogs [43] constituting the ligand classes of pipercolate-ketoamids and pipercolate-sulfonamides. Then computational studies suggested that bridged bicycles fit well in the binding pocket of FKBP51 [44,45]. Following the idea of bridging and rigidification [4.3.1]-bicyclic mimics of the pipercolate moiety lead the development of a class of highly potent, but unselective bicyclic FKBP ligands [46–53]. In 2015, the first selective ligands for FKBP51 were identified. The ligands were designed to use a bump-and-hole approach to artificially enable selectivity for engineered FKBP mutants over their wild type counterparts. Strikingly, one of the ligands still displayed affinity for wild type FKBP51 but not wild type FKBP52. Co-crystal structures revealed a conformational change was induced in FKBP51 and Phe67 was displaced by the ‘bump’ of the ligand. Subsequent optimization of the ligand led to the selective antagonists of FKBP51 by induced-fit (SAFit) family [54]. The compounds of the SAFit class retain the induced-fit binding mode and feature selectivity over FKBP52. SAFit2 binds with high affinity to FKBP51 ( $K_D = 6 \pm 2$  nM), displays >10000 selectivity over FKBP52 and is the gold standard for FKBP51 pharmacology [55]. Additionally, recent approaches focus on the macrocyclization of linear SAFit-type ligands to improve drug-relevant properties [56,57]. Macrocyclization can pre-organize a bio-active conformation to minimize an entropic loss upon binding and thus increase the affinity [58]. Additionally, this approach can also improve cell permeability of ligands. Macrocycles can have the ability to change their conformation when traversing hydrophobic lipid membranes thereby burying polar groups that are normally solvent-exposed in aqueous solution [59]. Up to date, a focused library of >1000 FKBP ligands has been assembled in the Hausch Lab (Figure 3) [46–54,56,57,60–64].

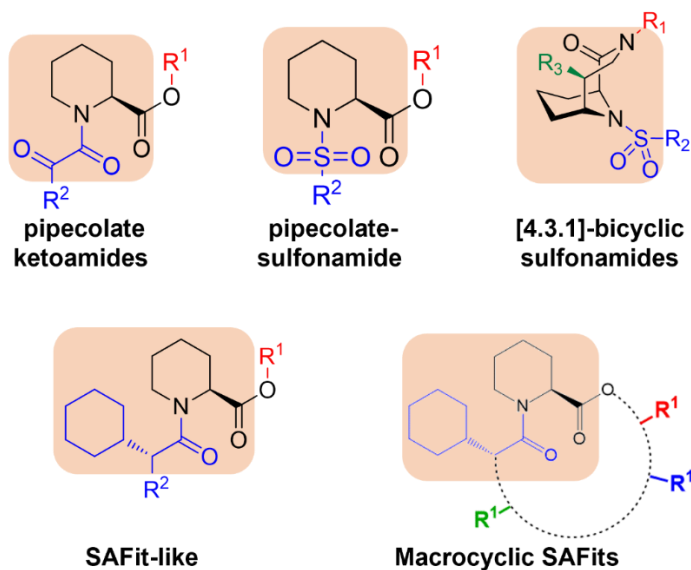


**Figure 3** General chemical structures of different classes of FKBP-ligands in the in-house focused library. Protein-interaction core motifs are shaded in salmon.

### 3.2. Molecular glues<sup>1</sup>

Molecular glues (MG), here defined as small molecules that engage two protein surfaces to induce or enhance the affinity between the two proteins, have historically been considered a rarity and peculiarity of some natural products. In the late nineteen nineties the molecular glue mechanisms of the immunosuppressive drugs FK506, Rapamycin and Cyclosporin were unraveled and led to initial enthusiasm. But synthetic approaches to develop *de novo* molecular glues to induce protein-protein interactions (PPIs) were not met with success at that time. However, the enthusiasm was revived with the development of proteolysis-targeting chimeras (PROTACs) and serendipitous discovery of several PPI inducing MGs. As a general mode of action MGs bind an accessory protein (AP, adapter protein or presenter protein) to act together on a protein-of-interest (POI or target protein). If the accessory protein forms beneficial PPIs with the composite POI surface (positive cooperativity) MGs can enable targeting of POI surfaces that would otherwise not be addressable (Figure 4A). That effect is evident for FK506 and Cyclosporin A as well as Rapamycin. These natural products address shallow surfaces on the phosphatase calcineurin and the kinase mTORC1 together with their respective APs FKBP12 and Cyclosporin. Thereby, they inhibit signaling and enable immune suppression. In that case,

<sup>1</sup> This chapter contains excerpts and adaptations thereof as well as figures and adaptations thereof from the previously published review:

Geiger, T. M.\*\*, Schäfer, S. C., Dreizler, J. K., Walz, M., & Hausch, F.\* (2022). Clues to molecular glues. *Current Research in Chemical Biology*, 2, 100018. \* , \*\*: Corresponding author

---

the AP acts as an interaction relay. The MG tightly engages with the AP and moieties of the small molecule that would normally protrude unproductively in the solvent, engage in interactions to the POI (Figure 4A red lines). In turn, the AP and POI can reinforce ternary complex formation through direct interactions of their surfaces (Figure 4A green lines). Additionally, MGs can act as PPI stabilizers if the accessory protein and the POI interact substantially with each other by nature (Figure 4B). Here, the POI and AP are often in a functional context and the affinities of the MG are more moderate. When gluing enzymes MGs can act catalytically and redirect enzyme activities to neo-substrates (Figure 4C). This case is most apparent for E3 ligases and degradative MGs but theoretically not limited to that enzyme class. Here, the catalytic mode of action can enable effectiveness even for weak MGs that feature low target recruitment. Additionally, MGs can confer tissue specificity depending on the abundance of the respective AP (Figure 4D). This was first transferred to practice by a VHL-based BCL-XL PROTAC which spared BCL-XL degradation in cells that poorly expressed VHL [65]. Finally, the AP and POI engaging moiety can be integrated into one compact scaffold as for strict MGs like FK506 or be clearly separated by a linker as in PROTACs (Figure 4E).

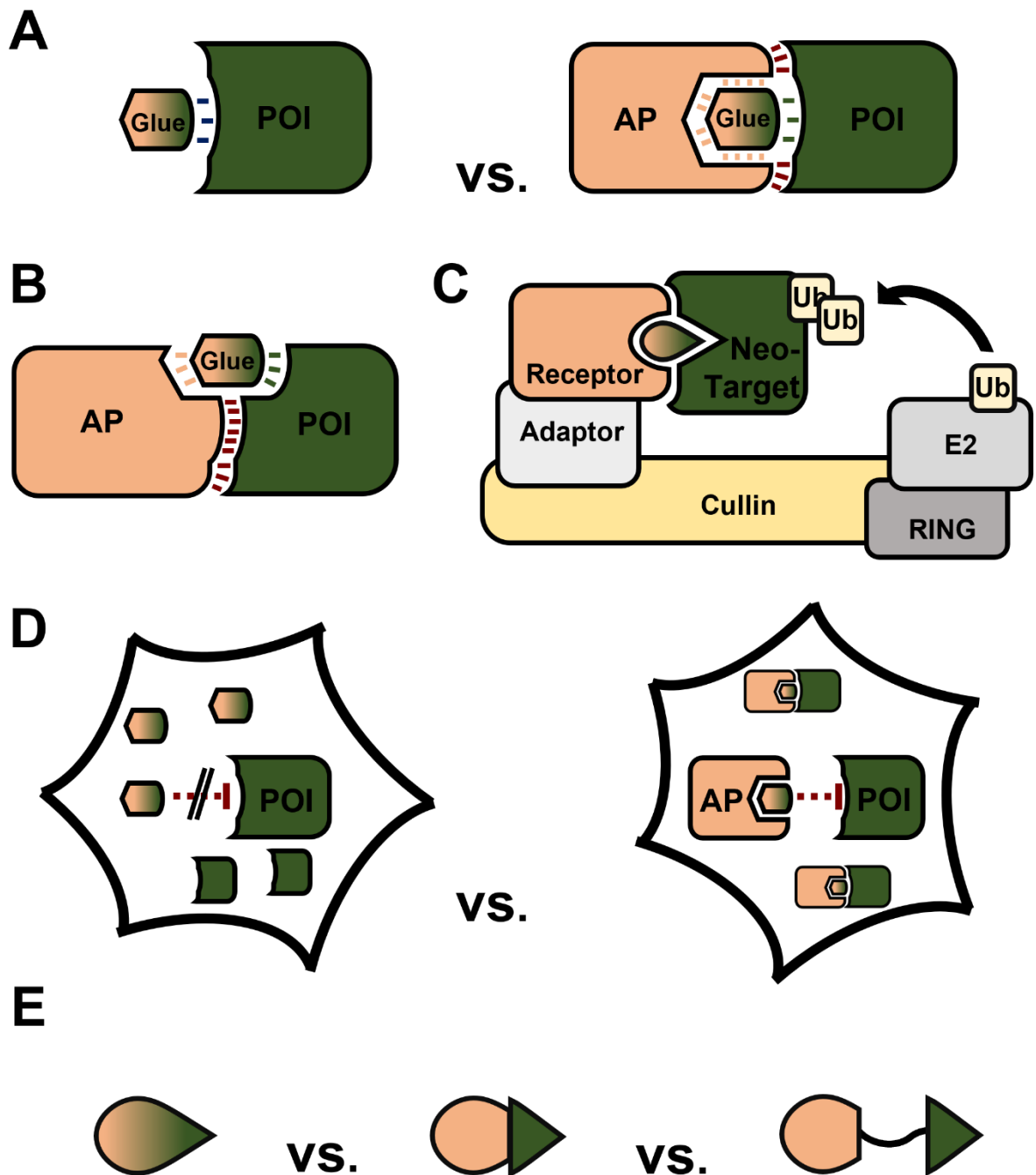


**Figure 4** **A** Shallow surfaces without ligandable pockets of the protein of interest (dark green) can be addressed with help of accessory protein (pale orange). **B** MGs can act as stabilizers for complexes of two proteins (dark green and pale orange) with preexisting PPIs (dark red). **C** MGs can act catalytically at sub stoichiometric concentrations if enzymes are glued. **D** MGs should work in cell-type specific manner according to the APs expression. **E** MGs are bifunctional as they engage two proteins (POI and AP) with their POI- and AP interacting parts (pale orange and dark green, respectively) These parts can be intertwined like for IMiDs or clearly separated as in PROTACs. Figure taken from [66].

### 3.2.1. Natural Immunophilin-based molecular glues

The Cyclophilin 18 (Cyp18)-binding Cyclosporin A (CsA) (Figure 5A) was first discovered in an antibiotic screening program [67] and found to be immunosuppressive, however initially the mode of action was unclear. Later, it was unraveled that a binary Cyp18:CsA complex, but not CsA alone, can engage the calcium/calmodulin-dependent serine–threonine protein phosphatase calcineurin (CN) [68]. Thereby, access to CN substrates such as NFAT (nuclear factor of activated T cells) is allosterically restricted ultimately reducing the function of effector T-cells [69]. Additionally, Sanglifehrins were discovered in a screening program directed to identify compounds that block the CsA-Cyp18 interaction [70]. However, Sanglifehrin A (SfA) (Figure 5B) does not target CN but still modulates cell growth. Structural analysis revealed that SfA engages the CsA-binding site in Cyp18 but large parts of the molecule are solvent exposed. Later it was identified that the SfA:Cyp18 complex targets the inosine-50-monophosphate dehydrogenase 2 (IMPDH2), but IMPDH2's catalytic activity remained unaffected. While it is clear that IMPDH2 is involved in *de novo* guanine nucleotide biosynthesis, which is increased in proliferating cells, the precise mode of action of SfA is still unclear [71].

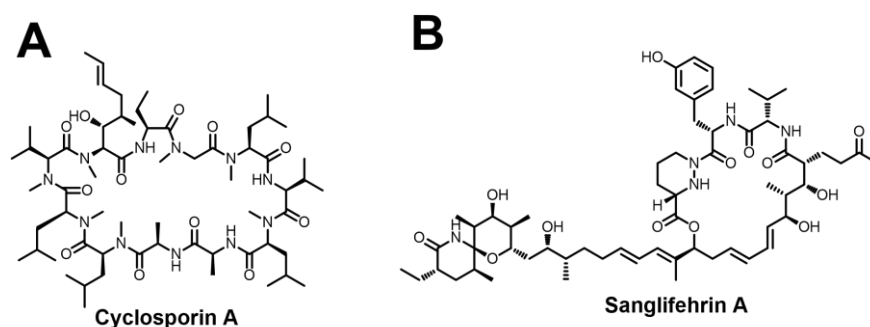


**Figure 5** Chemical structure of **A** Cyclosporin A and **B** Sanglifehrin A. Figure adapted from [66].

FK506 and Rapamycin (Figure 6C&D) are immunosuppressive drugs that tightly bind FKBP12 [72] instead of cyclophilins. Similar to CsA's mode of action, FK506 first engages its AP (FKBP12) and then the FK506:FKBP12 complex binds CN [73,74] thereby blocking access to down-stream targets of the phosphatase (Figure 6B). Rapamycin on the other hand associates with FKBP12 to bind the FKBP-Rapamycin binding domain of mTOR (FRB) to allosterically inhibit the mammalian (or mechanistic) target of Rapamycin kinase complex 1 (mTORC1) (Figure 6A) [75,76]. Inhibition of this kinase severely impacts cell growth and proliferation due to its regulatory role of protein synthesis. This natural product is a prime example of MGs as it tightly binds FKBP12, but not to FRB alone and no direct binding of FKBP12 and FRB is detectable. Only when bound to FKBP12, Rapamycin leads to stable ternary complex formation [4,72].

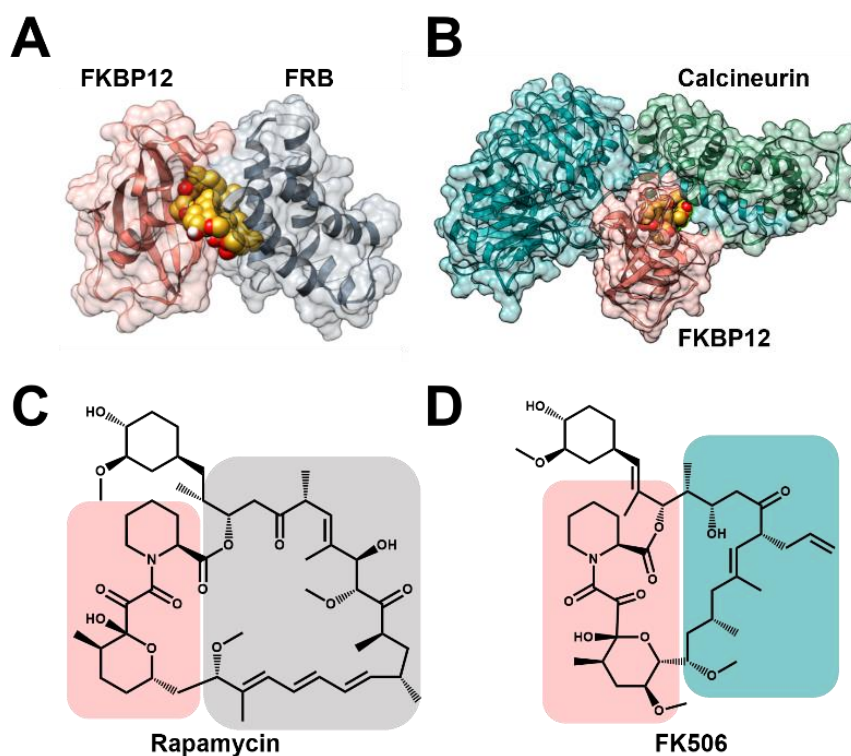


**Figure 6** FK506 and Rapamycin-induced FKBP:protein interactions. **A** FKBP12-Rapamycin-FRB complex (pdb: 1FAP) [4] and **B** FKBP12-FK506-Calcineurin complex (pdb: 1TCO) [74]. Chemical structures of **C** Rapamycin and **D** FK506. Protein interactions domains are shaded in salmon for FKBP12 and in grey and blue for the respective target proteins FRB and Calcineurin. Figure adapted from [66].

Next to Rapamycin and FK506 several ‘orphan’ molecular glues (Meridamycin [77], 3-Normerdamycin [78], and Antascomicins [79]) for the AP FKBP12 are postulated but their respective ternary target protein partners are still to be elucidated.

Nature repeatedly resorted to immunophilin-based molecular glues to address otherwise undruggable shallow surfaces which highlights that immunophilins might be ideal adapter proteins. Additionally, most of these natural products or analogs thereof have been or are still clinically used as evidenced by the drugs (Sandimmune, Tacrolimus, Sirolimus etc.). This demonstrates that pharmacological inhibition of Cyp18 and FKBP12 is generally tolerated. However, it is still not fully clear how rare or rather how prevalent immunophilin-based molecular glues really are, especially among synthetic FKBP ligands. Progress is being made to answer that question. Guo and coworkers generated a 45,000-molecule library – termed Rapafucins – of hybrid macrocycles consisting of an optimized FKBP-binding domain of Rapamycin and a combinatorically assembled tetrapeptide effector domain. Phenotypic

---

screening of this library revealed Rapadocin that bound nucleoside transporter hENT1 ( $K_i = 180$  nM) alone but binding was 30-fold enhanced in presence of FKBP12 [80].

### 3.2.2. Synthetic degradative molecular glues

Thalidomide (Figure 7C) originally sold in the 1950s as a sedative under the brand names Contergan or Thalomid lead to catastrophic effects among new-born children when administered during pregnancy which resulted in removal from the market in 1961. This medical disaster became known as the Contergan or thalidomide scandal. However, in 1998 thalidomide was reinstated and approved for the treatment of cancer by the FDA as the compound was demonstrated to have immunomodulatory and anti-inflammatory properties. Hence, the name IMiDs (Immunomodulatory imide drugs) for the compound class comprising thalidomide and its analogs was formed. In 2010, cereblon (CBRN) and the associated DDB1 (damaged DNA binding protein 1) were identified as primary binding partners [81]. In the following, it was demonstrated that IMiD binding redirects the E3 ligase substrate receptor CBRN to ZFK1 and ZFK3 transcription factors that are recognized as neo-substrates and subsequently degraded [82–84] (Figure 7A&B). Today, several additional neo-substrates of IMiD:CBRN complexes have been identified such as ZFP91 [85], casein kinase 1 alpha (CSNK1A1) [86] or GSPT1 [87].



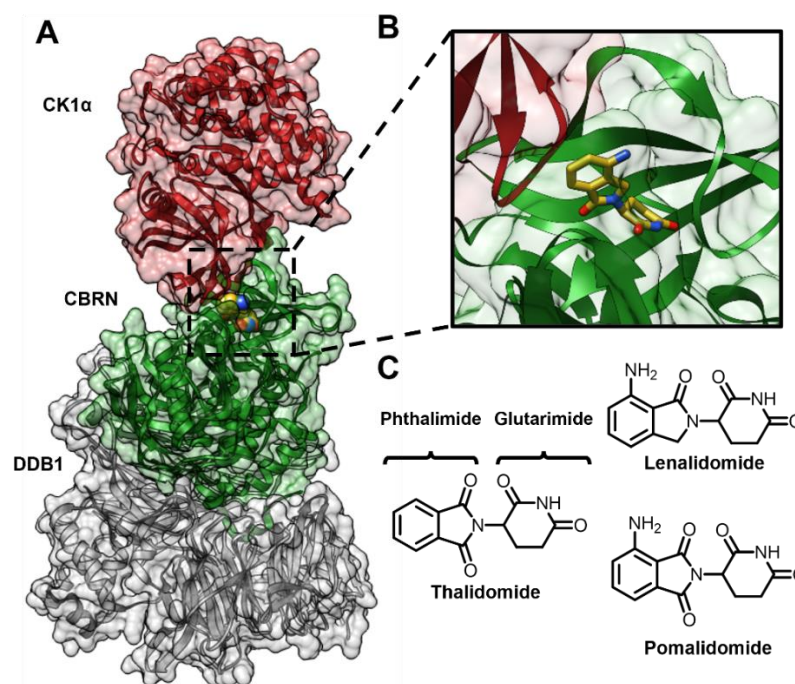


**Figure 7 A, B** Cartoon representation of CK1α (red), Lenalidomide (spheres or stick model), Cereblon (CBRN) (green) and DDB1 (grey) [88]. **C** Chemical structures of Thalidomide, and its close analogs Lenalidomide and Pomalidomide. Figure adapted from [66].

Strikingly the neo-substrates did not share any primary degron similarity except a glycine at a certain position in the recognized hairpin loop [85]. Furthermore, it became evident that hydrogen bonding of three backbone carbonyls in the surface exposed turn of the hairpin loop was essential for the induced interaction [82,88–90]. While the glutarimide ring is responsible for CBRN binding, the phthalimide moiety is (together with CBRN) responsible for neo-substrate recruitment. Thus, phthaloyl ring derivatization was explored to unlock new neo-substrates or to increase efficacy. This led to the development of second generation IMiDs for which the name ‘CELMoDs’ (Cereblon E3 ligase modulators) was coined [91].

After IMiDs, another class of molecular glue degraders were uncovered. Aryl-sulfonamides as Indisulam, Tasisulam, E7820 or CQS (Figure 8A) recruit the E3 ligase complex Cul4-DCAF15 to degrade the RNA-Binding Motif Protein 39 (RBM39) and its paralog RBM23 [92–94]. Additionally, a RBM39-selective degrader was discovered (Figure 8B) [95]. Different to IMiDs, aryl-sulfonamide degraders have very low affinities for DCAF15 alone ( $K_i > 50 \mu\text{M}$  for indisulam and tasisulam) but display synergistic binding in presence of both DCAF15 and RBM39 [96]. Hereby, a shallow pocket in DCAF15 is engaged. In the ternary complex, the aryl-sulfonamides are buried between the proteins and form direct and water-mediated contacts to both while the proteins engage in hydrophobic contacts to each other [96–98]. This mode of

action for ternary complex formations suggests that the AP does not need to be directly ligandable and high binary affinity is not a prerequisite for effective MGs.

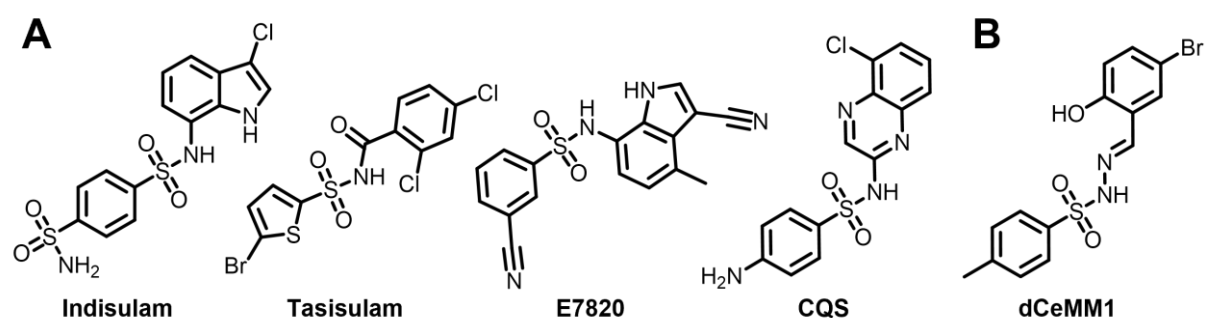
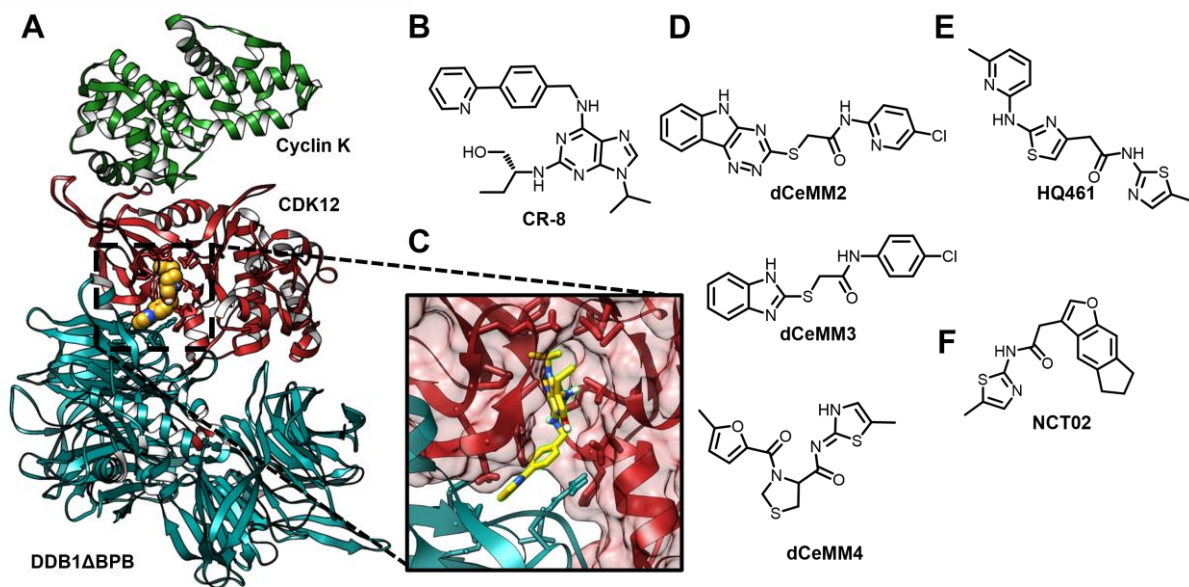


Figure 8 Aryl-sulfonamide recruiting Cul4:DCAF15 glues. Chemical structures of **A** Indisulam [92,94], Tasisulam [92], E7820 [94], CQS [92,94] and **B** of dCeMM1 [95]. Figure taken from [66].

With the rise and rise of IMiDs as cancer drugs [99], MGs started losing their reputation as peculiarities of natural products and the field focused increasingly on the rational discovery of MGs. Using different approaches, two of which directly aimed for discovery of degraders, four independent groups discovered structurally distinct cyclin K degraders. Słabicki *et al.* were the first to report such a molecule [100]. They systematically correlated cytotoxicity of a library of small molecules with E3 ligase expression levels across several cancer cell lines to discover CR-8. To unravel CR-8's mode of action they employed E3 ligase-focused CRISPR-Cas9 resistance screen. They were able to identify Cul4-RBX1-DDB1 complex as a crucial component but were unable to identify any cognate Cul4-DDB1 associated factors (DCAF) that normally serve for substrate recruitment. Instead, they subsequently employed a genome-wide CRISPR-Cas9 cyclin K\_eGFP reporter stability screen to identify the cyclin-dependent kinase 12 (CDK12), that binds to and depends on cyclin K for its activation, as essential for cyclin K destabilization. A crystal structure revealed that CR-8 binds the ATP-pocket of CDK12 and recruits the complex to DDB1. Thereby, CDK12 functions as a drug-induced substrate receptor to enable the degradation of its interaction partner cyclin K. Interestingly a weak binary affinity, although unlikely physiologically relevant, was reported for DDB1 and CDK12. Several CDK12 inhibitors that engage the same site, were able to recruit CDK12 to DDB1. *In vitro*, they induced cyclin K ubiquitination, albeit weaker than CR-8, but this recruitment did not lead cellular cyclin K degradation. This suggests the existence of a minimal ternary complex formation threshold that is necessary for degradation. In the following, Mayor-Ruiz *et al.* [95], Lv *et al.* [101] and Dieter *et al.* [102] also reported cyclin K degraders in quick succession. Mayor-Ruiz *et al.* used a comparative screening approach and tested 2000 cytostatic/cytotoxic molecules in neddylation proficient and hyponeddylated cells. The hyponeddylated cell line has broadly abrogated cullin-Ring ligase functions and the comparative approach allowed functional correlation of the small

molecule mode of action to cullin-Ring ligase activity. In that way, they were able to identify three cyclin K degraders. The other two studies serendipitously discovered cyclin K degraders in a luminescent reporter-based high-throughput screen for NRF2 inhibitors [101] and in a phenotypic cell viability screen against primary colorectal cancer tumor cells [102]. While structural confirmation of the ternary complex is still pending for the latter three studies, their results suggest a similar mode of action of all cyclin K degraders.



**Figure 9** Cyclin K degrader overview. **A, C** Cartoon representation of cyclin K (green), CDK12 (red) CR-8 (spheres or stick model) and DDB1 (cyan) (pdb: 6TD3, [100]). Chemical structures of **B** CR-8 [100], **D** dCeMM2, dCeMM3, dCeMM4 [95], **E** HQ461 [101] and **F** NCT02 [102]. Figure adapted from [66].

Like cyclin K degraders and distinct to IMiDs, BRD4 degrading molecular glues engage primarily their target and then recruit it to a E3 ligase. The bromo domain containing BRD4 is a transcriptional and epigenetic regulator that has been repeatedly targeted for proteasomal degradation with PROTACs [103–105]. However, a patent disclosure [106] described a monovalent BRD4 degrader that consists of the classical BET inhibitor JQ-1 functionalized with propargyl amine tail (Figure 10A), but the mode of action was not reported. Recently, Shergalis and colleagues resynthesized the compound and used arrayed CRISPR knock-out screens to identify DCAF16 as the relevant substrate recognition receptor [107]. Additionally, close analogs of GNE-0001 with covalent warheads (Figure 10B) were recently reported to target BRD4 for degradation in a DCAF16-dependent manner and covalently modify DCAF16 [108], which was confirmed by cryo-EM structures of the BRD4<sup>BD2</sup>:glue:DCAF16 complex. A second patent [109] recently disclosed a BRD4 degrader (Figure 10C) with a DC<sub>50</sub> of 150 pM that displayed strong growth inhibition in several cancer cell lines and outclassed the prominent

BRD4 PROTACs MZ-1 and ARV-771. The PROTAC-like structure of the compound comprises the bromodomain ligand JQ-1 which is tethered to the core structure of aryl-sulfonamide E7820, which indicates that compound was likely aimed to degrade BRD4 in DCAF15-dependent manner. However, the Ciulli lab discovered in competition experiments with the sulfonamide warhead E7820 that degradation was not blocked. Additionally, the PROTAC-like compound was still active in DCAF15 knockout cells. Instead, they revealed DCAF16 as the relevant E3 ligase. Strikingly, a cryo-EM structure showed that the compound bivalently binds both bromodomains of BRD4 and glues the complex to DCAF16. [110]

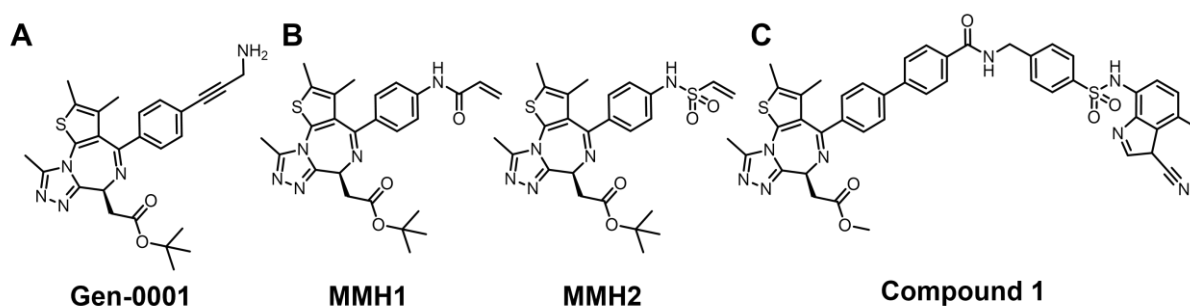


**Figure 10** Chemical structures of BRD4 degrading molecular glues. **A** Gen-0001, **B** MMH1 and MMH2, **C** Compound 1

The discovery of BCL6 degraders suggested another distinct mode of action for degradative MGs. A subset of Inhibitors of BCL6 which bind the BCL6-BTB domain and aimed to abolish the interaction to co-repressor proteins were demonstrated to be potent BCL6 degraders [111]. Hereby, the degraders surpassed the efficacy of non-degrading inhibitors. Interestingly, these degraders induced precipitation of their target protein in biophysical assays. In structural studies it was later shown that a solvent exposed moiety of BI-3802 (Figure 11C) induced homomultimer formation through interaction with a neighboring BTB-domain, which then leads to higher-order filaments (Figure 11B). Genome-wide CRISPR-Cas9 screens revealed the E3 ligase SIAH1 to be responsible for drug-induced and endogenous BCL6 degradation. SIAH1 recognized a VxP motif and displayed a weak affinity for isolated BCL6 but the affinity was strongly enhanced for BCL6 filaments. [112] These finding suggest ligand-induced multimerization of target-proteins as new mechanism for targeted protein degradation.

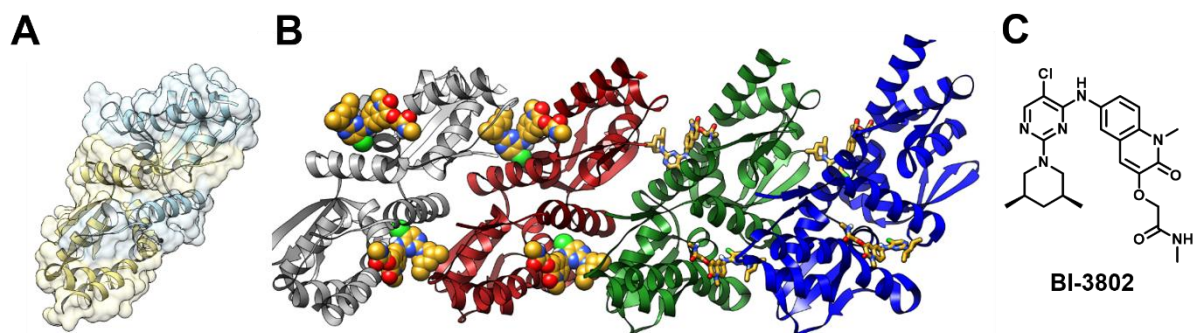


**Figure 11** Overview of BCL6 degrader BI-3802. **A** BCL6 BTB domain dimer (monomers coloured in khaki and light blue respectively pdb: 3E4U). **B** BI-3802-induced (spheres) higher order filaments (BCL6 dimers labelled in distinct colours, pdb: 6XMX). **C** Chemical structure of BI-3802. Figure taken from [66].

Noteworthy in the context of primary target-engaging degraders are also selective estrogen receptor degraders (SERDs) such as fulvestrant (Figure 12). It is hypothesized that fulvestrant binding to ER induces conformational changes leading to increased surface hydrophobicity, which ultimately results in degradation [113]. Despite the clinical use of fulvestrant the precise mode of action is not known.

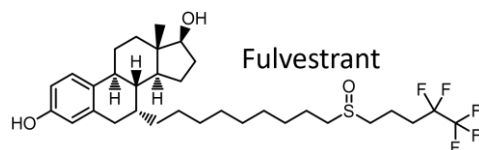


**Figure 12** Chemical structure of fulvestrant.

Together these discoveries highlight that primarily target-engaging molecules principally can be degraders through different mechanisms. The question of to which extent degraders or more generally molecular glues can be found in targeted libraries is still the subject of ongoing research and difficult to estimate. It appears to be important that the ligands feature either solvent exposed moieties or remodel the protein structurally.

---

### 3.2.3. Screening for molecular glues

Molecular glues have matured into a new modality in drug discovery. One of the key questions is how to discover molecular glues and which approach to take. Phenotypic screenings have been prevalent in drug discovery and repeatedly lead to the discovery of MGs [114]. They detect a functional outcome (e.g., cell death) but are generally agnostic towards the mode of action and glue-like mechanisms have been uncovered in follow-up validation. To identify degraders, phenotypic screens can be biased towards a degradative mode of action (e.g., for a dependence on a functional cullin E3 ligase machinery [95]). Alternatively, POI-degradation can be functionally coupled to an gain [115] or loss of a signal, if the POI is predetermined. CRISPR knockout-screens are a reoccurring method to subsequently identify the relevant E3 ligase components. Knockouts of relevant E3 ligase components block POI degradation, which can be coupled to a fluorescence or luminescence readout through e.g. POI\_eGFP or POI\_HiBiT fusions [100,107,110]. Thereby, the sgRNA libraries can focus on the ubiquitin-proteasome system or be genome-wide. An elegant approach where the E3 ligase is predetermined was recently used to discovery MGs in target agnostic manner [116]. Here, recruitment of a neo-target shielded the HiBiT-fused E3 ligase DCAF15 from self-ubiquitination and degradation which lead to a luminescence increase. If both POI and AP are predetermined assays that intentionally detect proximity such as HTRF- or AlphaLISA-based methods, can be employed. However, here a functional outcome of the induced interaction is not guaranteed. Taken together, the most appropriate approach depends on the POI and the desired functional outcome.

### 3.3. Bivalent functional tools

Bivalent functional (or hetero-bifunctional) tools consist of two ligands, in most cases of differing specificity, which are connected via a linker (Figure 13). Following this principle, they can be rationally designed given that ligands for the protein of interest and the accessory protein are available. In practice, empirical exploration using different POI and AP exit vectors as well as linkers differing in length is often required to find functionally active molecules. In the ternary complex hetero-bifunctionals engage both proteins via their respective ligands. Yet structural studies revealed that, beneficial PPIs (Figure 13 red lines), linker:protein (Figure 13 purple lines) and ligand contacts to the non-cognate binding partner often contribute to complex formation (positive cooperativity) [103,117,118].

Proteolysis targeting chimeras (PROTACs) might be the most prominent members of this type of compounds. They induce the degradation of their target protein, by recruiting an E3 ligase that ubiquitinates the target protein which is then recognized by the proteasome. This general principle of hetero-bifunctionals has not changed since the first proof of concept study [119] demonstrated that the ubiquitin-proteasome-system (UPS) can be hijacked. Since then, the classes of addressed accessory proteins were extended from E3 ligases to different protein classes. Next to PROTACs, lysosome-targeting chimeras (LYTACs) [120], autophagy-targeting chimeras (AUTACs) [121] and Hsp90-mediated targeting chimeras (HEMTACs) [122] have been described that induce degradation via lysosome and autophagy pathways, or likely via Hsp90-associated E3 ligases, respectively. Today several non-degrading bifunctional molecules are being explored that depending on the AP's function control different post-translational modifications such as de-ubiquitination [123,124], phosphorylation [125–127] and dephosphorylation [128–131] or acetylation [132,133]. Furthermore, first reports on bifunctional molecules that control the cellular localization of the targeted proteins are emerging [134].

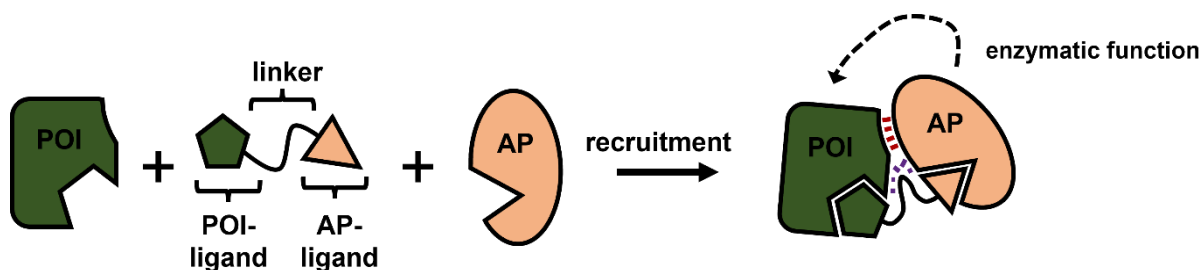


**Figure 13** Hetero-bifunctionals consist of a ligand for a protein of interest (POI) and of a ligand for an accessory protein (AP), which are connected by a linker. If the AP is an enzyme the POI can be modified. Red lines indicate non-cognate PPIs, purple lines indicate beneficial linker:protein contacts.

### 3.3.1. PROTACs

PROTACs are hetero-bifunctional molecules that comprise a POI ligand that is connected to an E3 ligase ligand via a linker. In favorable cases, PROTACs redirect the E3 ligase to induce POI (poly)ubiquitination and subsequent degradation of the target protein (Figure 14). The first proof of concept for a fully synthetic PROTAC to hijack the ubiquitin-proteasome system *in vitro* was demonstrated in 2001 by linking a small molecule ligand of the E3 ligase TrCP to a phospho-peptide recognition motif of the peptidase MetAP-2, to induce ubiquitination and degradation of Met-AP2 in extracts from unfertilized *Xenopus laevis* eggs [119]. Three years later, the first cell-penetrating PROTACs were reported based on the peptide from hypoxia-inducible factor 1 subunit- $\alpha$  (HIF1 $\alpha$ ) that bound the E3 ligase von Hippel–Lindau tumour suppressor (VHL) [135]. Notably, this publication also marked the first FKBP12-PROTAC although for the FKBP12<sup>F36V</sup> mutant. The first non-peptidic small molecule PROTAC was designed in 2008. It was based on nutlin-3a, a ligand for the E3 ligase mouse double minute 2 (MDM2) and degraded the androgen receptor [136]. Albeit the human proteome features approximately 600 E3 ligases, only a handful can be currently addressed by synthetic ligands and used in PROTACs. However, the E3 ligase ligand toolbox is steadily expanding [137]. CBRN and VHL ligands are the front runners in the field and most frequently used for PROTAC development as they combine strong specific binding affinities with an acceptable physiochemical profile [137,138].

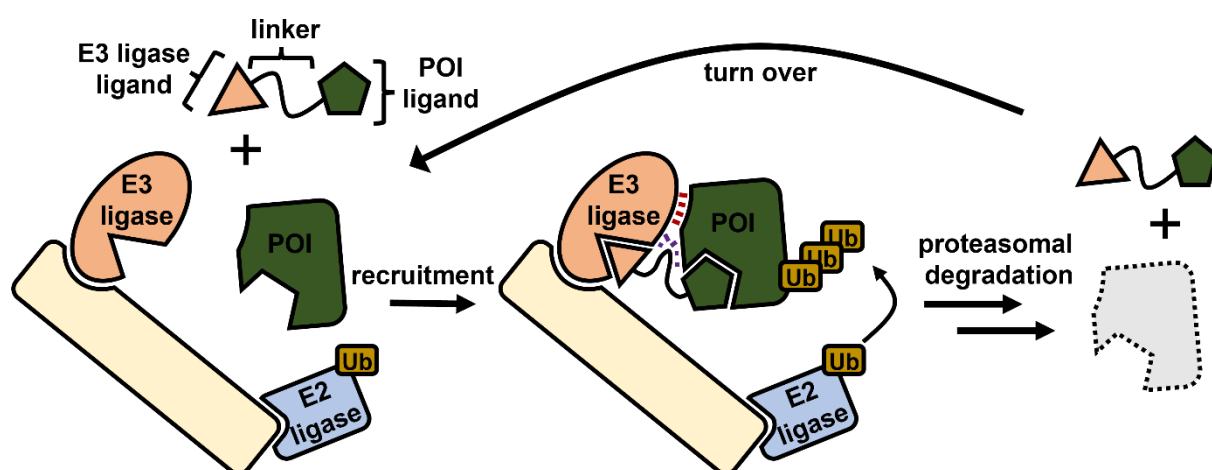


**Figure 14** PROTACs mode of action. PROTACs recruit the POI to E3 ligase complexes, in which the POI is polyubiquitinated and in the following degraded by the proteasome. The PROTAC is then released and recycled.

PROTACs can have several advantages over traditional occupancy-driven drugs. (i) They act through a catalytic event-driven mechanism to degrade more than one target per molecule leading to sub-stoichiometric efficacy [139]. (ii) A PROTAC's affinity for the POI and



---

degradation efficacy do not necessarily correlate [140], which is a double-edged sword: high affinities do not guarantee an active PROTAC, but on the other side this also implies that a low affinity PROTACs can induce rapid degradation. Indeed, this was demonstrated for PROTAC featuring a promiscuous kinase warhead that displayed a low binary affinity for p38 $\alpha$  ( $K_D = 5.3 \mu\text{M}$ ) but induced rapid degradation thereof [140]. (iii) A loss in binary affinity of the ligand upon integration into a PROTAC scaffold [117] or during PROTAC optimization [141] can be compensated and lead to functionally active degraders. (iv) PROTACs can in principle confer tissue specificity depending on the expression level of the engaged E3 ligase. This was first demonstrated by a VHL-based BCL-XL PROTAC which spared BCL-XL degradation in cells that poorly expressed VHL [65]. The development of ligands for E3 ligases with a more restricted expression profile compared to VHL or CBRN might lead to a more common translation of this principle into practice. (v) A PROTAC's degradation selectivity can substantially exceed the parent ligand selectivity [105,142] likely due to the importance of ternary complex stability [103]. One of the most important prospects of targeted protein degradation is that it can in principle enable a fundamentally different pharmacology over traditional ligands by addressing all protein functions via target depletion. Hence, ligands of functionally silent binding pockets can be turned into functionally active PROTACs. While this is a long-standing hypothesis, examples have been rare [117,143–145] most likely since high-quality ligands are usually not developed for non-functional binding pockets. Due to the size and high molecular weight of PROTACs they usually occupy a space of poor physiochemical properties beyond Lipinski's rule of five [146] and are not likely to be bioavailable. Yet, oral bioavailability is possible and used as a route of administration in clinical trials [147]. Additionally, the bifunctional nature of PROTACs is accompanied by the hook effect. At high concentrations bifunctional molecules can saturate the binding sites of the POI and AP in binary complexes, which consequently impairs efficacy as the required ternary complexes is not formed.

---

### 3.3.2. FKBP PROTACs

Chemical dimerizers for FKBP12 or its FKBP12<sup>F36V</sup> mutant have been extensively studied in chemical biology [43] and the proteins were used as model proteins to demonstrate the proof of principle for VHL- [135], CBRN- [148], DCAF11- [149], and DCAF16-based [150] PROTACs. Furthermore, bumped FKBP12 ligands containing chloroalkanes for the hole-modified FKBP12<sup>F36V</sup> mutant were used to recruit HaloTag-fused E3 ligases to FKBP12<sup>F36V</sup>\_eGFP reporter constructs in order to access the E3 ligases for small molecule induced protein degradation [151]. FKBP12 also served as a model protein to demonstrate the efficacy and practicality of global PROTAC-induced protein knockdown (sparing the brain if administered i.p.) in mice and rats as well as in larger mammals (Bama pigs and rhesus monkeys) [152]. Additionally, chemical–genetic model systems to control the levels of target\_FKBP12<sup>F36V</sup> fusion proteins with PROTACs based on bumped FKBP12 ligands were established in 2018 [153].

Although FKBP12 and the larger FKBP51 and FKBP52 are homologs, none of the studies on FKBP12 reported induced degradation of FKBP51 or FKBP52. In 2016, the Hausch lab started the generation of FKBP PROTAC candidates to address the lack of FKBP51 degrading tools. The aim was to study FKBP51's diverse functions and overcome limitations of traditional occupancy driven pharmacology. Therefore, Dr. Tianqi Mao assembled a library of 60 PROTAC candidates during her dissertation [154].

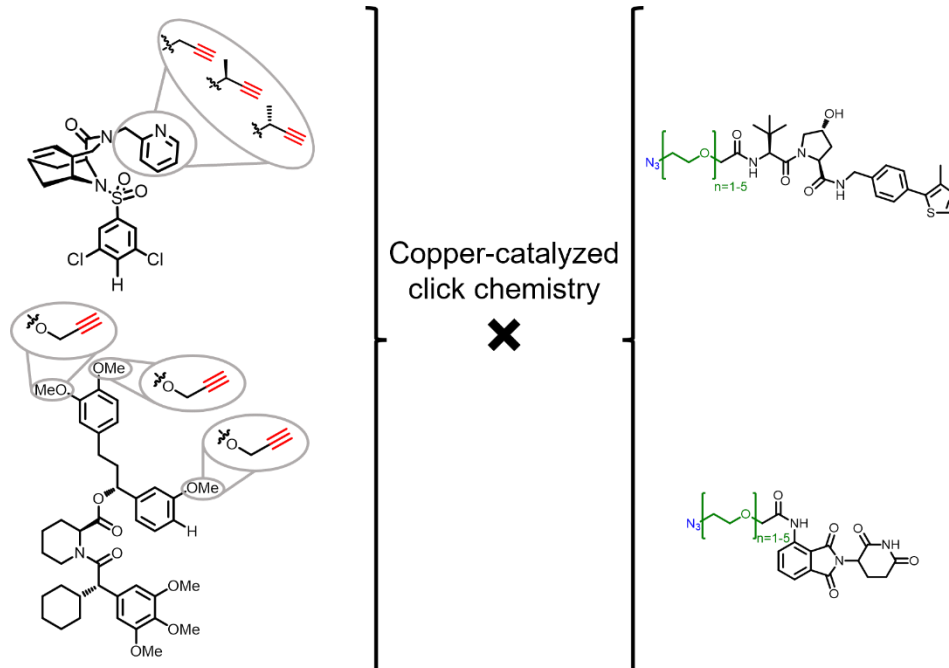


**Figure 15** FKBP PROTAC candidate library synthesized by Tianqi Mao during her PhD studies [154]. Alkyne-functionalized FKBP ligands (left) are combinatorially connected to azide-functionalized E3 ligase ligand building blocks (right) via copper-catalysed click chemistry.

Initial testing and characterization by Dr. Andreas Hähle during his dissertation yielded MTQ202 (or 10a4 in this work) as the only active FKBP51 PROTAC [155].

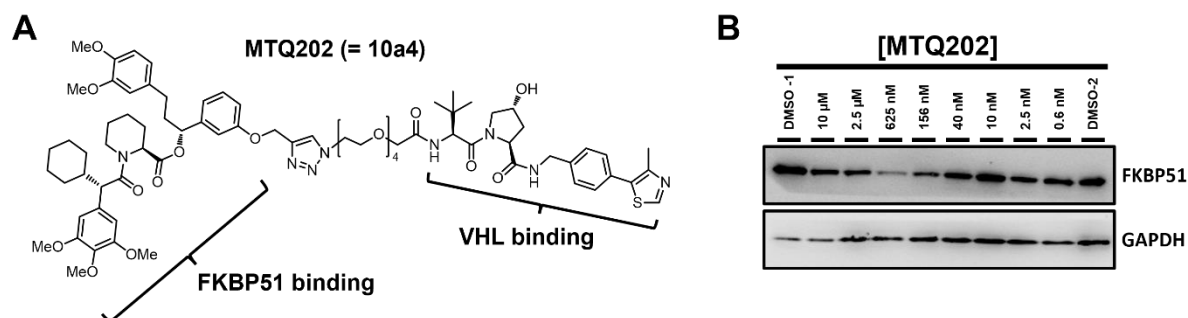


**Figure 16** Chemical structure of **A** MTQ202 [154] and **B** Western blot of MTQ202-mediated FKBP51 degradation in HEK293T cells after 24 hour treatment.

However, MTQ202 (Figure 16A) displayed only moderate activity and a strong hook effect (Figure 16B) and thus fell short as useful tool compound.

---

## 4. Results and Discussion

---

To support the development of FKBP-directed drugs, I first established a panel of assays to address key biochemical and molecular biological aspects of FKBP.

### 4.1. HTRF-binding assay for FKBP ligands

Binding affinities are commonly used to evaluate ligands and rank them in order of their binding strength. This in turn can be used to derive structure-affinity-relationships that build the foundation for subsequent optimization. Nowadays, FKBP12 ligands with picomolar binding affinities can be routinely synthesized [51,53]. The precise determination of sub-nanomolar  $K_D$  values, however, is challenging. Up to now, competitive fluorescence polarization (FP) assays have been used to measure binding affinities of FKBP ligands [156]. However, these assays utilize tracer concentrations that are below the protein concentration. For ultra-high affinity ligands, this results in an almost full tracer displacement as soon as the ligand concentration exceeds the protein concentration. In turn, this results in very steep tracer displacement curve. Small errors in the protein concentration, thereby directly translate to a shift in the tracer displacement curve and hence to an error in the determined ligand  $K_D$  value. To enable precise affinity determination, especially for high-affinity ligands, an orthogonal competitive homogeneous time-resolved fluorescence (HTRF) FKBP-ligand binding assay was developed (Figure 17). Competitive HTRF-binding assays have the advantage, that very high tracer concentrations are tolerated, as the unbound tracer does not contribute to the measured HTRF signal.

Additionally, the high tracer concentrations result in less steep tracer displacement curves with more data points in the dynamic range for ultra-high affinity ligands. These curves can robustly be fit and enable a precise  $K_D$  determination.

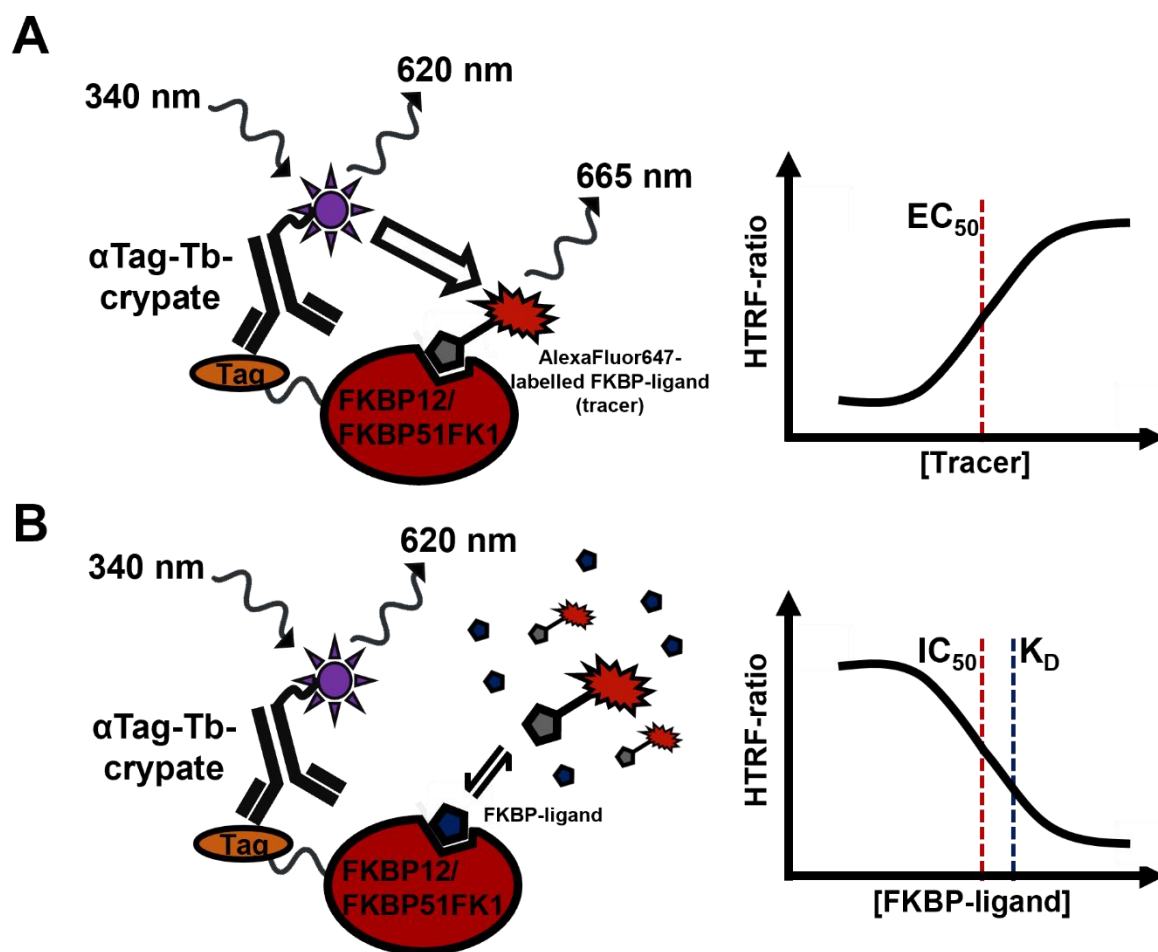


**Figure 17** A Scheme of a homogeneous time-resolved fluorescence (HTRF) assay that enables the precise affinity determination of FKBP ligands. **A** In presence of tagged FKBP, the terbium (Tb) cryptate-labelled  $\alpha$ tag antibody comes in proximity to the AlexaFluor647 (A647) labelled tracer. Upon excitation (340 nm) the donor (Tb cryptate) will transfer energy to an acceptor fluorophore (A647) in proximity. The donor fluorescence is also measured at 620 nm, which allows calculation of the HTRF ratio (665 nm / 620 nm). **B** Increasing concentrations of FKBP ligands competitively displace the tracer resulting in a decreasing HTRF ratio. The binding affinities of the ligands can subsequently be determined by fitting the displacement curves.

The general assay setup consists of a tagged FKBP, an AlexaFluor647 (A647)-labelled FKBP binding tracer and an anti-tag-antibody which is labelled with Terbium cryptate (Tb cryptate) (Figure 17A). In presence of all components, both the tracer and the antibody bind the tagged FKBP and upon excitation of the Tb cryptate at 340 nm, energy can be transferred to the acceptor fluorophore (A647), which subsequently emits light at 665 nm. The donor (Tb cryptate) fluorescence is also measured at 620 nm which is used for normalization of the acceptor signal to yield the HTRF ratio. Changes in the HTRF ratio are indicative for changes of proximity between the tracer and the Tb cryptate antibody. Upon addition of increasing concentrations of unlabeled FKBP-ligands, the tracer is dose-dependently displaced which results in a dose-dependent decrease of the HTRF ratio (Figure 17B). The generated tracer

displacement curves can be used to determine binding affinities of the ligand through displacement curve fitting [157].

#### 4.1.1. HTRF-binding assay development

In a first step, AlexaFluor647 coupled tracers (Figure 18) were assembled by connecting alkyne-functionalized FKBP ligands with commercially available azide-functionalized AlexaFluor647 through copper-catalyzed click chemistry.

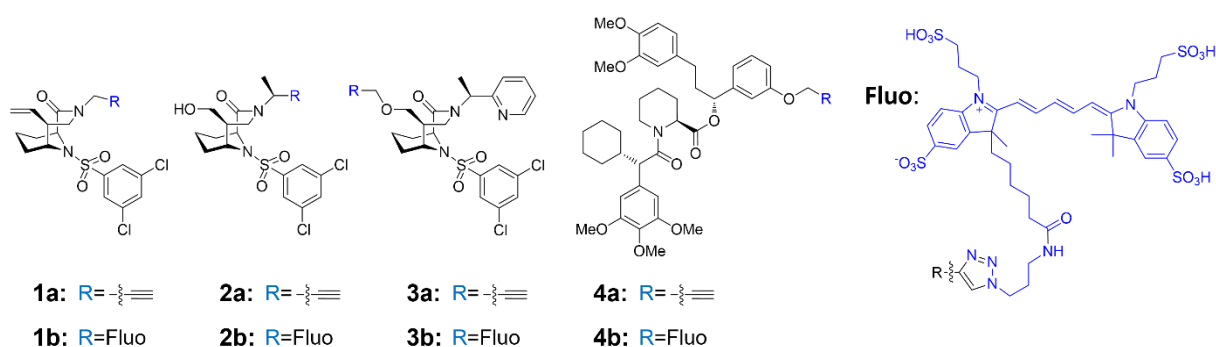


**Figure 18** Chemical structures of HTRF tracers and unclicked alkyne building blocks. Tracers were synthesized by Dr. Michael Walz (1b (MWa146); 4b (MWa144)) and Johannes Dreizler (2b (JKD649); 3b (JKD645)).

Tracer affinities for FKBP12 as well as FKBP51 were determined by a fluorescence polarization binding assay. Therefore, the proteins were titrated at a constant tracer concentration and the fluorescence polarization was measured. The  $K_D$  values were subsequently determined by curve fitting [157] and are summarised in Table 1.

**Table 1** Binding affinities of HTRF-tracers for His-FKBP12 and His-FKBP51<sup>FK1</sup>. Binding constants  $\pm$  standard deviation from three replicates. The binding affinities were determined by fluorescence polarization binding curves (Figure 66 and Figure 67).

Tracer	$K_D(\text{FKBP12}) / \text{nM}$	$K_D(\text{FKBP51}^{\text{FK1}}) / \text{nM}$
1b	$0.79 \pm 0.10$	$37.69 \pm 4.28$
2b	$0.18 \pm 0.04$	$2.62 \pm 0.27$
3b	$0.21 \pm 0.04$	$1.63 \pm 0.20$
4b	$33.99 \pm 5.53$	$2.55 \pm 0.39$

All bicyclic tracers 1b-3b bound with similar affinities to FKBP12, but tracer 1b bound substantially weaker to FKBP51<sup>FK1</sup>. Tracer 4b, which is based on the SAFit-scaffold displayed

good affinity for FKBP51<sup>FK1</sup> but bound weaker to FKBP12, which is in accordance with the selectivity profile of SAFit-like ligands.

In pilot experiments, different assay setups were tested. Therefore, purified proteins with His6- or Flag-tags were tested in combination with different tracers and the respective anti-tag Tb cryptate antibodies for their suitability to yield HTRF signals.

Towards this aim, Flag-FKBP51-His6 (N-terminal Flag-tag) as well as His6-FKBP51-Flag and His6-Tev-FKBP12-Flag (C-terminal Flag-tag) were purified by immobilized metal affinity chromatography (IMAC) and in case of both FKBP51 constructs by subsequent size exclusion chromatography (SEC).

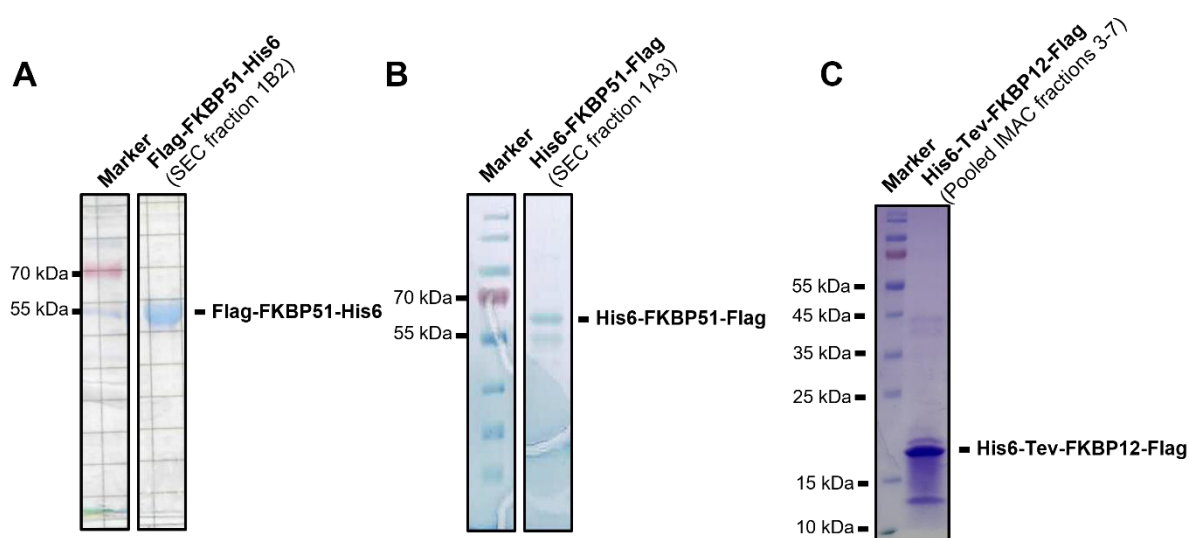


**Figure 19** SDS Page and Coomassie stain analysis of purified Flag-tagged FKBP51s. **A** Gel analysis of concentrated SEC-fraction 1B2 of Flag-FKBP51-His6. SEC chromatogram and gel analysis of all collected SEC fractions are depicted in Figure 68 and Figure 69. **B** SDS Page and Coomassie stain analysis of concentrated SEC-fraction 1A3 of His6-FKBP51-Flag. SEC chromatogram and gel analysis of all collected SEC fractions are depicted in Figure 70 and Figure 71. **C** SDS Page and Coomassie stain analysis of pooled IMAC fractions after purification of His6-Tev-FKBP12-Flag. All collected IMAC fractions are depicted in Figure 72. SDS Page and Coomassie stain analysis pooled IMAC fractions after purification of His6-Tev-FKBP12-Flag was performed by Wisley Oki Sugiarto under my supervision. Marker: PageRuler™ Prestained Protein Ladder (#26616).

After purification, the protein concentration was determined by spectrophotometric analysis at 280 nm. Total amounts of 26 mg Flag-FKBP51-His6, 7.4 mg His6-FKBP51-Flag and 36.4 mg His6-Tev-FKBP12-Flag were obtained. In the following, the integrity of the FK506-binding pockets and binding-active protein concentrations were determined by active-site titrations (Figure 20).

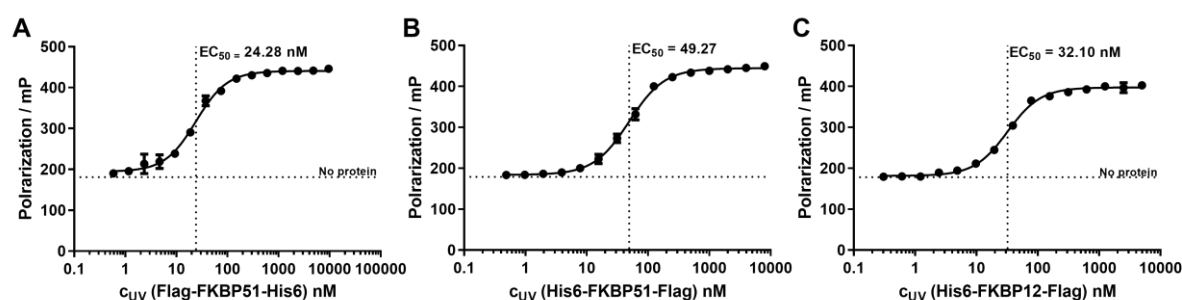


**Figure 20** Active site titrations of **A** Flag-FKBP51-His6, **B** His6-FKBP51-Flag and **C** His6-Tev-FKBP12-Flag. Individual data points and error bars represent mean and standard deviation of three replicates. The proteins were titrated at a constant concentration (50 nM) of the high affinity FKBP tracer MTQ238. The fluorescence polarization was measured using the following spectral adjustments: Ex.: 535 nm, Em.: 590 nm. EC<sub>50</sub> values were derived from a four-parameter IC<sub>50</sub> fit.

The active-site titrations demonstrated that the Flag-tagged proteins are binding-active and yielded active-site concentrations of 126.7  $\mu$ M for Flag-FKBP51-His6, 35  $\mu$ M for His6-FKBP51-Flag and 460  $\mu$ M for His6-Tev-FKBP12-Flag.

Next, the suitability to yield HTRF signals with an anti-Flag-Tb cryptate antibody was tested for Flag-FKBP51-His6 and His6-FKBP51-Flag as well as His6-Tev-FKBP12-Flag constructs in combination with the tracer 1b and 4b, respectively (Figure 21). The tracers 2b and 3b were not yet synthesized at that time.

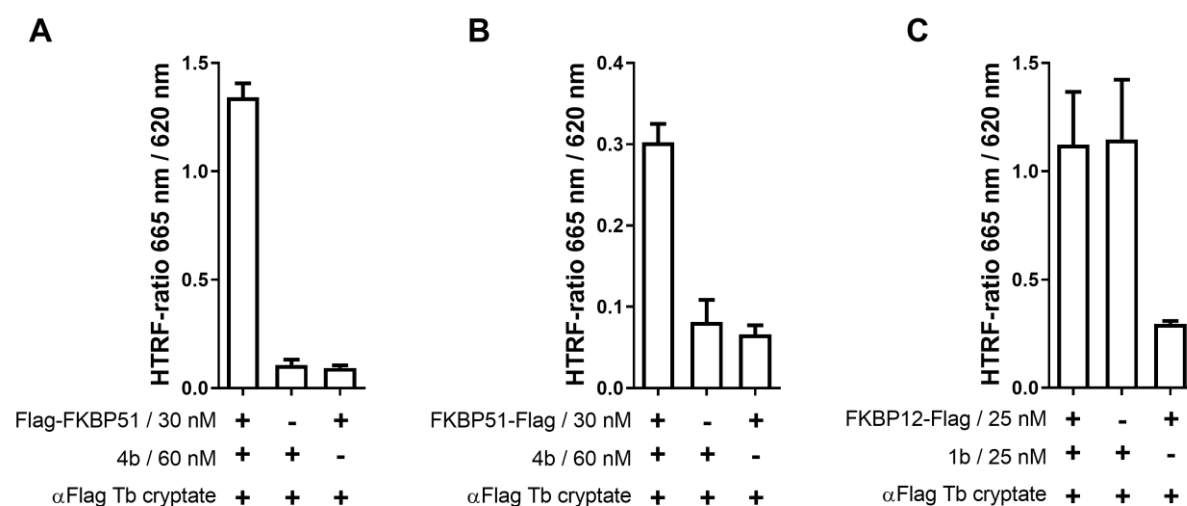


**Figure 21** Combinations of **A** 4b:Flag-FKBP51-His6 and **B** 4b: His6-FKBP51-Flag but not **C** 1b:His6-Tev-FKBP12-Flag yielded HTRF signals in presence of an anti-Flag-Tb cryptate antibody (concentration 0.5% (v/v)) above tracer background. Individual data points represent mean and standard deviation of three replicates. Fluorescence values at 665 nm and 620 nm are depicted in Figure 73.

Flag-tagged FKBP12, did not yield a HTRF signal in combination with tracer 1b. On the other hand, the Flag-tagged FKBP51 constructs, yielded HTRF signals in combination with tracer 4b.



The assay setup utilizing Flag-tagged proteins was not further pursued in favor of the setup using His6-tagged proteins and an anti-His6-Tb cryptate antibody. However, the purified Flag-tagged FKBP51 proteins were used in collaboration with the Gassen lab in pull down experiments to study the role of FKBP51 in autophagy [158].

Additionally, a second HTRF assay setup with (only) His-tagged FKBP12 and FKBP51<sup>FK1</sup>, in combination with the high affinity tracers (2b for FKBP12 and 3b for FKBP51<sup>FK1</sup>) and an anti-His6 Tb cryptate antibody, was tested for their suitability to yield HTRF signals. Therefore, the tracer was titrated at different FKBP concentrations and constant amounts of Tb cryptate-labelled anti-His6 antibody (Figure 22).

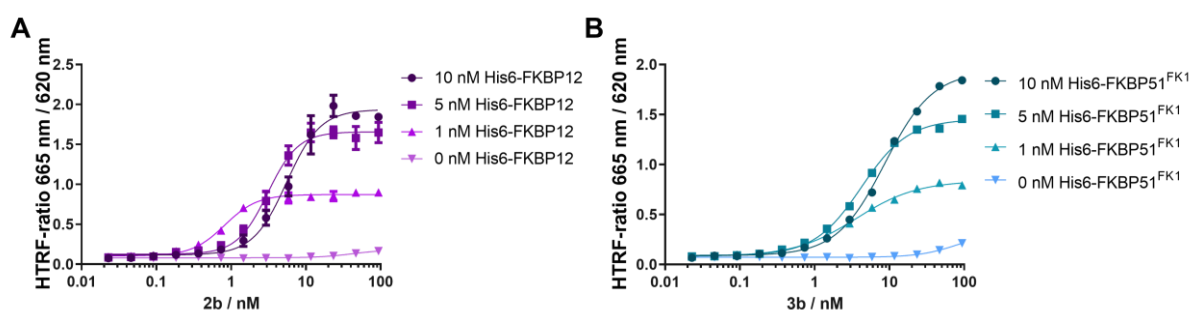


**Figure 22** Combinations of **A** 2b:His6-FKBP12 and **B** 3b:His6-FKBP51<sup>FK1</sup> yielded dose-responsive HTRF signals in presence an  $\alpha$ His6-Tb cryptate antibody (concentration 0.25% (v/v)). Individual data points represent mean and standard deviation of three replicates.

Both His6-protein:tracer combinations yielded both tracer- and protein-dose-dependent HTRF ratios and were further pursued. The upper plateau of the tracer binding curves indicates full saturation of the proteins with their respective tracer. A concentration of 5 nM protein was chosen to explore a competitive assay setup (Figure 23) as this concentration combined a good assay window and relatively low protein concentrations.

To demonstrate the assay's suitability to determine binding affinities of FKBP ligands the well characterized ligand 18<sup>(S-Me)</sup> was titrated at constant protein and antibody concentrations and at different tracer concentrations (Figure 23).

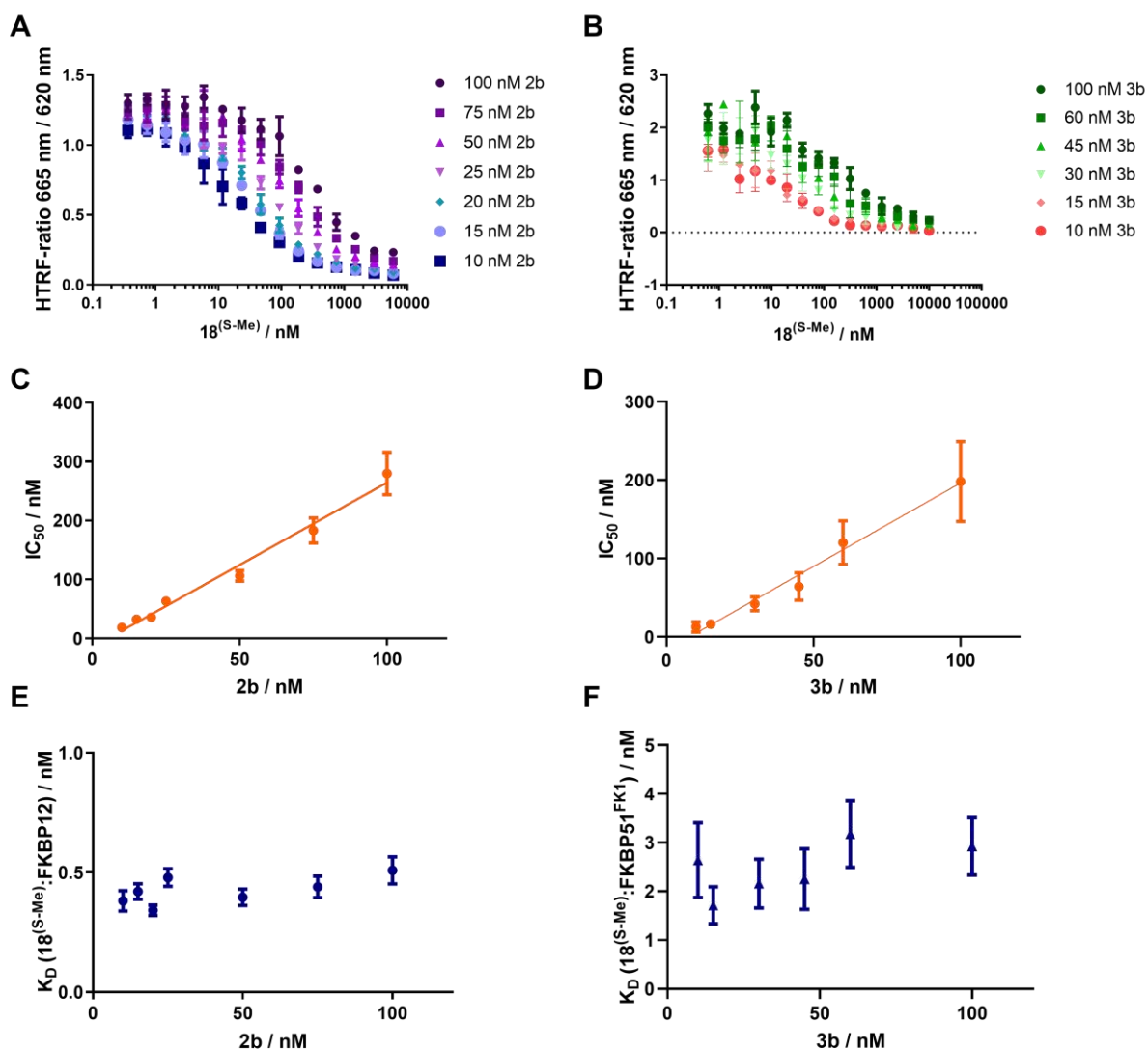


**Figure 23** Competitive HTRF binding assay for the FKBP ligand  $18^{(S-Me)}$  and **A** FKBP12 or **B** FKBP51<sup>FK1</sup>. Increasing amounts of the pan-selective FKBP ligand  $18^{(S-Me)}$  were titrated at the indicated tracer concentrations in presence of constant amounts of the respective FKBP (5 nM) and  $\alpha$ His6-Tb cryptate antibody (concentration 0.25% (v/v)). HTRF ratios were calculated after fluorescence measurements using the following spectral parameters: Ex.: 340 nm; Em: 620 nm and Ex.: 340 nm; Em: 665 nm; lag time: 150  $\mu$ s, integration time: 500  $\mu$ s. Individual points and error bars represent mean and standard deviation of three replicates.  $IC_{50}$  values and standard error for competitive **C** FKBP12 and **D** FKBP51<sup>FK1</sup> binding were determined by a four-parameter  $IC_{50}$  fit.  $K_D$  values and standard error for  $18^{(S-Me)}$  and **E** FKBP12 or **F** FKBP51<sup>FK1</sup> binding were determined by a  $K_D$  fit [157]. The competitive binding experiment for FKBP51<sup>FK1</sup> was performed by Wisely Oki Sugiarto under my supervision.

The generated displacement curves (Figure 23A&B) can be used to derive the  $IC_{50}$  values (Figure 23, C&D) by four-parameter  $IC_{50}$  fitting.

$IC_{50}$  values depend on the tracer concentration. The theoretical linear dependence of measured  $IC_{50}$  values and given apparent  $K_i$  values (or more generally apparent  $K_D$  values) of a competitive inhibitor was originally reported in context of enzyme inhibition and classical Michaelis-Menten kinetics [159].

---

Cheng-Prusoff equation:

$$IC_{50} = K_i * \left(1 + \frac{S}{K_m}\right) \text{ [159]}$$

$K_i$ : Inhibitor dissociation constant;  $S$ : Substrate concentration,  $K_m$ : Michaelis constant of the substrate ( $S$ )

The Cheng-Prusoff equation can be adapted to competitive binding experiments and used to approximate apparent  $K_i$  values of the tracer and the competitive ligand [160]:

$$IC_{50} = K_i * \left(1 + \frac{T}{K_D}\right) \text{ [160]}$$

$T$ : tracer concentration;  $K_i$ : Inhibitor dissociation constant;  $K_D$ : Tracer dissociation constant.  $K_i$ ,  $K_D$  defined as the concentration of the ligand and tracer respectively, that occupies 50% of binding sites in absence of competition.

The equation describes a linear dependency between the tracer concentration and the obtained  $IC_{50}$  values, if the following assumptions for the underlying equation are met: (i) the system is at equilibrium; (ii) tracer and ligand compete for a single binding site; (iii) binding is reversible and not cooperative and (iv) there is no significant depletion of either ligand or tracer, i.e. the free ligand or tracer concentration can be approximated by the total ligand and tracer concentrations respectively. Given the high affinities of both the tracer and the ligands in combination with a protein concentration  $> K_D$  this last assumption is not satisfied.

In this system, however, the protein concentration is known. The  $K_D$  values (Figure 23E&F) were determined by using a  $K_D$ -fit equation directly derived from the mass law [157] for the compound 18<sup>(S-Me)</sup> at every tracer concentration. The derived  $K_D$  values across different tracer concentration for both proteins are constant and in good agreement with the literature values derived from competitive FP-binding assays of 0.29 nM and 2.6 nM for FKBP12 and FKBP51<sup>FK1</sup>, respectively [51]. This demonstrates the usefulness of the orthogonal assay. Additionally, these experiments show that very high tracer concentrations ( $> 50$  nM) can be utilized. This will be useful to precisely determine the affinity of ultra-high affinity FKBP ligands (e.g.,  $K_D < 100$  pM). Higher tracer concentrations lead to less steep curves (see Figure 23A&B) with many points in the dynamic range that can be robustly fitted. In the FP binding assay, where tracer concentrations have to be below the protein concentrations, the displacement curves for ultra-high affinity ligands in the FKBP ligand would be very steep, with few points in the dynamic

range. In this case, the competitive HTRF binding assay can be employed to enable a more precise affinity determination.

#### 4.2. NanoBRET-based intracellular FKBP ligand target engagement assay

FKBP occupancy in living cells is thought to be necessary for FKBP ligands to interfere with the endogenous functions of the most prominent cytosolic FKBP12, FKBP12.6, FKBP51 and FKBP52. To profile the target engagement and selectivity of FKBP ligands, a NanoBRET target engagement assay was developed for these FKBP.

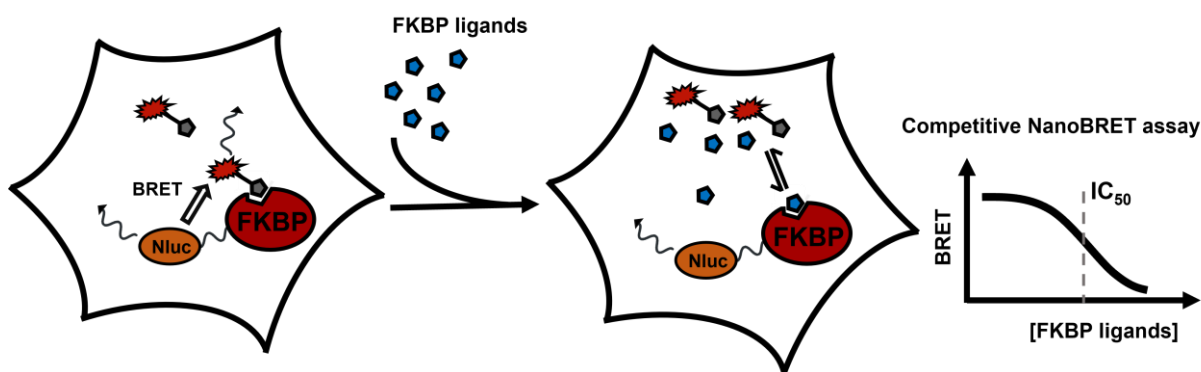


**Figure 24** NanoBRET-based FKBP ligand target engagement assay scheme. HEK293T cells stably expressing FKBP-Nluc fusion proteins generate a BRET signal in presence of the NanoBRET tracer. Addition of FKBP ligands leads to dose-dependent displacement of the tracer which results in decreasing BRET signals.  $IC_{50}$  values can be derived subsequently through four-parameter-fitting of the displacement curves and are indicative for the intracellular target engagement.

Monika T. Gnatzy and Angela Kühn worked under my supervision in their respective master and bachelor thesis on the development of FKBP-NanoBRET target engagement assay. Both contributed substantially to this project, which ultimately led to a publication in ChemBioChem with the title ‘Development of NanoBRET-Binding Assays for FKBP-Ligand Profiling in Living Cells’ by us [162]. The publication describes the development of a NanoBRET-based target engagement assay for FKBP ligands and for the most prominent FKBP51, 12.6, 51 and 52. The assay was used to demonstrate (i) the selectivity of SAFit-type ligands for FKBP51 over FKBP52 in cells and (ii) revealed a substantial offset in intracellular target engagement activity for this ligand class compared to smaller bicyclic ligands or macrocyclic natural products. However, the initially developed NanoBRET assay for FKBP51 showed – compared to the other FKBP51 – a very small assay window (approx. two-fold over background) and hence lacked robustness. While a small group of widely used FKBP ligands was profiled in the study, broader FKBP ligand profiling was warranted to guide ligand optimization. Therefore, I optimized the FKBP51 NanoBRET assay and established a high-throughput protocol.

#### 4.2.1. Optimization of the FKBP51-engagement assay

To increase the assay window and enable a higher robustness of the FKBP51 NanoBRET assay, the FK1 domain of FKBP51 was directly fused to a nanoluciferase (Nluc).

Both N- and C-terminal FKBP51<sup>FK1</sup>-Nluc tagged expression vectors were generated and tested for their suitability to induce BRET signals in pilot experiments. Therefore, HEK293T cells were transiently transfected with the respective expression constructs and the NanoBRET-tracer was titrated and compared to the published cell line stably expressing full-length FKBP51-Nluc (Figure 25A).

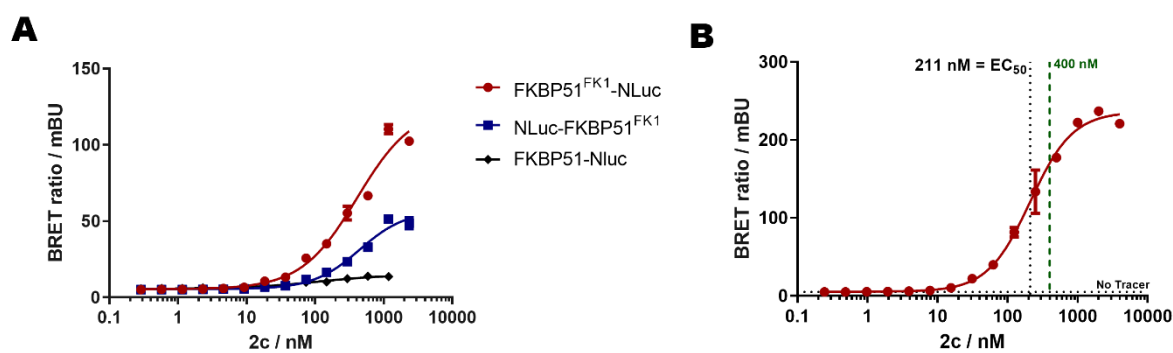


**Figure 25** Overview of tracer titration curves for different FKBP51-Nluc fusion constructs. **A** Tracer titration experiments in cells transiently expressing FKBP51<sup>FK1</sup>-Nluc and Nluc-FKBP51<sup>FK1</sup> or stably expressing FKBP51-Nluc fusion proteins. **B** Tracer titration experiments in cells stably expressing FKBP51<sup>FK1</sup>-Nluc fusion proteins. Individual data points represent mean and standard deviation of three replicates. Tracer titrations in A were performed by Monika T. Gnatzy and in case of the stable cell line in A, the graph was taken from [162].

Both the N- and C-terminally Nluc-tagged FKBP51<sup>FK1</sup> generated dose-dependent BRET signals and featured a drastically larger assay window compared to the FKBP51-Nluc construct (Figure 25A). As transiently transfected constructs were found to show substantial batch-to-batch variations, a stable FKBP51<sup>FK1</sup>-Nluc HEK293T cell line was created. The HEK293T cell line stably expressing FKBP51<sup>FK1</sup>-Nluc fusion proteins was generated by Monika T. Gnatzy. In a similar manner to the pilot experiments, tracer titration experiments in the stable FKBP51<sup>FK1</sup>-Nluc cell line showed dose-dependent BRET signals. Ultimately, a tracer (2c [162]) concentration of 400 nM slightly above the EC<sub>50</sub> of approx. 200 nM was chosen for competitive FKBP ligand profiling (Figure 25B).

#### 4.2.2. Development towards a semi-automatic high throughput assay and cost reduction

The competitive NanoBRET assays described in the publication [162] were performed by generating dilution series in DMSO starting with a 1000-fold ligand concentration. These DMSO dilution stocks were subsequently used to generate a 2-fold dilutions in Opti-MEM (0.2% DMSO), which were then transferred to the assay plate. However, all steps were performed by hand, which prevented the required higher throughput. To enable a higher throughput, the protocol was amended towards a semi-automatic assay in which the laborious steps (dilution series at 100-fold concentration, generation of two-fold dilutions (2% DMSO) and the transfer to the assay plates) were performed by a robot. Thomas Stipp contributed to this as a student under my supervision in an internship.

In a first step, it was confirmed that a higher final DMSO concentration (1% vs. 0.1% in [162]) is tolerated in the cellular assay and resulted in a similar  $IC_{50}$  for SAFit2. Indeed, the same  $IC_{50}$  value for SAFit2 – a well-established control compound – was obtained at both DMSO concentrations (Figure 74). Afterwards, the robot protocol was tested using the well-established control compounds JK384 and SAFit2. Therefore, six independent replicates of the dilution series (100-fold) and subsequent predilutions in Opti-MEM (2-fold) were performed and transferred to three distinct assay plates by the robot to generate triplicates of each replicate. Subsequently, the two-fold cell tracer mix was added by hand and the BRET signals were measured after 2 hours incubation. Using the triplicates of each dilution series, the  $IC_{50}$  values and standard errors were determined with a four-parameter  $IC_{50}$  fit (Table 2).

**Table 2** FKBP51<sup>FK1</sup>-NanoBRET target engagement assays for SAFit2 and JK384.  $IC_{50}$  values and standard errors represents three biological replicates. The experiment was performed by Thomas Stipp under my supervision.

Replicate no.	SAFit2 $IC_{50} \pm$ error / nM	JK384 $IC_{50} \pm$ error / nM
1	451 $\pm$ 197	174 $\pm$ 24
2	615 $\pm$ 139	147 $\pm$ 22
3	688 $\pm$ 137	143 $\pm$ 16
4	520 $\pm$ 103	122 $\pm$ 14
5	638 $\pm$ 110	149 $\pm$ 18
6	547 $\pm$ 125	210 $\pm$ 20

The  $IC_{50}$  values of the replicates for SAFit2 and JK384 were in agreement within each other and to the literature values of approx. 200 nM and 180 nM, respectively, for full-length

FKBP51-Nluc NanoBRET assays [162]. The three-fold higher  $IC_{50}$  values for SAFit2 compared to the literature can likely be attributed to slightly inaccurate predilution combined with normal two- to three-fold inter-assay deviations.

NanoBRET assays are generally pricy due to the high costs of reagents. To decrease the cost per assay point, an alternative substrate (26dl [163], Figure 26) and extracellular Nanoluciferase inhibitor (compound 43, [164]) were explored.

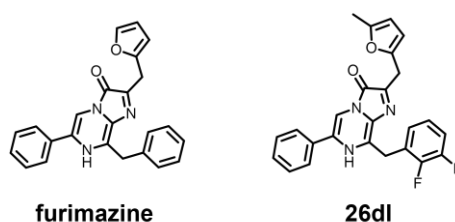


**Figure 26** Chemical structures of the Nluc substrates furimazine (sold by Promega) and the furimazine derivate 26dl [163].

In initial experiments without the extracellular Nanoluciferase inhibitor sold by Promega, it became evident that the BRET signal (assay window) drops significantly depending on the cell batch in absence of the inhibitor (data not shown). Unfortunately, the Promega Nluc-inhibitor is not sold separately. Thus, a literature known cell-impermeable Nluc inhibitor (compound 43, [164]) was re-synthesized (RCD339, Figure 27A) by Robin Deutscher and tested subsequently (Figure 27).

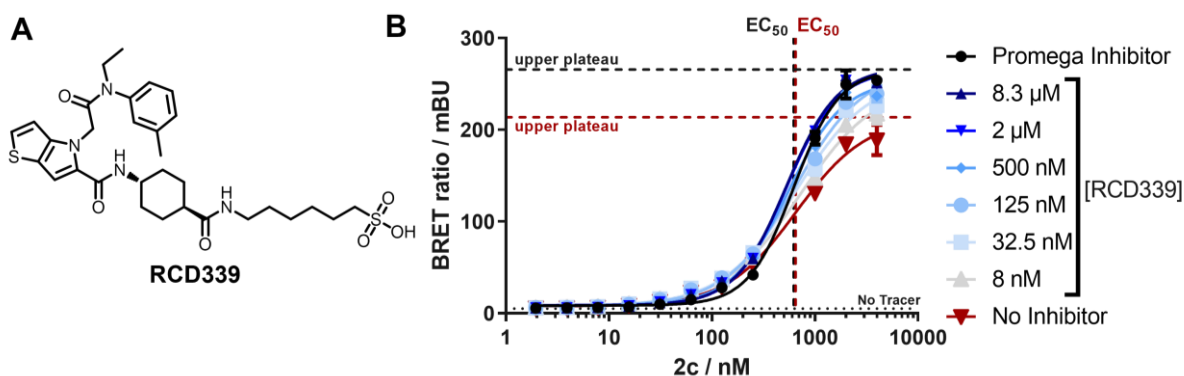


**Figure 27** Tracer titrations in presence or absence of extracellular Nluc inhibitor. **A** Chemical structure of the cell-impermeable Nanoluciferase inhibitor RCD339 (= compound 43 [164]). **B** The extracellular Nluc inhibitor elevates the assay window without changing the half maximal effective concentration. Experiment performed with HEK293T cells stably expressing FKBP51<sup>FKL</sup>-Nluc fusion proteins. Donor and acceptor signals were measured after addition of Luciferase substrate ((26dl [163]), final concentration 6  $\mu$ M) in presence of the indicated extracellular Nluc inhibitors.

The assay window dropped in absence of any extracellular Nluc inhibitor (Figure 27B, horizontal red dashed line) compared to the assay window in presence of the Promega inhibitor (Figure 27B, horizontal black dashed line). However, the  $EC_{50}$  values remained unaffected

---

(Figure 27B, vertical dashed lines). The synthesized cell-impermeable Nluc Inhibitor (RCD339) fully rescued the effect at concentrations  $> 2 \mu\text{M}$  and was consequently used in subsequent NanoBRET assays at a final concentration of  $2.5 \mu\text{M}$  to stabilize the BRET signal.



### 4.2.3. Characterization of FKBP ligands by competitive NanoBRET target-engagement assays

The established semi-automated NanoBRET target engagement assay was used to profile 189 and 148 in-house FKBP ligands of different chemical classes for intracellular FKBP51<sup>FK1</sup> and FKBP12 occupancy, respectively.

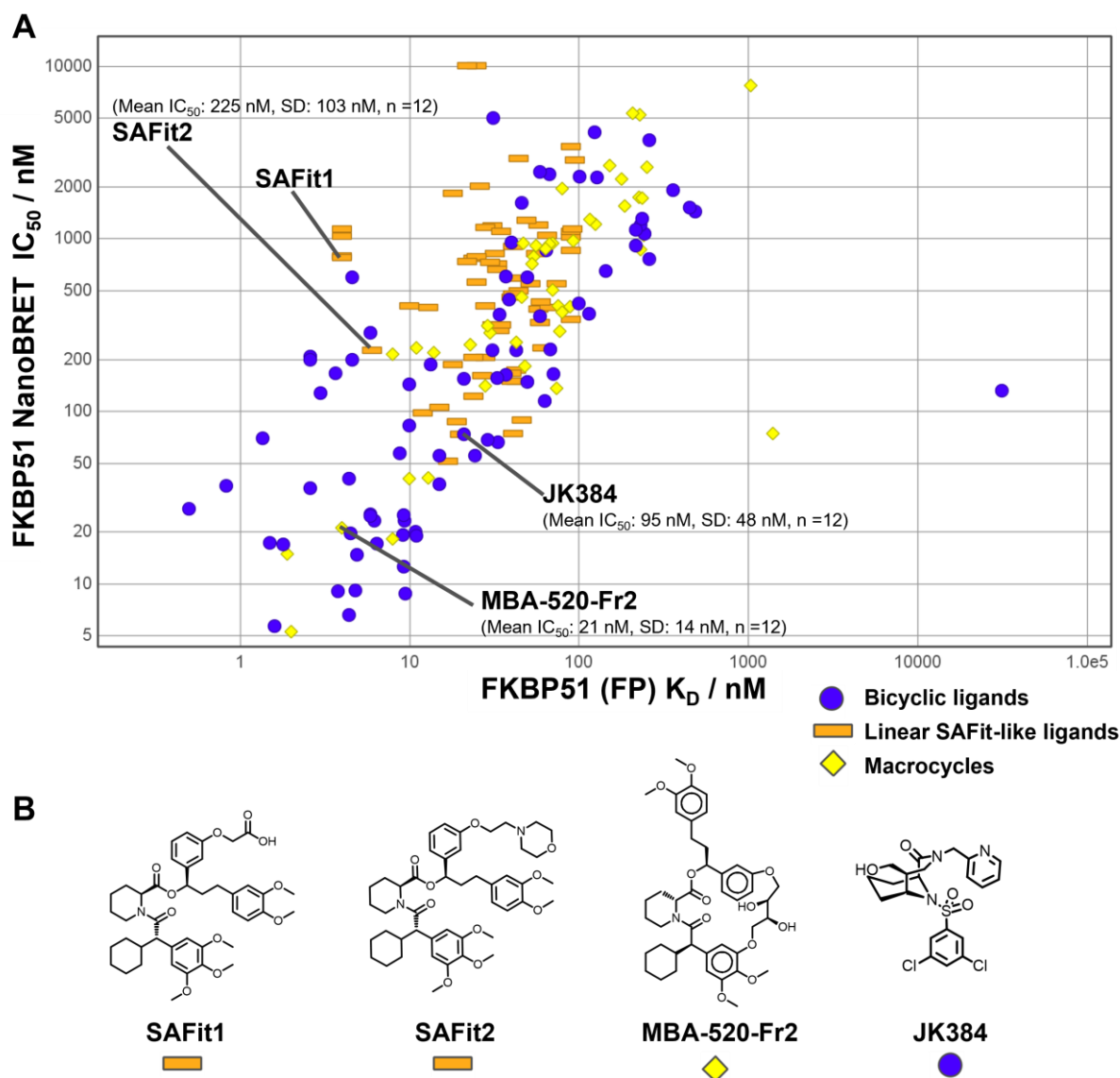


**Figure 28** High-throughput FKBP51<sup>FK1</sup>-Nluc assay links intracellular target engagement to biochemical binding affinities. **A** IC<sub>50</sub> values are plotted on the y-axis and are derived from competitive NanoBRET tracer displacement curves at 400 nM 2c [162] in living HEK293T cells stably expressing FKBP51<sup>FK1</sup>-Nluc fusionproteins. Corresponding K<sub>D</sub> values derived from fluorescence polarization assays are plotted on the x-axis. Data points corresponding to individual compounds are colour- and shape-coded according to their chemical classes. In case of the control compounds SAFit2, MBA-520-Fr2 and JK384, the IC<sub>50</sub> values and errors correspond to mean standard deviation of twelve independent experiments. **B** Chemical structures of SAFit1 [54], SAFit2 [54], MBA-520-Fr2 (64a [57]) and JK384 (FK[4.3.1]-16j [49]). Biochemical fluorescence polarization assays and K<sub>D</sub> determination were performed by Dr. Stephanie Merz and Wisely Oki Sugiarto.

The results obtained for FKBP51 indicate that the obtained  $IC_{50}$  values correlate with the binding affinities to FKBP51 for bicyclic and macrocyclic compounds. However, on average there is a substantial offset (approx. factor 5) between the respective NanoBRET versus FP assay values, which might be attributed to the high tracer concentration of 400 nM. For linear SAFit-type ligands the best  $IC_{50}$  values reach the 5-fold offset. For this compound class, the NanoBRET values correlate poorly with the binding affinity.

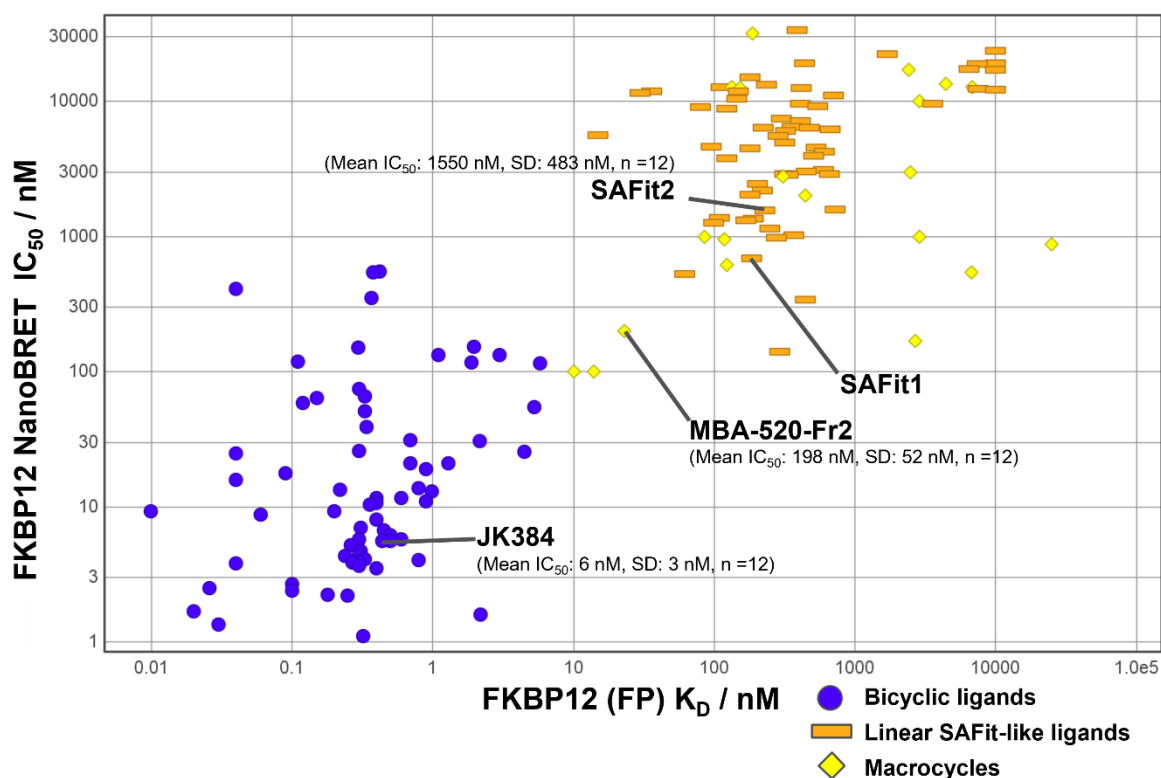


**Figure 29** High-throughput FKBP12-Nluc assay links intracellular target engagement to biochemical binding affinities.  $IC_{50}$  values are plotted on the y-axis and derived from competitive NanoBRET tracer displacement at 20 nM 2b [162] in living HEK293T cells stably expressing FKBP12-Nluc fusionproteins. Corresponding  $K_D$  values derived from fluorescence polarization assays are plotted on the x-axis. Data points corresponding to individual compounds are colour- and shape-coded according to their chemical classes. In case of the control compounds SAFit2, MBA-520-Fr2 and JK384, the  $IC_{50}$  values and errors correspond to mean standard deviation of twelve independent experiments. Biochemical fluorescence polarization assays and  $K_D$  determination were performed by Dr. Stephanie Merz and Wisely Oki Sugiarto.

For the FKBP12 NanoBRET assays, a similar correlation between  $IC_{50}$  values and binding affinities as well as an offset between the respective values became evident. Additionally, several bicyclic molecules engaged FKBP12 with lower  $IC_{50}$  values than the natural products FK506 ( $IC_{50} = 5.6$  nM [162]) and Rapamycin ( $IC_{50} = 8.5$  nM [162]) under similar conditions. Furthermore, the  $IC_{50}$  values of bicyclic high affinity ligands ( $K_D < 1$  nM) indicate a lower plateau between 1 and 10 nM for intracellular target-engagement. This could be due to the ligands first having to saturate tracer-unbound FKBP12 and FKBP12-Nluc before the tracer can

---

displaced from the overexpressed FKBP-Nluc. A more precise ranking of intracellular target-engagement could be achieved by repeating the assay with higher tracer concentration.

Taken together, the NanoBRET values confirm the intracellular FKBP binding of FKBP ligands, but especially linear SAFit-type ligands had reduced cellular potency. Additionally, it became evident from structural comparative analysis of close analogs (e.g., SAFit1 and SAFit2 in Figure 28), that under assay conditions charged groups like carboxylic acids greatly impair intracellular target engagement. The results add valuable insights to the cellular potencies of individual molecules. In consequence, the established NanoBRET assay has been used to: (i) determine which compounds penetrate cells [53]; (ii) confirm that the, at the time, new class of macrocyclic compounds [56] occupy FKBP51 in living cells; (iii) demonstrate that the enhanced ligand efficiency of  $\alpha$ -methylated bicyclic ligands compared to their respective non-methylated analogs translates to an enhanced cellular potency [51]; and to choose compounds for cellular profiling, when the biochemical potencies are similar [52]. Additionally, this assay will guide FKBP ligand optimization in future projects. Especially further macrocyclization approaches appear promising as members of the macrocycle class repeatedly outperformed linear SAFit-type molecules of similar binding affinity and molecular weight in terms of cellular potency. This effect can likely be attributed to the chameleonic effect of macrocycles, which can allow them to bury normally solvent exposed polar groups and expose normally buried hydrophobic groups when they pass hydrophobic membranes.

### 4.3. Glucocorticoid receptor reporter gene assays

The large FKBP51 and FKBP52 are well established as regulators of the glucocorticoid receptor. While FKBP51 suppresses GR activity, FKBP52 acts antagonistically to the former and increases GR activity. To study the effects of FKBP ligands on FKBP-mediated GR regulation a dual luciferase reporter gene assay was established in HEK293T cells using the dual reporter plasmids pGL4.36 (MMTV-luc2p) and pGL4.74 (TK-hRluc). pGL4.36 features a firefly luciferase (*luc2p*) reporter gene that is controlled by Murine Mammary Tumor Virus (MMTV) Long Terminal Repeat. This promoter drives transcription in response to stimulation of several nuclear receptors such as the glucocorticoid receptor. pGL4.74, on the other hand, drives transcription of the renilla luciferase (*hRluc*) reporter gene through a constitutively active promoter (HSV-TK) and can be used for transfection and expression control. Luc2p and hRluc luminescence can subsequently be assessed in the same sample. Normalization of the former to the latter (norm. luc) results in a more robust measurement as it accounts for fluctuating variables such as cell growth or transfection efficacy.

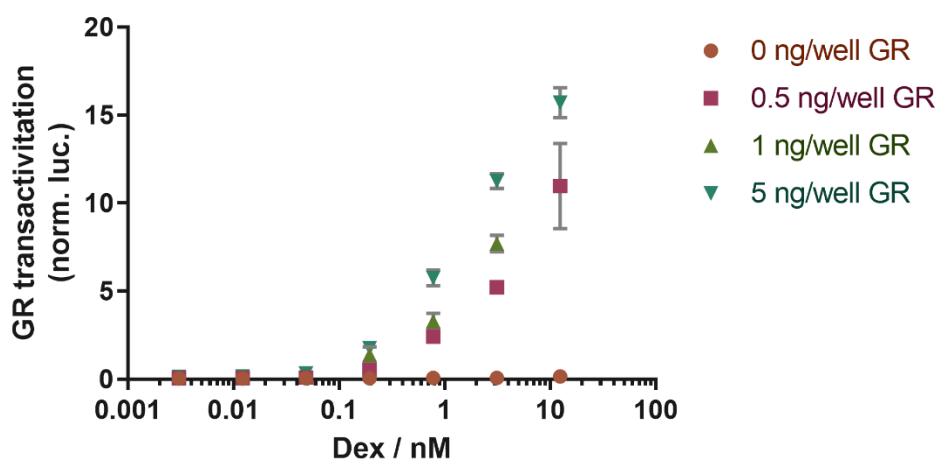


**Figure 30** Glucocorticoid receptor overexpression is required to stimulate dexamethasone induced reporter expression in HEK293T cells. HEK293T cells were transiently transfected (24 hours) with the dual luciferase reporter plasmids (pGL4.36 (MMTV-luc2p), pGL4.74 (TK-hRluc)) and the indicated amount of a GR-expression plasmid, followed by stimulation (24 hours) with the indicated concentration of dexamethasone (Dex). Reporter expression was quantified by luminescence measurements in lysates and the normalized luciferase (norm. luc.) was calculated by normalizing luc2p luminescence to hRluc luminescence. Individual points and error bars represent mean and standard deviation of biological triplicates. Raw data are depicted in Figure 75.

To establish the assay, HEK293T cells were transiently transfected with the dual luciferase reporter plasmids and increasing amounts of an GR expression plasmid and subsequently stimulated with the synthetic GR agonist dexamethasone (Dex). GR stimulation with increasing Dex concentrations resulted in a clear increase in GR activation (Figure 30). Notably, the effect

is due to changes in luc2p expression and not in the hRluc expression, which remained rather unchanged (Figure 75). Overexpression of the GR was essential in HEK293T cells to activate luc2p expression and increasing amounts enhanced the assay window. While HEK293T cells endogenously express the GR, the level might not be high enough to drive reporter stimulation. Ultimately, the highest GR expression plasmid transfection dose was used for further assays as it resulted in the highest assay window.

In the following, FKBP51 and FKBP52 were co-expressed in addition to GR and their effects on GR activation were tested at different Dex concentrations to determine the optimal Dex concentrations for ligand profiling (Figure 31).

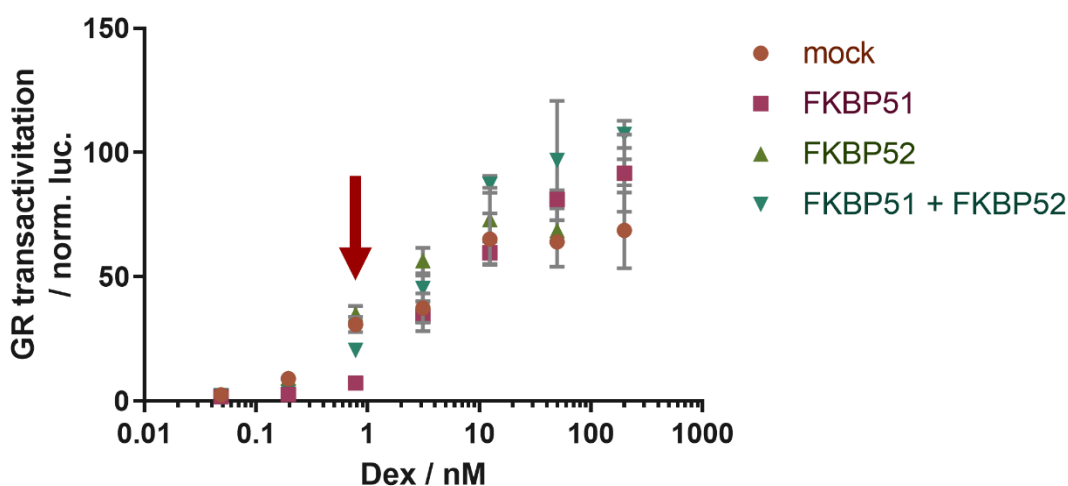


**Figure 31** FKBP51 suppresses GR activity, while FKBP52 blocks FKBP51's effect at low dexamthasone concentration. HEK293T cells were transiently transfected for 24 hours with the dual luciferase reporter plasmids (pGL4.36 (MMTV-luc2p), pGL4.74 (TK-hRluc) and 5 ng/well GR expression as well as FKBP51 (10 ng/well), FKBP52 (10 ng/well) and or mock plasmid (20 ng/well (mock), 10 ng/well (FKBP51, FKBP52)) and subsequently (24 hours) stimulated with dexamthasone (Dex). Reporter expression was quantified by luminescence measurements in lysates and the normalized luciferase (norm. luc.) was calculated by normalizing MMTV promotor driven luc2p luminescence to constitutive hRluc luminescence. Individual points and error bars represent mean and standard deviation of biological triplicates. Raw data are depicted in Figure 76. Red arrow indicates Dex concentrations at which the FKBP effect was observed.

The GR suppressive effects of FKBP51 became evident at low Dex concentrations around 1 nM (Figure 31, red arrow). Additionally, FKBP52 co-expression could reactivate GR signaling, rescuing FKBP51-mediated GR suppression but did not significantly increase GR activation alone, which is in line with previously published data [26]. This could indicate the ability of FKBP52 to displace FKBP51 from Hsp90:FKBP51:GR complexes and thereby relieving FKBP51's GR suppressive pressure as the main driver of FKBP52's GR activating function. This is

---

supported by a finding were co-expression of the TPR domain-containing protein Cyp40 was also able to rescue FKBP51-mediated GR suppression [32]

A Dex concentration of 1 nM was chosen to study the effects of FKBP ligands on GR signaling in further experiments as FKBP51's suppressive effect was most evident at low Dex concentrations and this stimulation condition still resulted in a good assay window.

In parallel to the establishment of the reporter gene assays, the Hausch lab investigated the molecular architecture of FKBP51- or FKBP52-containing Hsp90:FKBP:apoGR complexes [165], termed 'pre-activation complexes'. In brief, the study used site-specific incorporation of the photo-reactive amino acid para-benzoyl phenyl alanine (pBpa) into FKBP51, FKBP52 and the GR. Subsequently, in-cell photo-crosslinking and crosslinking-adduct formation analysis by western blot and or ELISA assays was employed to study the molecular architecture of pre-activation complexes. The formed crosslinks are indicative of direct proximity between the site-specifically incorporated pBpa and the crosslinked partner and hence allow investigation of the complex architecture and collectively the role for complex formation of distinct domains. The study revealed that (i) the interaction interfaces between the FKBP51 and GR spanned from the FK1 domain to the tip of the TPR domain and were very similar between FKBP51 and FKBP52 as both wrap around the GR. Additionally, it was demonstrated that (ii) crosslinks (FKBP→GR) in the FK1 but not in the FK2 or TPR domains of FKBP51 and FKBP52 were sensitive to SAFit2 or 18<sup>(S-Me)</sup> treatment, respectively. This, indicates that (iii) FK1 domain to GR contacts are largely dispensable, while (iv) the FK2- and TPR-domain contacts mainly drive Hsp90:FKBP:apoGR complex formation, and (v) FKBP ligands remodeled but did not disrupt the complex as they displaced the FK1 but not the FK2 domain from the GR surface.

To analyze the functional consequences of FK506-binding site occupation and FKBP ligand-induced complex remodeling on GR signaling 18<sup>(S-Me)</sup>, SAFit2 and FK506 were tested in reporter gene assays. The following results (Figure 32 & Figure 77) are part of the manuscript "Large-scale in-cell photocrosslinking at single residue resolution reveals the molecular basis for glucocorticoid receptor regulation by immunophilins" [165], which is currently in press at Nature Structural and Molecular Biology.

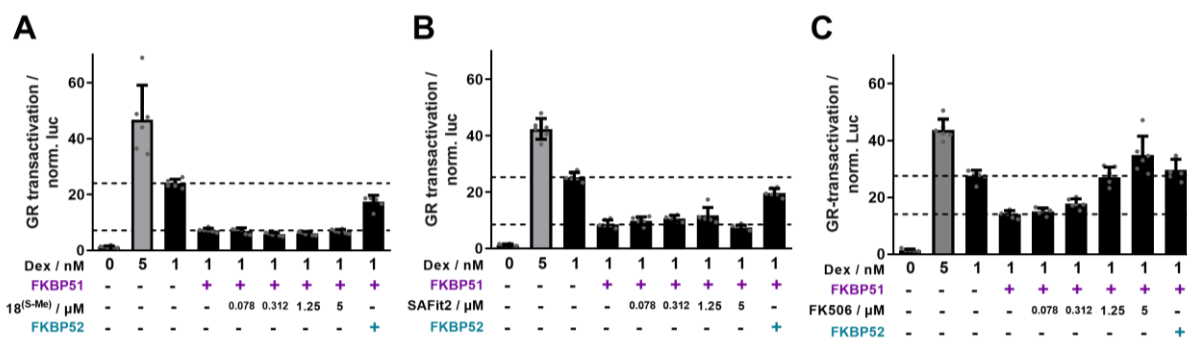


**Figure 32** Treatment with FK506 **C** but not 18<sup>(S-Me)</sup> **A** or SAFit2 **B** dose-dependently blocks GR suppression. HEK293T cells were transiently transfected (24 hours) with the dual luciferase reporter plasmids (pGL4.36 (MMTV-luc2p), pGL4.74 (TK-hRluc)), 5 ng/well GR expression plasmid and FKBP51 (10 ng/well) and/or an 3-fold excess of FKBP52 expression plasmids, respectively, and subsequently stimulated (24 hours) with dexamethasone (Dex) in presence of the indicated concentrations of FKBP ligands. Reporter expression was quantified by luminescence measurements in lysates and the normalized luciferase (norm. luc.) was calculated by normalizing luc2p luminescence to hRluc luminescence. Individual points and error bars represent mean and standard deviation of biological hexaplicates. Raw data are depicted in Figure 77. The data presented in this figure are part of the manuscript “Large-scale in-cell photocrosslinking at single residue resolution reveals the molecular basis for glucocorticoid receptor regulation by immunophilins” [165], which is currently in press at Nature Structural and Molecular Biology

Co-expression of FKBP52 principally reversed the GR signaling repressing effect of FKBP51. However, neither the selective FKBP51 ligand SAFit2 nor the bicyclic ligand 18<sup>(S-Me)</sup> affected the GR signaling suppressing effect of FKBP51 (Figure 32A&B). Notably, the tested ligand concentrations used were drastically higher (100-fold) than necessary for remodeling of the FKBP51:GR complex [165] and also at least 10-fold higher than the IC<sub>50</sub> values derived from competitive NanoBRET assays (see Figure 28). These findings indicate that FKBP51’s GR-suppressive effect does not depend on the FK506-binding site per se. This result is consistent with a study that found the catalytically dead FKBP51<sup>F67D/D68V</sup> mutant to retain GR suppression [26]. Strikingly, the larger macrocyclic ligand FK506 dose-dependently reverted the FKBP51-mediated GR suppression (Figure 32C) at concentrations consistent with intra-molecular FK506-binding site occupation [162]. Importantly, FK506 protrudes much further from the binding site compared to SAFit2 or 18<sup>(S-Me)</sup>. My results imply that the FKBP51:GR contacts which are retained after complex remodeling by small ligands have regulatory effects. Yet, FK506 can disrupted these regulatory contacts and re-active GR signaling. This has profound implications for the FKBP51-directed drug discovery. My findings, indicate that larger ligands are more disruptive and that it is principally possible to pharmacologically reactivate FKBP51-repressed GR signaling although the FK506-binding site is not required. However, it remains to be elucidated how FK506 differentially remodels the Hsp90:FKBP51:GR complex and how exactly compound size influences FKBP51-mediated GR regulation.

Next, it was investigated if FKBP52 occupation by FKBP ligands effects GR-signaling (Figure 33).

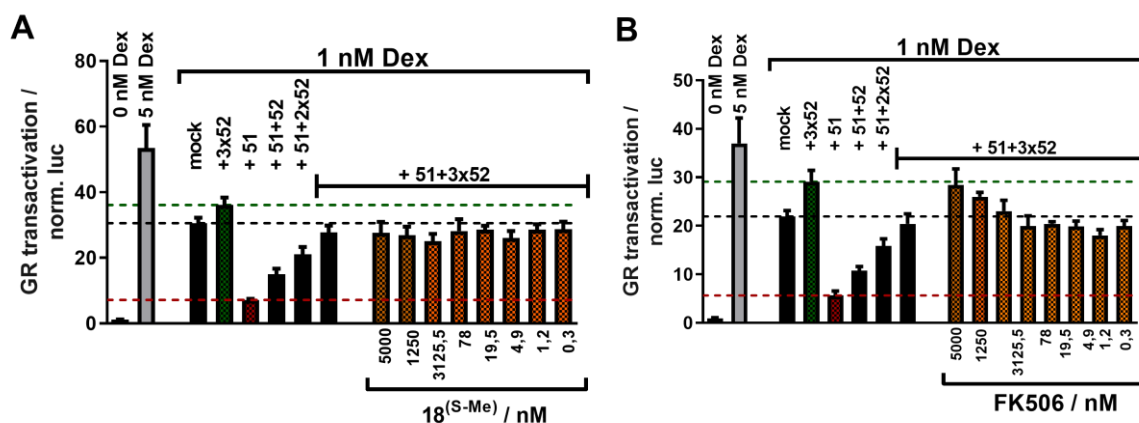


**Figure 33** Neither treatment with **A** 18<sup>(S-Me)</sup> nor **B** FK506 affects FKBP52-mediated GR reactivation. HEK293T cells were transiently transfected (24 hours) with the dual luciferase reporter plasmids (pGL4.36 (MMTV-luc2p), pGL4.74 (TK-hRluc)), 5 ng/well GR expression vector and FKBP51 expression vector (10 ng/well) and/or an indicated fold excess of FKBP52 expression vector, followed by stimulation (24 hours) with dexamethasone (Dex) in presence of the indicated concentrations of FKBP ligands. Reporter expression was quantified by luminescence measurements in lysates and the normalized luciferase (norm. luc.) was calculated by normalizing MMTV promoter luc2p luminescence to hRluc luminescence. Individual points and error bars represent mean and standard deviation of biological hexaplicates. Raw data are depicted in Figure 78.

During assay establishment, it became evident that FKBP52 overexpression principally, as previously published [26], reverted the FKBP51-mediated GR suppression, but did not strongly increase GR-signaling alone (Figure 31). Higher transfection doses (Figure 33, green dashed lines) only slightly increased GR-signaling over the mock control (Figure 33, black dashed lines) possibly by reverting the GR-suppressive effect of endogenous FKBP51. Thus, the effects of ligands on FKBP52's role was investigated indirectly by testing if they would block FKBP52's ability to reactivate FKBP51-suppressed GR signaling. Therefore, the FKBP51-suppressive effect (Figure 33, red dashed line) was reverted by co-transfection of a 3-fold excess of FKBP52 expression plasmid and compounds were added during stimulation. FK506, which blocks FKBP51-mediated GR suppression (Figure 32C), dose-dependently increased GR-signaling (Figure 33B) if FKBP52 was co-expressed next to FKBP51. It is unlikely, that a 3-fold excess of FKBP52 compared to FKBP51 expression plasmid transfection doses results in FKBP52 levels high enough to completely displace FKBP51 from GR containing complexes. FK506 might increase GR signaling here by blocking FKBP51's suppressive effect in the remaining complexes thus enhancing GR signaling. The pan-selective FKBP ligand 18<sup>(S-Me)</sup> that did not block FKBP51's effect (Figure 32A) also did not block FKBP52's ability to revert the GR-suppressive effect of FKBP51 (Figure 33A) indicating that FKBP52 effects is not FK506-binding site dependent. Conversely, the catalytically dead FKBP52<sup>F67D/D68V</sup> mutant was shown to not potentiate GR



---

signaling [31,166] and FK506 was shown to block FKBP52 mediated GR potentiation in yeast [31,166].

Collectively the experiments confirmed (i) FKBP51 as a negative regulator of GR signaling and FKBP52 as an antagonistic counterpart. Investigation of FKBP ligands demonstrated that (ii) the FK506-binding site is functionally silent, but (iii) FK506 that protrudes far from the binding site can block FKBP51's suppressive effect. This shows (iv) that pharmacological reactivation of FKBP51-suppressed GR-signaling is principally possible. Furthermore, the data suggest that (v) FKBP51 has an 'active' role in GR regulation, while FKBP52 'passively' regulates GR signaling by displacing FKBP51 from Hsp90:FKBP51:GR complexes. To investigate this hypothesis in more detail, it will be necessary to investigate FKBP51 and FKBP52's roles in FKBP51- and/or FKBP52-deficient cells.

#### 4.4. Development of a fluorescent reporter assay for FKBP51 and FKBP12 level

PROTACs degrade the POI and consequently target all protein functions. Thus, they possess a fundamentally different pharmacology than ligands. Screening of a large PROTAC candidate library by western blot is laborious and can be the rate-limiting step. Therefore, an alternative screening method was warranted to enable a higher throughput.

To rapidly analyze FKBP51 and FKBP12 levels in cells, I investigated a fluorescent FKBP-level reporter assay featuring eGFP-tagged FKBP-fusion proteins (Figure 34). Eukaryotic expression plasmids were generated that allow the co-expression of FKBP12- and FKBP51-eGFP fusion proteins (N-terminally or C-terminally tagged) as well as mCherry mediated by an IRES2 element. Degradation of the FKBP-eGFP fusion proteins decreases the eGFP signal, while the mCherry signal remains unaffected by FKBP-degrader treatment and serves for normalization. The ratio of the respective eGFP and mCherry signals directly allows an assessment of a PROTAC's induced maximal degradation ( $D_{max}$ ) and the half maximal degradation concentration ( $DC_{50}$ ).

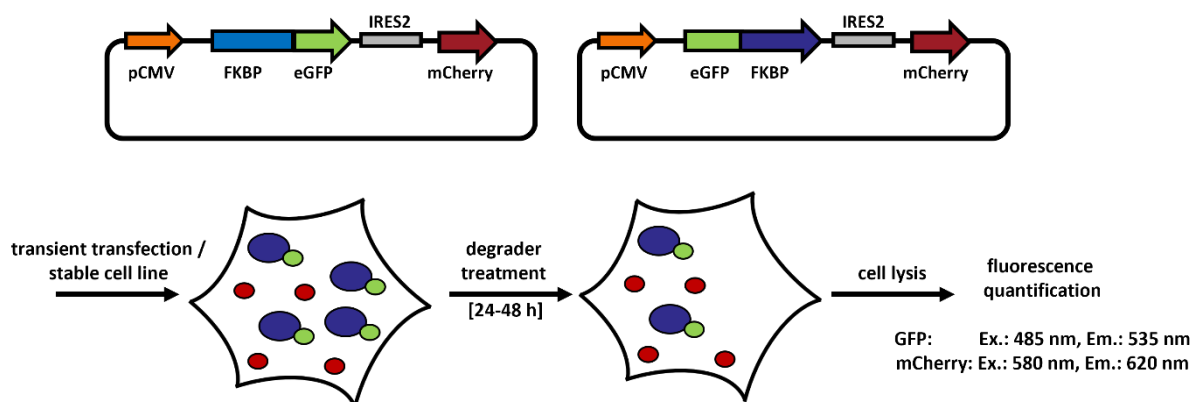


**Figure 34** Fluorescent FKBP-level reporter assay scheme. Reporter plasmids co-express N- or C-terminally eGFP-fused FKBP as well as mCherry upon transient transfection or in generated stable cell lines. Upon FKBP degrader treatment the FKBP-eGFP fusion protein level decreases while the mCherry levels remain unaffected and is used for normalization. Decreasing eGFP/mCherry ratios are indicative of FKBP-eGFP fusion protein degradation.

To assess the suitability of the fluorescent reporter assay, HEK293T cells were transiently transfected with the FKBP-level reporter constructs and subsequently treated with PROTACs. The PROTACs 10a4 (MTQ202) and 6a1 (MTQ508) were previously identified as FKBP51 [155] and FKBP12 degraders, respectively, by Western blotting.

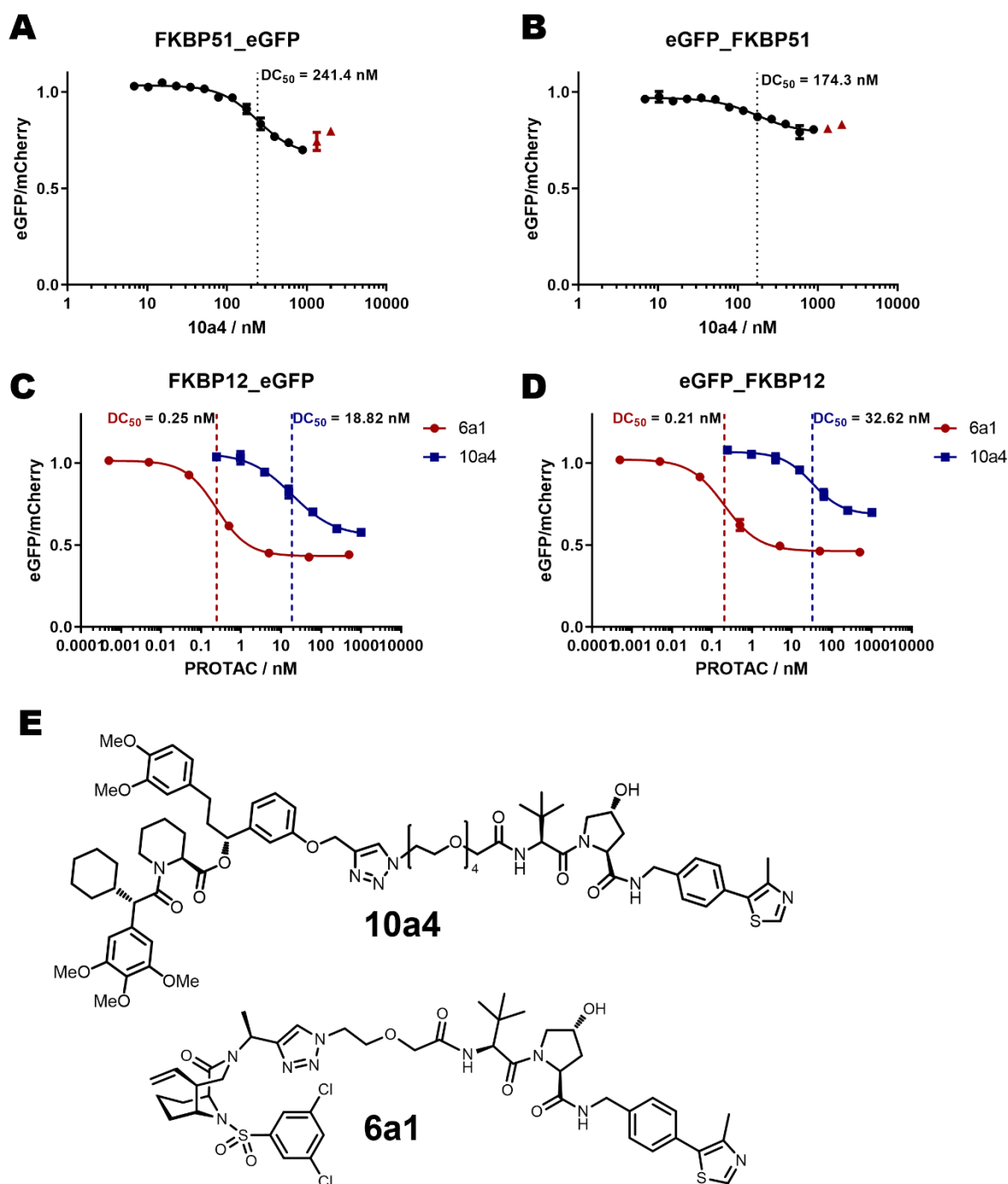


**Figure 35** PROTACs dose-dependently decrease the eGFP/mCherry ratio. Cells transiently transfected with 12.5 ng/well co-expression plasmids for mCherry and **A** FKBP51\_eGFP, **B** eGFP\_FKBP51, **C** FKBP12\_eGFP and **D** eGFP\_FKBP12 were treated for 24 hours with the indicated PROTAC before cell lysis and eGFP (Ex.: 485 nm, Em.: 525 nm) and mCherry (Ex.: 580 nm, Em.: 620 nm) fluorescence quantification. Individual data points and error bars represent mean and standard deviation of biological triplicates.  $DC_{50}$  values were determined by a four-parameter fit (red triangles in **A** and **B** excluded for the fit). **E** Chemical structures of 10a4 and 6a1.

All reporter constructs enabled detection of PROTAC-mediated FKBP-eGFP degradation as evidenced by a decrease of the eGFP/mCherry ratio upon treatment (Figure 35). While the  $DC_{50}$  values are almost identical between the N- and C-terminal tagged FKBP (compare Figure 35 A

to B and C to D) the assay windows were generally better for the C-terminally eGFP-tagged FKBP reporters. Hence, they were chosen for further profiling.

To further streamline the PROTAC profiling process, the generation of stable cell lines expressing FKBP51\_eGFP and mCherry or FKBP12\_eGFP and mCherry was conducted. In brief, HEK293T cells were transfected with the respective reporter plasmid, selected for Hygromycin B resistance and individual clones were expanded and tested for FKBP\_eGFP and mCherry expression by measuring the respective fluorescence in lysates. While the generation of a FKBP51\_eGFP-IRES2-mCherry cell line was not successful, for the FKBP12\_eGFP-IRES2-mCherry construct several clones could be generated and were further profiled (Figure 36).

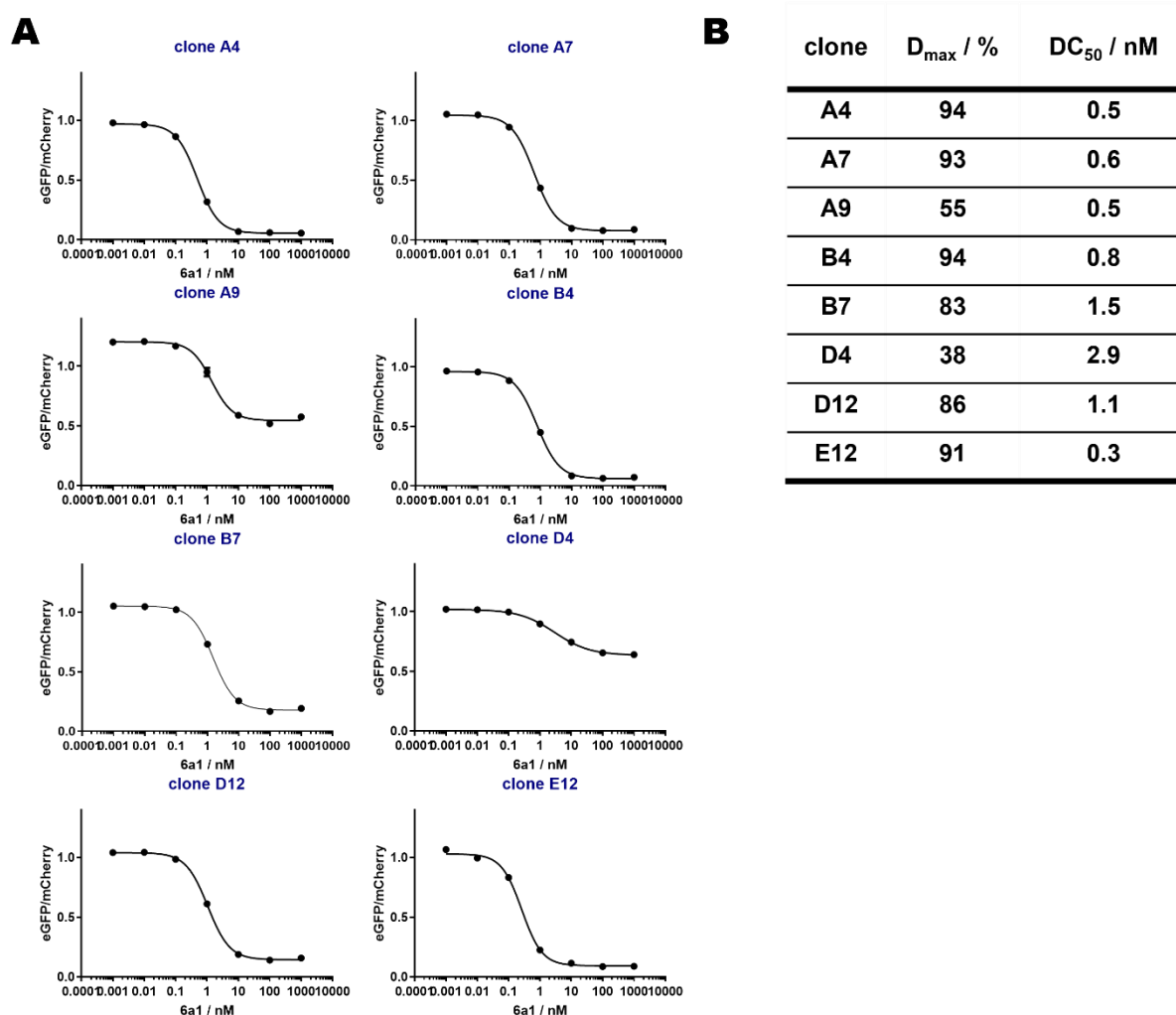


**Figure 36** Suitability test of HEK293T clones stably expressing FKBP12\_eGFP and mCherry for FKBP12-PROTAC profiling. **A** Cells were treated for 24 hours with the active FKBP12-PROTAC 6a1 before cell lysis and eGFP (Ex.: 485 nm, Em.: 525 nm) and mCherry (Ex.: 580 nm, Em.: 620 nm) fluorescence quantification. eGFP fluorescence was normalized on the respective mCherry fluorescence (eGFP/mCherry). Individual data points and error bars represent mean and standard deviation of

biological duplicates. **B** Half maximal degradation values ( $DC_{50}$  values) and maximal induced reporter degradation  $D_{max}$  values (indicated by the lower plateau) were determined by a four-parameter fit.

The PROTAC 6a1 decreased the eGFP/mCherry ratio dose-dependently in all clones with comparable ( $DC_{50}$  values) but to different extents ( $D_{max}$ ) indicating that the maximal potency and therefore the assay window depends on the strength of the reporter expression. Next, PROTAC-mediated FKBP12\_eGFP reporter degradation in the best clones (highest  $D_{max}$ ) A4, A7 and B4 was validated by Western blotting after treatment with the comparatively weak FKBP-PROTAC 10a4 (Figure 37).

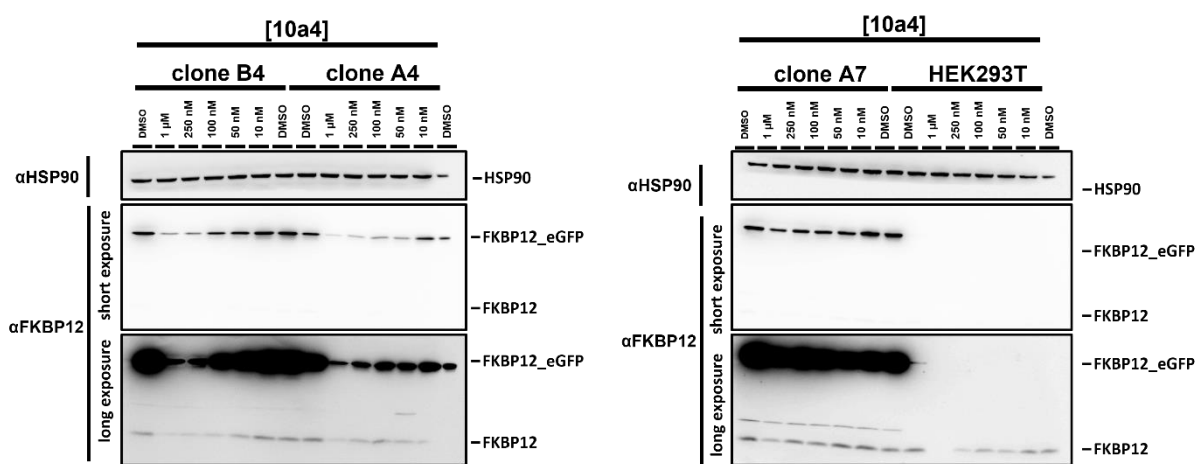


**Figure 37** Western blot of 10a4-mediated FKBP12 and FKBP12\_eGFP degradation after 24 h treatment of the indicated clones stably expressing FKBP12\_eGFP and mCherry. Hsp90 serves as a loading control.

Strong FKBP12\_eGFP degradation was evident in clones A4 and B4 and correlated with the degradation of endogenous FKBP12. Ultimately, clone B4 was chosen for PROTAC profiling as it featured a combination of a high detectable assay window, a correlating degradation of endogenous FKBP12 and the FKBP12\_eGFP reporter and generally high reporter expression. Lastly, the optimal treatment duration for screening was investigated in a time course experiment (Figure 38).

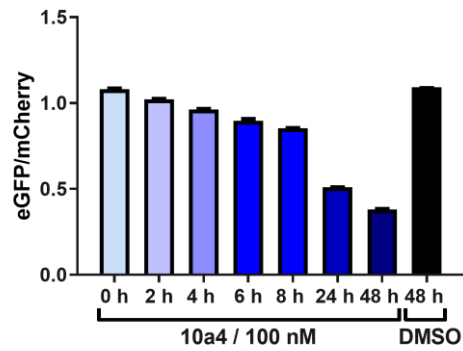


**Figure 38** FKBP12\_eGFP degradation kinetics of 10a4 in FKBP12\_eGFP reporter clone B4. Bars and error bars represent mean and standard deviation of biological triplicates.

10a4 continuously decreases FKBP12\_eGFP levels for up to 48 hours (Figure 38). Additionally, previous experiments revealed similar effects for endogenous FKBP51 [155]. Therefore, a treatment duration of 48 hours was chosen to profile the activity of the library of PROTAC candidates for FKBP12- and FKBP51-eGFP reporter degradation.

#### 4.5. Development of an HTRF-based FKBP52 quantification assay

For the quantification of endogenous FKBP52 levels in cell lysates a homogenous time-resolved fluorescence (HTRF) based assay (Figure 39A) was developed. The setup consists of a primary antibody that binds the TPR domain of FKBP52, a secondary europium cryptate (Eu cryptate) labelled antibody that binds the first, a AlexaFluor647 (A647) labelled FKBP-ligand (MWa146, Figure 39B) as well as FKBP52. In presence of all components, the Eu cryptate will come in close proximity to A647 and excitation (320 nm) of the Eu cryptate leads to emission of A647 (665 nm) additional to its own emission (620 nm), which is used for normalization. The changes in the HTRF ratio 665 nm / 620 nm are therefore indicative for an in- or decrease of proximity of the components or in case of constant antibody and tracer concentrations for a change in the quantity of FKBP52.

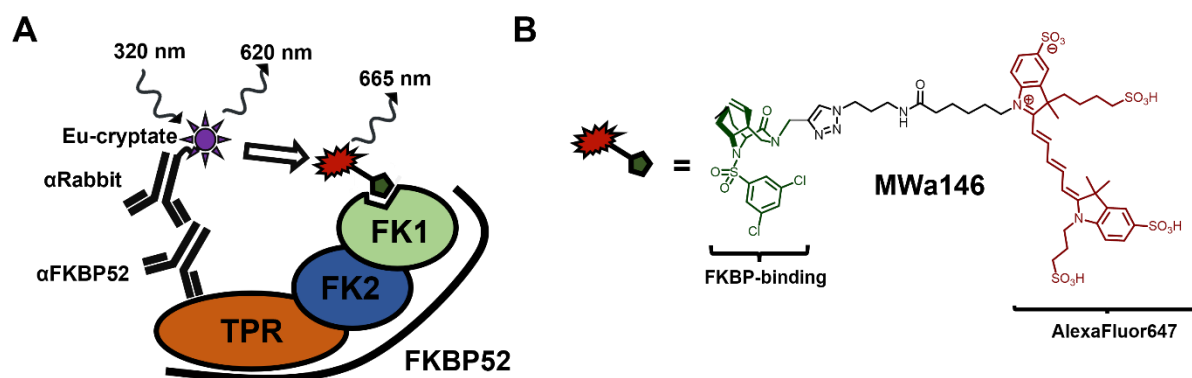


**Figure 39** HTRF-based FKBP52 quantification assay. **A** Schematic visualisation of the assay setup. In presence of FKBP52 the anti-FKBP52 and Eu cryptate labelled anti-rabbit antibody pair comes in close proximity to the tracer (MWa146) yielding an HTRF signal. **B** Chemical structure of the tracer MWa146 (FKBP ligand: green, AlexaFLuor647: red; synthesized by Dr. Michael Walz).

First, FKBP52-binding of the tracer (MWa146) was confirmed in a fluorescence polarization assay with a  $K_D$  of  $61 \pm 4$  nM (Figure 79). Then, the HTRF setup was tested by titrating purified FKBP52 and MWa146 against each other in presence of constant antibody concentrations (Figure 40A). The HTRF signal increased in both FKBP52- and MWa146-dependent manner. However, in presence of a high FKBP52 concentration (1000 nM) and MWa146 concentrations  $\leq 100$  nM the HTRF-signal decreased due to the hook effect. In principle, that could be avoided by using drastically higher antibody concentrations, but here economic reasons are the limiting factor. Next, the assay setup was tested directly in cell lysates on endogenous FKBP52 (Figure 40B). The HTRF ratio increased with increasing total protein concentrations and therefore with increasing FKBP52 concentrations for MWa146 concentrations  $\geq 30$  nM. The highest tested

tracer concentration of 120 nM resulted in the best signal to background ratio and was therefore chosen for further assay validation.

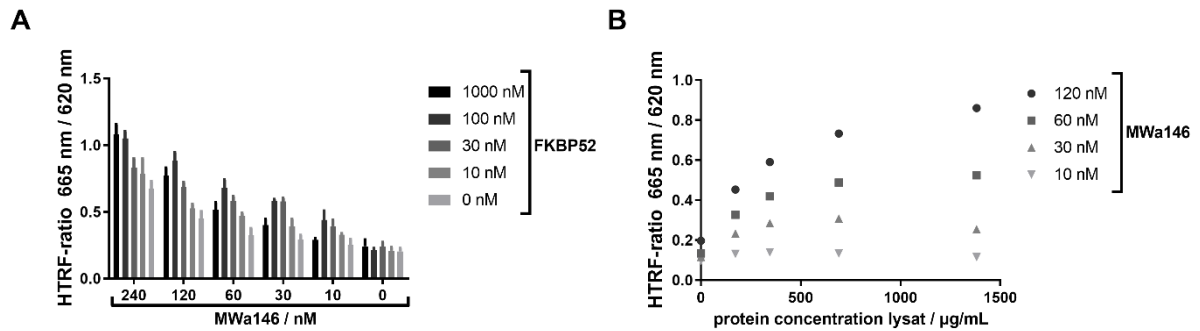


**Figure 40** Comparison of HTRF ratio derived from different MWa146:FKBP52 concentration pairings. **A** HTRF-ratios of different concentration pairings (MWa146 and purified FKBP52) as well as **B** HTRF ratios of different concentration pairings (MWa146 and lysates) with the indicated total protein concentration in presence of 1.2 nM anti-rabbit-Eu cryptate and 1.25 nM anti-FKBP52 antibodies.

In order to test the suitability of the assay to detect changes in the amount of cellular FKBP52, the FKBP52 levels was either decreased by siRNA mediated FKBP52-knockdown, left unchanged or increased by transient FKBP52 overexpression. Then, Western blotting (Figure 41A) and the HTRF assay (Figure 41B) were employed to quantify FKBP52 levels in cell lysates. Decreased FKBP52 levels could be detected in both undiluted and diluted lysates using the HTRF assay. However, overexpression of FKBP52 resulted also in lower HTRF ratios compared to the untransfected control in undiluted lysates. Upon dilution of the lysates and therefore a reduction of the FKBP52 levels the HTRF ratio increased, indicating that the lower HTRF signal in undiluted lysates was due to the hook effect.

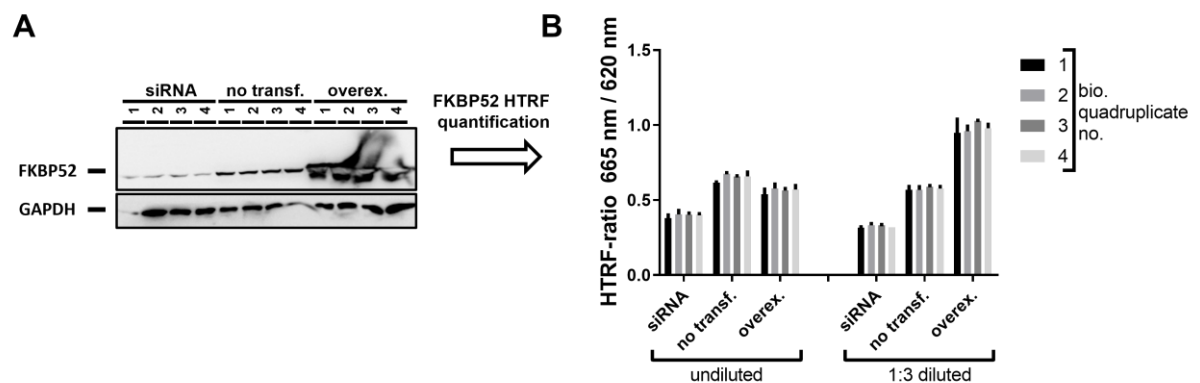


**Figure 41** HTRF-based FKBP52 quantification enables detection of de- or increased FKBP52 levels in cell lysates. **A** Western blot of HEK293T cells transiently transfected with 20 pmol/well anti-FKBP52 siRNA (siRNA), 200 ng/well pcDNA3-Flag-FKBP52 (overex.) or untransfected (no transf.) cells in 12 well plates (quadruplicates). **B** HTRF ratios of the lysates from A in presence of 120 nM MWa146, 1.2 nM anti-rabbit-Eu cryptate and 1.25 nM anti-FKBP52 antibodies. Bar and error bars represent mean and standard deviation of technical duplicates.



---

Lastly, it was tested if the HTRF assay is suitable to detect a FKBP52 knockdown when the cells are cultured in a 24 well format (Figure 80). Similar to the 12 well format (Figure 41), siRNA-mediated FKBP52-knockdown was detectable using the HTRF-assay directly in cell lysates.

Taken together, assay conditions using 120 nM tracer (MWa146), 1.25 nM anti-FKBP52 antibody, 1.2 nM anti-Rb-Eu cryptate antibody and cell lysates originating from 24 well plates were suitable to detect a decrease in FKBP52 levels. Consequently, the assay was employed to test PROTAC candidates for FKBP52 degradation.

## 4.6. FKBP-PROTACs

### 4.6.1. Cellular assessment of PROTAC activity

All copper-catalyzed click chemistry-assembled PROTAC candidates (Figure 42A) were tested in FKBP51\_eGFP and FKBP12\_eGFP reporter assays (Figure 42B). FKBP52-binding candidates (based on alkyne A1-A7) were profiled in FKBP52-quantification HTRF assays and/or by Western blotting (Figure 83 and Figure 84), if they had not previously been tested for FKBP52 degradation by Dr. Andreas Hähle.

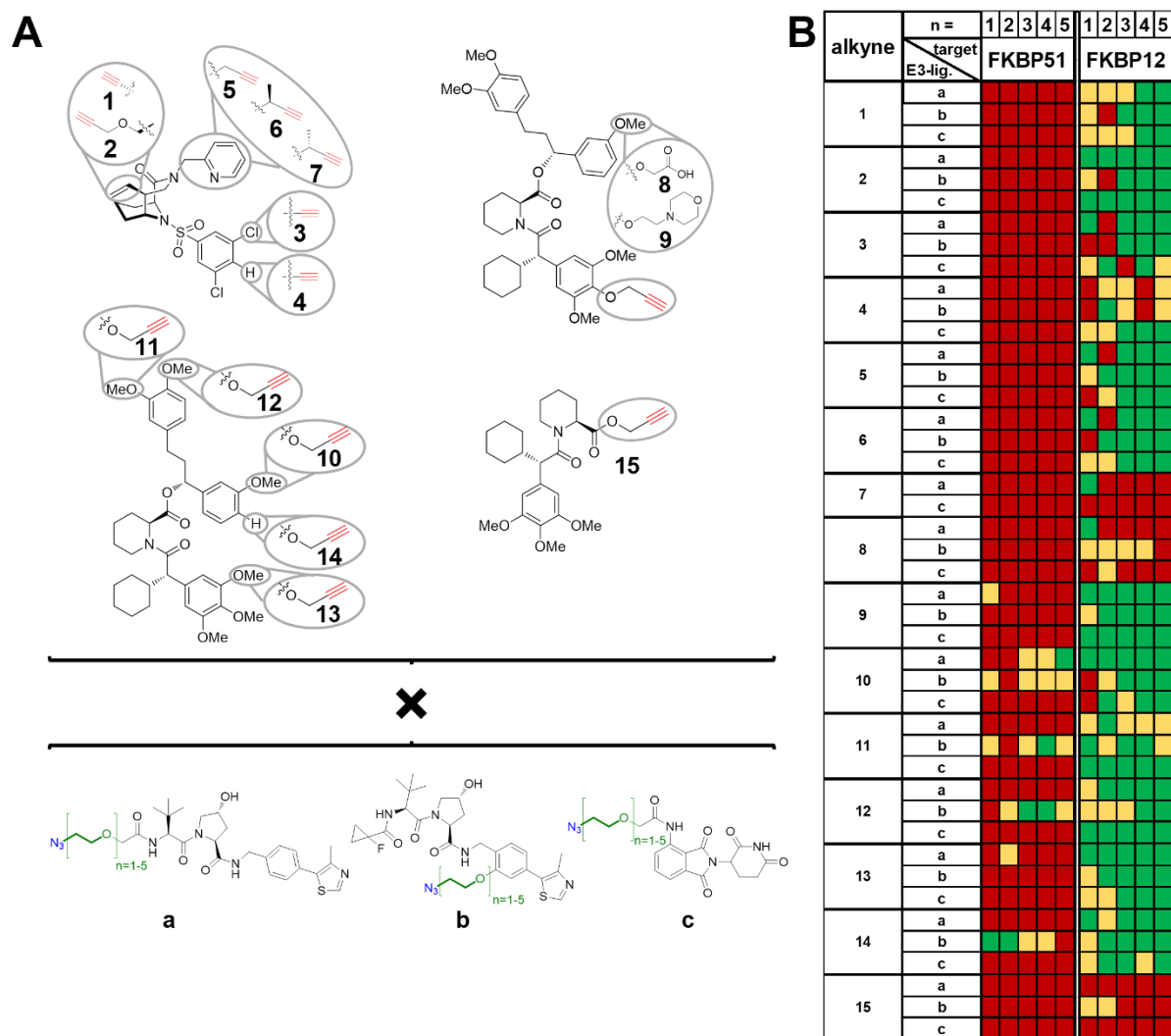


**Figure 42** Activity overview of FKBP PROTACs. **A** PROTAC candidates resulting from copper-catalysed click chemistry of alkyne-functionalized FKBP ligands (top) and azide-functionalized linker-E3 ligase ligand building blocks (bottom). **B** Degradation activity profile in FKBP51\_eGFP (transient expression) and FKBP12\_eGFP (stable expression) reporter assays (green: >50 % reporter degradation; yellow: 50-25 % reporter degradation; red < 25 % reporter degradation after 48 h treatment). PROTAC candidates were synthesized by Dr. Tianqi Mao [154] and Dr. Michael Walz [167].

Preliminarily active PROTACs were validated by western blotting for degradation of endogenous FKBP12 (Figure 43A and Figure 82) and FKBP51 (Figure 43B and Figure 81), respectively.

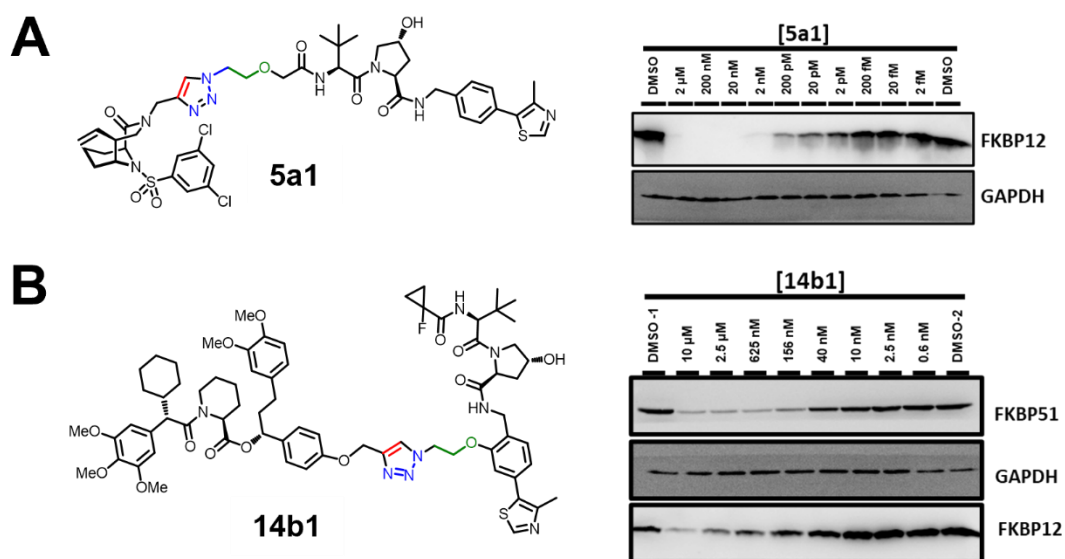


**Figure 43** Cellular activity of the initially best FKBP12 and FKBP51 PROTACs. **A** Chemical structure of PROTAC 5a1 and western blot of 5a1-dependent FKBP12 degradation (24 h treatment). **B** Chemical structure of PROTAC 14b1 and western blot of 14b1-dependent FKBP12 and FKBP51 degradation (24 h treatment).

Strikingly, the majority of PROTAC candidates efficiently degraded FKBP12 but only a small fraction of the candidates was active on FKBP51 (Figure 42B). Additionally, some PROTACs were false positive in HTRF-based FKBP52 quantification assay and could not be validated by Western blotting (Figure 83 and Figure 84). For FKBP12 PROTACs, activity was not limited to any E3 ligase ligand, linker length or FKBP ligand attachment point. In sharp contrast, active FKBP51 PROTACs showed a clear preference for SAFit-based FKBP ligands and the VHL-ligand **b**. Despite the higher preference for FKBP51 binding over FKBP12 binding of the SAFit-based scaffold, initial SAFit-based FKBP51-PROTACs retained substantial FKBP12-degrading activity. Collectively, these results demonstrate a strong degradation bias for FKBP12 over the larger FKBP51 and FKBP52. This highlights the advantage of TPD to establish a selective mode of action based on a pan-selective ligands. However, given the high similarity of FKBP12 to the FK1 domain of FKBP51 or FKBP52 this is hard to explain. Next to their size, one clear difference between FKBP12 and FKBP51 is that FKBP51 binds to Hsp90 via its TPR domain which could trap FKBP51 in degradation-resistant complexes (see Figure 2, and Figure 44A).

#### 4.6.2. Degradability assessment of FKBP51 and FKBP12 reporter swap mutants

To gain further insights into the basis of selective degradation, FKBP12/FKBP51 swap mutant reporter constructs were generated. Therefore, the FK1 domain of FKBP51 was directly fused to eGFP, reducing the size as well as abolishing the ability to associate with Hsp90. Furthermore, the FK2 and TPR domains of FKBP51 were fused to FKBP12 increasing the size and likely facilitating binding to Hsp90. The eGFP-fused mutant-constructs (Figure 44B) mimic the FKBP12-eGFP and FKBP51-eGFP reporter, respectively.

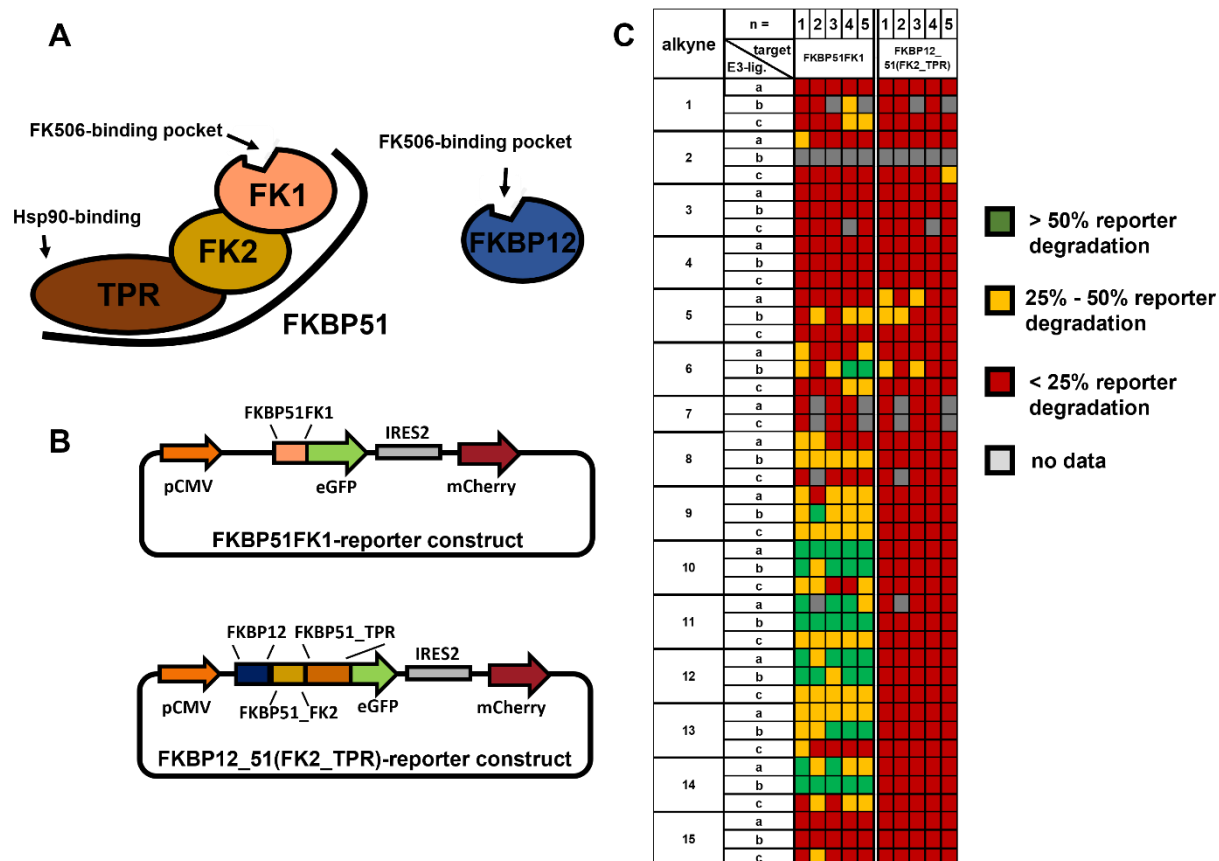


**Figure 44** Activity overview of FKBP PROTAC candidates for FKBP12/FKBP51 swap mutants. **A** Schematic representation of FKBP51 and FKBP12. **B** Visualization of the FKBP12/FKBP51 swap mutant reporter plasmids. **C** Degradation activity profile in FKBP51<sup>FK1</sup>\_eGFP and FKBP12\_FKBP51<sup>(FK2-TPR)</sup>\_eGFP reporter assays (green: >50 % reporter degradation; yellow: 50-25 % reporter degradation; red < 25 % reporter degradation after 48 h treatment).

Testing of the PROTAC candidate library for both mutant-reporter constructs (Figure 44C) revealed, that (i) the FKBP51<sup>FK1</sup> reporter is ‘easier’ to degrade than the FKBP51-full-length reporter construct; (ii) fusing FKBP51’s FK2 and TPR domain to FKBP12 strongly decreases degradability; (iii) the PROTAC series differing in linker length that featured active PROTACs for full-length FKBP51 (10a1-5, 11b1-5, 12b1-5, 14b1-5) showed also more active (green) PROTACs for the truncated construct. This indicates that the FK2 and TPR domain might block ubiquitination-productive ternary complex formation. However, it cannot be distinguished if a

---

limited rotatability of the protein by clashes of these domains and the E3 ligase or trapping of the FKBP51 or the FKBP12\_ (FKBP51FK2\_TPR) in degradation-resistant complex with Hsp90 is the reason here. Testing of a reporter construct featuring a Hsp90 binding-inactive TPR domain (FKBP51<sup>K352A</sup>) could give further insights into the role of Hsp90 binding for degradability.

### 4.6.3. Cellular characterization of FKBP12 PROTACs

Among the most efficacious FKBP12-PROTACs were compounds of series 5a and 6a (Figure 45A&B). 5a1 and 6a1 completely degraded endogenous FKBP12 ( $D_{\max} > 95\%$ ) with an  $DC_{50}$  of 20 pM (Figure 43A, Figure 82). Striking outliers in that series were compounds 5a2 and 6a2 that were degradation-inactive (Figure 45C&D).

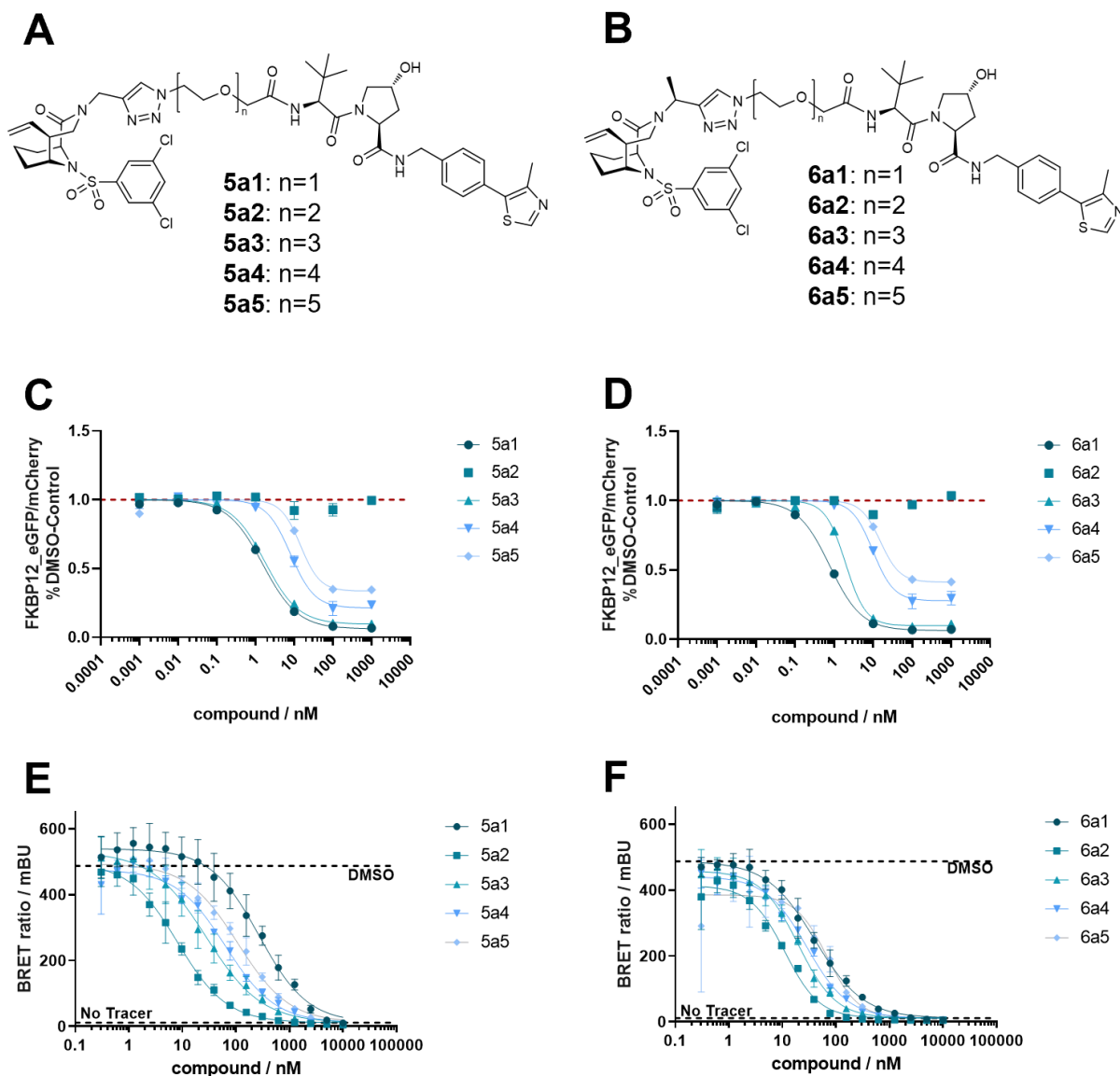


**Figure 45** Chemical structures **A** and **B** and FKBP12\_eGFP reporter degradation profiles **C** and **D** of PROTAC series 5a and 6a. Individual data points and error bars in **C** and **D** represent mean and standard deviation of biological duplicates. Compound **E** 5a1-5a5 and **F** 6a1-6a5 engage FKBP12 in living HEK293T cells stably overexpressing FKBP12-Nluc. Individual data points and error bars in **E** and **F** represent mean and standard deviation of biological triplicates. NanoBRET assays for PROTACs were performed in presence the neddylation inhibitor MLN4924 to block FKBP12-Nluc degradation.

---

Compounds of the series 5a and 6a tightly engaged FKBP12 in living cells (Figure 45E&F). Strikingly, the most potent PROTACs 5a1 and 6a1 showed the least efficient target occupation. Conversely, the degradation-inactive PROTAC candidates 5a2 and 6a2 displayed the strongest cellular target-engagement. This demonstrates 5a2 and 6a2's lack of degradation activity is not due to the lack FKBP12 binding in cells. On contrary, this could indicate that these compounds have the highest affinity for FKBP12 within their respective series. A possible reason for the degradation inactivity of 5a2 and 6a2 could be a pronounced negative cooperativity, where binary FKBP12-binding is favored over ternary complex formation. To test this hypothesis, it would be suitable to assess binding to VHL in presence and absence of FKBP12. If VHL binding is strongly decreases in presence of FKBP12, this would indicate that ternary complex formation is unfavorable and binary binding to FKBP12 is preferred. Hence, this could explain the lack of degradation activity as the ternary complex – a prerequisite for PROTAC-induced degradation – is not formed.

To establish the FKBP12-PROTACs 5a1 and 6a1 as useful chemical tools they were further characterized in mammalian cells.

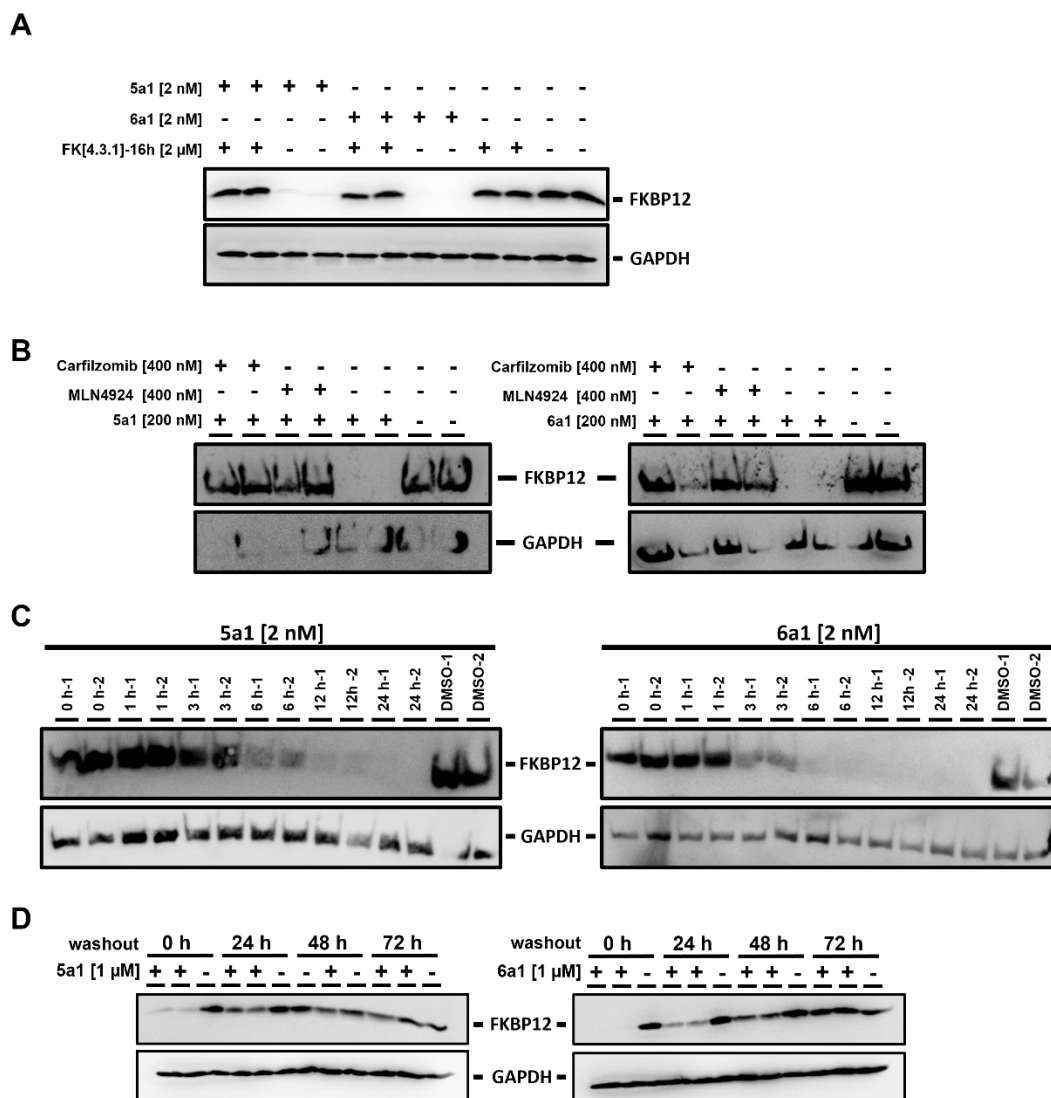


**Figure 46** Cellular characterization of 5a1 and 6a1 cells. **A** FK506-binding site and **B** neddylation as well as proteasome-dependent mode of action. **C** FKBP12 degradation kinetics of 5a1 and 6a1 in HEK293T cells. **D** Persisting effects of 5a1 and 6a1 after 24 hours treatment with 1 μM PROTAC in HEK293T cells.

5a1- and 6a1-induced degradation was blocked by the high affinity FKBP ligand FK[4.3.1]-16h [49] (Figure 46A), and by inhibition of neddylation and the proteasome by MLN4924 and carfilzomib, respectively (Figure 46B). The PROTACs achieved full degradation after 12 h and 6 h treatment, respectively, at low concentrations of 2 nM (Figure 46C) and FKBP12 levels gradually recovered after washout to normal levels after 72 h (Figure 46D).



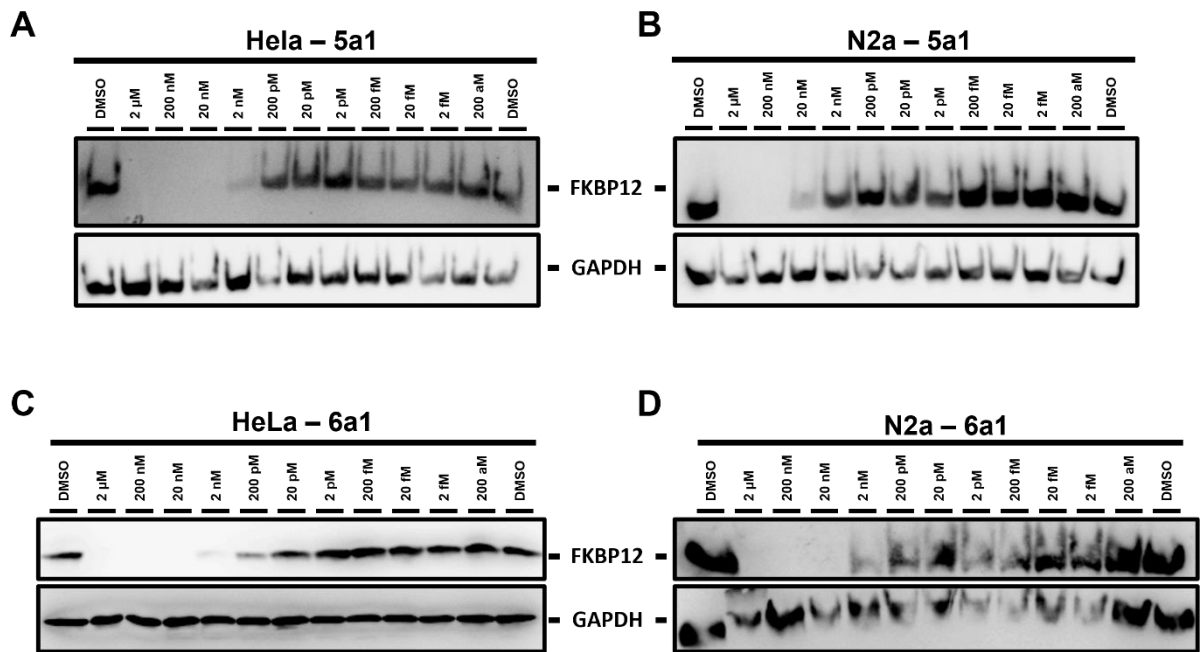


**Figure 47** Cellular activity of 5a1 and 6a1 in N2a and HeLa cells. Western blot of 5a1 and 6a1 mediated FKBP12 degradation in HeLa (A, C) and N2a (B, D) cells after 24 h treatment.

Additionally, profiling in HeLa and murine N2a cells demonstrated that 5a1 and 6a1 are active across different cell lines (Figure 47). Furthermore, quantitative proteomics confirmed the selectivity of 5a1 for FKBP12 with FKBP12 being the strongest and most significantly 5a1-downregulated protein in MOLT-4 cells (Figure 48).

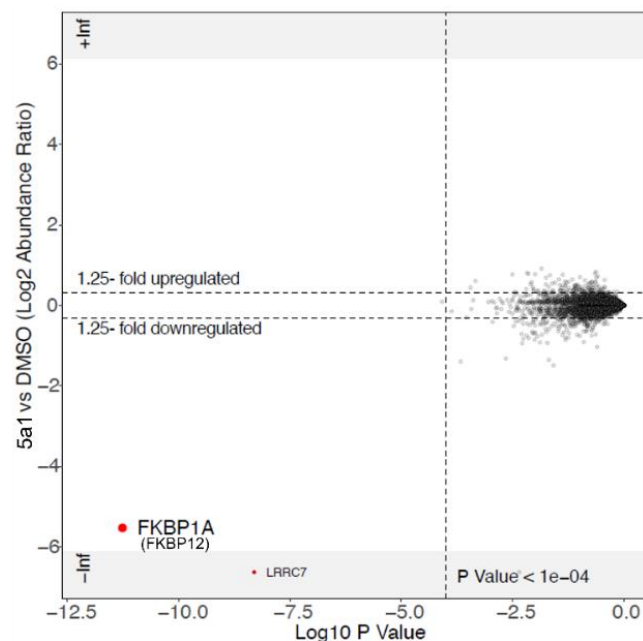


**Figure 48** Label free quantitative proteomics of MOLT-4 cell lysates after treatment (5 h) with 5a1 (1  $\mu$ M). FKBP12 (FKBP1A) is selectively degraded. +/- inf box (grey) contains proteins that were below detection level in all replicates of a specific treatment group. Global proteomics data were collected and analysed by Katherine A. Donovan, Eric S. Fischer and the Fischer Lab Degradation Proteomics Initiative.

#### 4.6.4. Optimization of first generation PROTACs yields the most selective and highly active FKBP51-PROTAC SelDeg51

Based on the slight preference for FKBP51 degradation over FKBP12, we chose 14b1 as a starting point for further optimization. In PROTAC optimization of already active PROTACs, the linker plays a key role and there are generally three strategies: (i) either the linker is evolved to further contribute to ternary complex through additional beneficial protein-linker contacts; (ii) the flexibility of the linker is reduced to preselect an ‘active’ conformation or to limit the degrees of freedom and hence reduce the entropic loss upon ternary complex formation; (iii) fine tuning of the linker length to improve ternary complex formation.

We explored systematic linker branching through addition of methyl groups to limit linker flexibility as well as fine-tuning the linker length by linker elongation through the insertion of one or two carbon atoms (Figure 85A). Dr. Michael Walz synthesized all 14b1 analogs [167].

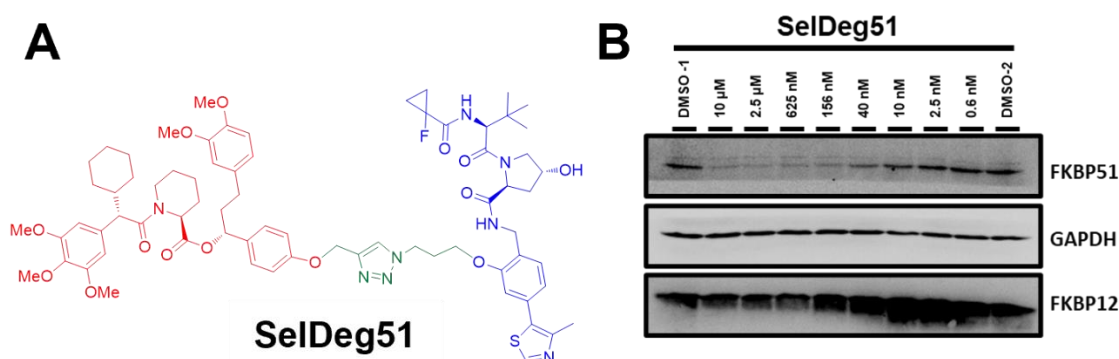


**Figure 49** Identification and binding mode of SelDeg51. **A** Chemical structure of SelDeg51 (red: FKBP ligand; green: linker; blue: VHL ligand). **B** SelDeg51-mediated FKBP51 and FKBP12 degradation after 24 h treatment of HEK293T cells. SelDeg51 was synthesized by Dr. Michael Walz.

Linker branching and insertion of two carbon atoms did not improve FKBP51 degradation efficacy (Figure 85B), but insertion of a single carbon atom yielded the Selective Degrader of FKBP51 (SelDeg51) (Figure 49A) with slightly improved cellular activity and a higher selectivity (Figure 49B). To establish SelDeg51 as a useful chemical tool I characterized the PROTAC in mammalian cells.

#### 4.6.5. Cellular characterization of SelDeg51

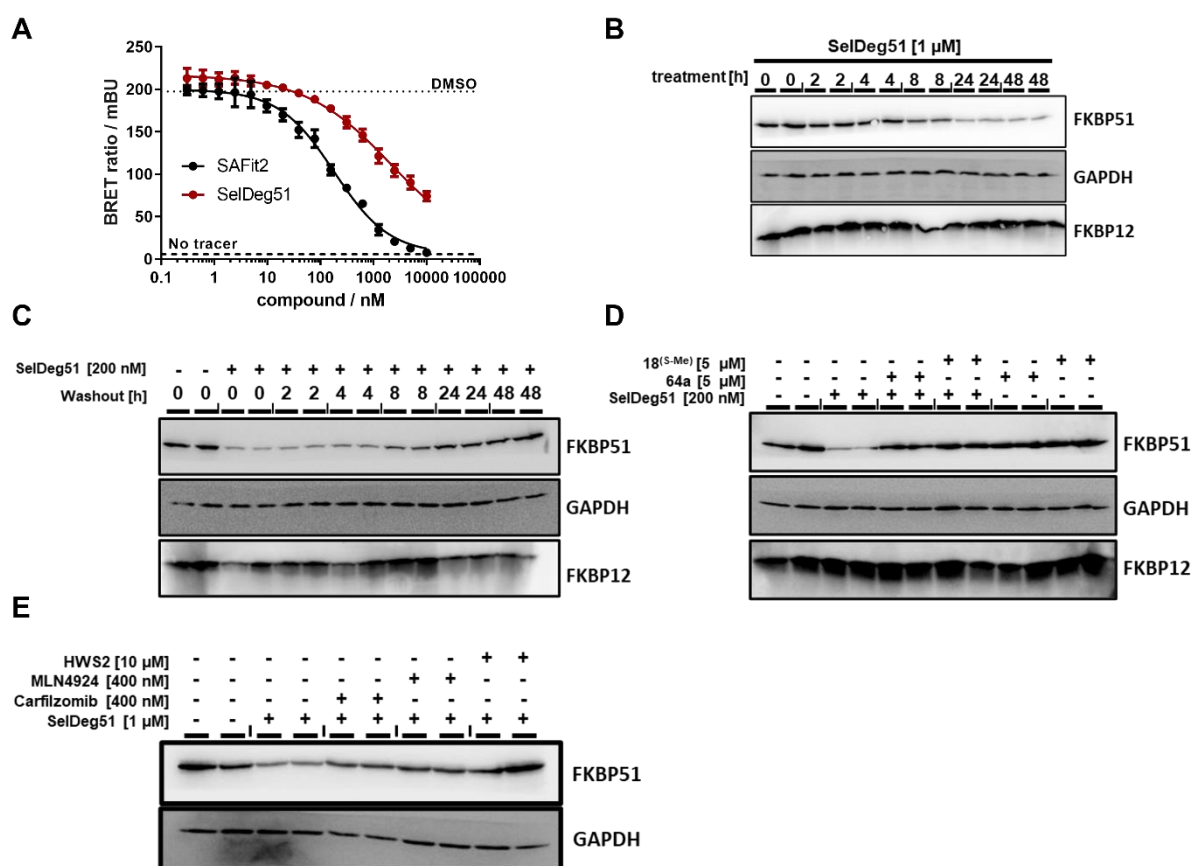


**Figure 50** Cellular characterization of SelDeg51. **A** SelDeg51 engages FKBP51 in living HEK293T cells stably overexpressing FKBP51<sup>FK1</sup>-Nluc. Individual data points and error bars in **A** represent mean and standard deviation of biological triplicates. NanoBRET assays for PROTACs were performed in presence the neddylation inhibitor MLN4924 to block FKBP51<sup>FK1</sup>-Nluc degradation **B** FKBP51 and FKBP12 degradation kinetics of SelDeg51 in HEK293T cells. **C** Persisting effects of SelDeg51 after washout. **D** FK506-binding site occupation and **E** VHL as well as proteasome and neddylation inhibition rescue degradation during 24 h and 8 h, respectively.

SelDeg51 engaged FKBP51 in living cells with an  $IC_{50}$  values of  $2160 \pm 147$  nM. Thereby, SelDeg51 displayed a lower potency (approx. 10-fold) than the parent FKBP51 ligand SAFit2 with an  $IC_{50}$  value of  $182 \pm 13$  nM in competitive FKBP51 NanoBRET assays (Figure 50A). This might be due to the bi-functional nature and hence larger size of the PROTAC compared to the parent ligand. The PROTAC achieved maximal degradation after 24 h at a concentration of  $1 \mu\text{M}$  (Figure 50B) and FKBP51 levels gradually recovered to normal levels after 24 h after washout (Figure 50C). Co-treatment with an excess of the FKBP ligands 18<sup>(S-Me)</sup> [49] and 64a [57] or the VHL ligand HWS2 blocked SelDeg51 mediated degradation (Figure 50D&E). Therefore, the expected mode of action of SelDeg51 was confirmed as FKBP51- and VHL-binding dependent. Additionally, both neddylation inhibition by MLN4924, which blocks cullin-Ring E3 ligase activity, and proteasome inhibition by Carfilzomib rescued degradation (Figure 50E). This confirmed a neddylation and proteasome dependent mode of action.

Furthermore, quantitative proteomics confirmed the selectivity of SelDeg51 with FKBP51 being the only significantly SelDeg51-downregulated protein in MOLT-4 cells (Figure 51).

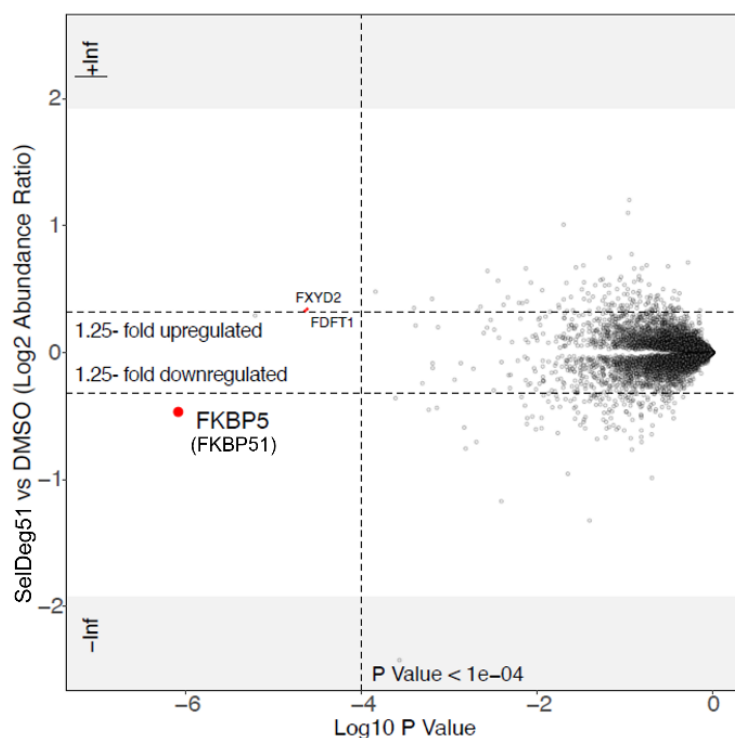


**Figure 51** Label free quantitative proteomics of MOLT-4 cell lysates after treatment (5 h) with SelDeg51 (1  $\mu$ M). FKBP51 (FKBP5) is selectively degraded. +/- inf box (grey) contains proteins that were below detection level in all replicates of a specific treatment group. Global proteomics data were collected and analysed by Katherine A. Donovan, Eric S. Fischer and the Fischer Lab Degradation Proteomics Initiative.

Taken together, these results establish SelDeg51 as useful chemical tool and confirm that FKBP51 is downregulated through PROTAC mediated degradation and not through off target effects or cytotoxicity.

---

#### 4.6.6. Cellular effects of FKBP51-degrading PROTACs surpass conventional ligands.

The Hsp90 cochaperone FKBP51 is a key regulator of steroid hormone signaling. During the course of this thesis, the structural basis of this regulation for the GR as a model system has been investigated by cryo-EM [168] and crosslinking [165] studies. These studies demonstrated that the FKBP51-GR interface extends from the FK1 domain to the tip of the TPR domain of FKBP51. Furthermore, it was demonstrated that (i) synthetic FKBP ligands engage FKBP51 in living cells (see chapter 4.2.3); (ii) remodel but not disrupt the FKBP51:apoGR:Hsp90 complex [165] and (iii) do not reactivate GR signaling (see chapter 4.3). This led to the conclusions (i) that the FK506-binding site is dispensable for GR regulation, (ii) synthetic FKBP ligands are functionally silent and (iii) that FKBP51 inhibits GR signaling through its scaffolding functionality. PROTACs degrade the target protein and consequently target all protein functions. To test if PROTAC-mediated FKBP51 degradation would target FKBP51's scaffolding function and relieve its inhibitive pressure on the GR, I assessed the ability of SelDeg51 to restore GR signalling in a GR reporter gene assay (Figure 52A).

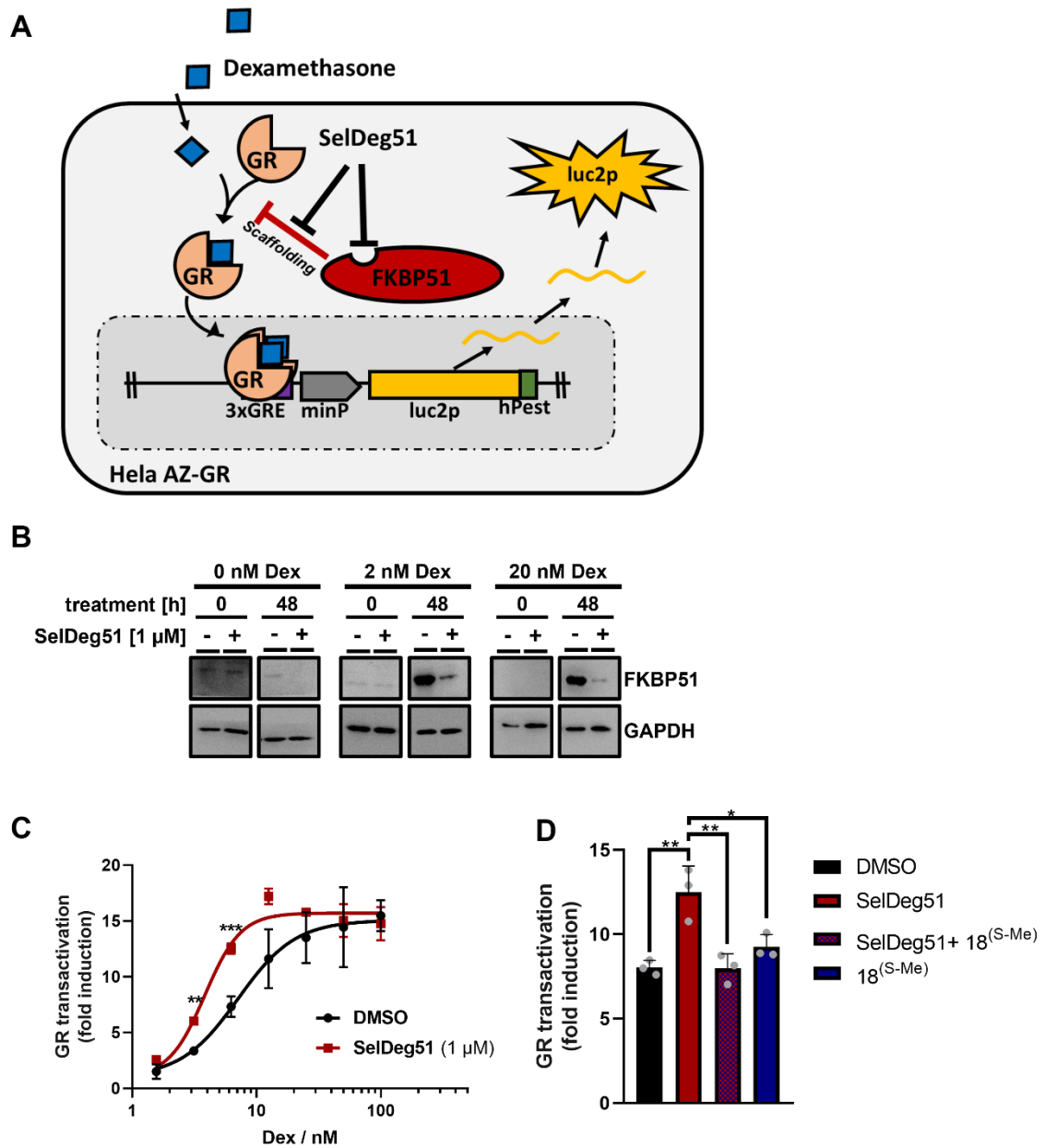


**Figure 52** SelDeg51 targets FKBP51's scaffolding function and reactivates glucocorticoid receptor signaling. **A** Schematic visualization of the glucocorticoid reporter gene assay in HeLa AZ-GR cells [161]. Stimulation of the GR by dexamethasone (Dex) results in expression of a luciferase (luc2p) which is controlled by glucocorticoid response elements (GRE). FKBP51 inhibits the GR through scaffolding, while the FK506-binding site not essential in that context. Luciferase expression is indicative of GR activation. **B** FKBP51 levels are robustly increased by dexamethasone treatment (Dex) and are efficiently diminished by SelDeg51 co-treatment. Full blots are depicted in Figure 86. **C** SelDeg51-mediated (1  $\mu$ M) FKBP51 degradation reactivates GR signaling in reporter gene assays in HeLa AZ-GR cell during 48 h co-treatment with Dex. **D** SelDeg51-mediated (250 nM) FKBP51 degradation but not FKBP ligands (2.5  $\mu$ M) reactivate GR-signalling in GR reporter gene assays during 48 h co-treatment with 6.25 nM Dex in HeLa AZ-GR cells. Luminescence values were normalized to the mean of the unstimulated control (no Dex, no compound/PROTAC) to yield fold induction values. Individual data points and error bars in C and D represent mean and standard deviation of three biological replicates. Asterisks indicate significance (\*:  $p < 0.05$ ; \*\*:  $p < 0.01$ ; \*\*\*:  $p < 0.001$ ).

---

In this reporter gene assay, luciferase (luc2p) expression is controlled by glucocorticoid response elements (GRE) resulting in induction after GR stimulation with dexamethasone. Therefore, luciferase levels are indicative for GR activation (Figure 52A) and can be easily assessed by luminescence measurements upon luciferase substrate addition. Moreover, *FKBP5* expression is also induced by the GR. FKBP51 negatively regulates GR signaling (see chapter 4.3), which constitutes an ultra-short negative feedback loop. Indeed, FKBP51 expression can be robustly induced by dexamethasone (Dex) during the 48 hours treatment. Importantly, Dex-stimulated FKBP51 levels can be drastically reduced by co-treatment with SelDeg51 (Figure 52B and Figure 86). Thereby, SelDeg51-mediated degradation of FKBP51 removed the inhibitory effect of FKBP51 on the GR and increased the sensitivity to Dex without influencing the maximal observed GR-activation (Figure 52C). As shown before (Figure 32), the FKBP ligand 18<sup>(S-Me)</sup> alone did not influence GR signalling, but it abrogated SelDeg51-mediated FKBP51 degradation (see Figure 50D) and the effect of SelDeg51 on GR signaling (Figure 52D).

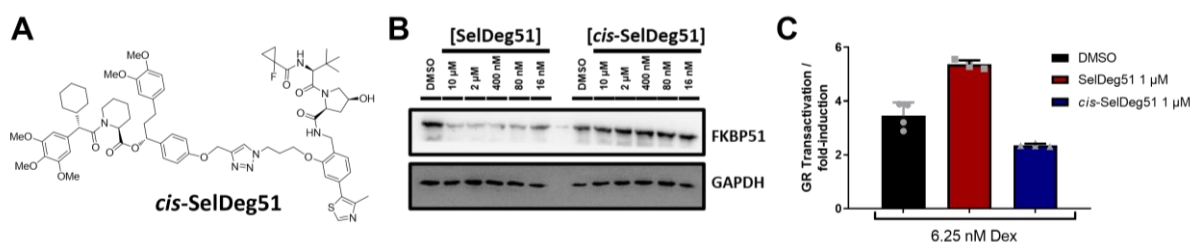


**Figure 53** Degradation-inactive *cis*-SelDeg51 does not target FKBP51's scaffolding function. **A** Chemical structure of *cis*-SelDeg51; **B** SelDeg51 but not *cis*-SelDeg51 degrades FKBP51 in HEK293T cells, and **C** reactivates GR-signaling in GR-reporter gene assays in HeLa AZ-GR cells. *Cis*-SelDeg51 was synthesized by Dr. Min Zheng.

As a further control, I tested *cis*-SelDeg51 (Figure 53A), that features an inverted stereocenter on the hydroxyproline moiety of the VHL ligand which abrogates VHL but not FKBP51 binding. This FKBP51 degradation-inactive compound *cis*-SelDeg51 (Figure 53B) also did not reactivate GR signaling in reporter gene assays (Figure 53C).

Taken together the results demonstrate that (i) synthetic high affinity FKBP ligands are functionally silent on GR signaling; (ii) but the potent FKBP51 PROTAC SelDeg51 is functionally active; (iii) the effects of SelDeg51 can be blocked by FKBP ligands; and (iv) the effects of SelDeg51 are mediated by FKBP51-degradation and not by binding alone. The experiments prove that degradation outperforms mere inhibition in this system and demonstrate that functionally silent binding pockets can still be used. This was achieved by switching from an occupation-driven strategy to an event-driven pharmacology by turning functionally silent small molecule ligands into an active PROTAC. While this possibility has been hypothesized for a long time, examples demonstrating a such fundamentally enhanced pharmacology of PROTACs compared to their parent ligands have been rare [117,143–145].



## 4.7. Cellular discovery of FKBP12-degrading molecular glues

Historically, degradative molecular glues have been rare and were mostly discovered serendipitously. Their rational discovery for desired targets still represents a major challenge. The high degradability of FKBP12 (see chapter 4.6.1) and that nature repeatedly resorted to FKBP12 to enable natural molecular glues (see chapter 3.2.1) indicate FKBP12 as an ideal model system to discover molecular glue degraders. Target focused libraries bear the possibility to contain molecular glues that in case of glueing E3 ligases can lead to target degradation (Figure 54). To test this hypothesis, I tested a FKBP-focused library for FKBP12-degrading molecular glues.

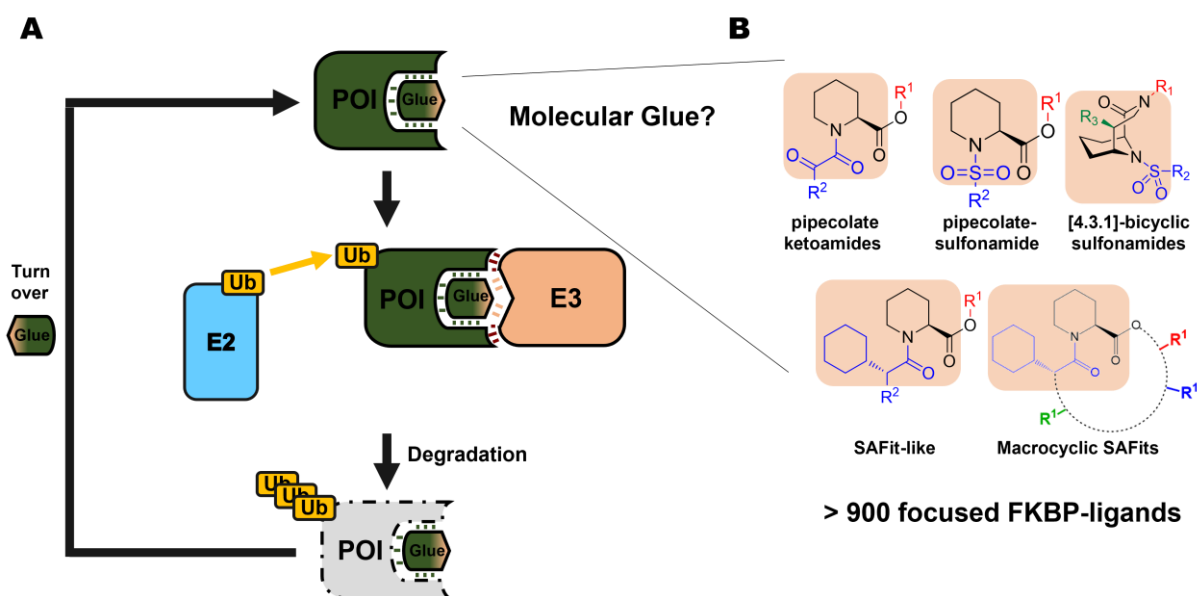


**Figure 54** Cellular identification of degrading molecular glues from focused libraries. **A** Target focused degradative molecular glues bind the protein of interest (POI). In favourable cases the solvent exposed parts of the ligand may recruit the binary complex to a E3 ligase. The POI may then be ubiquitinated and degraded, releasing the molecular glue to act catalytically. **B** Focused in-house FKBP ligand library of the Hausch lab.

#### 4.7.1. Cellular screening of a FKBP-focused ligand library for FKBP12-degrading molecular glues

The Hausch lab has assembled over the years a FKBP-focused library containing over 900 compounds that tightly bind FKBP12. Using the established fluorescent FKBP12\_eGFP level reporter assay (see chapter 4.4) the library was screened for FKBP12-degrading molecular glues in a cellular system (Figure 55).

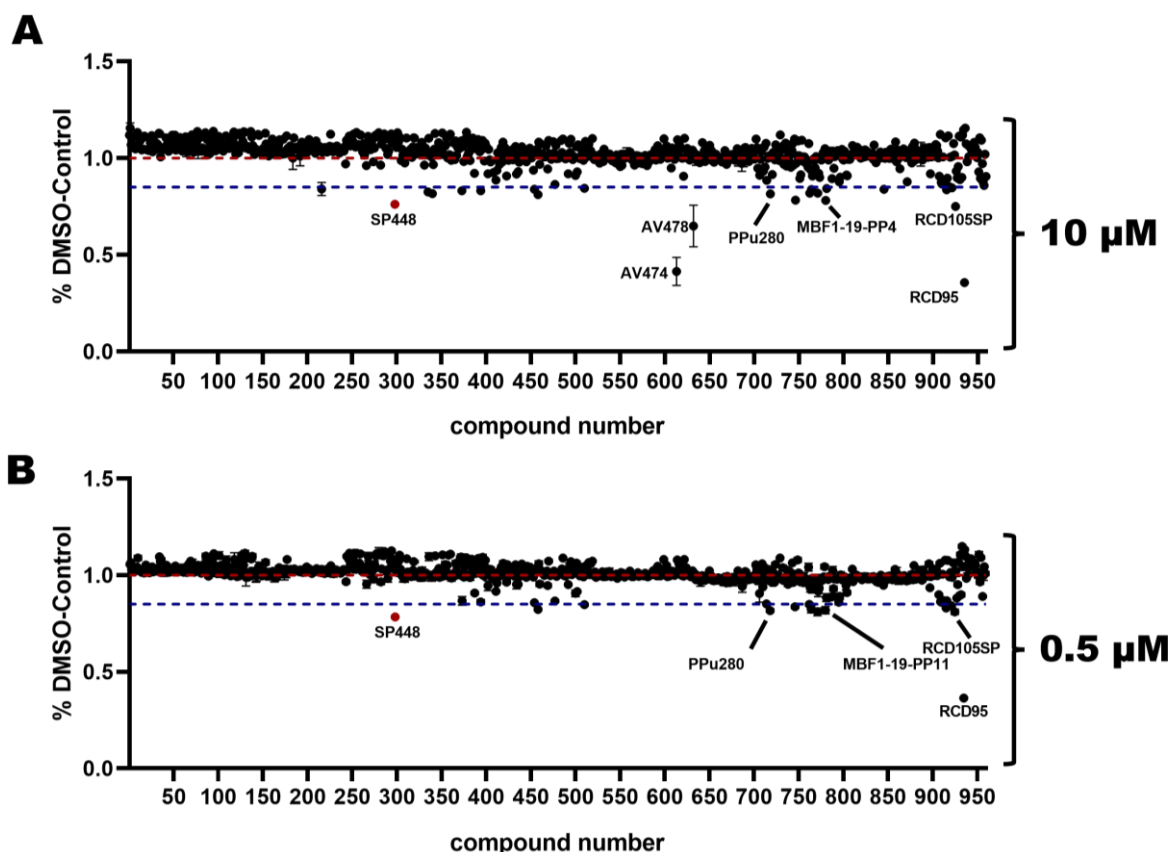


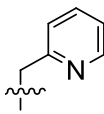
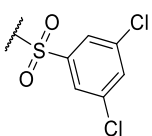
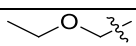
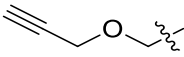
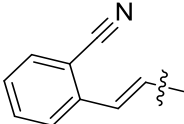
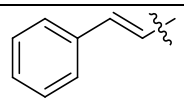
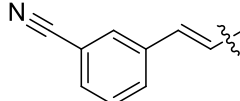
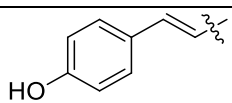
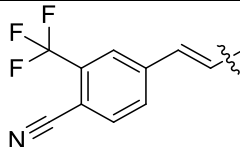
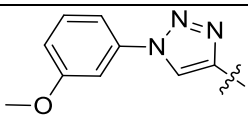
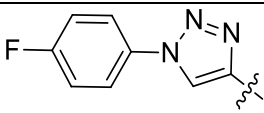
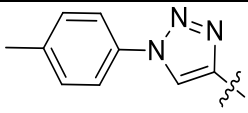
**Figure 55** Cellular screening of a FKBP-focused ligand library for FKBP12 degrading molecular glues. Several compounds induce FKBP12\_eGFP degradation in FKBP12\_eGFP reporter cells after 48 h treatment at **A** 10  $\mu$ M or **B** 0.5  $\mu$ M. Red dashed line represents mean of the DMSO control; blue dashed symbolizes an arbitrary 15% activity cut-off. Individual points and error bars represent the mean and standard deviation of independent biological duplicates. eGFP/mCherry ratios were normalized to the eGFP/mCherry ratio of the DMSO controls. The original eGFP and mCherry fluorescence data are provided in Figure 87.

Several FKBP ligands decreased the FKBP12\_eGFP/mCherry ratios compared to the DMSO control in FKBP12\_eGFP level reporter assays after 48 hours treatment (Figure 55). Compounds that induced degradation > 15% were regarded as hits and further profiled. AV474 and AV478 were not further investigated as they strongly decreased mCherry levels in addition to FKBP12\_eGFP levels likely indicating cytotoxicity (Figure 87C).

#### 4.7.2. SAR and optimization of FKBP12-degrading molecular glues

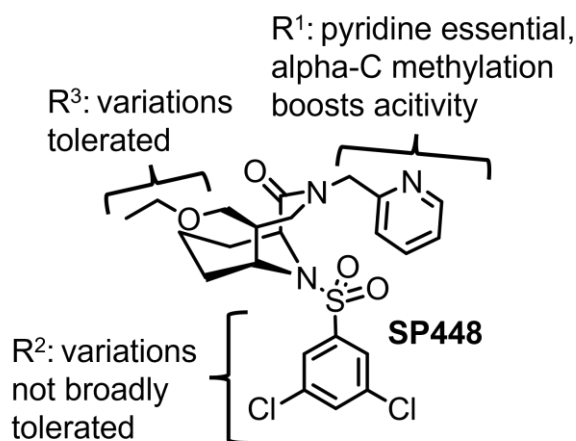
The primary hits from the initial screening and close analogs thereof (JK095, JK096, JK236) as control compounds were tested in dose-response experiments (Table 3 and Figure 88).

**Table 3** Chemical structures and activity in FKBP12\_eGFP level reporter assays of hits from the initial screening and close analogs thereof. Maximal achieved degradation ( $D_{max}$ ) and half maximal degradation ( $DC_{50}$ ) values were determined by a four-parameter fit. Corresponding dose-response curves are depicted in (Figure 88). JK095, JK096, JK236 were no hits in the initial screen and were included as controls.

Name	R1	R2	R3	$DC_{50}$ / nM	$D_{max}$ / %
SP448				16	24
MWa066				28	30
RCD14				20	12
RCD105SP				245	31
RCD3				23	13
RCD6				36	13
JK389				27	15
MFB1-19-P11				45	20
MBF1-19-PP4				38	14
MBF1-19-PP7				27	16

Name	R1	R2	R3	DC <sub>50</sub> / nM	D <sub>max</sub> / %
PPu280				23	17
MBF1-19-PP5				64	15
MBF1-19-PP10				28	14
RCD105SP				245	31
SP693				112	12
SP690				102	13
JK158				97	15
RCD95				-	< 5%
JK095/JK384				-	< 5%
JK236/PPu554				-	< 5%
JK096				-	< 10%
JK237				44	21

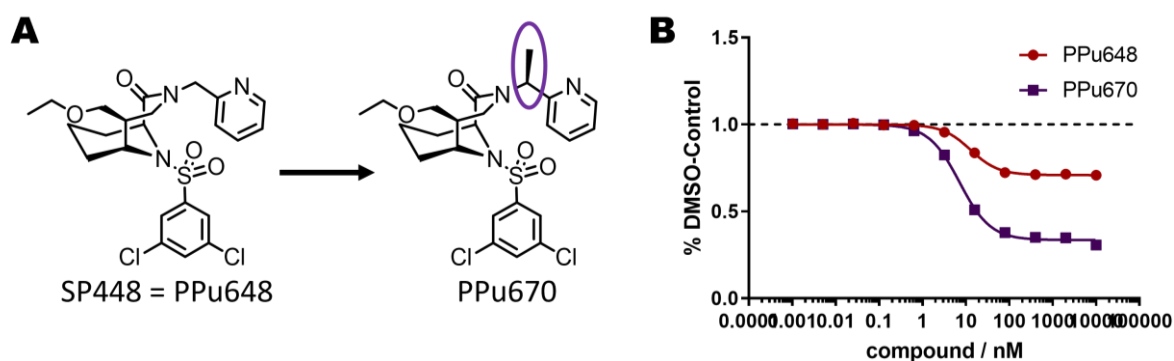
All hits from the initial hits except RCD95, which appeared to be a false primary positive hit, degraded the FKBP12\_eGFP reporter in dose-responsive manner.



**Figure 56** Initial summary of structure affinity relationship for FKBP12\_eGFP degrading molecular glues.

Initial structure-activity analysis (Figure 56 and Table 3) of the confirmed hits showed that (i) variations in the R<sup>3</sup> position were well tolerated. However, truncation to a free hydroxyl group abrogated activity as demonstrated by the JK236/JK237 analog pair; (ii) the pyridine moiety in R<sup>1</sup> appears to be essential; and (iii) the alpha-C methylation in S-configuration in R<sup>1</sup> can enable or boost activity as evidenced by the analog pair JK096 and JK237 that only differs in their R<sup>1</sup> alpha-C methylation status. Notably, R<sup>1</sup> alpha-C methylation boosts the affinity of the ligands for FKBP12 approximately by a factor of three [51]. (iv) R<sup>2</sup> substitutions are not broadly tolerated.

Based on the good activity and simplicity of its R<sup>3</sup> position, SP448 was chosen as a lead compound for further optimization over compounds with similar activity. The compound was resynthesized by Dr. Patrick Purder yielding PPU648. Based on the initial SAR findings he also installed a methyl group in S-configuration in the R<sup>1</sup> C-alpha position resulting in PPU670 (Figure 57).

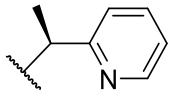
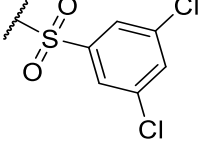
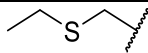
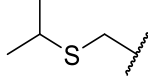
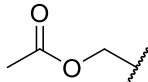
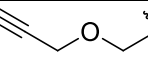
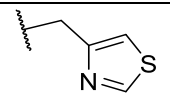
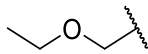
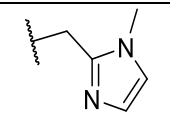
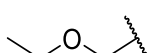


**Figure 57** Addition of a methyl group in S-configuration in the R<sup>1</sup>-C-alpha of SP448 yields compound PPU670 with increased potency in FKBP12\_eGFP level reporter assays. Dashed line indicates mean of the DMSO control. Individual data points and error bars represent mean and standard deviation of biological duplicates. Dr. Patrick Purder synthesized PPU648 and PPU670.

Addition of the methyl group in R<sup>1</sup> C-alpha position doubled the efficacy of PPU670 compared to the parent compound PPU648. In an attempt to further optimize the compound, Johannes Dreizler synthesized a library of 19 PPU670 analogs two of which not having the pyridine in R<sup>1</sup>.

**Table 4** Chemical structures and activity in FKBP12\_eGFP level reporter assays of focused PPU670 analogs. Maximal achieved degradation (D<sub>max</sub>) and half maximal degradation (DC<sub>50</sub>) values were determined by a four-parameter fit. Corresponding dose-response curves are depicted in (Figure 89). PPU670 analogs were synthesized by Johannes Dreizler.

Name	R1	R2	R3	DC <sub>50</sub> / nM	D <sub>max</sub> / %
PPu648				13	30
PPU670				7	66
JKD421				3	63
JKD428				7	23
JKD429				5	53
JKD437				15	36
JKD441				-	< 5%
JKD444				-	< 5%
JKD445				12	52
JKD446				15	45
JKD452				20	64
JKD453-1				17	48
JKD453-2				5	44
JKD464				22	51
JKD473				35	39

Name	R1	R2	R3	DC <sub>50</sub> / nM	D <sub>max</sub> / %
JKD477				18	56
JKD478				17	49
JKD480				18	22
JKD633				6	53
JKD525				-	< 5%
JKD548				-	< 5%

R<sup>3</sup> variations did not further improve FKBP12\_eGFP reporter degradation activity, but two PPU670 analogs (JKD421 and JKD452) displayed similar degradation efficacy. Taken together these results yield a more refined SAR for the R<sup>3</sup> position and show that (i) small aliphatic groups are tolerated if they are not too short as in JKD444; (ii) branching is generally disfavored; (iii) ether to thioether substitutions as in PPU670 compared to JKD477 are well tolerated; (iv) substitutions of the pyridine in R<sup>1</sup> to a thiazole or a substituted imidazole as in JKD525 and JKD548, respectively, abolished activity. This further strengthened the hypothesis that the pyridine moiety is essential.

### 4.7.3. Mechanistic insights in the mode of action

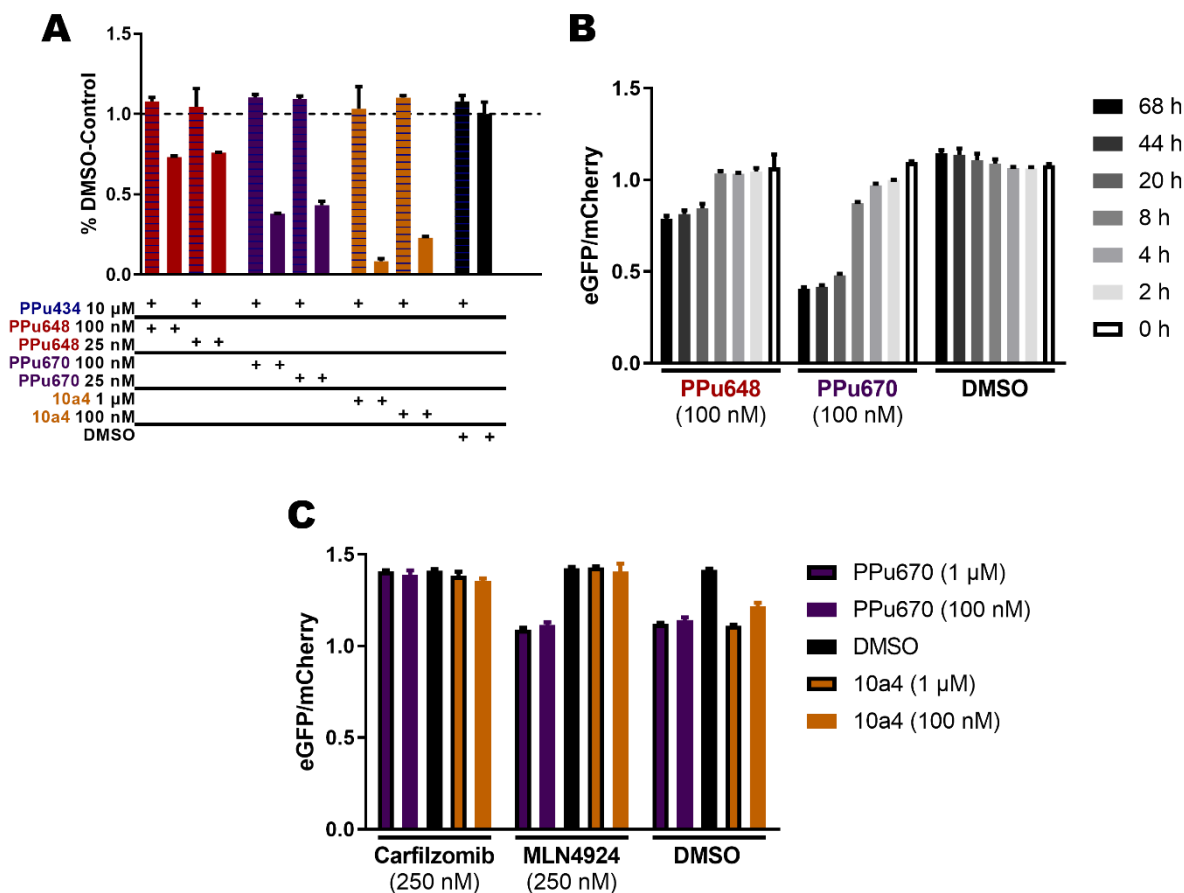


**Figure 58** Cellular characterization of PPU670's mode of action. **A** PPU670-mediated FKBP12\_eGFP reporter is FK506-binding site and **C** proteasome but not neddylation dependent. **B** PPU648 and PPU670 gradually reduce FKBP12\_eGFP reporter levels over time. FKBP12\_eGFP reporter cells were treated with the indicated compound concentrations for 48 h in A and 8 h in C. Bars and error bars indicate mean and standard deviation of biological quadruplicates.

Competition experiments with a high excess of the degradation-inactive high affinity FKBP12 ligand PPU434 revealed that the mode of action of the FKBP12\_eGFP degrading molecular glues is FK506-binding site dependent (Figure 58A). PPU648 or PPU670-mediated degradation could be rescued with an excess of PPU434 (Figure 58A). As a positive control, the PROTAC 10a4 was tested side-by-side. Both PPU648 and PPU670 gradually reduced FKBP12\_eGFP reporter level over time up to a maximal effect after 44 h (Figure 58B). However, the improved efficacy of PPU670 compared to PPU648 lead to a detectable reduction of FKBP12\_eGFP reporter levels already after 8 hours (Figure 58B). This allowed investigation of proteasome and neddylation dependence through co-treatment with the proteasome inhibitor Carfilzomib or the neddylation inhibitor MLN4924. For the experiments, shorter treatment time were required as both compounds reduce cell viability after prolonged treatment. Proteasome but not neddylation inhibition blocked PPU670-mediated FKBP12\_eGFP degradation. This result indicates that the



mode of action is relying on a functional proteasome but does not depend on a functional cullin-Ring E3 ligase machinery. On the other hand, the effects of the VHL-dependent and hence cullin-Ring E3 ligase dependent PROTAC 10a4 could be potentially blocked by MLN4924.

#### 4.7.4. FKBP12\_eGFP degradation is tag-dependent

For further validation, degradation of endogenous FKBP12 by PPU648 and PPU670 was investigated.

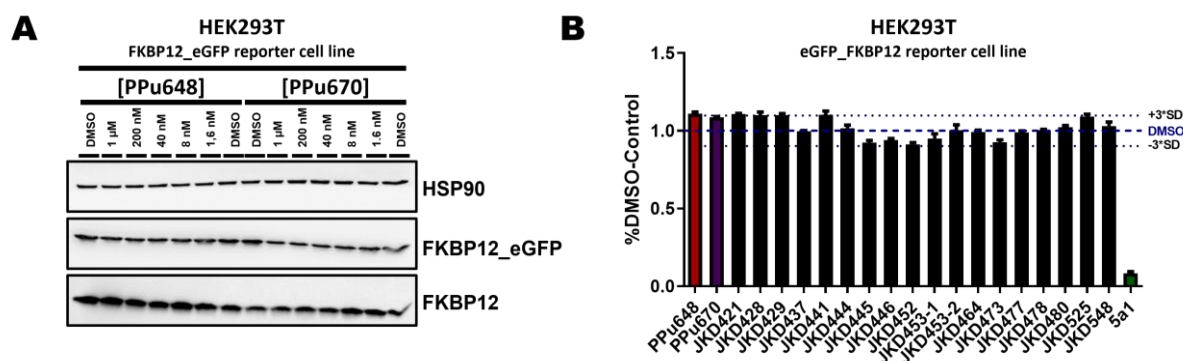


**Figure 59** Molecular glue-mediated FKBP12\_eGFP degradation is construct dependent. **A** PPU648 and PPU670 degrade FKBP12\_eGFP but not FKBP12 after 48 h treatment in the HEK293T FKBP12\_eGFP reporter cell line. **B** Focused PPU670 analogs do not degrade eGFP\_FKBP12 reporter levels after 48 h treatment in the HEK293T FKBP12\_eGFP reporter cell line. Bars and error bars represent mean and standard deviation of biological duplicates normalized to the DMSO control mean. Dashed and dotted lines represent mean and mean  $\pm 3 \times$  standard deviation of the DMSO control ( $n = 9$ ).

Unfortunately, Western blot analysis revealed that endogenous FKBP12 levels were not affected by PPU648 and PPU670 while the FKBP12\_eGFP reporter levels were slightly decreased upon treatment (Figure 59A). In order to validate this finding, an orthogonal but similar FKBP12 reporter assay was established by switching the orientation of FKBP12 and eGFP. Therefore, a stable eGFP\_FKBP12 (N-terminally eGFP-tagged FKBP12) reporter cell line was established (Figure 90). Using the eGFP\_FKBP12 reporter cell line, the focused library of PPU670 analogs (depicted in Table 4) was tested for reporter degradation. None of the tested compounds degraded the eGFP\_FKBP12 degrader construct, while the control PROTAC (5a1) was still active (Figure 59B). This indicated that the PPU670-mediated degradation is specific for the FKBP12\_eGFP reporter construct.

Yet, it was decided to continue with E3 ligase deconvolution as E3 ligases that can be targeted by molecular glues are rare and highly sought after in the TPD community.

#### 4.7.5. Elucidation and validation of UBR3 as the relevant E3 ligase

Genome-wide CRISPR screens provide an excellent strategy for target deconvolution if the phenotype can be translated into a fluorescence readout as in the case of our fluorescent FKBP12\_eGFP reporter assay in which eGFP fluorescence is reduced upon FKBP12\_eGFP degrader treatment. However, HEK293T cells have a complex karyotype with two or more copies of each chromosome [169] rendering them less suited for CRISPR screens. Therefore, the FKBP12\_eGFP-IRES2-mCherry construct was cloned into a lentiviral vector and a stable RPE1 FKBP12\_eGFP level reporter cell line was generated. RPE1 cells feature a near-diploid karyotype [170] and are more suitable for CRISPR screens.

Lentiviral FKBP12\_eGFP reporter vector and stable RPE1 cell line generation was performed by Dr. Yves Matthes.

I analyzed the PPU670-mediated FKBP12\_eGFP degradation to confirm that the compound is still active in RPE1 cells. Molecular glues can possess tissue or cell line specificity depending on the expression of the E3 ligase in the respective tissue or cell line (Figure 60).

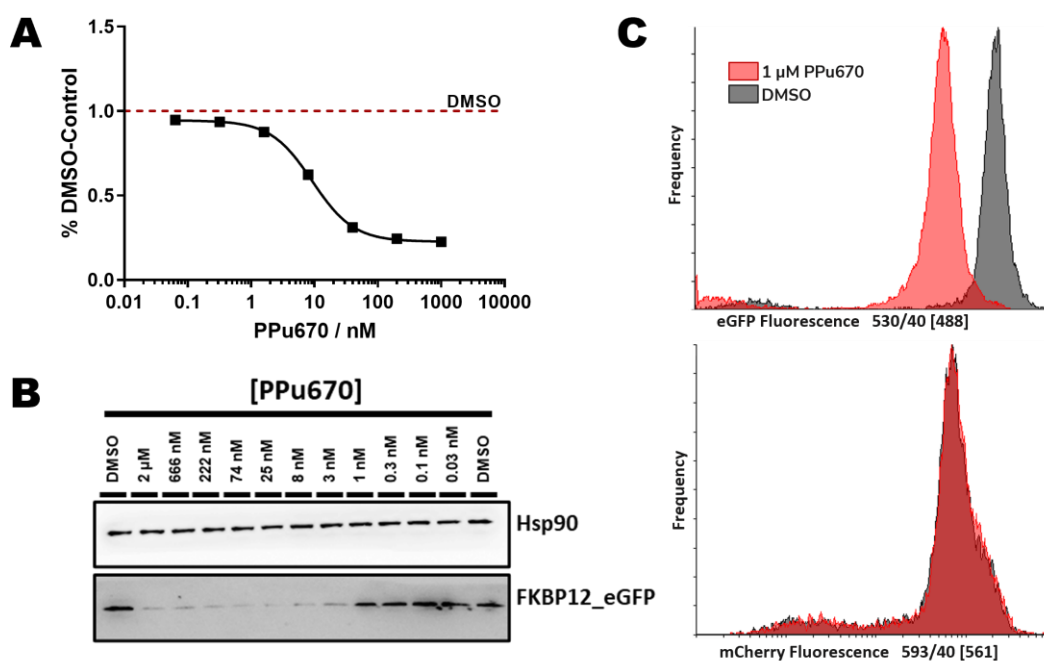


**Figure 60** PPU670 efficiently degrades FKBP12\_eGFP in RPE1 cells. FKBP12\_eGFP degradation analysed by fluorescence quantification **A**, by western blot **B** and in FACS assays **C** after 48 hours treatment. Individual points and error bars in **A** represent mean and standard deviation of biological duplicates. Flowcytometry images are depicted in Figure 91 and Figure 92. Lentiviral FKBP12\_eGFP-IRES2-mCherry vector and stable RPE1 reporter cell line generation were performed by Dr. Yves Matthes.

---

PPu670 degraded the FKBP12\_eGFP reporter in RPE1 cells with even greater potency compared to HEK293T FKBP12\_eGFP reporter cells (compare Figure 57 and Figure 59A to Figure 60A&B). This effect could be due to a higher expression of the relevant E3 ligase in RPE1 cells compared to HEK293T cells. Furthermore, FACS analysis showed almost baseline separated populations in treated versus untreated RPE1 reporter cells in the eGFP channel while mCherry levels were not affected (Figure 60C). Hence, the assay was suitable to conduct a genome-wide CRISPR screen to identify the relevant E3 ligase. Additionally, RPE1 reporter cells were analysed for degradation of endogenous FKBP12 upon PPU670 treatment. However, like in HEK293T cells endogenous FKBP12 levels remained unaffected (Figure 93).

The RPE1 reporter cell line was previously engineered to express Cas9. To deconvolute the relevant E3 ligase a genome-wide CRISPR screen was conducted. In brief, RPE1 reporter cells were transduced with an in-house genome wide sgRNA library enabling a puromycin resistance and featuring four sgRNAs per gene at a multiplicity of infection (MOI) of 0.5 and selected for puromycin resistance. Cell populations ( $8 \times 10^6$  cells corresponding to a 100-fold coverage of every sgRNA in the population) were treated with 1  $\mu$ M PPU670 for 48 hours. In the following, degradation-resistant (high eGFP) and degradation-sensitive (low eGFP) cells were gated and collected by FACS, while simultaneously gating for mCherry expression. Afterwards, the collected cells were amplified, NGS amplicons were generated, purified, and then quantified by next generation sequencing (NGS). Using MAGeCK, sgRNA enrichment was analysed for the respective high and low eGFP gates. The genome-wide CRISPR Screen including the following steps to next generation sequencing were performed by Dr. Yves Matthess. Data analysis was performed by Dr. Martin Wegner.

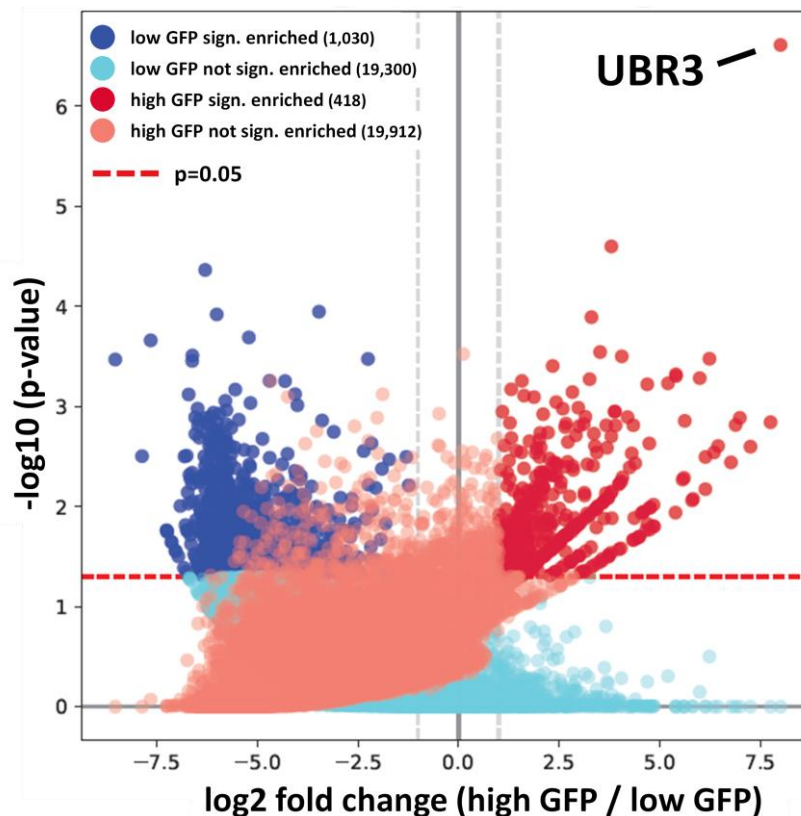


**Figure 61** Genome-wide CRISPR screening reveals UBR3 as the relevant E3 ligase. sgRNA enrichment was collapsed to gene level (4 sgRNA/gene) and calculated with MAGeCK. Red/orange and corresponding dark/light blue points indicate significance for log<sub>2</sub> fold enrichment of the respective gene in the high eGFP (red/orange) or in the low GFP gate (dark/light blue). Vertical dashed lines indicate a log<sub>2</sub>-fold change of -1 and 1 respectively. Red horizontal dashed line indicates a significance-threshold of  $p = 0.05$ . The genome-wide CRISPR Screen and statistical analysis of the NGS data set were performed by Dr. Yves Matthes and Dr. Martin Wegner, respectively.

The E3 ligase UBR3 was the most significant and most strongly enriched gene in the high GFP gate (log<sub>2</sub> fold change of approx. 8). This indicates that a UBR3 knock-out conferred resistance to PPU670 mediated FKBP12\_eGFP degradation. To validate this finding five different RPE1 FKBP12\_eGFP reporter UBR3-knockout cell lines were generated, by using the UBR3 sgRNAs featured in the in-house genome-wide sgRNA library (all four individually and a pool thereof). Then, the activity of PPU670 was tested in the resulting cell lines (Figure 62).

UBR3-knockout cell line generation and PPU670 activity analysis was performed by Dr. Yves Matthes.

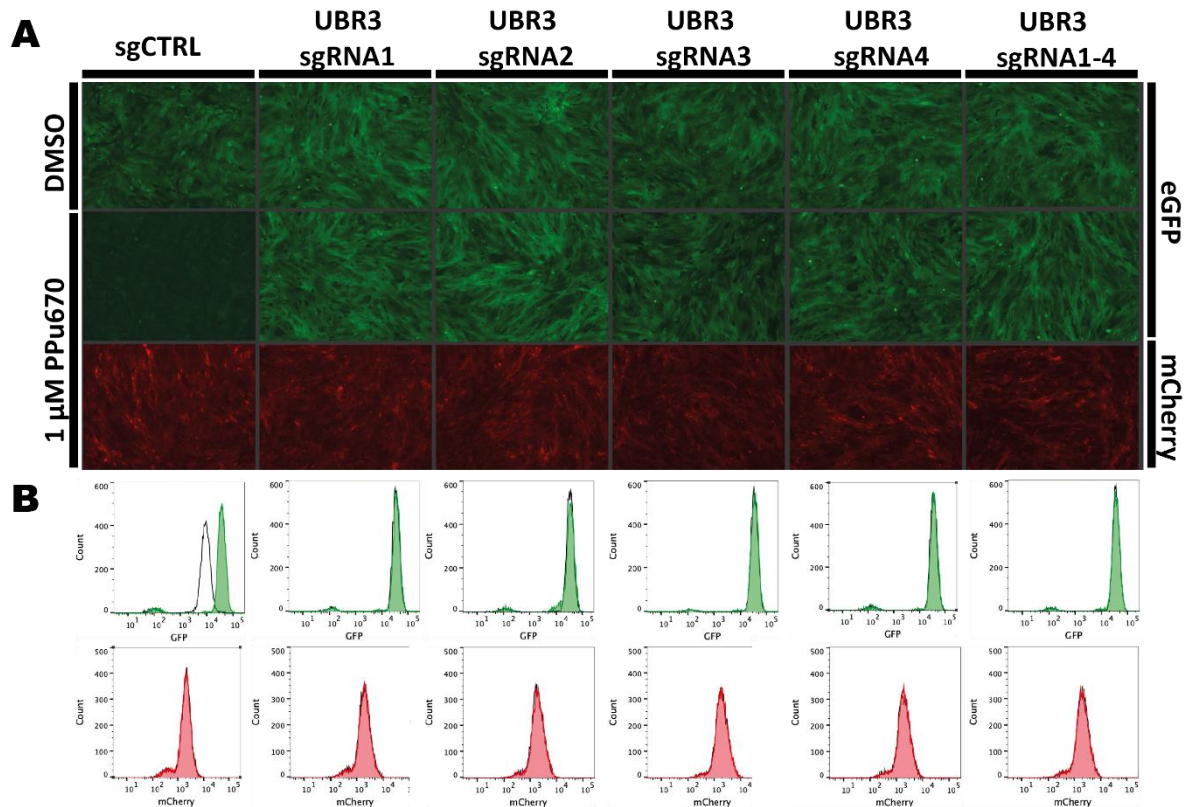


**Figure 62** UBR3-knockout blocks PPU670-mediated FKBP12\_eGFP degradation. **A** eGFP and mCherry fluorescence microscopy images of RPE1 FKBP12\_eGFP reporter UBR3-knockout cells after 48 h treatment. **B** Flow analysis of eGFP and mCherry fluorescence of RPE1 FKBP12\_eGFP reporter control and UBR3-knockout cells after 48 h treatment with 1  $\mu$ M PPU670 (black outline) or DMSO (green and red). Stable cell line generation, subsequent degrader treatment and FACS analyses were performed by Dr. Yves Matthes.

All UBR3 knockouts abrogated PPU670-mediated FKBP12\_eGFP reporter degradation, without affecting mCherry levels (Figure 62). This result ultimately validates PPU670's mode of action as UBR3-dependent and UBR3 as a relevant E3 ligase component. Notably, validation of UBR3 knockdown at the protein level through Western blotting was unsuccessful due to the lack of 'working' UBR3 antibodies.

UBR3 is a large (212 kDa) protein and so far poorly characterized. It contains a UBR box and Ring domain and is part of the UBR-box E3 ligase family. This family is not reliant on a cullin scaffold. This explains the insensitivity of PPU670's mode of action to neddylation inhibition. Generally, this class of E3 ligases contains a conserved UBR box domain that recognizes destabilizing N-terminal residues (N-degrons) and so far seven family members were identified in mammals (UBR1-7) [171]. However, substrates and cellular functions of UBR3 are not known [171]. The Ring domain of UBR3 likely facilitates association with a E2 ubiquitin ligase [172]. Interestingly, UBR3 has been suggested to have a regulatory role in sensory organs [173], which allows speculation that UBR3 is higher expressed in RPE1 (retinal pigment

---

epithelial cells) than in HEK293T cells and hence giving a potential reason for the differential activity of PPU670 in both cell lines.

In summary, the results demonstrate that (i) cellular testing of target-focused libraries can identify molecular glue degraders. However, (ii) control for tag-dependence is important. (iii) The approach is especially useful for solvent-exposed ligands that alter the potential interaction surface of the ensuing binary complex and (iv) as a PROTAC companion project where target degradation assays are likely already established, which results in a low entry barrier. (v) The E3 ligase UBR3 can be targeted by molecular glues to induce POI degradation. (vi) Molecular glue degraders may possess drastically different potencies in different tissues.

---

## 5. Conclusion and Outlook

---

I established a panel of FKBP-directed assays. The HTRF-binding assay for FKBP ligands enables the precise affinity determination of ultra-high affinity ligands (chapter 4.1). This will allow ranking of these compounds according to their binding affinity in future projects and thereby enable the establishment of reliable structure affinity relationship – the foundation for further optimization. Ultrahigh affinity FKBP ligands are especially attractive for molecular glues as they should facilitate an intracellular enrichment (intracellular trapping).

The NanoBRET-based FKBP ligand target engagement assays enable assessment of FKBP occupation in living cells (chapter 4.2). The assay thereby demonstrated that FKBP ligands engage FKBP in the environment where they have to act to achieve biologically relevant effects – inside living cells. In consequence, the established NanoBRET assay was used to: (i) determine which compounds potentially penetrate cells [53]; (ii) confirm that the, at the time, new class of macrocyclic compounds occupy FKBP51 in living cells [56]; (iii) demonstrate that the enhanced ligand efficiency of  $\alpha$ -methylated bicyclic ligands compared to their respective non-methylated analogs translates to an enhanced cellular potency [51]; and to choose compounds for cellular profiling, when the biochemical potencies are similar [52]. The NanoBRET assay bridges the gap between biochemical affinities and cellular effects or the lack thereof and has been incorporated in the standard profiling cascade of FKBP ligands.

I established GR signaling reporter gene assays (4.3) to analyze the roles of FKBP51 and FKBP52 in GR signaling as well as the effects of FK506-binding site occupation by FKBP ligands. Thereby, FKBP51 was confirmed as an inhibitor and FKBP52 as a potentiator of GR signaling. During the course of my studies, the molecular basis for FKBP-mediated GR regulation was investigated by photocrosslinking [165] and cryo-EM [168] studies. Together, these studies convincingly showed that the interaction interface of FKBP51 and FKBP52 with the GR extended from the FK1 domain to the tip of the TPR domain. Furthermore, it was demonstrated that (i) FKBP ligands remodel, but (ii) do not disrupt the FKBP:GR:Hsp90 complex [165]. Using the reporter gene assay, I linked ligand-induced complex remodeling and functional consequences. Strikingly, the FK506-binding site occupation and complex remodeling by synthetic FKBP ligands (including SAFit2) had no effects on GR signaling (Figure 63). This demonstrated that the FK506-binding site is per se dispensable for GR regulation and small synthetic FKBP ligands do not disrupt regulatory FKBP51:GR contacts. Based on the cryo-EM structure [168] it was postulated that SAFit2 does not clash with the GR and likely can be accommodated in the scaffold by GR chain rotations [168]. Conversely, effects of SAFit2, the

gold standard for pharmacological FKBP51 inhibition [55], have been repeatedly shown *in vivo* in animal models of stress disorders [61,174]. GR signaling and FKBP51-mediated regulation thereof is functionally linked to the stress response by the HPA axis. The disconnect between *in vivo* efficacy and lacking cellular effects could be explained (i) if an essential factor is missing in the currently studied cellular models or (ii) if FKBP51 ligands act *in vivo* via an additional pathway on GR signaling, in which the FK506-binding site is essential.

However, the large FKBP ligand FK506 protrudes far further from the binding site than SAFit2. Based on the cryo-EM structure of the FKBP51:GR:Hsp90 complex, FK506 was postulated to clash with the GR when bound to FKBP51 in the FKBP:GR:Hsp90 complex [168]. I was able to show the resulting functional consequences of this hypothesis – FK506 reactivated GR signaling in my reporter gene assays (Figure 63). The ability of FK506 to reactivate FKBP51-repressed GR signaling has profound implications for FKBP51-directed drugs: in principle, it is possible to reactive GR signaling by traditional ligands. It can be speculated that large ligands can abrogate regulatory FKBP51:GR contacts that are essential for GR regulation, but the precise mode of action is not clear. Therefore, it is currently not clear how to design occupation-driven ligands that reactivate GR signaling.

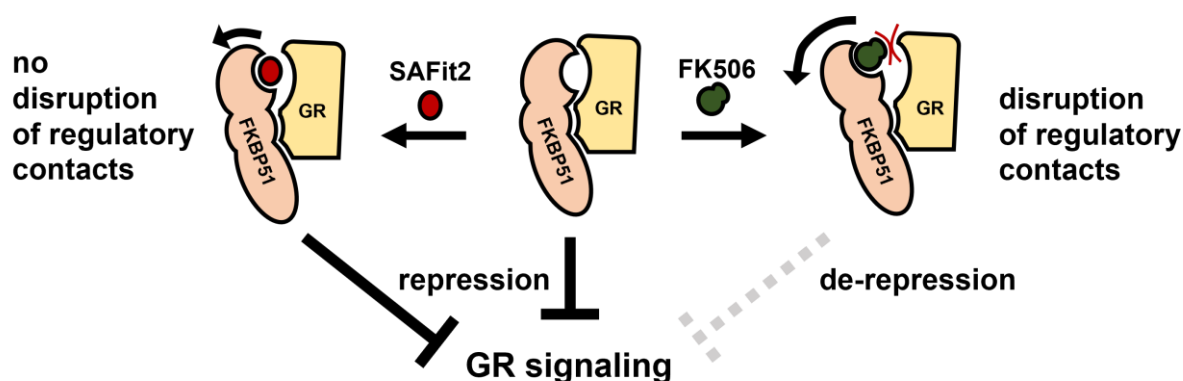


**Figure 63** FK506 but not SAFit2 reactivates GR signaling. Small ligands like SAFit2 do not disrupt regulatory FKBP51:GR contacts, whereas larger ligands that protrude far from the FK506-binding site disrupt regulatory FKBP51:GR contacts and relieve FKBP51-repressive effect on GR signaling.

Proteolysis targeting chimeras (PROTACs) possess a fundamentally different pharmacology compared to traditional ligands. PROTACs degrade their respective target protein and in consequence target all protein functions. Yet, they rely on traditional ligands as warheads for their creation. In practice, PROTAC generation often requires an empiric approach that relies on synthesis of PROTAC candidate libraries. Thereby, it can be required to explore a broad range of exit vectors, linker lengths and different E3 ligase ligands to find primary hits. A



---

building blocked-based plug and play approach can be useful to combinatorically assemble a library which covers a broad chemical space and different POI-ligand:linker:E3 ligase-ligand orientations. I established fluorescence-based FKBP-eGFP level reporter assays (chapter 4.4) that represent a cheap and effective screening method to identify primary hits in PROTAC candidate libraries. However, they require follow-up validation through orthogonal assays detecting the degradation of endogenous POI like Western blots or HTRF-based methods. This is especially important since commonly assessed parameters such as cellular target engagement, ternary complex stability, binding affinities, or cooperativity have rather inconsistent roles for degradation efficacy and are of limited use as predictors thereof [104,175]. A big challenge for TPD is that the degradability of a POI can hardly be predicted to date. PROTACs can have a strong degradability bias for a close homolog over another as demonstrated for FKBP12 over FKBP51 and FKBP52 (see chapter 4.6.1). Additionally, a large part of the proteome is rather resistant for TPD [175]. This can turn PROTAC discovery in a cumbersome endeavor. However, systematic scaffold hopping combined with linker optimization to fine-tune non-cognate protein-protein interactions and ligand-protein interactions can overcome those challenges as evidenced by the discovery of SelDeg51. A crystal structure for the ternary FKBP51:SelDeg51:VHL complex could enable further rational structure-based optimization (e.g., by macrocyclization). A first example in this direction was already demonstrated by the macrocyclization of the BRD4 PROTAC MZ-1 [141]. I strongly expect, that the fields of PROTACs and molecular glues will merge in the future and that the separated warheads of clear-cut hetero-bifunctional molecules become – through rigid structure-based optimization – more and more intertwined to become molecular glues.

PROTACs of the series 5a and 6a were very potent FKBP12 PROTACs except for the PROTAC candidates 5a2 and 6a2 which were degradation-inactive. I demonstrated that the inactivity of the 5a2 and 6a2 was not due to the lack of cellular FKBP12 engagement. On the contrary, they displayed the most potent cellular target engagement within their respective series (see 4.6.3). This can be explained if the binary FKBP12:PROTAC candidate complex is favored over the ternary complex and if 5a2 and 6a2 displayed a pronounced negative cooperativity. With an increasing availability of structural information of ternary complexes, positive cooperativity of active PROTACs – or ‘how a ternary complex forms’ – can often be explained in hindsight. However, a molecular understanding of negative cooperativity – or ‘why a ternary complex does not form’ – is largely lacking. To test my hypothesis, it would be suitable to assess the cooperativity of 5a2 and 6a2 by testing binding to VHL in presence and absence of FKBP12. If the PROTAC candidates display drastically lower binding affinity to VHL in presence of FKBP12 the negative cooperativity would be confirmed. Structural analysis of binary complexes with

---

FKBP12 and 5a2 or 6a2 could reveal the molecular basis for the negative cooperativity and provide a case study that enables a better understanding thereof. It remains to be seen if the molecular understanding for both active and inactive PROTACs enables computational approaches for PROTAC discovery in the future and how it will affect the *de-novo* discovery of PROTACs in general.

To establish PROTACs as useful functional tools, a profound confirmation of the mode of action and off-target controls are important. This is easily achievable by pharmacological inhibition of the relevant pathways, competition experiments, control for target engagement and synthesis of degradation-inactive analogs as demonstrated in this work. Additionally, global proteomics analysis can reveal potential off targets. While this is relevant for all PROTACs it is especially a concern for cereblon-based PROTACs as the included IMiD warhead can have substantial residual molecular glue degrader activity on IMiD off-targets [175].

I established SelDeg51 as a useful functional tool and demonstrated that SelDeg51 can reactivate GR signaling in reporter gene assays while small synthetic FKBP ligands could not rescue FKBP51-mediated GR-repression (Figure 63 & Figure 64). In context of the PROTAC field, this highlights that functionally silent ligands can be turned into active degraders and fundamentally outperform their parent molecules to convey a different pharmacology. While this is a long-standing hypothesis, examples demonstrating such cases have been rare [117,143–145]. For the FKBP51 community, SelDeg51 represents a unique tool to study FKBP51's function in cellular pathways without the need for genetic modifications. This is particularly intriguing when scaffolding functions of FKBP51 are suspected as in AKT signaling [7]. To study FKBP51 in GR signaling, FK506 could be a functional alternative. However, the immunosuppressive effects of FK506 limits its use. In a first step towards the application of SelDeg51 in mice, the effectiveness of SelDeg51 on murine FKBP51 must be confirmed. Additionally, given that SAFit2 is poorly orally available, specialized depot formulations or continuous injections are required for administration, SelDeg51 would likely have to follow a similar route in mice studies. Moreover, it is not clear if SelDeg51 has sufficient metabolic stability to act *in vivo*. For cellular models, SelDeg51 represents an easy-to-use tool that allows dose- and time-dependent control of FKBP51's level to answer the question whether FKBP51 levels matter in a certain cellular context.

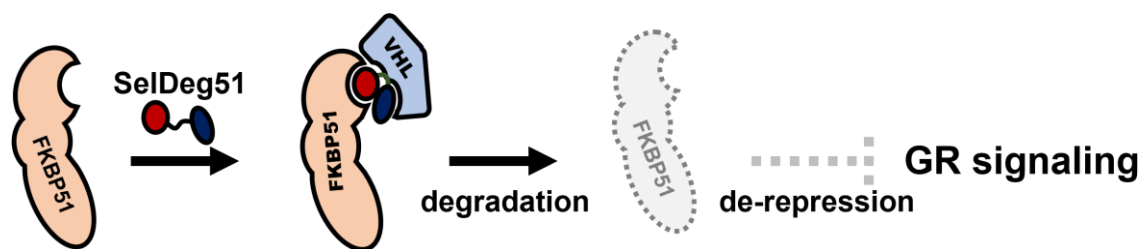


**Figure 64** SelDeg51 potentially degrades FKBP51 and abolishes FKBP51's scaffolding functions to de-repress GR signaling.

Molecular glues often preferentially bind either the protein of interest or the accessory protein. Focused libraries – by design – already bind one protein which greatly simplifies the recognition problem and enhances the likelihood to discover a molecular glue. To test this hypothesis, I used FKBP12, which showed a high degradability in the PROTAC studies, as a model system. I tested a focused FKBP-ligand library for FKBP12 degraders in E3 ligase-agnostic manner (Figure 65). Indeed, cellular testing of a FKBP-focused library in FKBP12\_eGFP level reporter assays led to the discovery of the molecular glue degrader SP448 as a validated hit. Subsequent rational optimization resulted in PPU670 with doubled cellular potency. Unfortunately, the discovered degraders appeared to act in an eGFP-tag-dependent manner, which highlights the importance of validation of primary hits in orthogonal assays.

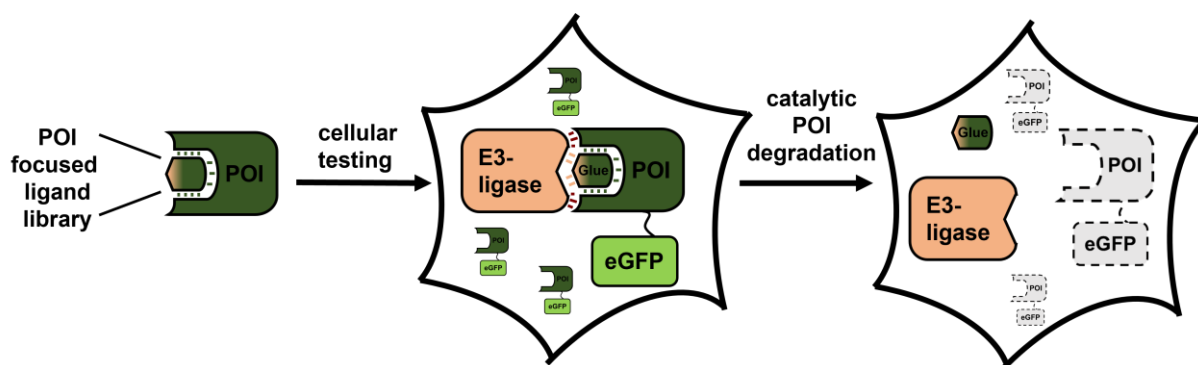


**Figure 65** Cellular testing of POI-focused ligand libraries may in favourable cases yield molecular glue degraders.

These findings, however, demonstrate that focused libraries can contain molecular glues. For drug discovery this implies that rescreening of target-focused libraries, which have historically been assembled during drug discovery campaigns might be rewarded with the discovery of ligands that have additional degradative properties. I expected POI degradation assays to be implemented in future drug discovery programs, especially for protein targets with solvent exposed binding sites. This approach is generally not limited to E3 ligases and degradation but can be applied to other classes of proteins. This can also result in functional inhibition of the POI. Nature repeatedly used FKBP12-based molecular glues (e.g., FK506, Rapamycin,

---

Antascomycin) to address ‘undruggable’ targets. This indicates that FKBP s might be highly versatile adapter proteins. Additionally, a FKBP-based Rapamycin-analog library was the basis for the discovery of Rapadocin [80]. In consequence, phenotypic or target-directed testing of FKBP12-focused libraries could be a fruitful approach to unravel more molecular glues to address otherwise undruggable proteins. The use of phenotypic screens – such as the FKBP12\_eGFP reporter assay – requires subsequent target deconvolution. In our case, degradation of the FKBP12\_eGFP reporter directly translated to the loss of a fluorescence signal and the reporter setup was transferred to a cell line that is more suitable for CRISPR screens. In RPE1 FKBP12\_eGFP reporter cells PPU670 displayed a greater potency compared to the HEK293T FKBP12\_eGFP reporter cell line. This effect could be due to a higher expression of the E3 ligase in RPE1 cells but this could not be confirmed due to the lack of specific UBR3 antibodies. Yet, this indicates that molecular glues can have context-specific potencies. Genome-wide CRISPR knockout screens deconvoluted UBR3 as the relevant E3 ligase for PPU670-mediated FKBP12\_eGFP degradation. In the following experiments, a UBR3-knockout fully rescued degradation, which confirmed UBR3 as an essential factor in the mode of action of PPU670. My findings demonstrate that UBR3 can be redirected to neo-substrates. Promiscuous E3 ligases are highly sought after for PROTAC development. However, the extent of UBR3’s promiscuity cannot be assessed based on one example. This E3 ligase is so far poorly characterized, and expression vectors are currently not available. In subsequent work it is necessary to generate UBR3 expression vectors and to show that UBR3 overexpression in UBR3-deficient cell lines can reestablish the effect of PPU670. If this is successful truncation constructs and mutants of the UBR3 expression construct can be used to determine functionally relevant domains of UBR3. Further steps could be the expression and purification of UBR3 (or functionally relevant domains thereof). This would enable a biochemical studies, ultimately including solving the crystal structure of the ternary UBR3:PPU670:FKBP12\_eGFP complex. This could enable subsequent structure-based optimization of the molecular glue. Currently, it is not clear, if PPU670 can direct un-tagged FKBP12 to UBR3, which is just not degraded, or if the C-terminal eGFP tag contributes to ternary complex formation through direct PPIs. This can be explored as soon as expression vectors become available, either in cellular NanoBRET assays or with purified proteins.

---

In summary, the development of SelDeg51 from systematic library generation to hit identification followed by linker-based optimization to a useful chemical tool adds to the understanding of the development of active PROTACs for hard-to-degrade proteins and exemplifies enhanced efficacy over traditional FKBP ligands. The discovery of FKBP12\_eGFP degrading molecular glues demonstrates that target-focused libraries can contain molecular glues and revealed UBR3 has a E3 ligase that can be chemically redirected to neo-targets. Molecular glues and hetero-bifunctional molecules possess gain-of-function mechanisms. I firmly believe they path a way for the development of smarter drugs, which can act in context-specific manner, have a better selectivity profile, higher efficacy or even enable addressing of ‘undruggable’ targets.

## 6. Materials and Methods

### 6.1. Materials

#### 6.1.1. General chemicals

**Table 5** List of general chemicals

<b>Chemical</b>	<b>Supplier/ Order Number</b>
2-Mercaptoethanol	Sigma, M6250
5 x passiv lysisbuffer	Promega, E194A
6x DNA Loading Dye	NEB, B7024S
Acetic acid 99-100 %	C. Roth, 7332.2
Agar-Agar, Kobe I	C. Roth, 5210.3
Agarose, universal	VWR, 35-1020
Ampicillin sodium salt	C. Roth, K09.5
Bovine serum albumin	Sigma, A7030
Calciumchlorid	C. Roth, CN 92.1
Carfilzomib	CST 15022
Dexamethasone	Fluka, 31381
Dimethylsulfoxid (DMSO)	C. Roth, 4720.4
di-potassium hydrogen phosphate	C. Roth, P749.1
Dithiothreitol (DTT)	C. Roth, 6908.1
Dual-Luciferase® Reporter Assay System	Promega, E1910
EDTA	C. Roth, 8043.3
Ethanol 70 % DAB	C. Roth, 7301.1
Ethanol denatured	C. Roth, K928.4
FK506 Tacrolimus	Beta Pharma, 56-01267
Glycerol 86 %	C. Roth, 4043.2
Glycine	C. Roth, 3908.2
Hepes	C. Roth, 9105.3
Hydrochloric acid (37%)	ThermoScientific, 124620010
Kanamycin sulfate	C. Roth, T832.1
LB Broth (Luria/Miller)	C. Roth, X968.2
LB-Agar	C. Roth, X969.2
Midori Green	Nippon Genetics, MG03
Milkpowder blotting grade	C. Roth, T145.3
MLN4924	CST 85923S
Nonidet® P-40 substitute	VWR Life Science, E109-50mL
PEI Prime	Sigma, 919012-100 mg
Phenylmethyl suphonyl fluoride	C. Roth, 6367.2
Ponceau S	C. Roth, 5938.2

<b>Chemical</b>	<b>Supplier/ Order Number</b>
Potassium carbonate	Alfa Aesar, A16625.36
Potassium dihydrogen phosphate	C. Roth, 3904.1
Potassium hydroxide	C. Roth, 6751.1
Potassium fluoride	VWR, 26821.230
Powdered milk	C. Roth, T145.3
Propan-2-ol	AppliChem, 603-117-00-0
Protease Inhibitor	ThermoScientific, A32953
Rapamycin	Alfa Aesar, J62473
Rotiphorese® Gel 30 (37.5:1)	C. Roth, 3029.1
Sodium chloride	C. Roth, 9265.3
Sodium dodecyl phosphate (SDS)	C. Roth, 0183.3
TEMED	C. Roth, 2367.3
Terrific-Broth-Medium	C. Roth, X972.3
Trichloroacetic acid	C. Roth, 8789.2
TRIS	C. Roth, 4855.2
TRIS hydrochlorid	C. Roth, 9090.3
Triton X-100	C. Roth, 3051.4
Tween 20	C. Roth, 9127.2

### 6.1.2. General plastics and materials

**Table 6** List of plastics and materials

<b>Plastics and materials</b>	<b>Supplier/ Order Number</b>
15 ml Falcon	Sarstedt, 62.554.502
50 ml Falcon	Sarstedt, 62.547.254
6 cm dish	Greiner Bio-one, 628166
10 cm dish	Sarstedt, 83.3902
12 well tissue culture plate	Sarstedt, 83.3921.005
24 well tissue culture plate	Sarstedt, 83.3923.005
96 well tissue culture plate	Sarstedt, 83.3924.005
Amersham™ Protran™ 0.2 μm, Nitrocellulose	GE Healthcare Life Sciences, 10600001
Combitips advanced (sterile) 1 ml	Eppendorf BIOPUR 0030089.642
Combitips advanced (sterile) 10 ml	Eppendorf BIOPUR 0030089.677
Combitips advanced (sterile) 2.5 ml	Eppendorf BIOPUR 0030089.650
Combitips advanced (sterile) 5 ml	Eppendorf BIOPUR 0030089.669
Combitips advanced 0,5 ml	Eppendorf 0030089.421

<b>Plastics and materials</b>	<b>Supplier/ Order Number</b>
Combitips advanced 10 ml	Eppendorf 0030089.464
Combitips advanced 5 ml	Eppendorf 0030089.456
CryoPure Tubes 1.8 ml white	Sarstedt, 72.379
Eppendorf tubes 5 ml	Eppendorf, 0030119401
Gelloader Pipette tips	Sarstedt, 70.1190.100
Micro tube 1.5 ml	Sarstedt, 72.691
Micro tube 1.5 ml protein LB	Sarstedt, 72.706.600
Micro tube 2 ml	Sarstedt, 72.691
Mini-PROTEAN empty cassettes	Bio-Rad, 4560005
PCR 8er Cap Strips	Biozym, 711050
Pipette tips 1000 $\mu$ L blue	Sarstedt, 70.3050.020
Pipette tips 20 $\mu$ L	Sarstedt, 70.3021
Pipette tips 200 $\mu$ L yellow	Sarstedt, 70.3030.020
Rotilabo®-Blottingpapiere, 0.35 mm	C. Roth, CL65.1
Serological pipette 5 ml	Sarstedt, 86.1253.001
Serological pipette 10 ml	Sarstedt, 86.1254.001
Serological pipette 25 ml	Sarstedt, 86.1285.001

### 6.1.3. Cell culture media and additives

Table 7 Cell culture media and additives

<b>Cell culture media and additives</b>	<b>Supplier</b>
0.25% Trypsin-EDTA	Gibco, 25200-056
DMEM	Gibco, 41966-052
DMEM/F12 (1:1)	Gibco, 11330-032
DPBS	Gibco, 14190-094
Heat inactivated FBS	Gibco, 10500-064
Hygromycin B	Roth, CP12.2
Opti-MEM	Gibco, 11058-021
Penicillin/Streptomycin	Gibco, 15140-122
Poly-D-Lysine	Gibco, A38904-01
Trypan Blue Stain 0.4%	Gibco, 15250-61



#### 6.1.4. Devices

**Table 8** List of Devices

Device	Supplier
1000 $\mu$ l, 200 $\mu$ l, 100 $\mu$ l, 20 $\mu$ l, 10 $\mu$ l, 2.5 $\mu$ l pipettes	Eppendorf
Biofuge Pico	Heraeus
Tecan Spark	Tecan
Tecan Genios Pro	Tecan
Nanodrop	DeNovix
Water Purification System	Simplicity
centrifuge 6-16K	Sigma
PCR-Cycler	Biometra
FACS	BD-Influx
Fujibox LAS3000	FUJIFILM
Mixing Block MB-102	BIOER
Turbo blotter	Bio-Rad
CO <sub>2</sub> incubator	Eppendorf, Thermo
centrifuge	Thermo
Mikroskop Wilovert S	Hund
Cell tank	Thermo
water bath	VWR
Incubator shaker innova 4000	NEW Brunswick scientific
Incubator shaker	Axon Labortechnik
Pipetting robot FXP	Biomek

#### 6.1.5. Tecan Reader

A Tecan GeniosPro or Tecan Spark were used for homogenous-time-resolved fluorescence, fluorescence polarization and fluorescence intensity measurements.

A Tecan Spark was used for luminescence measurements.

#### 6.1.6. Software

GraphPad Prism 8, Microsoft Office 365, UCDF Chimera [176], Flowing Software

### 6.1.7. Antibodies

**Table 9** Antibodies and conditions used in this work

Target	Name	Species	Dilution	Assay
$\alpha$ FKBP51	A301-430 (Bethyl)	rabbit	1:1000 in TBS + 5%(w/v) milk powder	Western Blot
$\alpha$ FKBP12	ab24373 (Abcam)	rabbit	1:1000 in TBS + 5% (w/v) BSA	Western Blot
$\alpha$ FKBP52	A301-427A (Bethyl)	rabbit	1:1000 in TBS + 5%(w/v) milk powder / final concentration of 1.25 nM in HTRF assays	Western Blot / HTRF
$\alpha$ GAPDH-HRP	14C10 (CST)	rabbit	1:1000 in TBS + 5% (w/v) BSA	Western Blot
$\alpha$ Hsp90	HSP90AA1/HSP90AB1 mAB, clone MBH90AB, MAB6457 Abnova	Mouse	1:1000 in TBS + 5%(w/v) milk powder	Western Blot
$\alpha$ Rabbit-IgG	A120-112P (Bethyl)	goat	1:1000 in TBS + 5%(w/v) milk powder	Western Blot
$\alpha$ Mouse-IgG	anti-mouse-HRP (NEB)	-	1:1000 in TBS + 5%(w/v) milk powder	Western Blot
$\alpha$ Flag	Tb cryptate-labeled anti-FLAG M2 antibody for capturing FLAG M2-tagged proteins (61FG2TLA, cisbio)	-	final dilution of 1:200 in HTRF assays	HTRF
$\alpha$ His6	MAB Anti-6HIS Tb cryptate Gold (61HI2TLB cisbio)	-	final dilution of 1:400 in HTRF assays	HTRF
$\alpha$ Rabbit IgG	pAB Anti Rabbit IgG-Eu cryptate (61PARKLA cisbio)	-	final concentration of 1.2 nM in HTRF assays	HTRF

**Table 10** Eukaryotic expression plasmids

Internal reference	Insert	Backbone	Created by
HG1218	FKBP51_eGFP-IRES2-mCherry	pEGFP-N	Thomas Geiger
HG1219	eGFP_FKBP51-IRES2-mCherry	pEGFP-C	Thomas Geiger
HG1252	FKBP12_eGFP-IRES2-mCherry	pcDNA3.1 (Hygro+)	Thomas Geiger
HG1250	eGFP_FKBP12-IRES2-mCherry	pcDNA3.1 (Hygro+)	Thomas Geiger
HG1436	FKBP51 <sup>FK1</sup> _eGFP-IRES2-mCherry	pEGFP-N	Thomas Geiger
HG1442	FKBP12_FKBP51 <sup>FK1-TPR</sup> _eGFP-IRES2-mCherry	pEGFP-N	Thomas Geiger
HG472	MMTV-luc2p	pGL4.36	Promega (E1360)
HG473	TK-hRluc	pGL4.74	Promega (E6921)
HG1215	Nluc -FKBP51 <sup>FK1</sup>	pNLF-1	Thomas Geiger
HG1217	FKBP51 <sup>FK1</sup> -Nluc	pNLF-1	Thomas Geiger
HG703	FKBP51-Flag	prK5	RG Rein (Max Planck Institute of Psychiatry)
HG206	FKBP52-Flag	prK5	RG Rein (Max Planck Institute of Psychiatry)
HG124	HA-GR	prK5	RG Rein (Max Planck Institute of Psychiatry)
HG39	-	prK5	-

**Table 11** Bacterial expression plasmids

Internal reference	Insert	Backbone	Created by
HG1015	His6-Tev-FKBP12(noCys)-Flag	pet30b(+)	Thomas Geiger
HG960	Flag-FKBP51-His6	pet30b(+)	Thomas Geiger
HG2	His6-FKBP51-Flag	pProexHTa	-

**Table 12** Purified proteins

Internal reference	Protein	Purified by
Aha399	His6-FKBP52-Strep	Andreas Hähle
CMe (Charge 180327)	His6-FKBP12	Christian Meyners
CMe (Charge 180613)	His6-TEV-FKBP51 <sup>FK1</sup> (16-140)	Christian Meyners
TGe245	His6-Tev-FKBP12(noCys)-Flag	Thomas Geiger
TGe231	Flag-FKBP51-His6	Thomas Geiger
TGe198	His6-FKBP51-Flag	Thomas Geiger

**Table 13** Stable cell lines

Name	Stable expression of	Antibiotic resistance	Created by
HEK293T FKBP12_eGFP-IRES2-mCherry	FKBP12_eGFP and mCherry	Hygromycin B	Thomas Geiger
HEK293T eGFP_FKBP12-IRES2-mCherry	eGFP_FKBP12 and mCherry	Hygromycin B	Thomas Geiger
RPE1 Cas9 NHTneo FKBP12_eGFP-IRES2-mCherry	FKBP12_eGFP and mCherry	Blasticidin	Yves Matthes (RG Kaulich)
HEK293T FKBP12-Nluc	FKBP12-Nluc	Hygromycin B	Monika Gnatzy (RG Hausch) [162]
HEK293T FKBP51 <sup>FK1</sup> -Nluc	FKBP51 <sup>FK1</sup> -Nluc	Hygromycin B	Monika Gnatzy (RG Hausch)
Hela AZ-GR	3xGRE-luc2p (inducible)	Hygromycin B	[161]

## 6.2. Biochemical methods

### 6.2.1. Agarose gel electrophoresis

For gel electrophoresis an 1.5% Agarose gel was prepared (1.5% (w/v) Agarose in 50 ml 1× TAE buffer (40 mM Tris, 20 mM acetic acid, 1 mM EDTA) with 10  $\mu$ L 1:10 prediluted Midori Green Advance DNA Stain (Nippon Genetics)). 5  $\mu$ L PCR product was mixed with 1  $\mu$ L 6× DNA loading Dye Purple (NEB) and loaded onto the gel. 5  $\mu$ L 1 kBp DNA Ladder (GeneRuler, Thermo Scientific) was used as a reference. Subsequently, the gel was run for 40 minutes at 120 V in 1× TAE buffer.

### 6.2.2. PCR

To generate PCR fragments for cloning, the PCR reaction was performed in single tubes in a final volume of 50  $\mu$ l following the general setup and protocol in Table 14 with the primers, templates and annealing temperatures listed in Table 15. PCR-products were cleaned up using the FastGene Gel/PCR Extraction Kit (Nippon Genetics) according to manufactures instructions and their size was verified by agarose gel electrophoresis (6.2.1). Primers were obtained from Sigma Aldrich or Merck Millipore.

Table 14 General PCR Setup (left) and protocol (right). Primers, Templates as well as annealing and elongation times are specified in Table 15.

10 $\mu$ L	5X Q5 Reaction Buffer (NEB)		98 °C	2 min
1 $\mu$ L	10 mM dNTPs (NEB)		98 °C	15 s
2,5 $\mu$ L	Primer 1 (10 $\mu$ M) (see Table 15)	30 x	Table 15	20 s
2,5 $\mu$ L	Primer 2 (10 $\mu$ M) (see Table 15)		72 °C	Table 15
1 $\mu$ L	Template (1-10 ng/ $\mu$ l) (see Table 15)		72 °C	2 min
0,5 $\mu$ L	Q5 High-Fidelity DNA Polymerase (NEB) 2000 units/ml		4 °C	Hold
23 $\mu$ L	MQ-H <sub>2</sub> O			

**Table 15** List of PCR-products generated by PCR with the respective primers, annealing and elongation times as well as the templates used. Primer sequences are listed in Table 16

PCR-product no.	Primers	Annealing temperature	Elongation time	Template
1	1407 + 1408	55 °C	300 s	HP833
2	1411 + 1413	65 °C	30 s	HP581
3	1414 + 1415	65 °C	30 s	HP702
4	1409 + 1410	55 °C	300 s	HP834
5	1412 + 1413	65 °C	30 s	HP581
6	1414 + 1416	65 °C	30 s	HP702
7	1611 + 1612	65 °C	240 s	HP1154
8	1613 + 1614	58 °C	30 s	HP1032
9	1615 + 1616	63 °C	70 s	HP1218
10	1617 + 1618	58 °C	30 s	HP834
11	1619 + 1620	58 °C	30 s	HP1032
12	1616 + 1621	63 °C	70 s	HP1228
13	1686 + 1687	50 °C	20 s	HP1218
14	1692 + 1694	60 °C	60 s	HP1252
15	1694 + 1695	60 °C	60 s	HP1218
16	669 + 1526	57 °C	20 s	HP703
17	1542 + 1527	57 °C	20 s	HP703
18	1125 + 1126	56 °C	45 s	HP684
19	1031 + 1032	56 °C	45 s	HP918

**Table 16** List of primers.

Primer no.	Sequence (5' → 3')
1407	GTACAAGTAAAGCGGCCGCGACTCTAGA
1408	GGGAGAGGGGTTACTTGTACAGCTCGTCCATGCC
1409	GGATCCACCGGATCTAGATAAC
1410	CTATACGTGGCCCTCAGG
1411	GTACAAGTAACCCCTCTCCCTCCCCCCC
1412	AACCTGAGGGCCACGTATAGCCCTCTCCCTCCCCCCC
1413	TGCTCACCATGGTTGTGGCCATATTATCATCGTGTTTTTCAAAGGAAAAC
1414	CGCGGCCGCTTTACTTGTACAGCTCGTCCATGCCGCCG

Primer no.	Sequence (5' → 3')
1415	TATCTAGATCCGGTGGATCCTTACTTGTACAGCTCGTCCATGCCGCCG
1611	TCTAGAGGGCCCGTTTAAAC
1612	GGATCCGAGCTCGGTACC
1613	TTGGTACCGAGCTCGGATCCATGGGAGTGCAGGTGGAAAC
1614	GTGGATCCTCTTCCAGTTTTAGAAGCTCCACATC
1615	AAAAC T GGAAGAGGATCCACCGGTCCGCC
1616	GTTTAAACGGGCCCTCTAGATTACTTGTACAGCTCGTCCATGCCGCC
1617	TTGGTACCGAGCTCGGATCCATGGTGAGCAAGGGCGAG
1618	GCACTCCCATAGAATTCTGAAGCTTGAGCTCG
1619	TTCGAATTCTATGGGAGTGCAGGTGGAAAC
1620	GGGAGAGGGGTCATTCCAGTTTTAGAAGCTCCAC
1621	ACTGGAATGACCCCTCTCCCTCCCCCCC
1686	TTCGAATTCTATGACTACTGA
1687	GGTGGATCCTCCTCTCCTTTGAAATCAAG
1692	GATCTCGAGCTCAAGCTTCGATGGGAGTGCAGGTGGAAAC
1693	TCTTCAAATAAATCCTCTCCTTCCAGTTTTAGAAGCTCCACATC
1694	GGAGAGGATTTATTTGAAGATGGAG
1695	CACCATGGTGGCGACCGGTGGATCCTCTACGTGGCCCTCAGGTTTC
669	GCCGCTCTAGA ACTACTGATGAAGGTGCCAAGAAC
1526	ATAGCGGCCGCTCACTCTCCTTTGAAATCAA
1542	GCGCGAATTCACCATGACTACTGATGAAGGTGCCAAG
1527	ATATCTAGACTCTCCTTTGAAATCAAGGA
1125	ATACATATGAGCTATTATCATCATCACC
1126	ATAGTCGACTTATTTATCATCATCATCTTTATAATCTTCCAGTTTCAGCAGTTCA A
1031	ATACATATGGATTATAAAGATGATGATGATAAAATGACCACCGATGAAGGCCG
1032	GTGCTCGAGCACATGACCTTCCGG

### 6.2.3. Restriction digest

The restriction digests were prepared according to the following general protocol (Table 17) and incubated for 3 hours at 37 °C. Afterwards, the restricted plasmids or PCR products were cleaned up using the FastGene Gel/PCR Extraction Kit (Nippon Genetics) according to manufactures instructions. All restriction enzymes (High-Fidelity) were purchased from New England Biolabs (NEB).

**Table 17** General setup for restriction digests

Component	50 $\mu$ l reaction
DNA / PCR product	1-5 $\mu$ g / 35 $\mu$ l
10 $\times$ rCutSmart Buffer	5 $\mu$ l
Restriction enzyme 1	1 $\mu$ l
Restriction enzyme 2	1 $\mu$ l
MQ-H <sub>2</sub> O	to 50 $\mu$ l

### 6.2.4. Gibson assembly

Gibson assembly was performed using the Gibson Assembly<sup>®</sup> Master Mix – Assembly Kit (NEB) according to the manufacturer’s instructions with the backbone fragment combinations listed in Table 18.

**Table 18** DNA fragments used for Gibson assembly.

Cloning of	PCR product no. (Vector) / restricted backbone (Table 15)	PCR product no. (Insert) (Table 15)	Fold molar excess of inserts
HP1218	1	2 + 3	2.5
HP1219	4	5 + 6	2.5
HP1252	7	8 + 9	2
HP1250	7	10 + 11 + 12	1
HP1442	HP1228 (EcoRI/BamHI) (generated by restriction of HP1228)	14 + 15	5



### 6.2.5. T4 ligation

T4 DNA ligase reactions were prepared according to the following protocol (Table 19) using the vector backbones and PCR products in Table 20 and incubated for 30 minutes at room temperature.

**Table 19** General setup for T4 DNA ligation

Component	10 $\mu$ l reaction
10 $\times$ T4 DNA Ligase Buffer (NEB)	1 $\mu$ l
Vector backbone	1 $\mu$ l
PCR product	2 $\mu$ l
T4 DNA Ligase (NEB) 400,000 units/ml	1 $\mu$ l
MQ-H <sub>2</sub> O	5 $\mu$ l

**Table 20** Restricted vector backbones and PCR product used for restriction ligation cloning. Restriction digests were performed as described in 6.2.3 with the indicated enzymes.

Cloning of	Fragment no. (backbone)	PCR product no. (Insert)
HP1215	HP672 (NotI/XbaI)	16 (NotI/XbaI)
HP1217	HP673 (EcoRI/XbaI)	17 (EcoRI/XbaI)
HP1436	HP1218 (EcoRI/BamHI)	13 (EcoRI/BamHI)
HP1015	HG107 (NdeI/SalI)	18 (NdeI/SalI)
HG960	HG107 (NdeI/XhoI)	19 (NdeI/XhoI)

### 6.2.6. Heat shock transformation

Chemically competent *Escherichia coli* DH5 $\alpha$  or *BL21 gold* cells (50  $\mu$ L) were thawed on ice, mixed with DNA (1  $\mu$ l plasmid stock, 10  $\mu$ l T4 ligation mix or 10  $\mu$ l Gibson assembly mix) and incubated on ice for 30 minutes. Cells were heat-shocked for 45 s at 42  $^{\circ}$ C, followed by 10 minutes incubation on ice. 500  $\mu$ l SOC medium was added and the cells were shaken for 1 hour at 37  $^{\circ}$ C. Afterwards, 200  $\mu$ l of the aliquot were plated onto LB agar containing the respective antibiotic (100  $\mu$ g/ml ampicillin or 50  $\mu$ g/ml kanamycin) and incubated overnight at 37  $^{\circ}$ C. The correct DNA sequence was verified by overnight sequencing (Ecoli Night Seq, Mircosynth Seqlab GmbH Göttingen). To generate glycerol stocks, 5 ml TB medium were inoculated with the

---

colony, shaken overnight at 37 °C and 650  $\mu$ l culture was added to sterile 650  $\mu$ l 50% glycerol and stored at -80 °C.

#### **6.2.7. Plasmid isolation**

6 ml or 100 ml TB-medium (100  $\mu$ g/ml ampicillin or 50  $\mu$ g/ $\mu$ L kanamycin) for mini- or midiplasmid preparations, respectively, were inoculated with a glycerol stock or colony and shaken overnight at 37 °C. The plasmids were extracted using High Copy Plasmid protocol of FastGene Plasmid Mini Kit (Nippon Genetics) or PureLink™ HiPure Plasmid-Midiprep-Kit (Invitrogen) following the manufactures instructions.

#### **6.2.8. Active-site titrations**

To determine the active-site concentration and confirm the structural integrity of the FK506-binding site of recombinantly expressed and purified FKBP, active-site titrations were performed. Towards this aim, triplicates of 1:2 serial dilution (14 steps) of the respective purified protein was performed in 40  $\mu$ L buffer (20 mM Hepes, 150 mM NaCl, 0.002% Triton X-100, pH 8.0) in black 384 well plates (Corning #3575). Afterwards, 10  $\mu$ L 250 nM TAMRA-labelled tracer (MTQ238) were added to every well to yield a final tracer concentration of 50 nM. Then, the plate was spun down and shaken at room temperature for 30 minutes. The fluorescence polarization and fluorescence intensities were measured using the following spectral adjustments: Ex.: 535 nm; Em.: 590 nm. The fluorescence polarization curves were fit by an four-parameter  $IC_{50}$  fit and the active-site concentration was calculated according to the following formula:  $c_{AST} = (c_{UV}/EC_{50}) \times 0.5 \times c_{tracer}$ .

#### **6.2.9. Fluorescence polarization binding curves**

Triplicates of 1:2 serial dilution (15 steps) of the respective purified protein was performed in 30  $\mu$ L buffer (20 mM Hepes, 150 mM NaCl, 0.002% Triton X-100, pH 8.0) in black 384 well plates (Greiner #781076 or Corning #3575). In the following, 10  $\mu$ L 4 nM Alexafluor647-labelled tracer were added to every well to yield a final tracer concentration of 1 nM. Then, the plate was spun down and shaken at room temperature for 30 minutes. The fluorescence polarization and fluorescence intensities were measured using the following spectral adjustments: Ex.: 580  $\pm$  20 nm; Em.: 665  $\pm$  8 nm; gain: optimal.

The  $K_D$  values were determined as described in [157].

### 6.2.10.HTRF binding assays

To assess the ability of tracer:protein (Flag-tagged) combinations to yield a HTRF signals in combination with an anti-Flag-Tb cryptate antibody, the assay setup was tested at a constant protein, tracer and anti-body concentration. Therefore, a 2-fold protein, a 4-fold tracer and a 4-fold antibody concentration were prepared in buffer (20 mM Hepes, pH 8.0, 150 mM NaCl, 0.002% Triton-X100 + 1 mM DTT). Subsequently, 10  $\mu$ L 2-fold protein dilution, 5  $\mu$ L 4-fold tracer dilution and 5  $\mu$ L 4-fold were transferred to a black 384 well plate (Corning #3575) in case of the FKBP51 constructs or in case of Flag-tagged FKBP12 to a white 384 well Proxiplate (Cisbio #6008280). Then, the plate was spun down, covered by a lid, and shaken at room temperature for 30 minutes.

To assess the suitability of tracer:protein combinations for HTRF assays of (only) His6-tagged proteins in combination with an anti-His6-Tb cryptate antibody, the assay window as evaluated for different protein and tracer concentrations. A 1:2 dilution series (15 steps) in 30  $\mu$ L buffer (20 mM Hepes, 150 mM NaCl, 0.015% Triton X-100, pH 8.0) of the respective tracer was performed in white 384 well plates (Greiner #781904). Subsequently, 10  $\mu$ L of a four-fold mixture of His6-tagged protein and anti-His6-Tb cryptate (1:100) in buffer (20 mM Hepes, 150 mM NaCl, 0.002% Triton X-100, pH 8.0) was added, the plate was spun down, covered by a lid, and shaken at room temperature for 30 minutes.

Competitive HTRF-binding assays were performed to determine the affinity of unlabeled FKBP ligands. Therefore, a 1:2 dilution series (15 steps) in 30  $\mu$ L buffer (20 mM Hepes, 150 mM NaCl, 0.002% Triton X-100, pH 8.0) of the respective ligand was performed in white 384 well plates (Greiner #781904). Subsequently, 10  $\mu$ L of a four-fold mixture of His6-tagged protein (20 nM), AlexaFluor647-labeled tracer (4 nM) and anti-His6-Tb cryptate (1:100) in buffer (20 mM Hepes, 150 mM NaCl, 0.002% Triton X-100, pH 8.0) was added, the plate spun down, covered by a lid, and shaken at room temperature for 30 minutes.

The HTRF signals were measured using the following spectral adjustments: donor signal Ex.: 340  $\pm$  35 nm; Em.: 620  $\pm$  10 nm; lag time: 150  $\mu$ s; integration time: 500  $\mu$ s; gain: optimal and acceptor signal: Ex.: 340  $\pm$  35 nm; Em.: 665  $\pm$  8 nm; lag time: 150  $\mu$ s; integration time: 500  $\mu$ s; gain: optimal. The HTRF-ratio (acceptor signal / donor signal) were calculated and the curves were fit by an four-parameter-IC<sub>50</sub> fit or to determine the K<sub>D</sub> of ligands as described by [157].

The measurement was performed in triplicates.

### 6.2.11. BCA protein quantification

The Pierce BCA Kit (Thermo Scientific) was used to calculate the total protein concentration of cell lysates. The assay was performed according to the manufacturer's instructions. Therefore, cells were lysed in HTRF-lysis buffer (DPBS (Gibco) + 400 mM KF + 0.5% Nonidet P-40 + PI (complete mini proteasome inhibitor (Roche)) + 1 mM PMSF), lysates were transferred to 1.5 mL Eppendorf tubes and spun down for 15 minutes at 4 °C and 15000 g. Additionally, an albumin standard (Thermo Scientific) dilution series was performed in HTRF-lysis-buffer. 6.25  $\mu$ l lysate or albumin standard were mixed with 50  $\mu$ l working solution (provided in the Kit) in a clear flat bottom 96 well plate (Greiner #655101) and incubated at 37 °C for 30 minutes. The absorbance was measured using a Tecan Spark at 562 nm and the protein concentration of the lysate was calculated using the generated albumin standard curve.

### 6.2.12. Expression of recombinant proteins

Recombinant protein expression was performed according to the following protocol: 50 to 200 ml TB medium with the respective antibiotic (100  $\mu$ g/ml ampicillin or 50  $\mu$ g/ $\mu$ L kanamycin) were inoculated with the *E. coli BL21 gold* cells, carrying the plasmid for protein expression, and shaken overnight at 37 °C. This preculture was used to inoculate 2 x 1 l main cultures at a OD<sub>600</sub> of 0.05 to 0.1. The main culture was shaken at 37 °C until a OD<sub>600</sub> of 0.5 was reached. Then, protein expression was induced with 0.5 ml IPTG (1 M) and the culture was shaken overnight at 25 °C. To harvest the cells, the cultures were centrifuged at 10,000 g at 4 °C and the supernatant was discarded. The cell pellets (originating from 1 l culture each) were frozen at -20 °C and stored at -20 °C for up to 2 weeks before the recombinant proteins were purified.

### 6.2.13. Cell lysis and recombinant protein purification

Flag-FKBP51-His6, His6-FKBP51-Flag and His6-Tev-FKBP12-Flag were purified according to the following protocol: each cell pellet (6.2.12) was thawed at room temperature, transferred to a 50 ml tube and resuspended in 20 ml lysis buffer (20 mM Hepes, 200 mM NaCl, 1 mM PMSF, 1 mM DTT, 2 mg/ml Lysozyme, 0.1 mg/ml DNase I). Afterwards, the lysates were mixed on a rolling device at 4 °C until the mixtures were homogenous. To disrupt the cell membranes, the mixtures were sonicated three times (Branson sonifier 450; 3 x 3 min, Duty cycle: 60%, output-control: 2-3, output  $\sim$  10) on ice. Afterwards, the mixtures were centrifuged at 4 °C and 15,000 g for 30 minutes.

For protein purification, 4 ml Ni-NTa agarose (50% slurry, cv = 2 ml, Macherey-Nagel) were equilibrated with 10 cv (=20 ml) lysis buffer. Then, the lysate was added to the column. The

---

flowthrough was collected and readded to the column. Then, the column bed was washed with 5 cv (= 10 ml) washing buffer (20 mM Hepes, 20 mM NaCl, 40 mM imidazole, pH 8.0) and the protein was eluted with elution buffer (20 mM Hepes, 20 mM NaCl, 300 mM imidazole, 1 mM DTT, pH 8.0). The eluate was collected in 1 ml fractions. Afterwards, the fractions were analyzed by SDS page and Coomassie staining and the target protein containing fraction were pooled.

In case of His6-TEV-FKBP12-Flag, the target protein containing fractions were dialyzed two times overnight at 4 °C in 1 l dialysis buffer (150 mM NaCl, 20 mM Hepes, pH 8.0). The protein concentration was analyzed photometrically at 280 nm ( $\epsilon = 14440/(M \times cm)$ ) and the protein was aliquoted, frozen in liquid nitrogen and stored at -80 °C until usage. The active-site concentration was determined as described in (6.2.8).

In case of Flag-FKBP51-His6 and His6-FKBP51-Flag, the target protein containing fractions were dialyzed two times overnight at 4 °C in 1 l dialysis buffer (150 mM NaCl, 20 mM Hepes, pH 8.0) and then further purified by size exclusion chromatography. Therefore, the pooled fractions were centrifuged (20,000 g, 4 °C, 30 min) and the supernatant was applied via a superloop to a HiLoad® 16/600 Superdex® 75 pg column (GE Healthcare), which was equilibrated in buffer (150 mM NaCl, 20 mM Hepes, pH 8.0). Protein elution was monitored by UV absorbance at 280 nm and the peaks were collected in 15 ml tubes. In the following, the fractions were analyzed by SDS page and Coomassie staining and the target protein containing fraction was concentrated using centrifugal filter (Amicon Ultra-15 MWCO: 3000 kDa; 10,000 g). Afterwards, the protein concentrations were analyzed photometrically at 280 nm ( $\epsilon = 41830/(M \times cm)$ ) and the protein was aliquoted, frozen in liquid nitrogen and stored at -80 °C until usage. The active-site concentration was determined as described in (6.2.8).

## 6.3. Cell culture

### 6.3.1. Mammalian cell culture

Human embryonic kidney 293T (HEK293T) cells and the stable cell lines (HEK293T FKBP12\_eGFP-IRES2-mCherry, HEK293T eGFP\_FKBP12-IRES2-mCherry, HEK293T FKBP12-Nluc, HEK293T FKBP51<sup>FK1</sup>-Nluc, Hela AZ-GR [161]) were maintained in Dulbecco's modified Eagle's medium (DMEM) (Gibco) supplemented with 10% fetal bovine serum (Gibco) + 1% Penicillin-Streptomycin (Gibco) and in case of stable cell lines with 200  $\mu$ g/mL Hygromycin B (Roth) at 37 °C and 5% CO<sub>2</sub> unless indicated otherwise.

Cell culturing was performed using sterility guidelines.

### **6.3.2. Mammalian cell passaging**

Cells were grown in 10 cm dishes for a maximum of 4 days. For passaging the culture medium was aspirated, the cells washed with prewarmed DBPS and 1 ml prewarmed Trypsin-EDTA solution was added and distributed. After 5 minutes incubation at 37 °C, the cells were collected and resuspended in 5 ml cell culture medium and spun down for 3 minutes at 1000 rpm. Afterwards, the supernatant was removed, and the cells suspended in 5 ml cell culture medium. An appropriate fraction of the cells transferred to a fresh 10 cm plate containing 10 ml of cell culture medium.

### **6.3.3. Surface coating**

Multiwell plates (Table 6) for cellular assays were coated in poly-D-lysine (PLD) (0.1 mg/ml (Gibco); diluted 1:50 in sterile MQ-H<sub>2</sub>O to a final concentration of 0.002 mg/ml). Half the recommended cell culture volume of the diluted PLD solution were added to the wells and the plate was placed in the incubator for 24-72 h. Afterwards, the PLD solution was aspirated, the wells washed with an equal volume of sterile water and left to air dry under a cell culture hood. Subsequently, the plates were tape-sealed and stored at 4 °C until usage, but for a maximum duration of three weeks.

### **6.3.4. Cell counting**

Before seeding, the cells were counted. A 10  $\mu$ L cell suspension obtained like in 6.3.2 was mixed with 10  $\mu$ L Trypan Blue solution and 10  $\mu$ L of the mixture were then transferred to a Neubauer Counting Chamber. The non-blue cells in four major quadrants were counted and the cell count in the original suspension calculated according to: 1 Neubauer count  $\hat{=}$  5\*10<sup>3</sup> cells/ml in the original suspension.

### **6.3.5. FKBP52 siRNA knockdown and transient overexpression**

To alter cellular FKBP52 levels HEK293T cells were transiently transfected with a FKBP52 targeting siRNA (ThermoFisher Silencer<sup>®</sup> Select 4390824 ID: s50) or a FKBP52 (pcDNA3-Flag-FKBP52) expression construct.

9×10<sup>4</sup> or 3.5×10<sup>4</sup> and 5×10<sup>4</sup> HEK293T cell/well were seeded in PLD-coated 12 and 24 well plates, respectively, and left to attach overnight. On the next day, transient transfection mixtures were prepared. The siRNA and Lipofectamin2000 were diluted to a concentration of 200 nM (24 well plate) or 100 nM (24 well plate) and 1.7% (v/v), respectively, in Opti-MEM and incubated for 5 minutes at room temperature. Subsequently, the solutions were mixed 1:1 and incubated at room temperature for 30 minutes. In the meantime, the cell culture medium

---

was aspirated and 400  $\mu\text{L}$  (24 well plate) or 800  $\mu\text{L}$  (12 well plate) fresh medium was added to the wells. Following the incubation period, 100  $\mu\text{L}/\text{well}$  (24 well plate) or 200  $\mu\text{L}/\text{well}$  (12 well plate) transfection mix was added to wells (final siRNA amount: 20 pmol/well) and the plate was placed in the incubator for 24 h. Control cells were prepared in a similar manner with sterile water instead of siRNA.

For transient FKBP52 overexpression  $9 \times 10^4$  HEK293T cell/well were seeded in PLD-coated 12 well plate and left to attach overnight. On the next day, transient transfection mixtures were prepared. pcDNA3-Flag-FKBP52 and Lipofectamine2000 (Invitrogen) were diluted to a concentration of 2 ng/ $\mu\text{l}$  and 1.7% (v/v), respectively, in Opti-MEM and incubated 5 minutes at room temperature. Subsequently, the solutions were mixed 1:1 and incubated at room temperature for 30 minutes. In the meantime, the cell culture medium was aspirated and 800  $\mu\text{L}$  fresh medium was added to the wells. Following the incubation period, 200  $\mu\text{L}/\text{well}$  transfection mix was added to wells and the plate was placed in the incubator for 24 h. Control cells were prepared in a similar manner with sterile water instead of siRNA.

Cell lysis and HTRF-based relative FKBP52 quantification were performed as in 6.3.6. with the exception that the DPBS + 400 mM KF + 0.5% Nonidet P-40 was used as lysis and HTRF Buffer.

### **6.3.6. HTRF-based relative FKBP52 quantification assay**

$3.5 \times 10^4$  HEK293T cells/well were seeded in PDL-coated 24 well plates. After overnight attachment, cells in two wells/plate were transiently transfected (Lipofectamine2000, Invitrogen) with 20 pmol/well anti-FKBP52 siRNA (Silencer Validated siRNA siRNA ID: s50, ThermoFisher) as described in 6.3.5. After overnight incubation, the medium of all wells was exchanged to medium containing PROTAC or DMSO for 24 hours. Then, the cells were washed with 500  $\mu\text{L}/\text{well}$  cold (4 °C) DBPS (Gibco) and lysed in lysis buffer (150 mM NaCl, 25 mM Tris-Cl, 200 mM KF, 0.5% Triton X-100, 0.5% sodium deoxycholate, 0.1% SDS, 5% (w/v) BSA, supplemented with protease inhibitor cocktail (Roche) and 1 mM PMSF, pH 8.0) on ice for 30 min. The lysates were transferred to 1.5 mL Eppendorf tubes and spun down for 20 min at 18,000 g at 4 °C. 16  $\mu\text{L}$  lysate were transferred to ProxiPlates (Cisbio #6008280) and 4  $\mu\text{L}$  (600 nM MWa146, 6.25 nM primary FKBP52 antibody (A301-427A (Bethyl)) and 6 nM secondary pAB anti Rabbit IgG-Eu cryptate (61PARKLA (Revvity)) in lysis buffer were added. After overnight incubation at 4°C, the HTRF signal was measured using the following spectral adjustments: donor signal Ex.:  $340 \pm 35$  nm; Em.:  $620 \pm 10$  nm; lag time: 150  $\mu\text{s}$ ; integration time: 500  $\mu\text{s}$ ; gain: optimal and acceptor signal: Ex.:  $340 \pm 35$  nm; Em.:  $665 \pm 8$  nm; lag time: 150  $\mu\text{s}$ ; integration time: 500  $\mu\text{s}$ ; gain: optimal.

### 6.3.7. Generation of stable cell lines

10<sup>6</sup> HEK293T cells were seeded in a 10 cm cell culture plates. On the next day, the cell culture medium was aspirated, and 9 mL fresh medium was added. pcDNA3.1(H+)-FKBP12\_eGFP-IRES2-mCherry (8  $\mu$ g) and pcDNA3.1(H+)-eGFP\_FKBP12-IRES2-mCherry (16  $\mu$ g) were mixed with 22.5  $\mu$ g PEI in 1 ml Opti-MEM (Gibco), respectively. Incubated for 30 min at room temperature and each transfection mixture was added a distinct plate. After overnight incubation, the medium was exchanged and after 48 hours the culture medium was replaced by selection medium (DMEM +10% FBS + 1% P/S + 900  $\mu$ g/mL Hygromycin B) for 14 days. During the selection period, the medium was exchanged every 2-3 days. To obtain monoclonal populations the cells were washed, trypsinized, and subcloned into 96 well plates at density of approx. 1 cell/well. After expansion, cells were screened for simultaneous expression of FKBP12-eGFP and mCherry.

### 6.3.8. Fluorescent FKBP-eGFP level reporter assays

FKBP12\_eGFP and eGFP\_FKBP12 level reporter assays using the stable HEK293T FKBP12\_eGFP-IRES2-mCherry or HEK293T eGFP\_FKBP12-IRES2-mCherry were performed according to the following protocol:

10<sup>4</sup> cells/well were seeded in black PDL-coated 96 well cell culture plates and left to attach overnight. The medium was aspirated and 50  $\mu$ L fresh medium (without Hygromycin B) was added. In case of mechanistic experiments, the medium was additionally supplemented with a 2-fold concentration of competitor compound, proteasome (Carfilzomib) or neddylation (MLN4924) inhibitor. Compound or PROTAC solutions at 2-fold concentration were prepared in medium (without Hygromycin B) and 50  $\mu$ L were added to the respective wells. If not otherwise indicated, after 48 h, the cells were washed with DPBS (Gibco) and lysed in 50  $\mu$ L NETN buffer (100 mM NaCl, 20 mM Tris-Cl, 0.5 mM EDTA, 0.5% (v/v) Nonidet P-40, pH 8.0 + proteasome inhibitor (Roche)) on ice for 30 minutes. The eGFP and mCherry fluorescence was measured using a Tecan Spark and the spectral adjustments: mCherry: Ex.: 580 nm, Em.: 620 nm; eGFP: Ex.: 485 nm, Em.: 525 nm. Following, eGFP to mCherry ratios were calculated and normalized to the eGFP/mCherry ratio of the DMSO control.

For dose-response experiments the data was analyzed with GraphPad Prism 8 and fitted by a four parameter IC<sub>50</sub> fit.



FKBP12\_eGFP reporter sequence:

MGVQVETISPGDGRFTPKRGQTCVVHYTGMLEDGKKFDSSRDRNKPFKFKMLGKQEVIRGWEEGVAQMSVGQ  
RAKLTISPDYAYGATGHPGIIPPHATLVFDVELLKLEEDPPVATMVSKGEELFTGVVPILVELDGDVNGHKFSVS  
GEGEGDATYGKLTCLKFICTTGKLPVPWPTLVTTLTLYGVQCFSRYPDHMKQHDFFKSAMPEGYVQERTIFFKDD  
GNYKTRAEVKFEGDTLVNRIELKGIDFKEDGNILGHKLEYNYNSHNVYIMADKQKNGIKVNFKIRHNIEDGSVQ  
LADHYQQNTPIGDGPVLLPDNHYLSTQSALS KDPNEKRDMVLEFVTAAGITLGMDELYK

eGFP\_FKBP12 reporter sequence:

MVSKGEELFTGVVPILVELDGDVNGHKFSVSGEGEGDATYGKLTCLKFICTTGKLPVPWPTLVTTLTLY  
GVQCFSRYPDHMKQHDFFKSAMPEGYVQERTIFFKDDGNYKTRAEVKFEGDTLVNRIELKGIDFKE  
DGNILGHKLEYNYNSHNVYIMADKQKNGIKVNFKIRHNIEDGSVQLADHYQQNTPIGDGPVLLPDN  
HYLSTQSALS KDPNEKRDMVLEFVTAAGITLGMDELYKSGLSRAQASNSMGVQVETISPGDGR  
TFPKRGQTCVVHYTGMLEDGKKFDSSRDRNKPFKFKMLGKQEVIRGWEEGVAQMSVGQRAKLTISP  
DYAYGATGHPGIIPPHATLVFDVELLKLE

FKBP51\_eGFP, FKBP51<sup>FK1</sup>\_eGFP and FKBP12\_FKBP51<sup>FK2-TPR</sup>\_eGFP level assays were performed using transient expression and according to the following protocol:

$2 \times 10^6$  HEK293T cells were seeded in a 10 cm plate. After overnight attachment, the medium was exchanged to 9 mL fresh medium and the cells were transiently transfected by adding a previously in 1 ml Opti-MEM reduced serum medium (Gibco) incubated (30 min, room temperature) mixture of 5  $\mu$ g pEGFP-N-FKBP51\_eGFP-IRES2-mCherry plasmid, of 2.5  $\mu$ g pEGFP-N-FKBP51<sup>FK1</sup>\_eGFP-IRES2-mCherry plasmid or 5  $\mu$ g pEGFP-N-FKBP12\_FKBP51<sup>FK2-TPR</sup>\_eGFP-IRES2-mCherry plasmid and 22.5  $\mu$ g PEI. Following overnight incubation, the cells were washed with DPBS (Gibco), trypsinized and  $2 \times 10^4$  transiently transfected cells in 50  $\mu$ l medium were added to each well of a black PDL-coated 96 well plate. Additionally, PROTAC solutions were prepared at 2-fold concentration in medium and added to the respective wells. After 48 h, the cells were washed with DPBS (Gibco) and lysed in 50  $\mu$ L NETN buffer (100 mM NaCl, 20 mM Tris-Cl, 0.5 mM EDTA, 0.5% (v/v) Nonidet P-40, pH 8.0 + proteasome inhibitor (Roche)) on ice for 30 minutes. The eGFP and mCherry fluorescence was measured using a Tecan Spark and the spectral adjustments: mCherry: Ex.: 580 nm, Em.: 620 nm; eGFP: Ex.: 485 nm, Em.: 525 nm. Following, eGFP to mCherry ratios were calculated and normalized to the eGFP/mCherry ratio of the DMSO control.

FKBP51\_eGFP reporter sequence:

MTTDEGAKNNEESPTATVAEQGEDITSKKDRGVLKIVKRVNGEETPMIGDKVYVHYKGKLSNGKK  
FDSSHDRNEPFVFSLGKGQVIKAWDIGVATMKKGEICHLCKPEYAYGSAGSLPKIPSNATLFFEIELL  
DFKGEDLFEDGGIIRRTKRKGEYGNPNEGATVEIHLEGRCGGRMFDCRDVAFTVGEGEDHDIPIGI  
DKALEKMQREEQCILYLGPYGFGEAGKPKFGIEPNAELIYEVTLKSFKAKESWEMDTKEKLEQAAI  
VKEKGTVYFKGGKYMQAVIQYKIVSWLEMEYGLSEKESKASESFLAAFLNLAMCYLKLREYTKAV  
ECCDKALGLDSANEKGLYRRGEAQLLMNEFESAKGDFEKVLEVNPQNKAARLQISMCQKKAKEHN  
ERDRRIYANMFKKFAEQDAKEEANKAMGKKTSEGVTNEKGTDSQAMEEEKPEGHVEDPPVATMVS  
KGEELFTGVVPILVELDGDVNGHKFVSVEGEGDATYGKLTCLKFICTTGKLPVPWPTLVTTLYGVQC  
FSRYPDHMKQHDFFKSAMPEGYVQERTIFFKDDGNYKTRAEVKFEGDTLVNRIELKGIDFKEDGNIL  
GHKLEYNYNSHNVYIMADKQKNGIKVNFKIRHNIEDGSVQLADHYQQNTPIGDGPVLLPDNHYLST  
QSALS KDPNEKRDHMLLEFVTAAGITLGMDELYK

FKBP51<sup>FK1</sup>\_eGFP reporter sequence:

MTTDEGAKNNEESPTATVAEQGEDITSKKDRGVLKIVKRVNGEETPMIGDKVYVHYKGKLSNGKK  
FDSSHDRNEPFVFSLGKGQVIKAWDIGVATMKKGEICHLCKPEYAYGSAGSLPKIPSNATLFFEIELL  
DFKGEEDPPVATMVS KGEELFTGVVPILVELDGDVNGHKFVSVEGEGDATYGKLTCLKFICTTGKLP  
VPWPTLVTTLYGVQCFSRYPDHMKQHDFFKSAMPEGYVQERTIFFKDDGNYKTRAEVKFEGDTLV  
NRIELKGIDFKEDGNILGHKLEYNYNSHNVYIMADKQKNGIKVNFKIRHNIEDGSVQLADHYQQNTPI  
IGDGPVLLPDNHYLSTQSALS KDPNEKRDHMLLEFVTAAGITLGMDELYK

FKBP12\_FKBP51<sup>FK2-TPR</sup>\_eGFP:

MGVQVETISPGDGRTPKRGQTCVVHYTGMLDGGKFDSSRDRNKPFKFMLGKQEVIRGWEEGVA  
QMSVGQRAKL TISPDYAYGATGHPGIIPPHATLVFDVELL KLEGEDLFEDGGIIRRTKRKGEYGNPN  
EGATVEIHLEGRCGGRMFDCRDVAFTVGEGEDHDIPIGIDKALEKMQREEQCILYLGPYGFGEAGK  
PKFGIEPNAELIYEVTLKSFKAKESWEMDTKEKLEQAAIVKEKGTVYFKGGKYMQAVIQYKIVSWL  
EMEYGLSEKESKASESFLAAFLNLAMCYLKLREYTKAVECCDKALGLDSANEKGLYRRGEAQLLMN  
EFESAKGDFEKVLEVNPQNKAARLQISMCQKKAKEHNERDRRIYANMFKKFAEQDAKEEANKAMG  
KKTSEGVTNEKGTDSQAMEEEKPEGHVEDPPVATMVS KGEELFTGVVPILVELDGDVNGHKFVSVEG  
EGEGDATYGKLTCLKFICTTGKLPVPWPTLVTTLYGVQCFSRYPDHMKQHDFFKSAMPEGYVQERT  
IFFKDDGNYKTRAEVKFEGDTLVNRIELKGIDFKEDGNILGHKLEYNYNSHNVYIMADKQKNGIKVN  
FKIRHNIEDGSVQLADHYQQNTPIGDGPVLLPDNHYLSTQSALS KDPNEKRDHMLLEFVTAAGITL  
GMDELYK

### 6.3.9. SDS page

SDS pages were cast in 1 mm disposable cassettes (Bio-Rad). Therefore, the separation gel was prepared according to the following protocol (Table 21):

**Table 21** Separation gel protocol

	8%	10%	12%	14%	16%
Acrylamide (30%) / Bisacrylamide (0.8%) (ml)	3.8	4.8	5.7	6.7	7.8
1 M Tris, pH 8.8) (ml)			5.3		
MQ-H <sub>2</sub> O (ml)	4.9	3.9	3.0	2.0	1.1
10% (v/v) SDS in MQ-H <sub>2</sub> O (μl)			140		
TEMED (μl)			17		
10% APS (v/v) in MQ-H <sub>2</sub> O (μl)			84		

The separation gel mixture was mixed and poured into the empty gel cassettes filling approx. 80% and overlaid with 300 μL isopropanol. After polymerization, the isopropanol was discarded and 5 ml stacking gel buffer (5.3% (v/v) acrylamide, 0.14% (v/v) bisacrylamide, 60 mM Tris, 0.1% (v/v) SDS, pH 6.8) was mixed with 25 μL 10% (v/v) APS in MQ-H<sub>2</sub>O and 5 μL TEMED and filled to the top in the cassettes. The combs were added directly afterwards. After polymerization the gels were wrapped in wet tissues and stored until usage in sealed plastic bags at 4 °C for up to 2 weeks.

### 6.3.10. Coomassie stain analysis

30 μl protein sample were mixed with 10 μL β-mercaptoethanol containing 4×Lämmli-buffer and heated to 95 °C for 10 minutes. Afterwards, the proteins were separated by SDS page and the gel was shaken in Coomassie staining solution (40% (v/v) ethanol, 10% (v/v) acetic acid, 1 g/L Coomassie Brilliant Blue R250) for 1 h. In the following, destaining was performed by shaken the gel in destaining solution (40% (v/v) ethanol, 10% (v/v) acetic acid) for at least 30 minutes until the protein band were visible.

### 6.3.11. Western blot

2×10<sup>5</sup> cells/well in case of HEK293T cells and stable cell lines thereof, 7.5 x 10<sup>5</sup> cells/well in case of the Hela AZ-GR cell line or 10<sup>5</sup> cells/well in case of the RPE1 FKBP12\_eGFP reporter cell line were seeded in PDL-coated 12 well plates and left to attach overnight. Cells were treated with the indicated concentrations of PROTACs and/or compounds for 24 h in 1 ml

medium unless indicated otherwise. After the incubation period, the medium was aspirated, the cells were washed with 500  $\mu\text{L}$  4°C DPBS (Gibco) and lysed in 100  $\mu\text{L}$ /well NETN buffer (100 mM NaCl, 20 mM Tris-Cl, 0.5 mM EDTA, 0.5% (v/v) Nonidet P-40, pH 8.0) + proteasome inhibitor (Roche)). Subsequently, lysates were transferred to 1.5 ml Eppendorf tubes and spun down for 15 minutes at 4 °C and 15000 g. Then, 60  $\mu\text{L}$  supernatant was mixed with 20  $\mu\text{L}$   $\beta$ -mercaptoethanol containing 4 $\times$ Lämmli-buffer and heated to 95 °C for 10 minutes. The proteins were subsequently separated by SDS page and transferred to nitrocellulose membrane (Amersham) using a Semi-Dry Rapid Blotting System (Bio-Rad). The membrane was cut at heights appropriate for different proteins, blocked in 5% milk powder (Roth) in TBS buffer for 30 minutes and probed overnight with the respective antibodies (Table 9). On the next day, the membranes were washed three times for 5 minutes in TBS buffer. If needed the membranes were probed for 2 hours with a secondary antibody (Table 9) followed by a second washing step (three times for 5 minutes in TBS). Proteins levels were visualized using Immobilon Western Chemiluminescent HRP Substrate (Millipore) and LAS-3000 (Fujifilm) device.

#### **6.3.12. FACS**

$1.5 \times 10^6$  RPE1 FKBP12\_eGFP reporter cells/plate were seeded in uncoated 10 cm cell culture plates. After overnight attachment, the cells were treated with 1  $\mu\text{M}$  PPU670 or DMSO (0.1%) for 48 hours. Subsequently, the cells were trypsinized, collected in medium, washed twice with prewarmed DPBS, resuspended in DPBS supplemented with 1 mM EDTA and stored on ice until FACS analysis. eGFP (Ex.: 488 nm; Em.:  $530 \pm 40$  nm) and mCherry (Ex.: 561 nm; Em.:  $593 \pm 40$  nm) fluorescence of at least  $10^4$  events per condition were recorded using BD-Influx cell sorter (research group Kolmar, under supervision of Dr. Andreas Christmann). Flow analysis was performed using Flowing Software 2.5. The recorded events were gated for SSC/FSC and TriggerPulse and the histograms correspond to at least  $9 \times 10^3$  events.

#### **6.3.13. GR reporter gene assays (Hela AZ-GR)**

$2 \times 10^4$  Hela AZ-GR [161] cells per well were seeded in PDL-coated 96 well cell culture plate. After overnight attachment, the medium was aspirated. 50  $\mu\text{L}$  2-fold concentrated Dexamethasone and 50  $\mu\text{L}$  2-fold concentrated PROTAC predilutions in medium were added. Or alternatively, in case of competition experiments, 50  $\mu\text{L}$  2-fold Dexamethasone, 25  $\mu\text{L}$  4-fold PROTAC and 25  $\mu\text{L}$  4-fold compound predilutions in medium were added. After 48 hours incubation, the cells were washed with 50  $\mu\text{L}$  4 °C DPBS and lysed in 60  $\mu\text{L}$  passive lysis buffer (Promega) for 30 minutes. Then, 20  $\mu\text{L}$  lysate were transferred to a white 96 well half area plate (Greiner #675075) and 20  $\mu\text{L}$ /well Bio-Glow Substrate (Promega) was added. After 5

minutes at room temperature, the luminescence was measured using a Tecan Spark plate reader (settle time: 1 s, integration time: 1 s). After the measurement, the luminescence values were normalized the unstimulated control (no Dex, no compound) to the fold-induction values and significance was tested by One-way or Two-way Anova tests as indicated using GraphPad Prism 8.

#### **6.3.14. GR reporter gene assays (HEK293T)**

$10^4$  HEK293T cells/well were seeded in a PDL-coated 96 well plate and left to attach overnight. Then, cells were transiently transfected with the dual reporter plasmids (pGL4.36 and pGL4.74 (Promega), prk5-HA-GR and/or prk5-FKBP51-Flag and prk5-FKBP52-Flag. Towards this, the plasmids were diluted in 10  $\mu$ l Opti-MEM (pGL4.36: 45 ng/well; pGL4.74: 5 ng/well; prk5-HA-GR, prk5-FKBP51-Flag, prk5-FKBP52-Flag and prk5 (empty vector); as indicated in the figure captions), 0.3  $\mu$ g/well PEI was added, and the mixture was incubated at room temperature for 30 minutes. Meanwhile, the medium was aspirated from the cells, 90  $\mu$ l/well fresh medium were added and after the incubation period, 10  $\mu$ l/well transfection mix were added to every well. On the next day, the cells were stimulated with dexamethasone, and depending on the experiment, co-treated with FKBP ligands or DMSO for 24 hours in a final volume of 100  $\mu$ l/well. Towards this, the transfection medium was removed and 50  $\mu$ l 2-fold Dexamethasone and 50  $\mu$ L 2-fold compound/DMSO dilutions in medium were added. Subsequently, the cells were washed with 50  $\mu$ l 4 °C DBPS and lysed in 60  $\mu$ L Passive Lysis Buffer (Promega) on ice for 30 minutes. For luminescence measurements, 20  $\mu$ L cell lysates were transferred to white 96 half area plates (Greiner) and 20  $\mu$ l/well Dual-Glo<sup>®</sup> Luciferase Reagent (Promega) were added. After 5 minutes at room temperature, the luc2p luminescence (settle time: 1 s, integration time: 1 s) was measured. Then, 20  $\mu$ l/well Dual-Glo<sup>®</sup> Stop & Glo<sup>®</sup> Reagent (Promega) were added, and the renellia luciferase signal was measured (settle time: 1 s, integration time: 1 s). Afterwards, the luminescence ratio was calculated ( $\text{luc2p}_{\text{lum.}} / \text{hRluc}_{\text{lum.}}$ ) and subsequently normalized to the ratio of the unstimulated mock (empty vector) control to obtain fold-induction values.

#### **6.3.15. NanoBRET assays**

Tracer titration experiments were used to determine the EC<sub>50</sub> of the tracer. A tracer 1:2 dilution series (14 steps) was performed in DMSO at a 100-fold concentration. Afterwards, the tracer dilutions in DMSO were prediluted 1:50 in Opti-MEM to yield a 2-fold concentrated stock and 20  $\mu$ L of this stock were transferred to a white non-binding 384 well plate (Greiner #781904) (triplicates for every tracer concentration). Afterwards, HEK293T cells stably expressing

FKBP51<sup>FK1</sup>-Nluc were collected, adjusted to a cell count of  $6.8 \times 10^5$  cells/ml in Opti-MEM, and 20  $\mu$ l were transferred to the assay plate. The plate was spun down, sealed with an aluminum foil, and shaken for 2 hours at 37 °C. After 15 minutes equilibration at room temperature, Nanoluciferase substrate and extracellular inhibitor were added as described in [162]. After 5 minutes at room temperature, the luminescence was measured using a Tecan Spark with the following spectral adjustments: well-wise measuring mode, donor signal: 445-470 nm integration time: 1s and acceptor signal: 610-700 nm integration time: 1s. Afterwards, the BRET ratio ( $\text{acceptor}_{\text{Signal}} / \text{donor}_{\text{Signal}}$ ) was calculated and EC<sub>50</sub> was obtained by a four-parameter IC<sub>50</sub> fit using GraphPad Prism 8.

For competitive FKBP-engagement profiling of FKBP ligands the following protocol was used: a dilution series at a 100-fold concentration of the final sample was prepared in DMSO using a pipetting robot. Subsequently, DMSO dilution stocks were diluted to a two-fold concentration in Opti-MEM. Afterwards, 20  $\mu$ l of the two-fold dilution were transferred to 3 distinct white non-binding 384 assay plates (Greiner #781904) to yield triplicates. The dilutions and transfer were performed by a pitting robot (Beckmann; Biomek FX<sup>P</sup>). Afterwards, HEK293T cells stably expressing FKBP12-Nluc or FKBP51<sup>FK1</sup>-Nluc were collected, and the cell count adjusted to  $9.8 \times 10^5$  cells/ml in Opti-MEM. The fluorescent tracer 2b [162] and 2c [162] were diluted to 160 nM and 3.2  $\mu$ M in Opti-MEM to yield an 8-fold tracer stock solution, respectively, for FKBP12 and FKBP51<sup>FK1</sup> NanoBRET assays. Then, cell suspension were mixed with tracer dilution in a ratio of 3:1 to obtain a 2-fold concentrated cell:tracer mixture, of which 20  $\mu$ L/well were added to the compound solutions. The plates were spun down, sealed with aluminum foil and shaken for 2 hours at 37°C. After 15 minutes equilibration at room temperature, Nanoluciferase substrate and extracellular inhibitor (Promega, N2160) was diluted in Opti-MEM as described in [162] or extracellular Nluc-Inhibitor (compound 43 [164]) and luciferin (compound 26dl [163]) were dissolved in Opti-MEM at concentrations of 7.5  $\mu$ M and 6.6  $\mu$ M. 20  $\mu$ l/well of the substrate-inhibitor mixture were added to the assay plates for BRET detection. After 5 minutes at room temperature, the luminescence was measured using a Tecan Spark with the following spectral adjustments: well-wise measuring mode wavelength donor signal: 445-470 nm integration time: 1s and acceptor signal: 610-700 nm integration time: 1s. Afterwards, the BRET ratio ( $\text{acceptor}_{\text{Signal}} / \text{donor}_{\text{Signal}}$ ) was calculated and IC<sub>50</sub> was obtained by a four-parameter IC<sub>50</sub> fit using GraphPad Prism 8.

To obtain the luciferin derivate 26dl [163] from the o-acetylated precursor, 1 mg 26dl-precursor, was dissolved in 200  $\mu$ L DMSO and then diluted with 300  $\mu$ L acidic ethanol (100  $\mu$ L

---

37% hydrochloric acid in 12 ml 100% ethanol). After overnight incubation, a stock solution of 4.22 mM was obtained and used without further purification. The stock solution was stored under argon at -80 °C until usage.

---

## 7. References

---

- [1] M.S. Weiss, A. Jabs, R. Hilgenfeld, Peptide bonds revisited, *Nat Struct Mol Biol* 5 (1998) 676. <https://doi.org/10.1038/1368>.
- [2] M.W. Harding, A. Galat, D.E. Uehling, S.L. Schreiber, A receptor for the immunosuppressant FK506 is a cis-trans peptidyl-prolyl isomerase, *Nature* 341 (1989) 758–760. <https://doi.org/10.1038/341758a0>.
- [3] J.J. Siekierka, S.H. Hung, M. Poe, C.S. Lin, N.H. Sigal, A cytosolic binding protein for the immunosuppressant FK506 has peptidyl-prolyl isomerase activity but is distinct from cyclophilin, *Nature* 341 (1989) 755–757. <https://doi.org/10.1038/341755a0>.
- [4] J. Choi, J. Chen, S.L. Schreiber, J. Clardy, Structure of the FKBP12-rapamycin complex interacting with the binding domain of human FRAP, *Science* 273 (1996) 239–242. <https://doi.org/10.1126/science.273.5272.239>.
- [5] A.R. Marks, Cellular functions of immunophilins, *Physiol. Rev.* 76 (1996) 631–649. <https://doi.org/10.1152/physrev.1996.76.3.631>.
- [6] W. Shou, B. Aghdasi, D.L. Armstrong, Q. Guo, S. Bao, M.J. Charng, L.M. Mathews, M.D. Schneider, S.L. Hamilton, M.M. Matzuk, Cardiac defects and altered ryanodine receptor function in mice lacking FKBP12, *Nature* 391 (1998) 489–492. <https://doi.org/10.1038/35146>.
- [7] A. Hähle, S. Merz, C. Meyners, F. Hausch, The Many Faces of FKBP51, *Biomolecules* 9 (2019). <https://doi.org/10.3390/biom9010035>.
- [8] K. Lee, A.C. Thwin, C.M. Nadel, E. Tse, S.N. Gates, J.E. Gestwicki, D.R. Southworth, The structure of an Hsp90-immunophilin complex reveals cochaperone recognition of the client maturation state, *Mol. Cell* 81 (2021) 3496-3508.e5. <https://doi.org/10.1016/j.molcel.2021.07.023>.
- [9] R. Zhao, M. Davey, Y.-C. Hsu, P. Kaplanek, A. Tong, A.B. Parsons, N. Krogan, G. Cagney, D. Mai, J. Greenblatt, C. Boone, A. Emili, W.A. Houry, Navigating the chaperone network: an integrative map of physical and genetic interactions mediated by the hsp90 chaperone, *Cell* 120 (2005) 715–727. <https://doi.org/10.1016/j.cell.2004.12.024>.
- [10] M. Ruiz-Estevez, J. Staats, E. Paatela, D. Munson, N. Katoku-Kikyo, C. Yuan, Y. Asakura, R. Hostager, H. Kobayashi, A. Asakura, N. Kikyo, Promotion of Myoblast Differentiation by Fkbp5 via Cdk4 Isomerization, *Cell Rep.* 25 (2018) 2537-2551.e8. <https://doi.org/10.1016/j.celrep.2018.11.006>.
- [11] B. Qiu, Z. Zhong, S. Righter, Y. Xu, J. Wang, R. Deng, C. Wang, K.E. Williams, Y.-Y. Ma, G. Tsechpenakis, T. Liang, W. Yong, FKBP51 modulates hippocampal size and function in



- post-translational regulation of Parkin, *Cell. Mol. Life Sci.* 79 (2022) 175.  
<https://doi.org/10.1007/s00018-022-04167-8>.
- [12] U.K. Jinwal, J. Koren, S.I. Borysov, A.B. Schmid, J.F. Abisambra, L.J. Blair, A.G. Johnson, J.R. Jones, C.L. Shults, J.C. O'Leary, Y. Jin, J. Buchner, M.B. Cox, C.A. Dickey, The Hsp90 cochaperone, FKBP51, increases Tau stability and polymerizes microtubules, *J. Neurosci.* 30 (2010) 591–599. <https://doi.org/10.1523/JNEUROSCI.4815-09.2010>.
- [13] L.J. Blair, B.A. Nordhues, S.E. Hill, K.M. Scaglione, J.C. O'Leary, S.N. Fontaine, L. Breydo, B. Zhang, P. Li, L. Wang, C. Cotman, H.L. Paulson, M. Muschol, V.N. Uversky, T. Klengel, E.B. Binder, R. Kaye, T.E. Golde, N. Berchtold, C.A. Dickey, Accelerated neurodegeneration through chaperone-mediated oligomerization of tau, *J. Clin. Invest.* 123 (2013) 4158–4169. <https://doi.org/10.1172/JCI69003>.
- [14] S. Tranguch, J. Cheung-Flynn, T. Daikoku, V. Prapapanich, M.B. Cox, H. Xie, H. Wang, S.K. Das, D.F. Smith, S.K. Dey, Cochaperone immunophilin FKBP52 is critical to uterine receptivity for embryo implantation, *Proc. Natl. Acad. Sci. U. S. A.* 102 (2005) 14326–14331. <https://doi.org/10.1073/pnas.0505775102>.
- [15] W. Yong, Z. Yang, S. Periyasamy, H. Chen, S. Yucel, W. Li, L.Y. Lin, I.M. Wolf, M.J. Cohn, L.S. Baskin, E.R. Sa Nchez, W. Shou, Essential role for Co-chaperone Fkbp52 but not Fkbp51 in androgen receptor-mediated signaling and physiology, *J. Biol. Chem.* 282 (2007) 5026–5036. <https://doi.org/10.1074/jbc.M609360200>.
- [16] M. Maiarù, K.K. Tochiki, M.B. Cox, L.V. Annan, C.G. Bell, X. Feng, F. Hausch, S.M. Géranton, The stress regulator FKBP51 drives chronic pain by modulating spinal glucocorticoid signaling, *Sci. Transl. Med.* 8 (2016) 325ra19.  
<https://doi.org/10.1126/scitranslmed.aab3376>.
- [17] M. Maiarù, O.B. Morgan, T. Mao, M. Breitsamer, H. Bamber, M. Pöhlmann, M.V. Schmidt, G. Winter, F. Hausch, S.M. Géranton, The stress regulator FKBP51: a novel and promising druggable target for the treatment of persistent pain states across sexes, *Pain* 159 (2018) 1224–1234. <https://doi.org/10.1097/j.pain.0000000000001204>.
- [18] J. Hartmann, K.V. Wagner, C. Liebl, S.H. Scharf, X.-D. Wang, M. Wolf, F. Hausch, T. Rein, U. Schmidt, C. Touma, J. Cheung-Flynn, M.B. Cox, D.F. Smith, F. Holsboer, M.B. Müller, M.V. Schmidt, The involvement of FK506-binding protein 51 (FKBP5) in the behavioral and neuroendocrine effects of chronic social defeat stress, *Neuropharmacology* 62 (2012) 332–339.  
<https://doi.org/10.1016/j.neuropharm.2011.07.041>.
- [19] J.C. O'Leary, S. Dharia, L.J. Blair, S. Brady, A.G. Johnson, M. Peters, J. Cheung-Flynn, M.B. Cox, G. de Erausquin, E.J. Weeber, U.K. Jinwal, C.A. Dickey, A new anti-depressive

- strategy for the elderly: ablation of FKBP5/FKBP51, *PLoS One* 6 (2011) e24840.  
<https://doi.org/10.1371/journal.pone.0024840>.
- [20] C. Touma, N.C. Gassen, L. Herrmann, J. Cheung-Flynn, D.R. Büll, I.A. Ionescu, J.-M. Heinzmann, A. Knapman, A. Siebertz, A.-M. Depping, J. Hartmann, F. Hausch, M.V. Schmidt, F. Holsboer, M. Ising, M.B. Cox, U. Schmidt, T. Rein, FK506 binding protein 5 shapes stress responsiveness: modulation of neuroendocrine reactivity and coping behavior, *Biol. Psychiatry* 70 (2011) 928–936.  
<https://doi.org/10.1016/j.biopsych.2011.07.023>.
- [21] S. Albu, C.P.N. Romanowski, M. Letizia Curzi, V. Jakubcakova, C. Flachskamm, N.C. Gassen, J. Hartmann, M.V. Schmidt, U. Schmidt, T. Rein, F. Holsboer, F. Hausch, M. Paez-Pereda, M. Kimura, Deficiency of FK506-binding protein (FKBP) 51 alters sleep architecture and recovery sleep responses to stress in mice, *J. Sleep Res.* 23 (2014) 176–185. <https://doi.org/10.1111/jsr.12112>.
- [22] G. Balsevich, A.S. Häusl, C.W. Meyer, S. Karamihalev, X. Feng, M.L. Pöhlmann, C. Dournes, A. Uribe-Marino, S. Santarelli, C. Labermaier, K. Hafner, T. Mao, M. Breitsamer, M. Theodoropoulou, C. Namendorf, M. Uhr, M. Paez-Pereda, G. Winter, F. Hausch, A. Chen, M.H. Tschöp, T. Rein, N.C. Gassen, M.V. Schmidt, Stress-responsive FKBP51 regulates AKT2-AS160 signaling and metabolic function, *Nat. Commun.* 8 (2017) 1725.  
<https://doi.org/10.1038/s41467-017-01783-y>.
- [23] L.A. Stechschulte, B. Qiu, M. Warrior, T.D. Hinds, M. Zhang, H. Gu, Y. Xu, S.S. Khuder, L. Russo, S.M. Najjar, B. Lecka-Czernik, W. Yong, E.R. Sanchez, FKBP51 Null Mice Are Resistant to Diet-Induced Obesity and the PPAR $\gamma$  Agonist Rosiglitazone, *Endocrinology* 157 (2016) 3888–3900. <https://doi.org/10.1210/en.2015-1996>.
- [24] T. Jääskeläinen, H. Makkonen, J.J. Palvimo, Steroid up-regulation of FKBP51 and its role in hormone signaling, *Curr. Opin. Pharmacol.* 11 (2011) 326–331.  
<https://doi.org/10.1016/j.coph.2011.04.006>.
- [25] T. Klengel, D. Mehta, C. Anacker, M. Rex-Haffner, J.C. Pruessner, C.M. Pariante, T.W.W. Pace, K.B. Mercer, H.S. Mayberg, B. Bradley, C.B. Nemeroff, F. Holsboer, C.M. Heim, K.J. Ressler, T. Rein, E.B. Binder, Allele-specific FKBP5 DNA demethylation mediates gene-childhood trauma interactions, *Nat. Neurosci.* 16 (2013) 33–41.  
<https://doi.org/10.1038/nn.3275>.
- [26] G.M. Wozniak, J. Rüegg, G.A. Abel, U. Schmidt, F. Holsboer, T. Rein, FK506-binding proteins 51 and 52 differentially regulate dynein interaction and nuclear translocation of the glucocorticoid receptor in mammalian cells, *J. Biol. Chem.* 280 (2005) 4609–4616.  
<https://doi.org/10.1074/jbc.M407498200>.

- 
- [27] A. Baischew, S. Engel, T.M. Geiger, M.C. Taubert, F. Hausch, Structural and biochemical insights into FKBP51 as a Hsp90 co-chaperone, *J. Cell. Biochem.* (2023).  
<https://doi.org/10.1002/jcb.30384>.
- [28] P.G. Febbo, M. Lowenberg, A.R. Thorner, M. Brown, M. Loda, T.R. Golub, Androgen mediated regulation and functional implications of fkbp51 expression in prostate cancer, *J. Urol.* 173 (2005) 1772–1777. <https://doi.org/10.1097/01.ju.0000155845.44729.ba>.
- [29] L. Ni, C.-S. Yang, D. Gioeli, H. Frierson, D.O. Toft, B.M. Paschal, FKBP51 promotes assembly of the Hsp90 chaperone complex and regulates androgen receptor signaling in prostate cancer cells, *Mol. Cell. Biol.* 30 (2010) 1243–1253.  
<https://doi.org/10.1128/MCB.01891-08>.
- [30] S. Periyasamy, T. Hinds, L. Shemshedini, W. Shou, E.R. Sanchez, FKBP51 and Cyp40 are positive regulators of androgen-dependent prostate cancer cell growth and the targets of FK506 and cyclosporin A, *Oncogene* 29 (2010) 1691–1701.  
<https://doi.org/10.1038/onc.2009.458>.
- [31] D.L. Riggs, M.B. Cox, H.L. Tardif, M. Hessling, J. Buchner, D.F. Smith, Noncatalytic role of the FKBP52 peptidyl-prolyl isomerase domain in the regulation of steroid hormone signaling, *Mol. Cell. Biol.* 27 (2007) 8658–8669. <https://doi.org/10.1128/MCB.00985-07>.
- [32] J.-P. Schülke, G.M. Wochnik, I. Lang-Rollin, N.C. Gassen, R.T. Knapp, B. Berning, A. Yassouridis, T. Rein, Differential impact of tetratricopeptide repeat proteins on the steroid hormone receptors, *PLoS One* 5 (2010) e11717.  
<https://doi.org/10.1371/journal.pone.0011717>.
- [33] C. Storer Samaniego, J.H. Suh, A. Chattopadhyay, K. Olivares, N. Guy, J.C. Sivils, P. Dey, F. Yumoto, R.J. Fletterick, A.M. Strom, J.-Å. Gustafsson, P. Webb, M.B. Cox, The FKBP52 Cochaperone Acts in Synergy with  $\beta$ -Catenin to Potentiate Androgen Receptor Signaling, *PLoS One* 10 (2015) e0134015. <https://doi.org/10.1371/journal.pone.0134015>.
- [34] E. Kirschke, D. Goswami, D. Southworth, P.R. Griffin, D.A. Agard, Glucocorticoid receptor function regulated by coordinated action of the Hsp90 and Hsp70 chaperone cycles, *Cell* 157 (2014) 1685–1697. <https://doi.org/10.1016/j.cell.2014.04.038>.
- [35] R.Y.-R. Wang, C.M. Noddings, E. Kirschke, A.G. Myasnikov, J.L. Johnson, D.A. Agard, Structure of Hsp90-Hsp70-Hop-GR reveals the Hsp90 client-loading mechanism, *Nature* 601 (2022) 460–464. <https://doi.org/10.1038/s41586-021-04252-1>.
- [36] I.-O. Ebong, V. Beilsten-Edmands, N.A. Patel, N. Morgner, C.V. Robinson, The interchange of immunophilins leads to parallel pathways and different intermediates in

- the assembly of Hsp90 glucocorticoid receptor complexes, *Cell Discov.* 2 (2016) 16002. <https://doi.org/10.1038/celldisc.2016.2>.
- [37] C.M. Noddings, R.Y.-R. Wang, J.L. Johnson, D.A. Agard, Structure of Hsp90-p23-GR reveals the Hsp90 client-remodelling mechanism, *Nature* 601 (2022) 465–469. <https://doi.org/10.1038/s41586-021-04236-1>.
- [38] H. Pei, L. Li, B.L. Fridley, G.D. Jenkins, K.R. Kalari, W. Lingle, G. Petersen, Z. Lou, L. Wang, FKBP51 affects cancer cell response to chemotherapy by negatively regulating Akt, *Cancer Cell* 16 (2009) 259–266. <https://doi.org/10.1016/j.ccr.2009.07.016>.
- [39] A.-K. Fabian, A. März, S. Neimanis, R.M. Biondi, C. Kozany, F. Hausch, InterAKTions with FKBP51—mutational and pharmacological exploration, *PLoS One* 8 (2013) e57508. <https://doi.org/10.1371/journal.pone.0057508>.
- [40] J. Yu, B. Qin, F. Wu, S. Qin, S. Nowsheen, S. Shan, J. Zayas, H. Pei, Z. Lou, L. Wang, Regulation of Serine-Threonine Kinase Akt Activation by NAD<sup>+</sup>-Dependent Deacetylase SIRT7, *Cell Rep.* 18 (2017) 1229–1240. <https://doi.org/10.1016/j.celrep.2017.01.009>.
- [41] M. Tufano, L. Marrone, C. D'Ambrosio, V. Di Giacomo, S. Urzini, Y. Xiao, M. Matuozzo, A. Scaloni, M.F. Romano, S. Romano, FKBP51 plays an essential role in Akt ubiquitination that requires Hsp90 and PHLPP, *Cell Death Dis.* 14 (2023) 116. <https://doi.org/10.1038/s41419-023-05629-y>.
- [42] K. Luo, Y. Li, Y. Yin, L. Li, C. Wu, Y. Chen, S. Nowsheen, Q. Hu, L. Zhang, Z. Lou, J. Yuan, USP49 negatively regulates tumorigenesis and chemoresistance through FKBP51-AKT signaling, *EMBO J.* 36 (2017) 1434–1446. <https://doi.org/10.15252/embj.201695669>.
- [43] J.M. Kolos, A.M. Voll, M. Bauder, F. Hausch, FKBP Ligands—Where We Are and Where to Go?, *Front. Pharmacol.* 9 (2018) 1425. <https://doi.org/10.3389/fphar.2018.01425>.
- [44] R.E. Babine, T.M. Bleckman, E.S. Littlefield, H.E. Parge, L. Pelletier, C.T. Lewis, J.V. French, M. Imbacuan, S. Katoh, J.H. Tatlock, R.E. Showalter, J. Villafranca, Design, synthesis and X-ray crystallographic studies of [7.3.1] and [8.3.1] macrocyclic FKBP-12 ligands, *Bioorganic & Medicinal Chemistry Letters* 6 (1996) 385–390. [https://doi.org/10.1016/0960-894x\(96\)00032-7](https://doi.org/10.1016/0960-894x(96)00032-7).
- [45] R.E. Babine, T.M. Bleckman, C.R. Kissinger, R. Showalter, L.A. Pelletier, C. Lewis, K. Tucker, E. Moomaw, H.E. Parge, J. Villafranca, Design, synthesis and X-ray crystallographic studies of novel FKBP-12 ligands, *Bioorg. Med. Chem. Lett.* 5 (1995) 1719–1724. [https://doi.org/10.1016/0960-894x\(95\)00290-A](https://doi.org/10.1016/0960-894x(95)00290-A).

- [46] R. Gopalakrishnan, C. Kozany, S. Gaali, C. Kress, B. Hoogeland, A. Bracher, F. Hausch, Evaluation of synthetic FK506 analogues as ligands for the FK506-binding proteins 51 and 52, *J. Med. Chem.* 55 (2012) 4114–4122. <https://doi.org/10.1021/jm201746x>.
- [47] R. Gopalakrishnan, C. Kozany, Y. Wang, S. Schneider, B. Hoogeland, A. Bracher, F. Hausch, Exploration of pipercolate sulfonamides as binders of the FK506-binding proteins 51 and 52, *J. Med. Chem.* 55 (2012) 4123–4131. <https://doi.org/10.1021/jm201747c>.
- [48] Y. Wang, A. Kirschner, A.-K. Fabian, R. Gopalakrishnan, C. Kress, B. Hoogeland, U. Koch, C. Kozany, A. Bracher, F. Hausch, Increasing the efficiency of ligands for FK506-binding protein 51 by conformational control, *J. Med. Chem.* 56 (2013) 3922–3935. <https://doi.org/10.1021/jm400087k>.
- [49] S. Pomplun, C. Sippel, A. Hähle, D. Tay, K. Shima, A. Klages, C.M. Ünal, B. Rieß, H.T. Toh, G. Hansen, H.S. Yoon, A. Bracher, P. Preiser, J. Rupp, M. Steinert, F. Hausch, Chemogenomic Profiling of Human and Microbial FK506-Binding Proteins, *J. Med. Chem.* 61 (2018) 3660–3673. <https://doi.org/10.1021/acs.jmedchem.8b00137>.
- [50] S. Pomplun, Y. Wang, A. Kirschner, C. Kozany, A. Bracher, F. Hausch, Rational design and asymmetric synthesis of potent and neurotrophic ligands for FK506-binding proteins (FKBPs), *Angew. Chem. Int. Ed Engl.* 54 (2015) 345–348. <https://doi.org/10.1002/anie.201408776>.
- [51] J.M. Kolos, S. Pomplun, S. Jung, B. Rieß, P.L. Purder, A.M. Voll, S. Merz, M. Gnatzy, T.M. Geiger, I. Quist-Løkken, J. Jatzlau, P. Knaus, T. Holien, A. Bracher, C. Meyners, P. Czodrowski, V. Krewald, F. Hausch, Picomolar FKBP inhibitors enabled by a single water-displacing methyl group in bicyclic 4.3.1 aza-amides, *Chem. Sci.* 12 (2021) 14758–14765. <https://doi.org/10.1039/d1sc04638a>.
- [52] R.C. Deutscher, C. Meyners, S.C. Schäfer, M.L. Repity, W.O. Sugiarto, J. Kolos, T. Heymann, T.M. Geiger, S. Knapp, F. Hausch, Discovery of fully synthetic FKBP12-mTOR molecular glues, 2023.
- [53] R. Deutscher, M.S. Karagöz, P. Purder, J. Kolos, C. Meyners, W.O. Sugiarto, P. Krajczyk, F. Tebbe, T. Geiger, C. Ünal, U. Hellmich, M. Steinert, F. Hausch, 4.3.1 Bicyclic FKBP ligands inhibit *Legionella pneumophila* infection by LpMip-dependent and LpMip independent mechanisms, *Chembiochem* (2023) e202300442. <https://doi.org/10.1002/cbic.202300442>.
- [54] S. Gaali, A. Kirschner, S. Cuboni, J. Hartmann, C. Kozany, G. Balsevich, C. Namendorf, P. Fernandez-Vizarra, C. Sippel, A.S. Zannas, R. Draenert, E.B. Binder, O.F.X. Almeida, G. Rührter, M. Uhr, M.V. Schmidt, C. Touma, A. Bracher, F. Hausch, Selective inhibitors of

- the FK506-binding protein 51 by induced fit, *Nat. Chem. Biol.* 11 (2015) 33–37.  
<https://doi.org/10.1038/nchembio.1699>.
- [55] V. Buffa, F.H. Knaup, T. Heymann, M. Springer, M.V. Schmidt, F. Hausch, Analysis of the Selective Antagonist SAFit2 as a Chemical Probe for the FK506-Binding Protein 51, *ACS Pharmacol. Transl. Sci.* 6 (2023) 361–371. <https://doi.org/10.1021/acscptsci.2c00234>.
- [56] A.M. Voll, C. Meyners, M.C. Taubert, T. Bajaj, T. Heymann, S. Merz, A. Charalampidou, J. Kolos, P.L. Purder, T.M. Geiger, P. Wessig, N.C. Gassen, A. Bracher, F. Hausch, Macrocyclic FKBP51 Ligands Define a Transient Binding Mode with Enhanced Selectivity, *Angew. Chem. Int. Ed Engl.* 60 (2021) 13257–13263.  
<https://doi.org/10.1002/anie.202017352>.
- [57] M. Bauder, C. Meyners, P.L. Purder, S. Merz, W.O. Sugiarto, A.M. Voll, T. Heymann, F. Hausch, Structure-Based Design of High-Affinity Macrocyclic FKBP51 Inhibitors, *J. Med. Chem.* 64 (2021) 3320–3349. <https://doi.org/10.1021/acs.jmedchem.0c02195>.
- [58] E.M. Driggers, S.P. Hale, J. Lee, N.K. Terrett, The exploration of macrocycles for drug discovery--an underexploited structural class, *Nat. Rev. Drug Discov.* 7 (2008) 608–624.  
<https://doi.org/10.1038/nrd2590>.
- [59] A. Whitty, M. Zhong, L. Viarengo, D. Beglov, D.R. Hall, S. Vajda, Quantifying the chameleonic properties of macrocycles and other high-molecular-weight drugs, *Drug Discov. Today* 21 (2016) 712–717. <https://doi.org/10.1016/j.drudis.2016.02.005>.
- [60] F.H. Knaup, C. Meyners, W.O. Sugiarto, S. Wedel, M. Springer, C. Walz, T.M. Geiger, M. Schmidt, M. Sisignano, F. Hausch, Structure-Based Discovery of a New Selectivity-Enabling Motif for the FK506-Binding Protein 51, *J. Med. Chem.* 66 (2023) 5965–5980.  
<https://doi.org/10.1021/acs.jmedchem.3c00249>.
- [61] S. Gaali, X. Feng, A. Hähle, C. Sippel, A. Bracher, F. Hausch, Rapid, Structure-Based Exploration of Pipercolic Acid Amides as Novel Selective Antagonists of the FK506-Binding Protein 51, *J. Med. Chem.* 59 (2016) 2410–2422.  
<https://doi.org/10.1021/acs.jmedchem.5b01355>.
- [62] X. Feng, C. Sippel, F.H. Knaup, A. Bracher, S. Staibano, M.F. Romano, F. Hausch, A Novel Decalin-Based Bicyclic Scaffold for FKBP51-Selective Ligands, *J. Med. Chem.* 63 (2020) 231–240. <https://doi.org/10.1021/acs.jmedchem.9b01157>.
- [63] X. Feng, C. Sippel, A. Bracher, F. Hausch, Structure-Affinity Relationship Analysis of Selective FKBP51 Ligands, *J. Med. Chem.* 58 (2015) 7796–7806.  
<https://doi.org/10.1021/acs.jmedchem.5b00785>.

- [64] M. Bischoff, C. Sippel, A. Bracher, F. Hausch, Stereoselective construction of the 5-hydroxy diazabicyclo[4.3.1]decane-2-one scaffold, a privileged motif for FK506-binding proteins, *Org. Lett.* 16 (2014) 5254–5257. <https://doi.org/10.1021/ol5023195>.
- [65] S. Khan, X. Zhang, D. Lv, Q. Zhang, Y. He, P. Zhang, X. Liu, D. Thummuri, Y. Yuan, J.S. Wiegand, J. Pei, W. Zhang, A. Sharma, C.R. McCurdy, V.M. Kuruvilla, N. Baran, A.A. Ferrando, Y.-M. Kim, A. Rogojina, P.J. Houghton, G. Huang, R. Hromas, M. Konopleva, G. Zheng, D. Zhou, A selective BCL-XL PROTAC degrader achieves safe and potent antitumor activity, *Nat. Med.* 25 (2019) 1938–1947. <https://doi.org/10.1038/s41591-019-0668-z>.
- [66] T.M. Geiger, S.C. Schäfer, J.K. Dreizler, M. Walz, F. Hausch, Clues to molecular glues, *Current Research in Chemical Biology* 2 (2022) 100018. <https://doi.org/10.1016/j.crchbi.2021.100018>.
- [67] J.F. Borel, Z.L. Kis, T. Beveridge, The History of the Discovery and Development of Cyclosporine (Sandimmune®), in: V.J. Merluzzi, J. Adams (Eds.), *The search for anti-inflammatory drugs: Case histories from concept to clinic*, Birkhäuser, Boston, 1995, pp. 27–63.
- [68] J. Liu, J.D. Farmer, W.S. Lane, J. Friedman, I. Weissman, S.L. Schreiber, Calcineurin is a common target of cyclophilin-cyclosporin A and FKBP-FK506 complexes, *Cell* 66 (1991) 807–815. [https://doi.org/10.1016/0092-8674\(91\)90124-h](https://doi.org/10.1016/0092-8674(91)90124-h).
- [69] Q. Huai, H.-Y. Kim, Y. Liu, Y. Zhao, A. Mondragon, J.O. Liu, H. Ke, Crystal structure of calcineurin-cyclophilin-cyclosporin shows common but distinct recognition of immunophilin-drug complexes, *Proc. Natl. Acad. Sci. U. S. A.* 99 (2002) 12037–12042. <https://doi.org/10.1073/pnas.192206699>.
- [70] J.J. Sanglier, V. Quesniaux, T. Fehr, H. Hofmann, M. Mahnke, K. Memmert, W. Schuler, G. Zenke, L. Gschwind, C. Maurer, W. Schilling, Sanglifehrins A, B, C and D, novel cyclophilin-binding compounds isolated from *Streptomyces* sp. A92-308110. I. Taxonomy, fermentation, isolation and biological activity, *J. Antibiot. (Tokyo)* 52 (1999) 466–473. <https://doi.org/10.7164/antibiotics.52.466>.
- [71] K.H. Pua, D.T. Stiles, M.E. Sowa, G.L. Verdine, IMPDH2 Is an Intracellular Target of the Cyclophilin A and Sanglifehrins A Complex, *Cell Rep.* 18 (2017) 432–442. <https://doi.org/10.1016/j.celrep.2016.12.030>.
- [72] A.M. März, A.-K. Fabian, C. Kozany, A. Bracher, F. Hausch, Large FK506-binding proteins shape the pharmacology of rapamycin, *Mol. Cell. Biol.* 33 (2013) 1357–1367. <https://doi.org/10.1128/MCB.00678-12>.

- [73] C.R. Kissinger, H.E. Parge, D.R. Knighton, C.T. Lewis, L.A. Pelletier, A. Tempczyk, V.J. Kalish, K.D. Tucker, R.E. Showalter, E.W. Moomaw, Crystal structures of human calcineurin and the human FKBP12-FK506-calcineurin complex, *Nature* 378 (1995) 641–644. <https://doi.org/10.1038/378641a0>.
- [74] J.P. Griffith, J.L. Kim, E.E. Kim, M.D. Sintchak, J.A. Thomson, M.J. Fitzgibbon, M.A. Fleming, P.R. Caron, K. Hsiao, M.A. Navia, X-ray structure of calcineurin inhibited by the immunophilin-immunosuppressant FKBP12-FK506 complex, *Cell* 82 (1995) 507–522. [https://doi.org/10.1016/0092-8674\(95\)90439-5](https://doi.org/10.1016/0092-8674(95)90439-5).
- [75] S.L. Schreiber, Immunophilin-sensitive protein phosphatase action in cell signaling pathways, *Cell* 70 (1992) 365–368. [https://doi.org/10.1016/0092-8674\(92\)90158-9](https://doi.org/10.1016/0092-8674(92)90158-9).
- [76] G.R. Crabtree, S.L. Schreiber, Three-part inventions: intracellular signaling and induced proximity, *Trends Biochem. Sci.* 21 (1996) 418–422. [https://doi.org/10.1016/s0968-0004\(96\)20027-1](https://doi.org/10.1016/s0968-0004(96)20027-1).
- [77] G.M. Salituro, D.L. Zink, A. Dahl, J. Nielsen, E. Wu, L. Huang, C. Kastner, F.J. Dumont, Meridamycin: A novel nonimmunosuppressive FKBP12 ligand from streptomyces *hygroscopicus*, *Tetrahedron Letters* 36 (1995) 997–1000. [https://doi.org/10.1016/0040-4039\(94\)02425-B](https://doi.org/10.1016/0040-4039(94)02425-B).
- [78] M.Y. Summers, M. Leighton, D. Liu, K. Pong, E.I. Graziani, 3-Normeridamycin: A Potent Non-Immunosuppressive Immunophilin Ligand is Neuroprotective in Dopaminergic Neurons, *ChemInform* 37 (2006). <https://doi.org/10.1002/chin.200639221>.
- [79] T. Fehr, J.J. Sanglier, W. Schuler, L. Gschwind, M. Ponelle, W. Schilling, C. Wioland, Antascomicins A, B, C, D and E. Novel FKBP12 binding compounds from a *Micromonospora* strain, *J. Antibiot. (Tokyo)* 49 (1996) 230–233. <https://doi.org/10.7164/antibiotics.49.230>.
- [80] Z. Guo, S.Y. Hong, J. Wang, S. Rehan, W. Liu, H. Peng, M. Das, W. Li, S. Bhat, B. Peiffer, B.R. Ullman, C.-M. Tse, Z. Tarmakova, C. Schiene-Fischer, G. Fischer, I. Coe, V.O. Paavilainen, Z. Sun, J.O. Liu, Rapamycin-inspired macrocycles with new target specificity, *Nat. Chem.* 11 (2019) 254–263. <https://doi.org/10.1038/s41557-018-0187-4>.
- [81] T. Ito, H. Ando, T. Suzuki, T. Ogura, K. Hotta, Y. Imamura, Y. Yamaguchi, H. Handa, Identification of a primary target of thalidomide teratogenicity, *Science* 327 (2010) 1345–1350. <https://doi.org/10.1126/science.1177319>.
- [82] J. Krönke, N.D. Udeshi, A. Narla, P. Grauman, S.N. Hurst, M. McConkey, T. Svinkina, D. Heckl, E. Comer, X. Li, C. Ciarlo, E. Hartman, N. Munshi, M. Schenone, S.L. Schreiber, S.A. Carr, B.L. Ebert, Lenalidomide causes selective degradation of IKZF1 and IKZF3 in



- multiple myeloma cells, *Science* 343 (2014) 301–305.  
<https://doi.org/10.1126/science.1244851>.
- [83] G. Lu, R.E. Middleton, H. Sun, M. Naniong, C.J. Ott, C.S. Mitsiades, K.-K. Wong, J.E. Bradner, W.G. Kaelin, The myeloma drug lenalidomide promotes the cereblon-dependent destruction of Ikaros proteins, *Science* 343 (2014) 305–309.  
<https://doi.org/10.1126/science.1244917>.
- [84] A.K. Gandhi, J. Kang, C.G. Havens, T. Conklin, Y. Ning, L. Wu, T. Ito, H. Ando, M.F. Waldman, A. Thakurta, A. Klippel, H. Handa, T.O. Daniel, P.H. Schafer, R. Chopra, Immunomodulatory agents lenalidomide and pomalidomide co-stimulate T cells by inducing degradation of T cell repressors Ikaros and Aiolos via modulation of the E3 ubiquitin ligase complex CRL4(CRBN.), *Br. J. Haematol.* 164 (2014) 811–821.  
<https://doi.org/10.1111/bjh.12708>.
- [85] J. An, C.M. Ponthier, R. Sack, J. Seebacher, M.B. Stadler, K.A. Donovan, E.S. Fischer, pSILAC mass spectrometry reveals ZFP91 as IMiD-dependent substrate of the CRL4CRBN ubiquitin ligase, *Nat. Commun.* 8 (2017) 15398.  
<https://doi.org/10.1038/ncomms15398>.
- [86] J. Krönke, E.C. Fink, P.W. Hollenbach, K.J. MacBeth, S.N. Hurst, N.D. Udeshi, P.P. Chamberlain, D.R. Mani, H.W. Man, A.K. Gandhi, T. Svinkina, R.K. Schneider, M. McConkey, M. Järås, E. Griffiths, M. Wetzler, L. Bullinger, B.E. Cathers, S.A. Carr, R. Chopra, B.L. Ebert, Lenalidomide induces ubiquitination and degradation of CK1 $\alpha$  in del(5q) MDS, *Nature* 523 (2015) 183–188. <https://doi.org/10.1038/nature14610>.
- [87] M.E. Matyskiela, G. Lu, T. Ito, B. Pagarigan, C.-C. Lu, K. Miller, W. Fang, N.-Y. Wang, D. Nguyen, J. Houston, G. Carmel, T. Tran, M. Riley, L. Nosaka, G.C. Lander, S. Gaidarova, S. Xu, A.L. Ruchelman, H. Handa, J. Carmichael, T.O. Daniel, B.E. Cathers, A. Lopez-Girona, P.P. Chamberlain, A novel cereblon modulator recruits GSPT1 to the CRL4(CRBN) ubiquitin ligase, *Nature* 535 (2016) 252–257.  
<https://doi.org/10.1038/nature18611>.
- [88] G. Petzold, E.S. Fischer, N.H. Thomä, Structural basis of lenalidomide-induced CK1 $\alpha$  degradation by the CRL4(CRBN) ubiquitin ligase, *Nature* 532 (2016) 127–130.  
<https://doi.org/10.1038/nature16979>.
- [89] A.D. Buhimschi, C.M. Crews, Evolving Rules for Protein Degradation? Insights from the Zinc Finger Degrome, *Biochemistry* 58 (2019) 861–864.  
<https://doi.org/10.1021/acs.biochem.8b01307>.
- [90] Q.L. Sievers, G. Petzold, R.D. Bunker, A. Renneville, M. Słabicki, B.J. Liddicoat, W. Abdulrahman, T. Mikkelsen, B.L. Ebert, N.H. Thomä, Defining the human C2H2 zinc

- finger degrome targeted by thalidomide analogs through CRBN, *Science* 362 (2018).  
<https://doi.org/10.1126/science.aat0572>.
- [91] M. Costacurta, J. He, P.E. Thompson, J. Shortt, *Molecular Mechanisms of Cereblon-Interacting Small Molecules in Multiple Myeloma Therapy*, *J. Pers. Med.* 11 (2021).  
<https://doi.org/10.3390/jpm11111185>.
- [92] T. Han, M. Goralski, N. Gaskill, E. Capota, J. Kim, T.C. Ting, Y. Xie, N.S. Williams, D. Nijhawan, *Anticancer sulfonamides target splicing by inducing RBM39 degradation via recruitment to DCAF15*, *Science* 356 (2017). <https://doi.org/10.1126/science.aal3755>.
- [93] T.C. Ting, M. Goralski, K. Klein, B. Wang, J. Kim, Y. Xie, D. Nijhawan, *Aryl Sulfonamides Degrade RBM39 and RBM23 by Recruitment to CRL4-DCAF15*, *Cell Rep.* 29 (2019) 1499-1510.e6. <https://doi.org/10.1016/j.celrep.2019.09.079>.
- [94] T. Uehara, Y. Minoshima, K. Sagane, N.H. Sugi, K.O. Mitsushashi, N. Yamamoto, H. Kamiyama, K. Takahashi, Y. Kotake, M. Uesugi, A. Yokoi, A. Inoue, T. Yoshida, M. Mabuchi, A. Tanaka, T. Owa, *Selective degradation of splicing factor CAPER $\alpha$  by anticancer sulfonamides*, *Nat. Chem. Biol.* 13 (2017) 675–680.  
<https://doi.org/10.1038/nchembio.2363>.
- [95] C. Mayor-Ruiz, S. Bauer, M. Brand, Z. Kozicka, M. Siklos, H. Imrichova, I.H. Kaltheuner, E. Hahn, K. Seiler, A. Koren, G. Petzold, M. Fellner, C. Bock, A.C. Müller, J. Zuber, M. Geyer, N.H. Thomä, S. Kubicek, G.E. Winter, *Rational discovery of molecular glue degraders via scalable chemical profiling*, *Nat. Chem. Biol.* 16 (2020) 1199–1207.  
<https://doi.org/10.1038/s41589-020-0594-x>.
- [96] T.B. Faust, H. Yoon, R.P. Nowak, K.A. Donovan, Z. Li, Q. Cai, N.A. Eleuteri, T. Zhang, N.S. Gray, E.S. Fischer, *Structural complementarity facilitates E7820-mediated degradation of RBM39 by DCAF15*, *Nat. Chem. Biol.* 16 (2020) 7–14.  
<https://doi.org/10.1038/s41589-019-0378-3>.
- [97] X. Du, O.A. Volkov, R.M. Czerwinski, H. Tan, C. Huerta, E.R. Morton, J.P. Rizzi, P.M. Wehn, R. Xu, D. Nijhawan, E.M. Wallace, *Structural Basis and Kinetic Pathway of RBM39 Recruitment to DCAF15 by a Sulfonamide Molecular Glue E7820*, *Structure* 27 (2019) 1625-1633.e3. <https://doi.org/10.1016/j.str.2019.10.005>.
- [98] D.E. Bussiere, L. Xie, H. Srinivas, W. Shu, A. Burke, C. Be, J. Zhao, A. Godbole, D. King, R.G. Karki, V. Hornak, F. Xu, J. Cobb, N. Carte, A.O. Frank, A. Frommlet, P. Graff, M. Knapp, A. Fazal, B. Okram, S. Jiang, P.-Y. Michellys, R. Beckwith, H. Voshol, C. Wiesmann, J.M. Solomon, J. Paulk, *Structural basis of indisulam-mediated RBM39 recruitment to DCAF15 E3 ligase complex*, *Nat. Chem. Biol.* 16 (2020) 15–23.  
<https://doi.org/10.1038/s41589-019-0411-6>.

- [99] S.A. Holstein, P.L. McCarthy, Immunomodulatory Drugs in Multiple Myeloma: Mechanisms of Action and Clinical Experience, *Drugs* 77 (2017) 505–520.  
<https://doi.org/10.1007/s40265-017-0689-1>.
- [100] M. Ślábicki, Z. Kozicka, G. Petzold, Y.-D. Li, M. Manojkumar, R.D. Bunker, K.A. Donovan, Q.L. Sievers, J. Koepfel, D. Suchyta, A.S. Sperling, E.C. Fink, J.A. Gasser, L.R. Wang, S.M. Corsello, R.S. Sellar, M. Jan, D. Gillingham, C. Scholl, S. Fröhling, T.R. Golub, E.S. Fischer, N.H. Thomä, B.L. Ebert, The CDK inhibitor CR8 acts as a molecular glue degrader that depletes cyclin K, *Nature* 585 (2020) 293–297.  
<https://doi.org/10.1038/s41586-020-2374-x>.
- [101] L. Lv, P. Chen, L. Cao, Y. Li, Z. Zeng, Y. Cui, Q. Wu, J. Li, J.-H. Wang, M.-Q. Dong, X. Qi, T. Han, Discovery of a molecular glue promoting CDK12-DDB1 interaction to trigger cyclin K degradation, *Elife* 9 (2020). <https://doi.org/10.7554/eLife.59994>.
- [102] S.M. Dieter, C. Siegl, P.L. Codó, M. Huerta, A.L. Ostermann-Parucha, E. Schulz, M.K. Zowada, S. Martin, K. Laaber, A. Nowrouzi, M. Blatter, S. Kreth, F. Westermann, A. Benner, U. Uhrig, K. Putzker, J. Lewis, A. Haegerbarth, D. Mumberg, S.J. Holton, J. Weiske, L.-M. Toepper, U. Scheib, G. Siemeister, C.R. Ball, B. Kuster, G. Stoehr, H. Hahne, S. Johannes, M. Lange, F. Herbst, H. Glimm, Degradation of CCNK/CDK12 is a druggable vulnerability of colorectal cancer, *Cell Rep.* 36 (2021) 109394.  
<https://doi.org/10.1016/j.celrep.2021.109394>.
- [103] M.S. Gadd, A. Testa, X. Lucas, K.-H. Chan, W. Chen, D.J. Lamont, M. Zengerle, A. Ciulli, Structural basis of PROTAC cooperative recognition for selective protein degradation, *Nat. Chem. Biol.* 13 (2017) 514–521.  
<https://doi.org/10.1038/nchembio.2329>.
- [104] J. Krieger, F.J. Sorrell, A.A. Wegener, B. Leuthner, F. Machrouhi-Porcher, M. Hecht, E.M. Leibrock, J.E. Müller, J. Eisert, I.V. Hartung, S. Schlesiger, Systematic Potency and Property Assessment of VHL Ligands and Implications on PROTAC Design, *ChemMedChem* 18 (2023) e202200615. <https://doi.org/10.1002/cmdc.202200615>.
- [105] M. Zengerle, K.-H. Chan, A. Ciulli, Selective Small Molecule Induced Degradation of the BET Bromodomain Protein BRD4, *ACS Chem. Biol.* 10 (2015) 1770–1777.  
<https://doi.org/10.1021/acscchembio.5b00216>.
- [106] R.A. Blake, P. Dragovich, L.J. Gazzard, S. Kaufman, T. Kleinheinz, T. Pillow, S. Staben, B. Wei (GENENTECH INC [US]; HOFFMANN LA ROCHE [CH]) WO2020055976 (A1), 2019.
- [107] A.G. Shergalis, V.L. Marin, D.Y. Rhee, S. Senaweera, R.L. McCloud, J.A. Ronau, C.W. Hutchins, S. McLoughlin, K.R. Woller, S.E. Warder, A. Vasudevan, J.M. Reitsma, CRISPR

- Screen Reveals BRD2/4 Molecular Glue-like Degradator via Recruitment of DCAF16, *ACS Chem. Biol.* 18 (2023) 331–339. <https://doi.org/10.1021/acscchembio.2c00747>.
- [108] Y.-D. Li, M.W. Ma, M.M. Hassan, M. Hunkeler, M. Teng, K. Puvar, R. Lumpkin, B. Sandoval, C.Y. Jin, S.B. Ficarro, M.Y. Wang, S. Xu, B.J. Groendyke, L.H. Sigua, I. Tavares, C. Zou, J.M. Tsai, P.M.C. Park, H. Yoon, F.C. Majewski, J.A. Marto, J. Qi, R.P. Nowak, K.A. Donovan, M. Słabicki, N.S. Gray, E.S. Fischer, B.L. Ebert, Template-assisted covalent modification of DCAF16 underlies activity of BRD4 molecular glue degraders, *bioRxiv* (2023). <https://doi.org/10.1101/2023.02.14.528208>.
- [109] 清. 大場, 靖. 丹羽, 鉄. 松平, 田. 真. 浜, 竜. 山崎, 達. 伊吹 (MITSUBISHI TANABE PHARMA CORP [JP]; YAKULT HONSHA KK [JP]) WO2021157684 (A1), 2021.
- [110] O. Hsia, M. Hinterndorfer, A.D. Cowan, K. Iso, T. Ishida, R. Sundaramoorthy, M.A. Nakasone, A. Rukavina, K. Husnjak, M. Wegner, A. Correa-Sáez, C. Craigon, C. Maniaci, A. Testa, M. Kaulich, I. Dikic, G.E. Winter, A. Ciulli, An intramolecular bivalent degrader glues an intrinsic BRD4-DCAF16 interaction, 2023.
- [111] N. Kerres, S. Steurer, S. Schlager, G. Bader, H. Berger, M. Caligiuri, C. Dank, J.R. Engen, P. Etmayer, B. Fischerauer, G. Flotzinger, D. Gerlach, T. Gerstberger, T. Gmaschitz, P. Greb, B. Han, E. Heyes, R.E. Jacob, D. Kessler, H. Kölle, L. Lamarre, D.R. Lancia, S. Lucas, M. Mayer, K. Mayr, N. Mischerikow, K. Mück, C. Peinsipp, O. Petermann, U. Reiser, D. Rudolph, K. Rumpel, C. Salomon, D. Scharn, R. Schnitzer, A. Schrenk, N. Schweifer, D. Thompson, E. Traxler, R. Varecka, T. Voss, A. Weiss-Puxbaum, S. Winkler, X. Zheng, A. Zoephel, N. Kraut, D. McConnell, M. Pearson, M. Koegl, Chemically Induced Degradation of the Oncogenic Transcription Factor BCL6, *Cell Rep.* 20 (2017) 2860–2875. <https://doi.org/10.1016/j.celrep.2017.08.081>.
- [112] M. Słabicki, H. Yoon, J. Koepfel, L. Nitsch, S.S. Roy Burman, C. Di Genua, K.A. Donovan, A.S. Sperling, M. Hunkeler, J.M. Tsai, R. Sharma, A. Guirguis, C. Zou, P. Chudasama, J.A. Gasser, P.G. Miller, C. Scholl, S. Fröhling, R.P. Nowak, E.S. Fischer, B.L. Ebert, Small-molecule-induced polymerization triggers degradation of BCL6, *Nature* 588 (2020) 164–168. <https://doi.org/10.1038/s41586-020-2925-1>.
- [113] A.C. Lai, C.M. Crews, Induced protein degradation: an emerging drug discovery paradigm, *Nat. Rev. Drug Discov.* 16 (2017) 101–114. <https://doi.org/10.1038/nrd.2016.211>.
- [114] J.A. Dewey, C. Delalande, S.-A. Azizi, V. Lu, D. Antonopoulos, G. Babnigg, Molecular Glue Discovery: Current and Future Approaches, *J. Med. Chem.* 66 (2023) 9278–9296. <https://doi.org/10.1021/acs.jmedchem.3c00449>.

- [115] V. Koduri, L. Duplaquet, B.L. Lampson, A.C. Wang, A.H. Sabet, M. Ishoey, J. Paulk, M. Teng, I.S. Harris, J.E. Endress, X. Liu, E. Dasilva, J.A. Paulo, K.J. Briggs, J.G. Doench, C.J. Ott, T. Zhang, K.A. Donovan, E.S. Fischer, S.P. Gygi, N.S. Gray, J. Bradner, J.A. Medin, S.J. Buhrlage, M.G. Oser, W.G. Kaelin, Targeting oncoproteins with a positive selection assay for protein degraders, *Sci. Adv.* 7 (2021). <https://doi.org/10.1126/sciadv.abd6263>.
- [116] A. Hanzl, E. Barone, S. Bauer, H. Yue, R.P. Nowak, E. Hahn, E.V. Pankevich, A. Koren, S. Kubicek, E.S. Fischer, G.E. Winter, E3-Specific Degradation Discovery by Dynamic Tracing of Substrate Receptor Abundance, *J. Am. Chem. Soc.* 145 (2023) 1176–1184. <https://doi.org/10.1021/jacs.2c10784>.
- [117] W. Farnaby, M. Koegl, M.J. Roy, C. Whitworth, E. Diers, N. Trainor, D. Zollman, S. Steurer, J. Karolyi-Oezguer, C. Riedmueller, T. Gmaschitz, J. Wachter, C. Dank, M. Galant, B. Sharps, K. Rumpel, E. Traxler, T. Gerstberger, R. Schnitzer, O. Petermann, P. Greb, H. Weinstabl, G. Bader, A. Zoephel, A. Weiss-Puxbaum, K. Ehrenhöfer-Wölfer, S. Wöhrle, G. Boehmelt, J. Rinnenthal, H. Arnhof, N. Wiechens, M.-Y. Wu, T. Owen-Hughes, P. Ettmayer, M. Pearson, D.B. McConnell, A. Ciulli, BAF complex vulnerabilities in cancer demonstrated via structure-based PROTAC design, *Nat. Chem. Biol.* 15 (2019) 672–680. <https://doi.org/10.1038/s41589-019-0294-6>.
- [118] C. Kofink, N. Trainor, B. Mair, S. Wöhrle, M. Wurm, N. Mischerikow, M.J. Roy, G. Bader, P. Greb, G. Garavel, E. Diers, R. McLennan, C. Whitworth, V. Vetma, K. Rumpel, M. Scharnweber, J.E. Fuchs, T. Gerstberger, Y. Cui, G. Gremel, P. Chetta, S. Hopf, N. Budano, J. Rinnenthal, G. Gmaschitz, M. Mayer, M. Koegl, A. Ciulli, H. Weinstabl, W. Farnaby, A selective and orally bioavailable VHL-recruiting PROTAC achieves SMARCA2 degradation in vivo, *Nat Commun* 13 (2022) 5969. <https://doi.org/10.1038/s41467-022-33430-6>.
- [119] K.M. Sakamoto, K.B. Kim, A. Kumagai, F. Mercurio, C.M. Crews, R.J. Deshaies, Protacs: chimeric molecules that target proteins to the Skp1-Cullin-F box complex for ubiquitination and degradation, *Proc. Natl. Acad. Sci. U. S. A.* 98 (2001) 8554–8559. <https://doi.org/10.1073/pnas.141230798>.
- [120] S.M. Banik, K. Pedram, S. Wisnovsky, G. Ahn, N.M. Riley, C.R. Bertozzi, Lysosome-targeting chimaeras for degradation of extracellular proteins, *Nature* 584 (2020) 291–297. <https://doi.org/10.1038/s41586-020-2545-9>.
- [121] D. Takahashi, J. Moriyama, T. Nakamura, E. Miki, E. Takahashi, A. Sato, T. Akaike, K. Itto-Nakama, H. Arimoto, AUTACs: Cargo-Specific Degradation Using Selective Autophagy, *Mol. Cell* 76 (2019) 797–810.e10. <https://doi.org/10.1016/j.molcel.2019.09.009>.

- [122] Z. Li, S. Ma, L. Zhang, S. Zhang, Z. Ma, L. Du, M. Li, Targeted Protein Degradation Induced by HEMTACs Based on HSP90, *J. Med. Chem.* 66 (2023) 733–751. <https://doi.org/10.1021/acs.jmedchem.2c01648>.
- [123] N.J. Henning, L. Boike, J.N. Spradlin, C.C. Ward, G. Liu, E. Zhang, B.P. Belcher, S.M. Brittain, M.J. Hesse, D. Dovala, L.M. McGregor, R. Valdez Misiolek, L.W. Plasschaert, D.J. Rowlands, F. Wang, A.O. Frank, D. Fuller, A.R. Estes, K.L. Randal, A. Panidapu, J.M. McKenna, J.A. Tallarico, M. Schirle, D.K. Nomura, Deubiquitinase-targeting chimeras for targeted protein stabilization, *Nat. Chem. Biol.* 18 (2022) 412–421. <https://doi.org/10.1038/s41589-022-00971-2>.
- [124] J. Liu, X. Yu, H. Chen, H.Ü. Kaniskan, L. Xie, X. Chen, J. Jin, W. Wei, TF-DUBTACs Stabilize Tumor Suppressor Transcription Factors, *J. Am. Chem. Soc.* 144 (2022) 12934–12941. <https://doi.org/10.1021/jacs.2c04824>.
- [125] S.U. Siriwardena, D.N.P. Munkanatta Godage, V.M. Shoba, S. Lai, M. Shi, P. Wu, S.K. Chaudhary, S.L. Schreiber, A. Choudhary, Phosphorylation-Inducing Chimeric Small Molecules, *J. Am. Chem. Soc.* 142 (2020) 14052–14057. <https://doi.org/10.1021/jacs.0c05537>.
- [126] V.M. Shoba, D.N.P. Munkanatta Godage, S.K. Chaudhary, A. Deb, S.U. Siriwardena, A. Choudhary, Synthetic Reprogramming of Kinases Expands Cellular Activities of Proteins, *Angew. Chem. Int. Ed Engl.* 61 (2022) e202202770. <https://doi.org/10.1002/anie.202202770>.
- [127] R. Pergu, V.M. Shoba, S.K. Chaudhary, D.N.P. Munkanatta Godage, A. Deb, S. Singha, U. Dhawa, P. Singh, V. Anokhina, S. Singh, S.U. Siriwardena, A. Choudhary, Development and Applications of Chimera Platforms for Tyrosine Phosphorylation, *ACS Cent. Sci.* 9 (2023) 1558–1566. <https://doi.org/10.1021/acscentsci.3c00200>.
- [128] S. Yamazoe, J. Tom, Y. Fu, W. Wu, L. Zeng, C. Sun, Q. Liu, J. Lin, K. Lin, W.J. Fairbrother, S.T. Staben, Heterobifunctional Molecules Induce Dephosphorylation of Kinases-A Proof of Concept Study, *J. Med. Chem.* 63 (2020) 2807–2813. <https://doi.org/10.1021/acs.jmedchem.9b01167>.
- [129] P.-H. Chen, Z. Hu, E. An, I. Okeke, S. Zheng, X. Luo, A. Gong, S. Jaime-Figueroa, C.M. Crews, Modulation of Phosphoprotein Activity by Phosphorylation Targeting Chimeras (PhosTACs), *ACS Chem. Biol.* 16 (2021) 2808–2815. <https://doi.org/10.1021/acscchembio.1c00693>.
- [130] Z. Hu, P.-H. Chen, W. Li, T. Douglas, J. Hines, Y. Liu, C.M. Crews, Targeted Dephosphorylation of Tau by Phosphorylation Targeting Chimeras (PhosTACs) as a Therapeutic Modality, *J. Am. Chem. Soc.* (2023). <https://doi.org/10.1021/jacs.2c11706>.

- [131] Q. Zhang, X. Wu, H. Zhang, Q. Wu, M. Fu, L. Hua, X. Zhu, Y. Guo, L. Zhang, Q. You, L. Wang, Protein Phosphatase 5-Recruiting Chimeras for Accelerating Apoptosis-Signal-Regulated Kinase 1 Dephosphorylation with Antiproliferative Activity, *J. Am. Chem. Soc.* 145 (2023) 1118–1128. <https://doi.org/10.1021/jacs.2c10759>.
- [132] W.W. Wang, L.-Y. Chen, J.M. Wozniak, A.M. Jadhav, H. Anderson, T.E. Malone, C.G. Parker, Targeted Protein Acetylation in Cells Using Heterobifunctional Molecules, *J. Am. Chem. Soc.* 143 (2021) 16700–16708. <https://doi.org/10.1021/jacs.1c07850>.
- [133] M. Kabir, N. Sun, X. Hu, T.C. Martin, J. Yi, Y. Zhong, Y. Xiong, H.Ü. Kaniskan, W. Gu, R. Parsons, J. Jin, Acetylation Targeting Chimera Enables Acetylation of the Tumor Suppressor p53, *J. Am. Chem. Soc.* 145 (2023) 14932–14944. <https://doi.org/10.1021/jacs.3c04640>.
- [134] W.J. Gibson, A. Sadagopan, V.M. Shoba, A. Choudhary, M. Meyerson, S.L. Schreiber, Bifunctional small molecules that induce nuclear localization and targeted transcriptional regulation, *bioRxiv* (2023). <https://doi.org/10.1101/2023.07.07.548101>.
- [135] J.S. Schneekloth, F.N. Fonseca, M. Koldobskiy, A. Mandal, R. Deshaies, K. Sakamoto, C.M. Crews, Chemical genetic control of protein levels: selective in vivo targeted degradation, *J. Am. Chem. Soc.* 126 (2004) 3748–3754. <https://doi.org/10.1021/ja039025z>.
- [136] A.R. Schneekloth, M. Pucheault, H.S. Tae, C.M. Crews, Targeted intracellular protein degradation induced by a small molecule: En route to chemical proteomics, *Bioorg. Med. Chem. Lett.* 18 (2008) 5904–5908. <https://doi.org/10.1016/j.bmcl.2008.07.114>.
- [137] T. Ishida, A. Ciulli, E3 Ligase Ligands for PROTACs: How They Were Found and How to Discover New Ones, *SLAS Discov.* 26 (2021) 484–502. <https://doi.org/10.1177/2472555220965528>.
- [138] G.M. Burslem, C.M. Crews, Proteolysis-Targeting Chimeras as Therapeutics and Tools for Biological Discovery, *Cell* 181 (2020) 102–114. <https://doi.org/10.1016/j.cell.2019.11.031>.
- [139] D.P. Bondeson, A. Mares, I.E.D. Smith, E. Ko, S. Campos, A.H. Miah, K.E. Mulholland, N. Routly, D.L. Buckley, J.L. Gustafson, N. Zinn, P. Grandi, S. Shimamura, G. Bergamini, M. Faelth-Savitski, M. Bantscheff, C. Cox, D.A. Gordon, R.R. Willard, J.J. Flanagan, L.N. Casillas, B.J. Votta, W. den Besten, K. Famm, L. Kruidenier, P.S. Carter, J.D. Harling, I. Churcher, C.M. Crews, Catalytic in vivo protein knockdown by small-molecule PROTACs, *Nat. Chem. Biol.* 11 (2015) 611–617. <https://doi.org/10.1038/nchembio.1858>.
- [140] D.P. Bondeson, B.E. Smith, G.M. Burslem, A.D. Buhimschi, J. Hines, S. Jaime-Figueroa, J. Wang, B.D. Hamman, A. Ishchenko, C.M. Crews, Lessons in PROTAC Design from

- Selective Degradation with a Promiscuous Warhead, *Cell Chem. Biol.* 25 (2018) 78-87.e5. <https://doi.org/10.1016/j.chembiol.2017.09.010>.
- [141] A. Testa, S.J. Hughes, X. Lucas, J.E. Wright, A. Ciulli, Structure-Based Design of a Macrocyclic PROTAC, *Angew. Chem. Int. Ed Engl.* 59 (2020) 1727–1734. <https://doi.org/10.1002/anie.201914396>.
- [142] A.C. Lai, M. Toure, D. Hellerschmied, J. Salami, S. Jaime-Figueroa, E. Ko, J. Hines, C.M. Crews, Modular PROTAC Design for the Degradation of Oncogenic BCR-ABL, *Angew. Chem. Int. Ed Engl.* 55 (2016) 807–810. <https://doi.org/10.1002/anie.201507634>.
- [143] B. Adhikari, J. Bozilovic, M. Diebold, J.D. Schwarz, J. Hofstetter, M. Schröder, M. Wanior, A. Narain, M. Vogt, N. Dudvarski Stankovic, A. Baluapuri, L. Schönemann, L. Eing, P. Bhandare, B. Kuster, A. Schlosser, S. Heinzlmeir, C. Sottriffer, S. Knapp, E. Wolf, PROTAC-mediated degradation reveals a non-catalytic function of AURORA-A kinase, *Nat. Chem. Biol.* 16 (2020) 1179–1188. <https://doi.org/10.1038/s41589-020-00652-y>.
- [144] R.P. Law, J. Nunes, C.-W. Chung, M. Bantscheff, K. Buda, H. Dai, J.P. Evans, A. Flinders, D. Klimaszewska, A.J. Lewis, M. Muelbaier, P. Scott-Stevens, P. Stacey, C.J. Tame, G.F. Watt, N. Zinn, M.A. Queisser, J.D. Harling, A.B. Benowitz, Discovery and Characterisation of Highly Cooperative FAK-Degrading PROTACs, *Angew. Chem. Int. Ed Engl.* 60 (2021) 23327–23334. <https://doi.org/10.1002/anie.202109237>.
- [145] X. Yu, D. Li, J. Kottur, Y. Shen, H.S. Kim, K.-S. Park, Y.-H. Tsai, W. Gong, J. Wang, K. Suzuki, J. Parker, L. Herring, H.Ü. Kaniskan, L. Cai, R. Jain, J. Liu, A.K. Aggarwal, G.G. Wang, J. Jin, A selective WDR5 degrader inhibits acute myeloid leukemia in patient-derived mouse models, *Sci. Transl. Med.* 13 (2021) eabj1578. <https://doi.org/10.1126/scitranslmed.abj1578>.
- [146] C.A. Lipinski, F. Lombardo, B.W. Dominy, P.J. Feeney, Experimental and computational approaches to estimate solubility and permeability in drug discovery and development settings, *Adv. Drug Deliv. Rev.* 46 (2001) 3–26. [https://doi.org/10.1016/s0169-409x\(00\)00129-0](https://doi.org/10.1016/s0169-409x(00)00129-0).
- [147] X. Han, L. Zhao, W. Xiang, C. Qin, B. Miao, D. McEachern, Y. Wang, H. Metwally, L. Wang, A. Matvekas, B. Wen, D. Sun, S. Wang, Strategies toward Discovery of Potent and Orally Bioavailable Proteolysis Targeting Chimera Degradable of Androgen Receptor for the Treatment of Prostate Cancer, *J. Med. Chem.* 64 (2021) 12831–12854. <https://doi.org/10.1021/acs.jmedchem.1c00882>.
- [148] G.E. Winter, D.L. Buckley, J. Paulk, J.M. Roberts, A. Souza, S. Dhe-Paganon, J.E. Bradner, DRUG DEVELOPMENT. Phthalimide conjugation as a strategy for in vivo target



- protein degradation, *Science* 348 (2015) 1376–1381.  
<https://doi.org/10.1126/science.aab1433>.
- [149] X. Zhang, L.M. Luukkonen, C.L. Eissler, V.M. Crowley, Y. Yamashita, M.A. Schafroth, S. Kikuchi, D.S. Weinstein, K.T. Symons, B.E. Nordin, J.L. Rodriguez, T.G. Wucherpfennig, L.G. Bauer, M.M. Dix, D. Stamos, T.M. Kinsella, G.M. Simon, K.A. Baltgalvis, B.F. Cravatt, DCAF11 Supports Targeted Protein Degradation by Electrophilic Proteolysis-Targeting Chimeras, *J. Am. Chem. Soc.* 143 (2021) 5141–5149.  
<https://doi.org/10.1021/jacs.1c00990>.
- [150] X. Zhang, V.M. Crowley, T.G. Wucherpfennig, M.M. Dix, B.F. Cravatt, Electrophilic PROTACs that degrade nuclear proteins by engaging DCAF16, *Nat. Chem. Biol.* 15 (2019) 737–746. <https://doi.org/10.1038/s41589-019-0279-5>.
- [151] P. Ottis, M. Toure, P.M. Cromm, E. Ko, J.L. Gustafson, C.M. Crews, Assessing Different E3 Ligases for Small Molecule Induced Protein Ubiquitination and Degradation, *ACS Chem. Biol.* 12 (2017) 2570–2578. <https://doi.org/10.1021/acscchembio.7b00485>.
- [152] X. Sun, J. Wang, X. Yao, W. Zheng, Y. Mao, T. Lan, L. Wang, Y. Sun, X. Zhang, Q. Zhao, J. Zhao, R.-P. Xiao, X. Zhang, G. Ji, Y. Rao, A chemical approach for global protein knockdown from mice to non-human primates, *Cell Discov.* 5 (2019) 10.  
<https://doi.org/10.1038/s41421-018-0079-1>.
- [153] B. Nabet, J.M. Roberts, D.L. Buckley, J. Paulk, S. Dastjerdi, A. Yang, A.L. Leggett, M.A. Erb, M.A. Lawlor, A. Souza, T.G. Scott, S. Vittori, J.A. Perry, J. Qi, G.E. Winter, K.-K. Wong, N.S. Gray, J.E. Bradner, The dTAG system for immediate and target-specific protein degradation, *Nat. Chem. Biol.* 14 (2018) 431–441.  
<https://doi.org/10.1038/s41589-018-0021-8>.
- [154] T. Mao, Development of Novel Small-Molecule Degraders of FK506-Binding Protein 51, 2020.
- [155] A. Haehle, Elucidation of the molecular and cellular mechanisms of FKBP51-selective inhibitors, 2020.
- [156] C. Kozany, A. März, C. Kress, F. Hausch, Fluorescent probes to characterise FK506-binding proteins, *Chembiochem* 10 (2009) 1402–1410.  
<https://doi.org/10.1002/cbic.200800806>.
- [157] Z.X. Wang, An exact mathematical expression for describing competitive binding of two different ligands to a protein molecule, *FEBS Lett.* 360 (1995) 111–114.  
[https://doi.org/10.1016/0014-5793\(95\)00062-e](https://doi.org/10.1016/0014-5793(95)00062-e).
- [158] S. Martinelli, E.A. Anderzhanova, T. Bajaj, S. Wiechmann, F. Dethloff, K. Weckmann, D.E. Heinz, T. Ebert, J. Hartmann, T.M. Geiger, M. Döngi, K. Hafner, M.L. Pöhlmann, L.

- Jollans, A. Philipsen, S.V. Schmidt, U. Schmidt, G. Maccarrone, V. Stein, F. Hausch, C.W. Turck, M.V. Schmidt, A.-K. Gellner, B. Kuster, N.C. Gassen, Stress-primed secretory autophagy promotes extracellular BDNF maturation by enhancing MMP9 secretion, *Nat. Commun.* 12 (2021) 4643. <https://doi.org/10.1038/s41467-021-24810-5>.
- [159] Y. Cheng, W.H. Prusoff, Relationship between the inhibition constant (K<sub>1</sub>) and the concentration of inhibitor which causes 50 per cent inhibition (I<sub>50</sub>) of an enzymatic reaction, *Biochem. Pharmacol.* 22 (1973) 3099–3108. [https://doi.org/10.1016/0006-2952\(73\)90196-2](https://doi.org/10.1016/0006-2952(73)90196-2).
- [160] P. Newton, P. Harrison, S. Clulow, A novel method for determination of the affinity of protein: protein interactions in homogeneous assays, *J. Biomol. Screen.* 13 (2008) 674–682. <https://doi.org/10.1177/1087057108321086>.
- [161] A. Novotna, P. Pavek, Z. Dvorak, Construction and characterization of a reporter gene cell line for assessment of human glucocorticoid receptor activation, *Eur. J. Pharm. Sci.* 47 (2012) 842–847. <https://doi.org/10.1016/j.ejps.2012.10.003>.
- [162] M.T. Gnatzy, T.M. Geiger, A. Kuehn, N. Gutfreund, M. Walz, J.M. Kolos, F. Hausch, Development of NanoBRET-Binding Assays for FKBP-Ligand Profiling in Living Cells, *Chembiochem* 22 (2021) 2257–2261. <https://doi.org/10.1002/cbic.202100113>.
- [163] E.P. Coutant, G. Gagnot, V. Hervin, R. Baatallah, S. Goyard, Y. Jacob, T. Rose, Y.L. Janin, Bioluminescence Profiling of NanoKAZ/NanoLuc Luciferase Using a Chemical Library of Coelenterazine Analogues, *Chemistry* 26 (2020) 948–958. <https://doi.org/10.1002/chem.201904844>.
- [164] J.R. Walker, M.P. Hall, C.A. Zimprich, M.B. Robers, S.J. Duellman, T. Machleidt, J. Rodriguez, W. Zhou, Highly Potent Cell-Permeable and Impermeable NanoLuc Luciferase Inhibitors, *ACS Chem. Biol.* 12 (2017) 1028–1037. <https://doi.org/10.1021/acscchembio.6b01129>.
- [165] A. Baischew, S. Engel, T.M. Geiger, F. Hausch, Large-scale in-cell photocrosslinking at single residue resolution reveals the molecular basis for glucocorticoid receptor regulation by immunophilins, 2023.
- [166] D.L. Riggs, P.J. Roberts, S.C. Chirillo, J. Cheung-Flynn, V. Prapapanich, T. Ratajczak, R. Gaber, D. Picard, D.F. Smith, The Hsp90-binding peptidylprolyl isomerase FKBP52 potentiates glucocorticoid signaling in vivo, *EMBO J.* 22 (2003) 1158–1167. <https://doi.org/10.1093/emboj/cdg108>.
- [167] M. Walz, Development of the first selective proteolysis targeting chimera for the FK506-binding protein 51, 2023.

- [168] C.M. Noddings, J.L. Johnson, D.A. Agard, Cryo-EM reveals how Hsp90 and FKBP immunophilins co-regulate the Glucocorticoid Receptor, *bioRxiv* (2023).  
<https://doi.org/10.1101/2023.01.10.523504>.
- [169] A.A. Stepanenko, V.V. Dmitrenko, HEK293 in cell biology and cancer research: phenotype, karyotype, tumorigenicity, and stress-induced genome-phenotype evolution, *Gene* 569 (2015) 182–190. <https://doi.org/10.1016/j.gene.2015.05.065>.
- [170] N.L. Hindul, A. Jhita, D.G. Oprea, T.A. Hussain, O. Gonchar, M.A.M. Campillo, L. O'Regan, M.T. Kanemaki, A.M. Fry, K. Hirota, K. Tanaka, Construction of a human hTERT RPE-1 cell line with inducible Cre for editing of endogenous genes, *Biol. Open* 11 (2022). <https://doi.org/10.1242/bio.059056>.
- [171] J.G. Kim, H.-C. Shin, T. Seo, L. Nawale, G. Han, B.Y. Kim, S.J. Kim, H. Cha-Molstad, Signaling Pathways Regulated by UBR Box-Containing E3 Ligases, *Int. J. Mol. Sci.* 22 (2021). <https://doi.org/10.3390/ijms22158323>.
- [172] M.B. Metzger, J.N. Pruneda, R.E. Klevit, A.M. Weissman, RING-type E3 ligases: master manipulators of E2 ubiquitin-conjugating enzymes and ubiquitination, *Biochim. Biophys. Acta* 1843 (2014) 47–60. <https://doi.org/10.1016/j.bbamcr.2013.05.026>.
- [173] T. Tasaki, R. Sohr, Z. Xia, R. Hellweg, H. Hörtnagl, A. Varshavsky, Y.T. Kwon, Biochemical and genetic studies of UBR3, a ubiquitin ligase with a function in olfactory and other sensory systems, *J. Biol. Chem.* 282 (2007) 18510–18520.  
<https://doi.org/10.1074/jbc.M701894200>.
- [174] J. Hartmann, K.V. Wagner, S. Gaali, A. Kirschner, C. Kozany, G. Rühler, N. Dedic, A.S. Häusl, L. Hoeijmakers, S. Westerholz, C. Namendorf, T. Gerlach, M. Uhr, A. Chen, J.M. Deussing, F. Holsboer, F. Hausch, M.V. Schmidt, Pharmacological Inhibition of the Psychiatric Risk Factor FKBP51 Has Anxiolytic Properties, *J. Neurosci.* 35 (2015) 9007–9016. <https://doi.org/10.1523/JNEUROSCI.4024-14.2015>.
- [175] K.A. Donovan, F.M. Ferguson, J.W. Bushman, N.A. Eleuteri, D. Bhunia, S. Ryu, L. Tan, K. Shi, H. Yue, X. Liu, D. Dobrovolsky, B. Jiang, J. Wang, M. Hao, I. You, M. Teng, Y. Liang, J. Hatcher, Z. Li, T.D. Manz, B. Groendyke, W. Hu, Y. Nam, S. Sengupta, H. Cho, I. Shin, M.P. Agius, I.M. Ghobrial, M.W. Ma, J. Che, S.J. Buhrlage, T. Sim, N.S. Gray, E.S. Fischer, Mapping the Degradable Kinome Provides a Resource for Expedited Degradation Development, *Cell* 183 (2020) 1714–1731.e10.  
<https://doi.org/10.1016/j.cell.2020.10.038>.
- [176] M.F. Sanner, A.J. Olson, J.-C. Spohner, Reduced surface: An efficient way to compute molecular surfaces, *Biopolymers* 38 (1996) 305–320.  
[https://doi.org/10.1002/\(SICI\)1097-0282\(199603\)38:3<305:AID-BIP4>3.0.CO;2-Y](https://doi.org/10.1002/(SICI)1097-0282(199603)38:3<305:AID-BIP4>3.0.CO;2-Y).

## 8. Supplemental Information

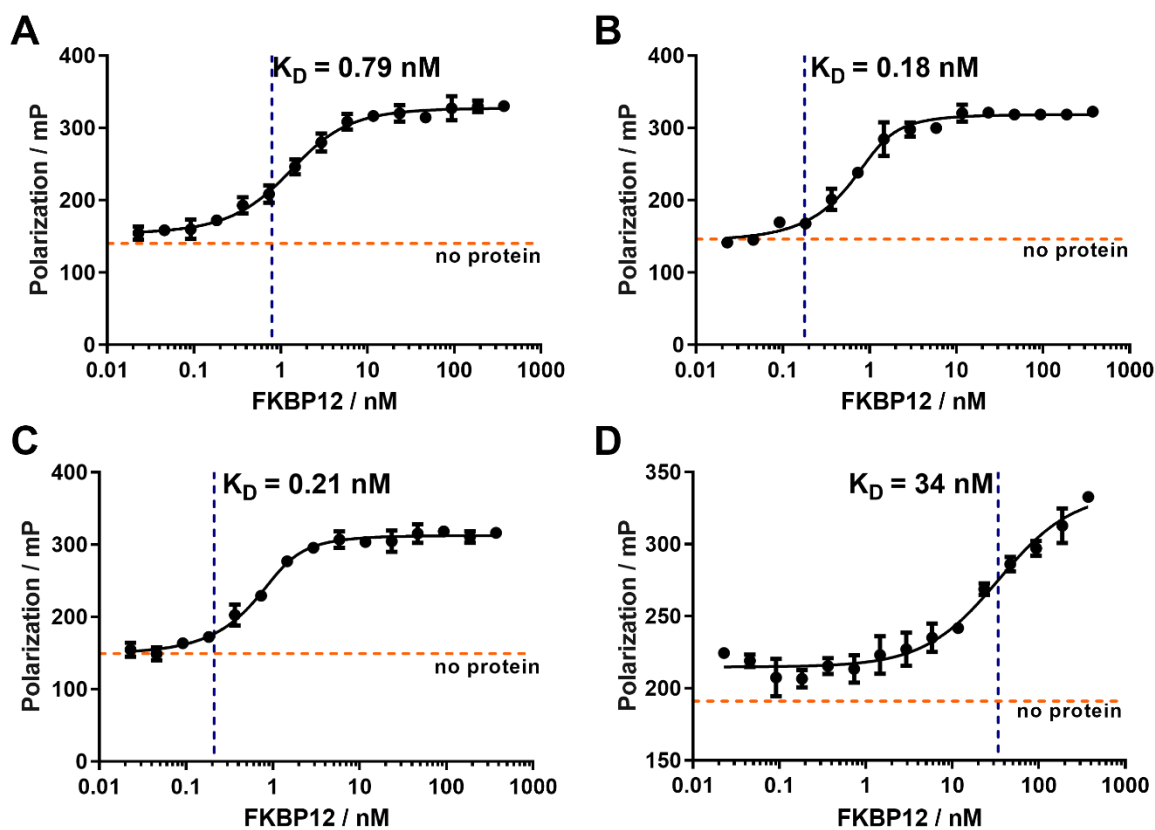


**Figure 66** Fluorescence polarization binding curves of HTRF-tracers (A: 1b; B: 2b; C: 3b; D: 4b) and FKBP12. His6-tagged FKBP12 was titrated at constant tracer concentrations of 1 nM and fluorescence polarization was measured using the following spectral parameters: Ex.: 580 nm; Em: 665 nm. Individual points and error bars represent mean and standard deviation of triplicates.

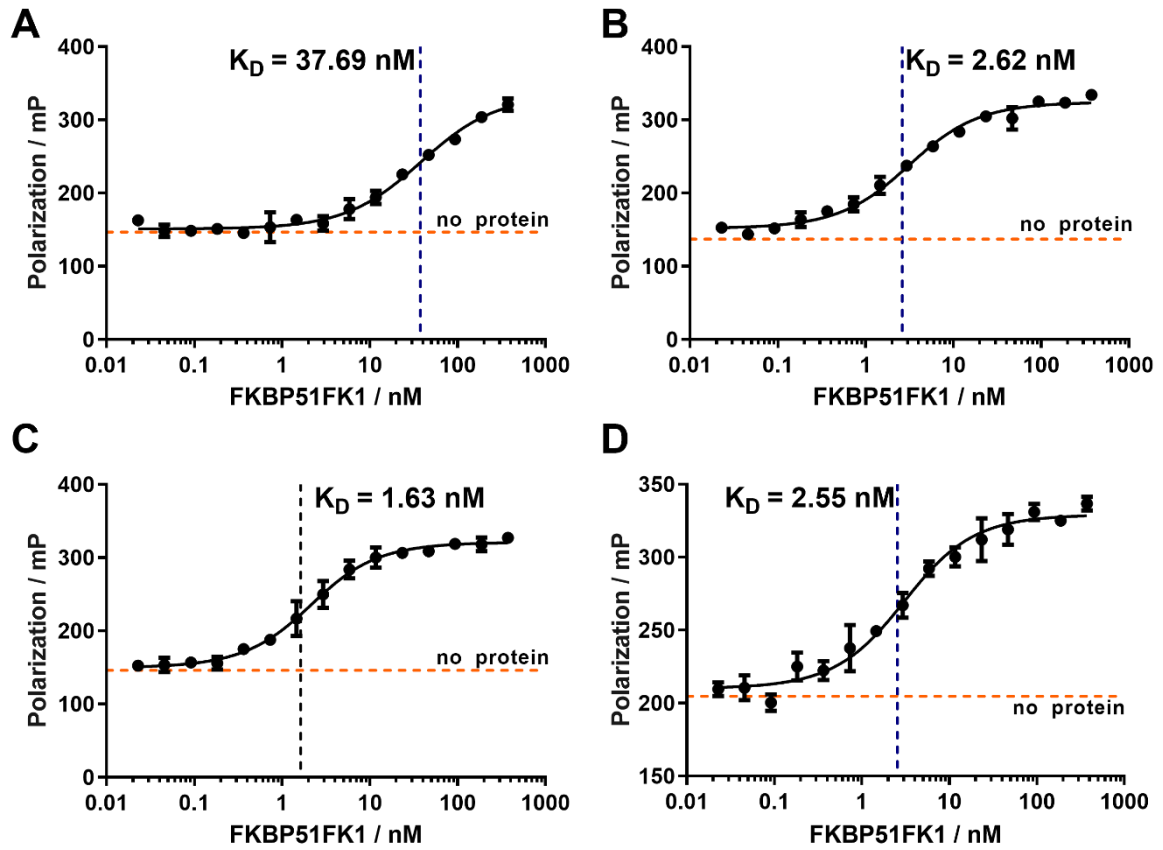


**Figure 67** Fluorescence polarization binding curves of HTRF-tracers (A: 1b; B: 2b; C:3b; D: 4b) and FKBP51<sup>FK1</sup>. His6-tagged FKBP51<sup>FK1</sup> was titrated at constant tracer concentrations of 1 nM and fluorescence polarization was measured using the following spectral parameters: Ex.: 580 nm; Em: 665 nm. Individual points and error bars represent mean and standard deviation of triplicates.

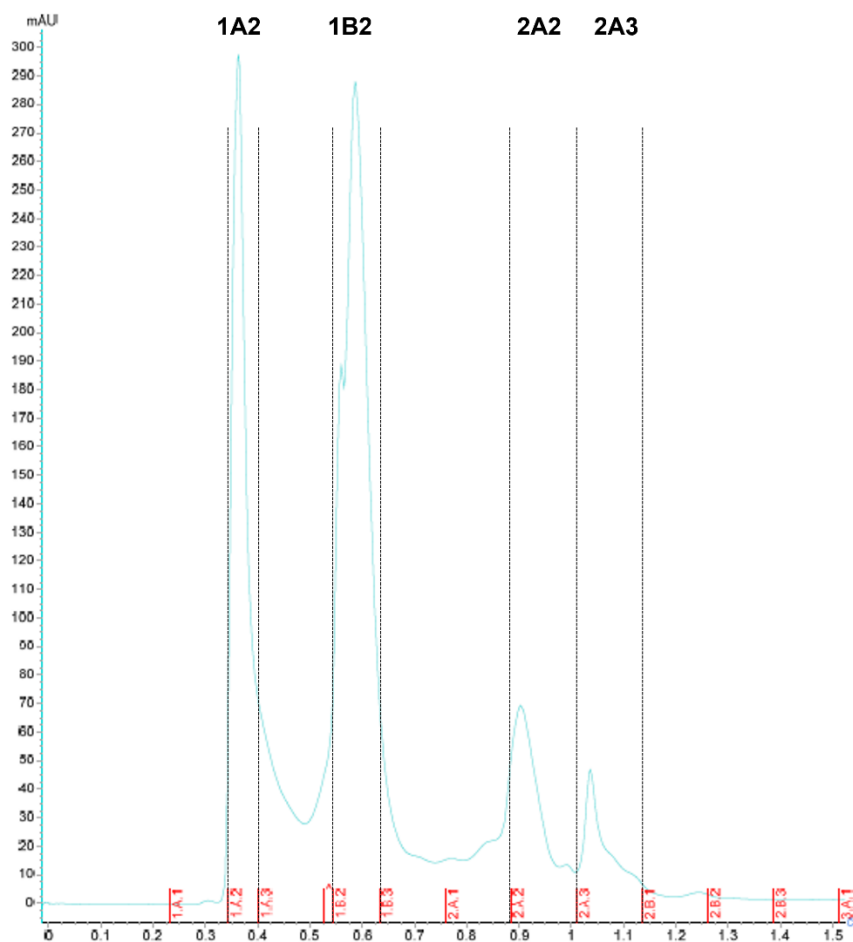


**Figure 68** Size Exclusion Chromatogram (SEC) of Flag-FKBP51-His6. Size exclusion chromatography (ÄKTA pure, GE Healthcare, Column: HiLoad 16/600 Superdex 75 pg, sample injection via superloop, UV trace: absorption at 280 nm (cyan)) was performed after Nickel affinity purification (IMAC). Running buffer: 150 mM NaCl, 20 mM HEPES, pH 8. The collected fractions (indicated by dashed vertical lines) were analysed by SDS Page and Coomassie staining (Figure 69).

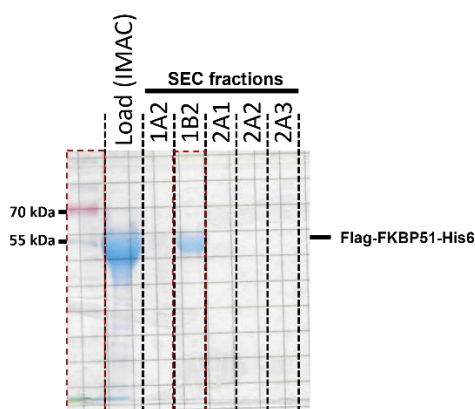


**Figure 69** Analysis of collected SEC fractions (Figure 68) during the purification Flag-FKBP51-His6 by SDS Page and Coomassie staining. Fraction 1B2 contains Flag-FKBP51-His6. Red dashed squares indicate the lanes depicted in Figure 19A. Marker: (PageRuler™ Prestained Protein Ladder, ThermoFischer #26166)

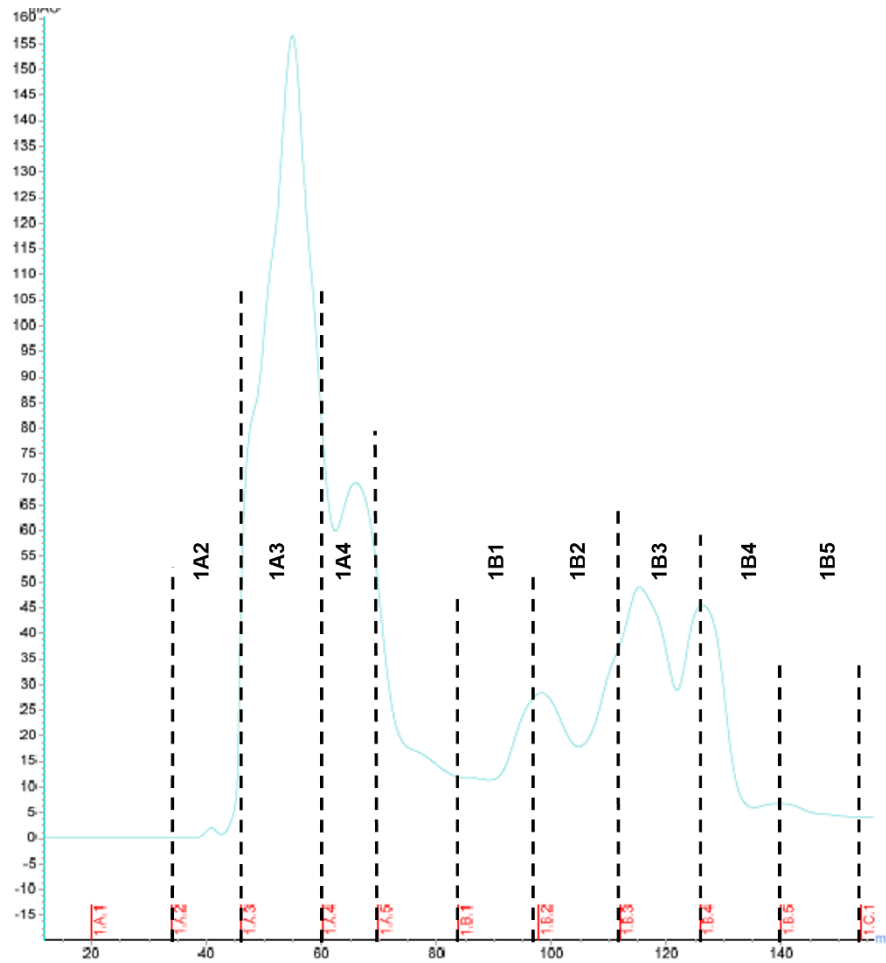


**Figure 70** Size Exclusion Chromatogram (SEC) of His6-FKBP51-Flag. Size exclusion chromatography (ÄKTA pure, GE Healthcare, Column: HiLoad 16/600 Superdex 75 pg, sample injection via superloop, UV trace: absorption at 280 nm (cyan)) was performed after Nickel affinity purification (IMAC). Running buffer: 150 mM NaCl, 20 mM HEPES, pH 8. The collected fractions (indicated by dashed vertical lines) were analysed by SDS Page and Coomassie staining (Figure 70).

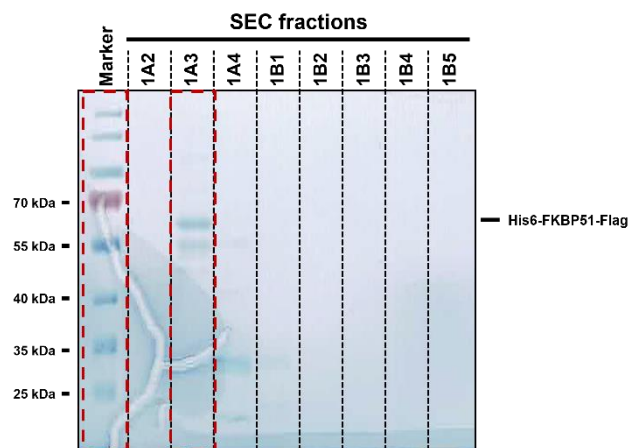


**Figure 71** Analysis of collected SEC fractions (Figure 70) during the purification His6-FKBP51-Flag of by SDS Page and Coomassie staining. Fraction 1A3 contains His6-FKBP51-Flag. Red dashed squares indicate the lanes depicted in Figure 19B. Marker: (PageRuler™ Prestained Protein Ladder, ThermoFischer #26166):

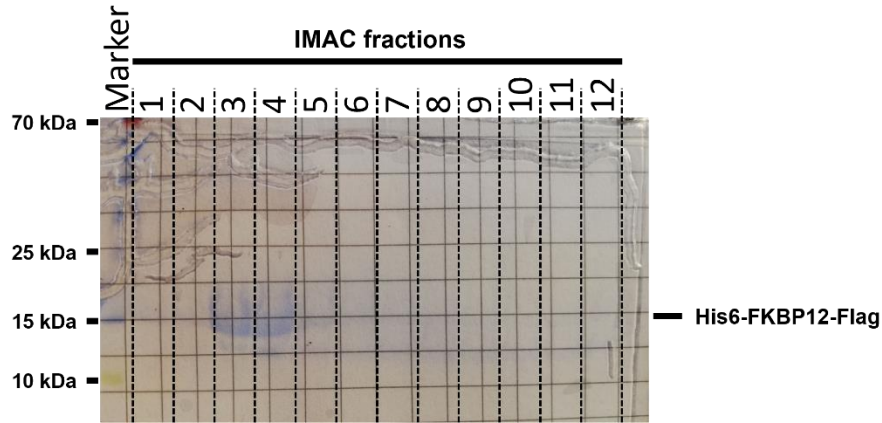


**Figure 72** Analysis of collected IMAC fractions during the His6-Tev-FKBP12-Flag purification by SDS Page and Coomassie staining. Fractions 3-7 were pooled and dialysed against 1 l buffer (150 mM NaCl, 20 mM Hepes, pH 8.0) in a Dialysis-membrane Typ20 MWCO 12-16 kDa, pore size 25 Å (Biomol). Marker: (PageRuler™ Prestained Protein Ladder, ThermoFischer #26166)

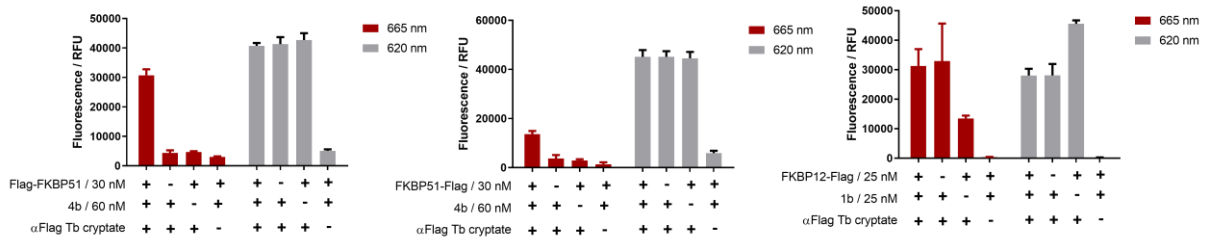


**Figure 73** Corresponding fluorescence intensity values at 665 nm (red) and 620 nm (grey) to the HTRF ratios of HTRF pilot experiments depicted in Figure 21. Combinations of **A** 4b:Flag-FKBP51 and **B** 4b:FKBP51-Flag but not **C** 1b:FKBP12-Flag yielded fluorescence intensity signals at 665 nm in presence a  $\alpha$ Flag-Tb cryptate antibody (concentration 0.5% (v/v)) above the tracer background. Individual data points represent mean and standard deviation of three replicates. Fluorescence intensities were measured using the following spectral parameters: fluorescence intensity at 665 nm: Ex.: 340 nm, Em: 665 nm, lag time: 150s, integration time: 150  $\mu$ s; fluorescence intensity at 620 nm: Ex.: 340 nm, Em: 620 nm, lag time: 150s, integration time: 150  $\mu$ s. His6-tagged FKBP51<sup>FK1</sup> was titrated at constant tracer concentrations of 1 nM and fluorescence polarization was measured using the following spectral parameters: Ex.: 580 nm; Em: 665 nm. Individual points and error bars represent mean and standard deviation of triplicates.



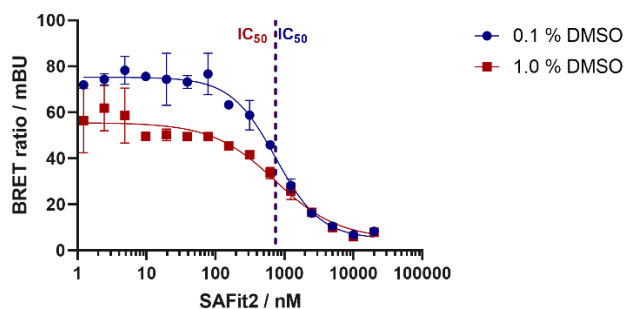


**Figure 74** FKBP51<sup>FK1</sup> NanoBRET engagement assays in presence of different DMSO concentrations. Experiment was performed by Thomas Stipp with HEK293T cells stably expressing FKBP51<sup>FK1</sup>-NLuc fusion proteins in presence of a final concentration 400 nM tracer 2c [162] and  $2.7 \times 10^5$  cells/well. Donor and acceptor signals were measured after 2 hours incubation after addition of luciferase substrate as described in [162].

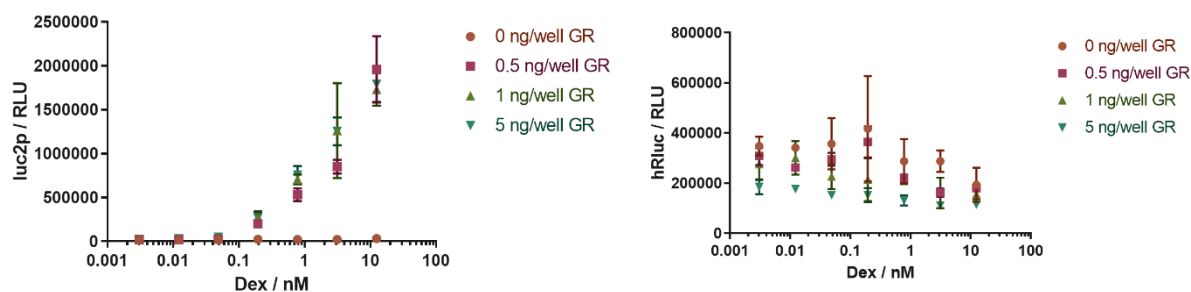


**Figure 75** Glucocorticoid receptor over expression is required to stimulate dexamethasone induced reporter expression. HEK293T cells were transiently transfected (24 hours) with the dual luciferase reporter plasmids (pGL4.36 (MMTV-luc2p), pGL4.74 (TK-hRluc) and the indicated amount of a GR-expression plasmid and followingly (24 hours) stimulated with dexamethasone (Dex). Reporter expression was quantified by luc2p (left) and hRluc (right) luminescence measurements. Individual points and error bars represent mean and standard deviation of biological triplicates. Normalized luminescence (norm. luc) is depicted in Figure 30.

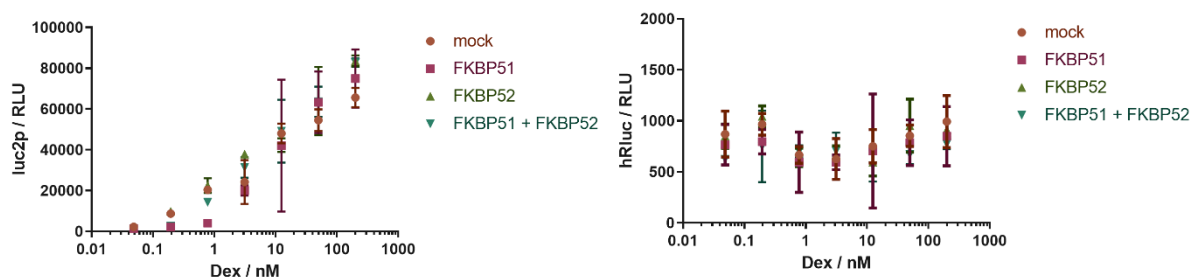


**Figure 76** FKBP51 suppresses GR activity, while FKBP52 blocks FKBP51's effect at low dexamethasone concentration. HEK293T cells were transiently transfected (24 hours) with the dual luciferase reporter plasmids (pGL4.36 (MMTV-luc2p), pGL4.74 (TK-hRluc)) and 5 ng/well GR expression as well as FKBP51 (10 ng/well), FKBP52 (10 ng/well) and or mock plasmid (20 ng/well (mock), 10 ng/well (FKBP51, FKBP52)) and followingly (24 hours) stimulated with dexamethasone (Dex). Reporter expression was quantified by luc2p (left) and hRluc (right) luminescence measurements. Individual points and error bars represent mean and standard deviation of biological triplicates. Normalized luminescence (norm. luc) is depicted in Figure 31.

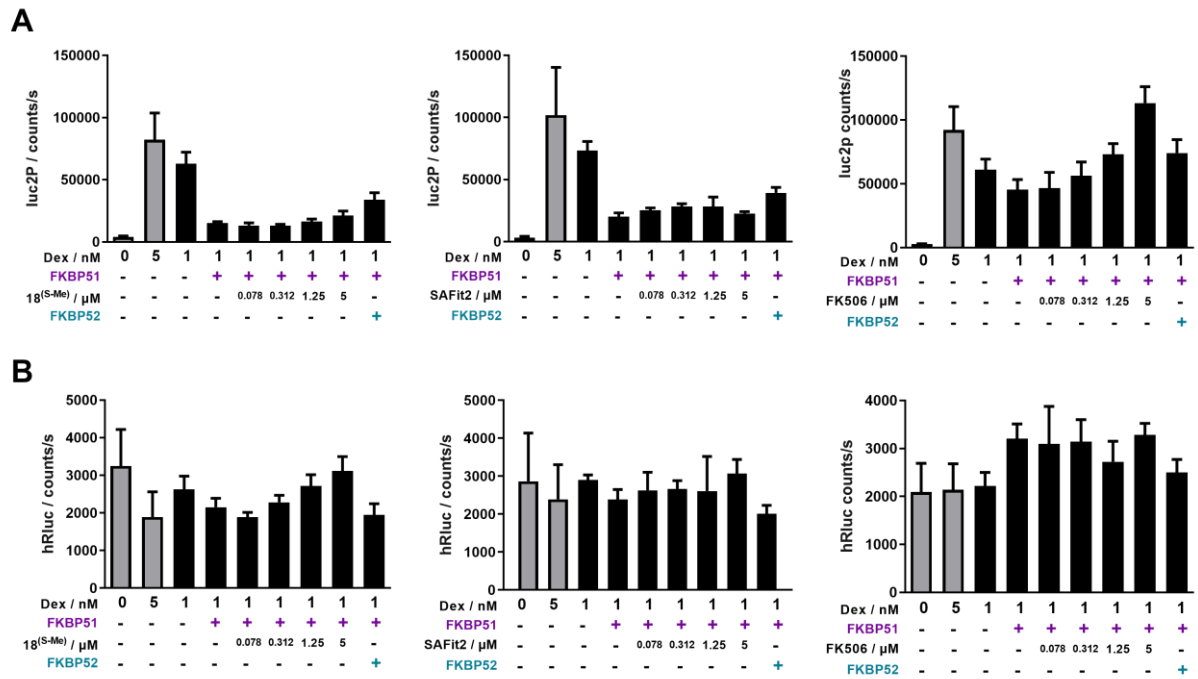


**Figure 77** Treatment with FK506, but not 18<sup>(S-Me)</sup> or SAFit2 dose-dependently blocks GR suppression. HEK293T cells were transiently transfected (24 hours) with the dual luciferase reporter plasmids (pGL4.36 (MMTV-luc2p), pGL4.74 (TK-hRluc), 5 ng/well GR expression plasmid and FKBP51 (10 ng/well) and/or a 3-fold excess of FKBP52 expression plasmids, respectively, and following (24 hours) stimulated with dexamethasone (Dex) in presence of the indicated concentrations of FKBP ligands. Reporter expression was quantified by luc2p **A** and hRluc **B** luminescence measurements. Individual points and error bars represent mean and standard deviation of biological hexaplicates. Normalized luminescence (norm. luc) is depicted in Figure 32. The data presented in this figure are part of the manuscript “Large-scale in-cell photocrosslinking at single residue resolution reveals the molecular basis for glucocorticoid receptor regulation by immunophilins” [165], which is currently in press at Nature Structural and Molecular Biology.

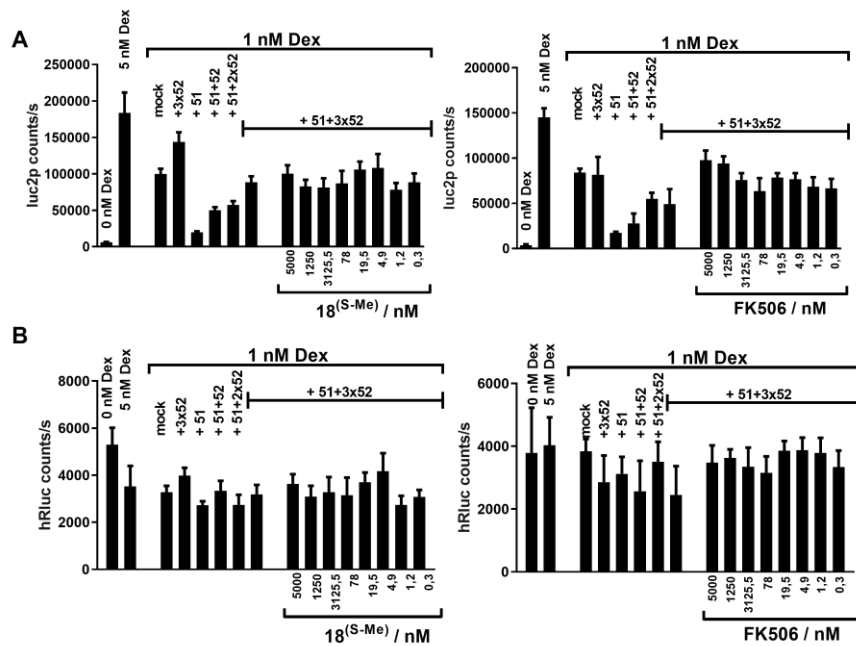


**Figure 78** Neither treatment with FK506 nor 18<sup>(S-Me)</sup> affects FKBP52-mediated GR reactivation. HEK293T cells were transiently transfected (24 hours) with the dual luciferase reporter plasmids (pGL4.36 (MMTV-luc2p), pGL4.74 (TK-hRluc)), 5 ng/well GR expression plasmid and FKBP51 (10 ng/well) and or an indicated fold excess of FKBP52 expression plasmids, respectively, and following (24 hours) stimulated with dexamethasone (Dex) in presence of the indicated concentrations of FKBP ligands. Reporter expression was quantified by luc2p **A** and hRluc **B** luminescence measurements. Individual points and error bars represent mean and standard deviation of biological hexaplicates. Normalized luminescence (norm. luc) is depicted in Figure 33.

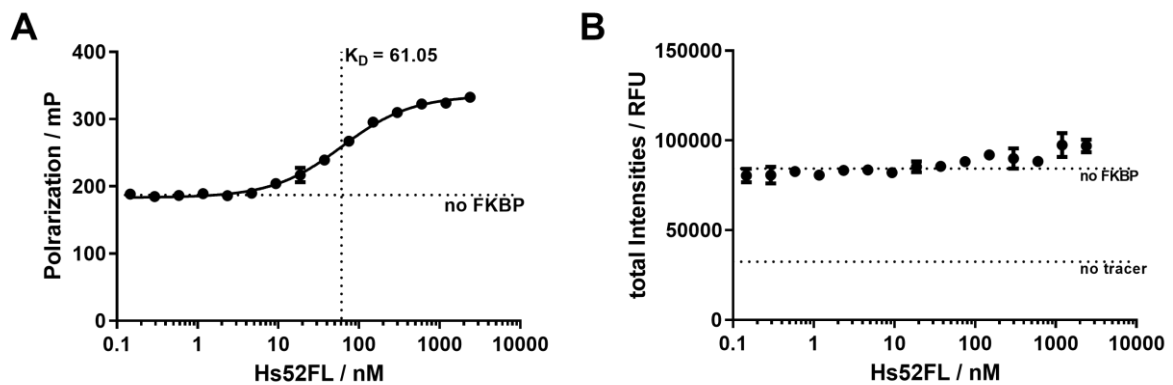


**Figure 79** Analysis of Mwa146 affinity for human full-length FKBP52 (Hs52FL) by fluorescence polarization measurements. Measurements were performed at a constant tracer concentration of 1 nM. Polarization **A** and total intensities **B** were measured using a tecan genios pro and the spectral adjustments: Ex.: 590 nm; Em.: 670 nm. Individual data points and error bars represent mean standard deviation of three replicates.

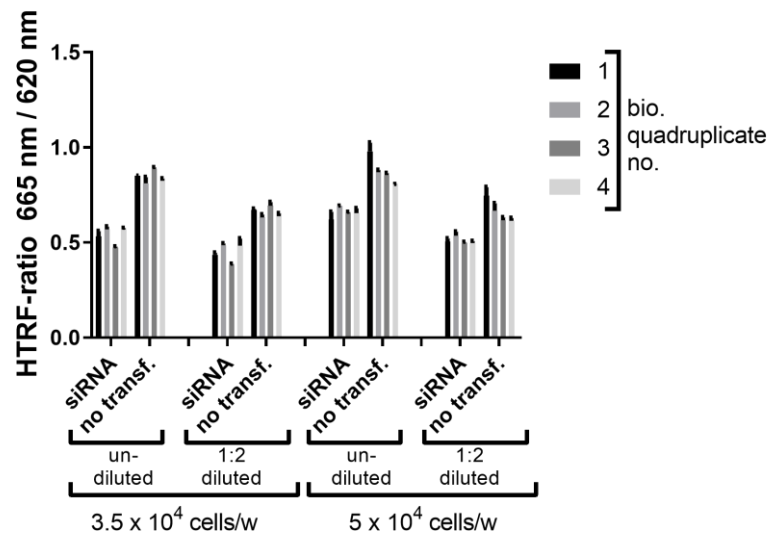


**Figure 80** Comparison of HTRF-ratio derived from undiluted or diluted lysates of cells transfected with a FKBP52 targeting siRNA (siRNA) or untransfected cells (no transf.) in presence of 120 nM Mwa146, 1.2 nM anti-rabbit-Eu cryptate and 1.25 nM anti-FKBP52 antibodies.

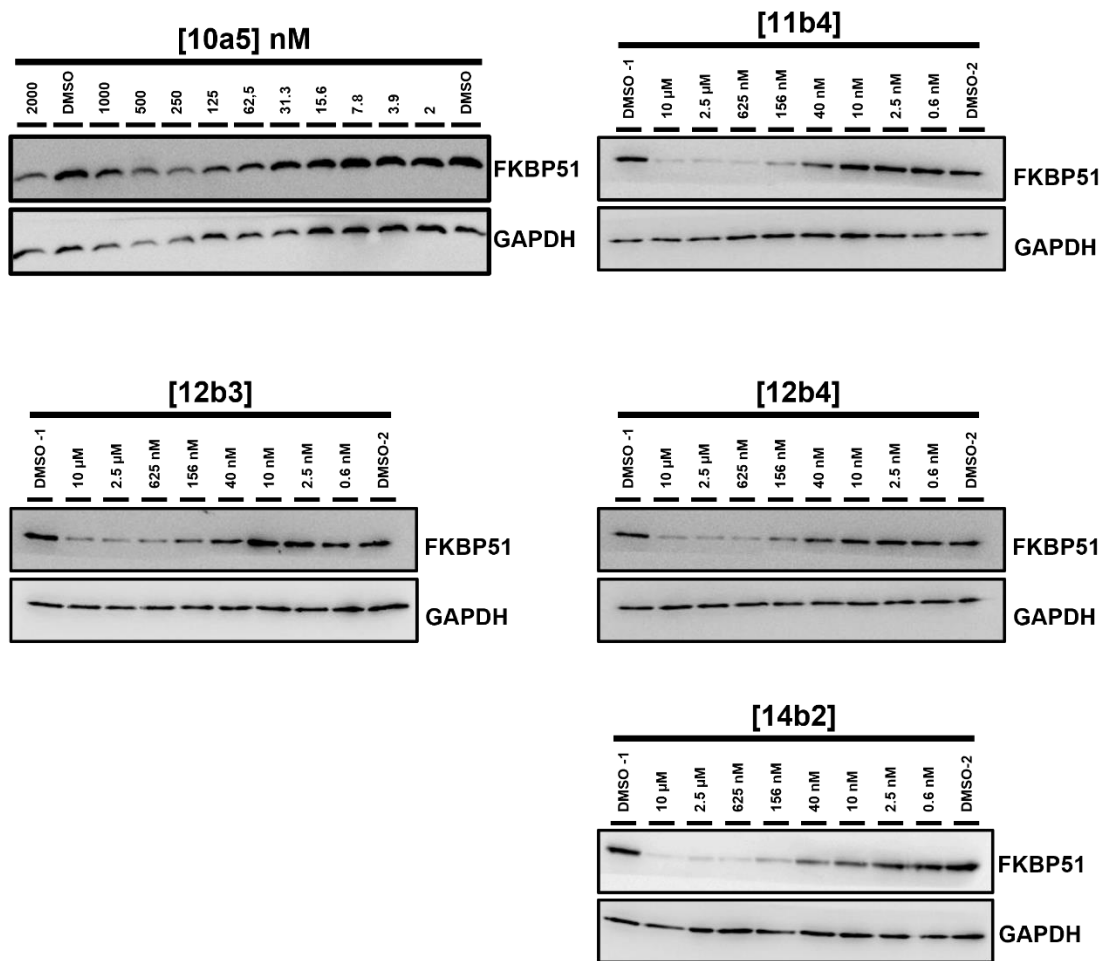


**Figure 81** PROTAC-mediated FKBP51 degradation in HEK293T cells after 24 h treatment.

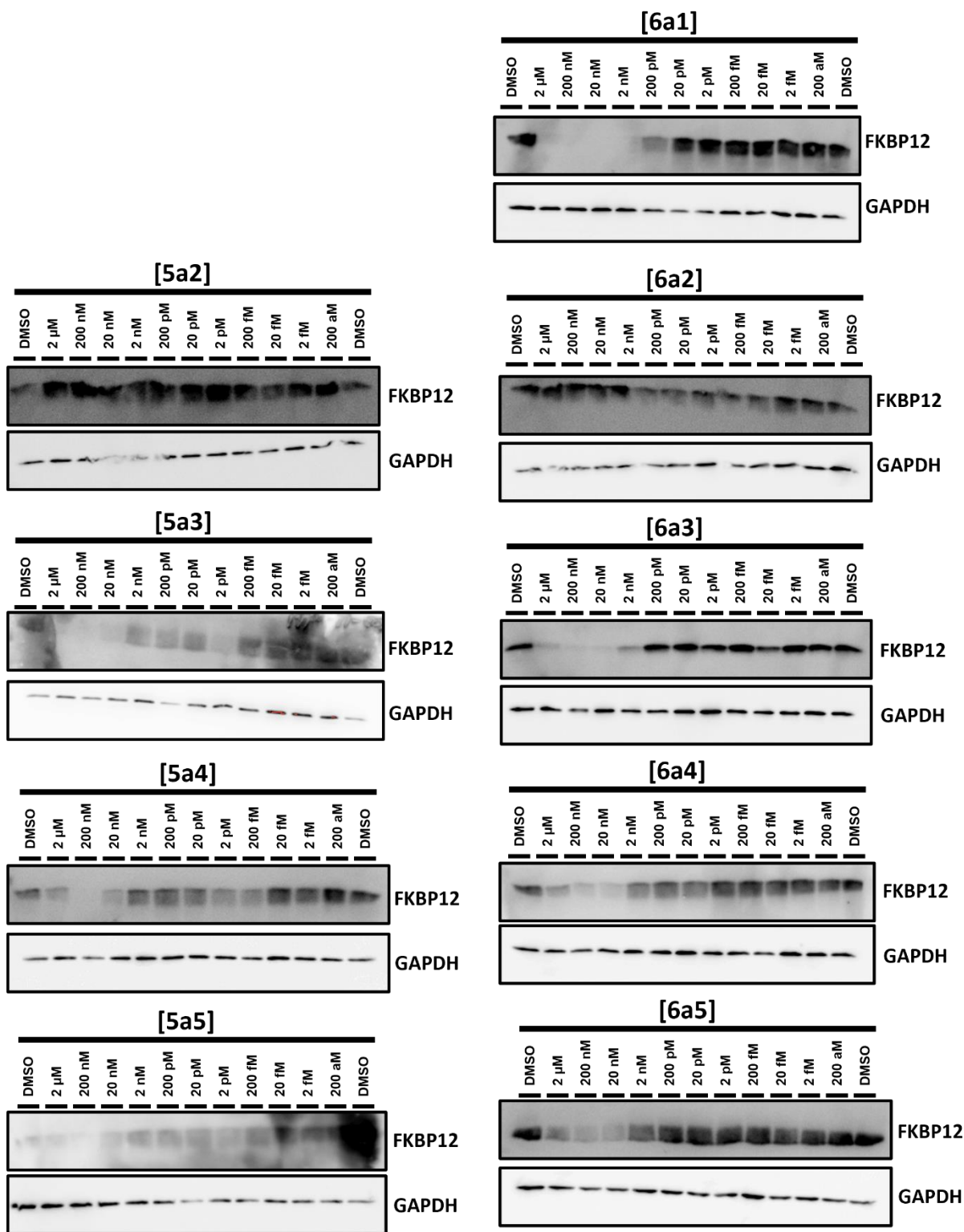


Figure 82 Part 1 of 5. PROTAC-mediated FKBP12 degradation in HEK293T cells after 24 h treatment.

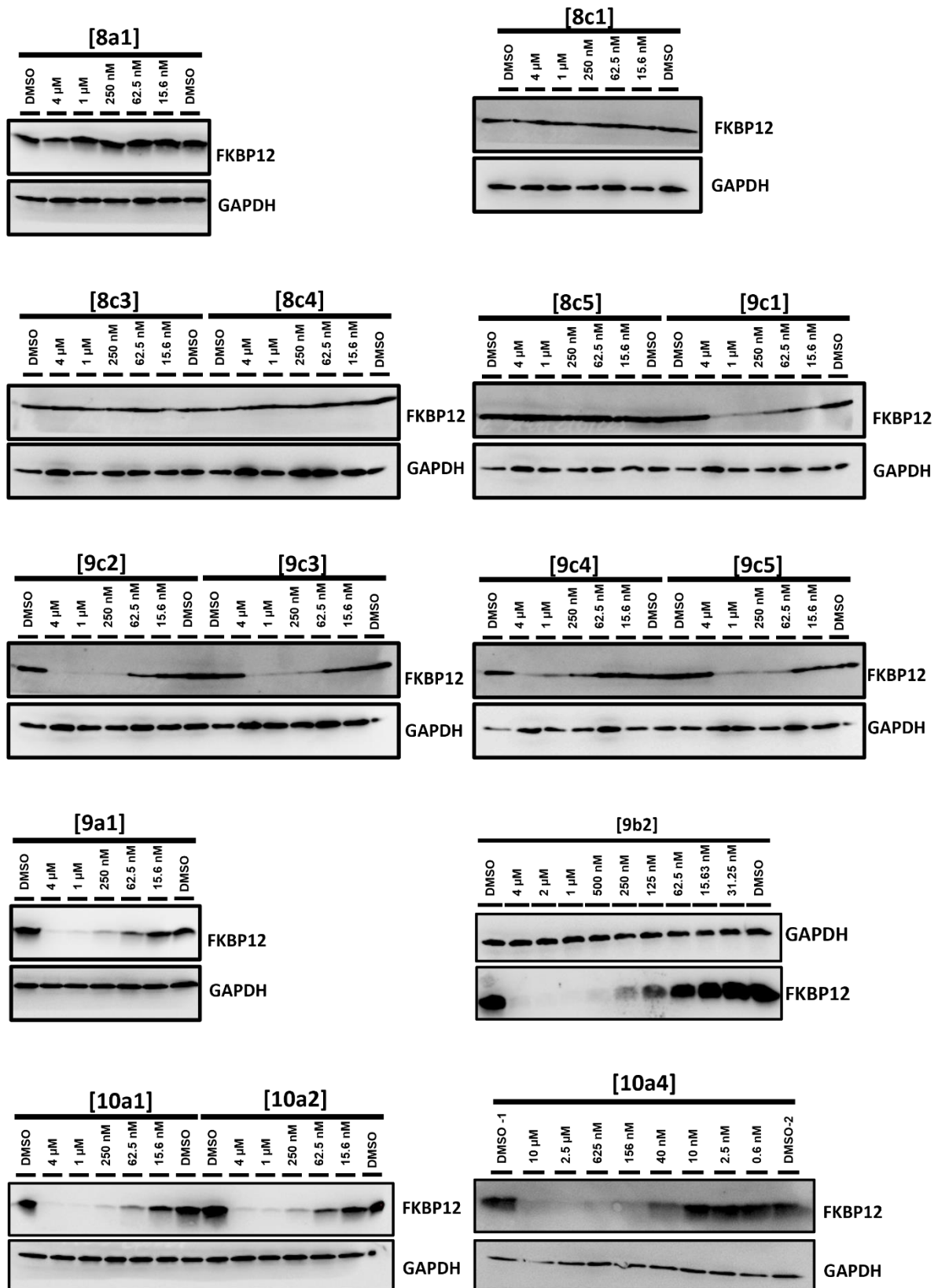


Figure 82 Part 2 of 5. PROTAC-mediated FKBP12 degradation in HEK293T cells after 24 h treatment

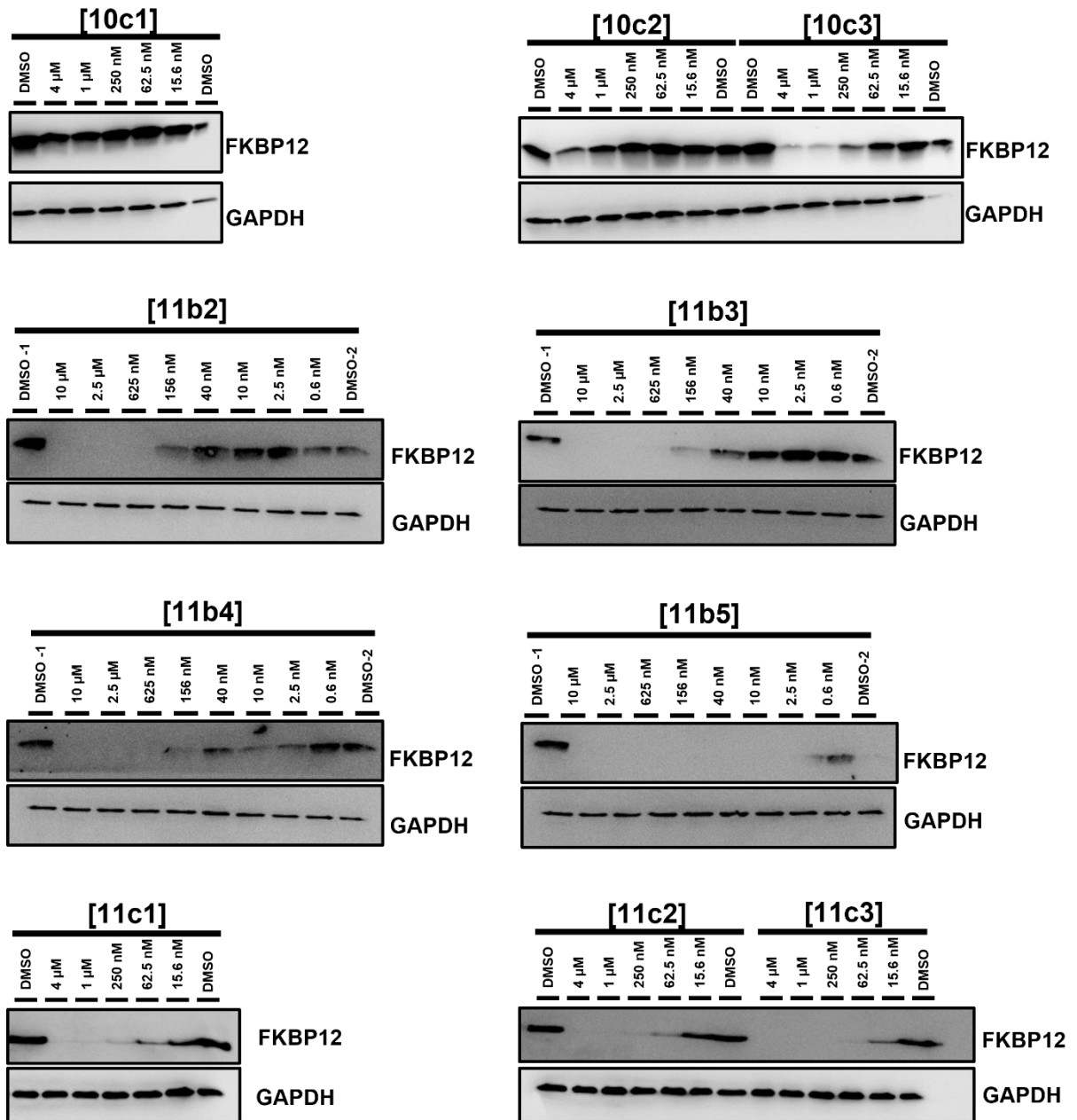


Figure 82 Part 3 of 5. PROTAC-mediated FKBP12 degradation in HEK293T cells after 24 h treatment.



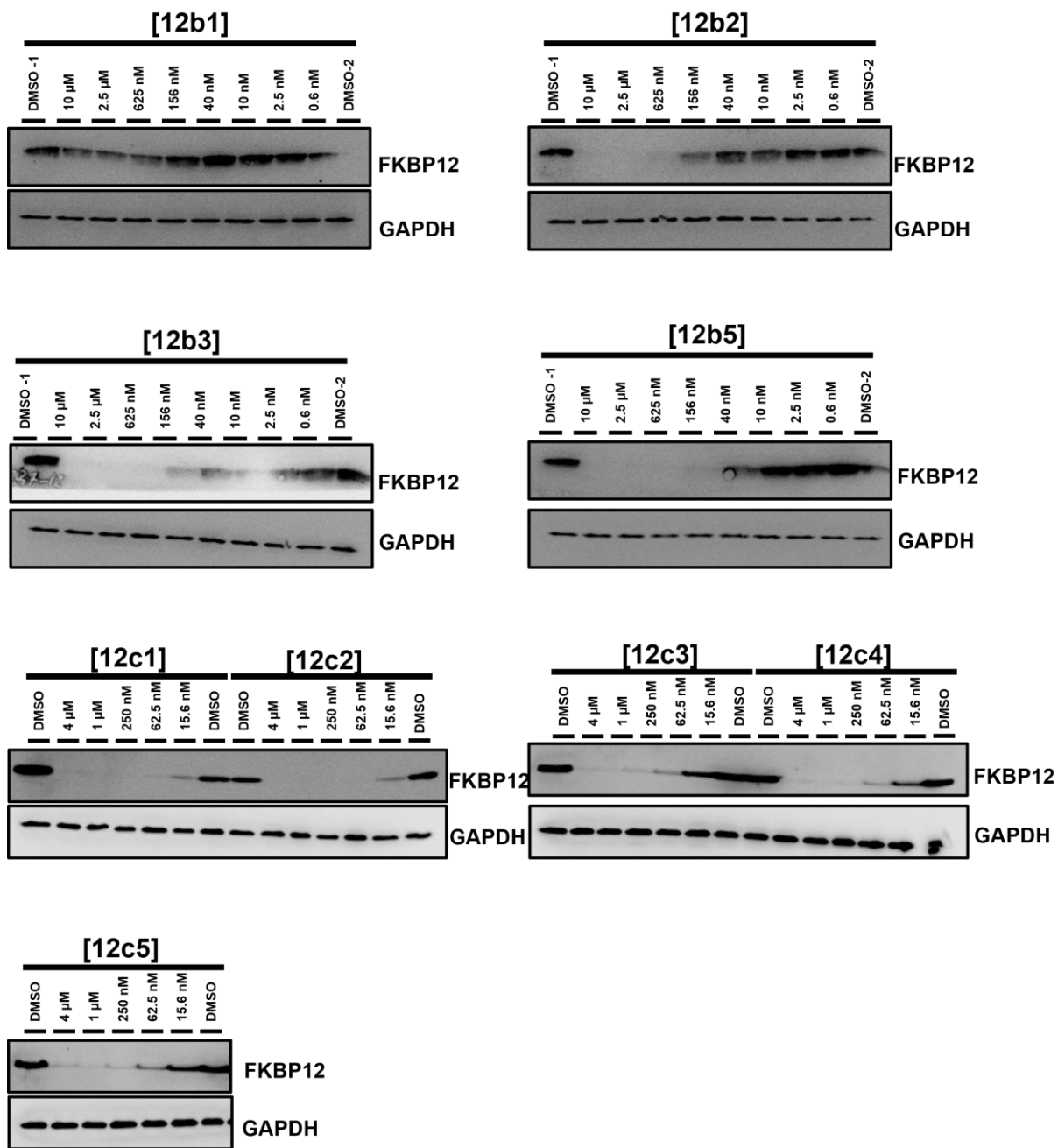


Figure 82 Part 4 of 5. PROTAC-mediated FKBP12 degradation in HEK293T cells after 24 h treatment.

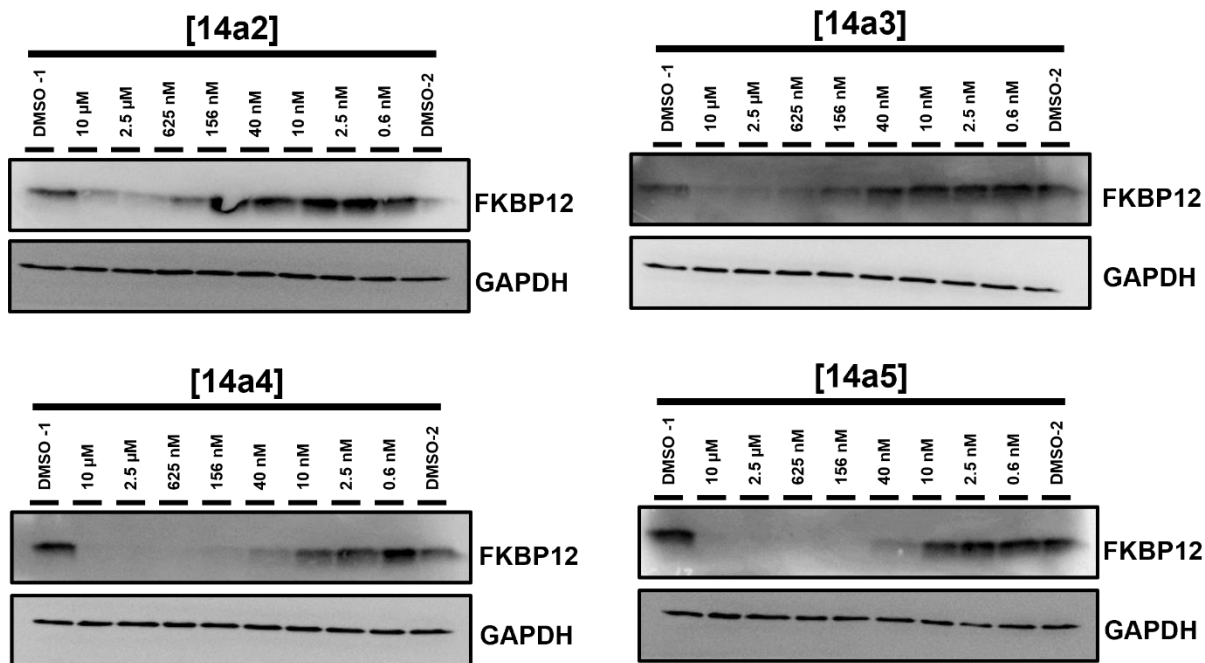
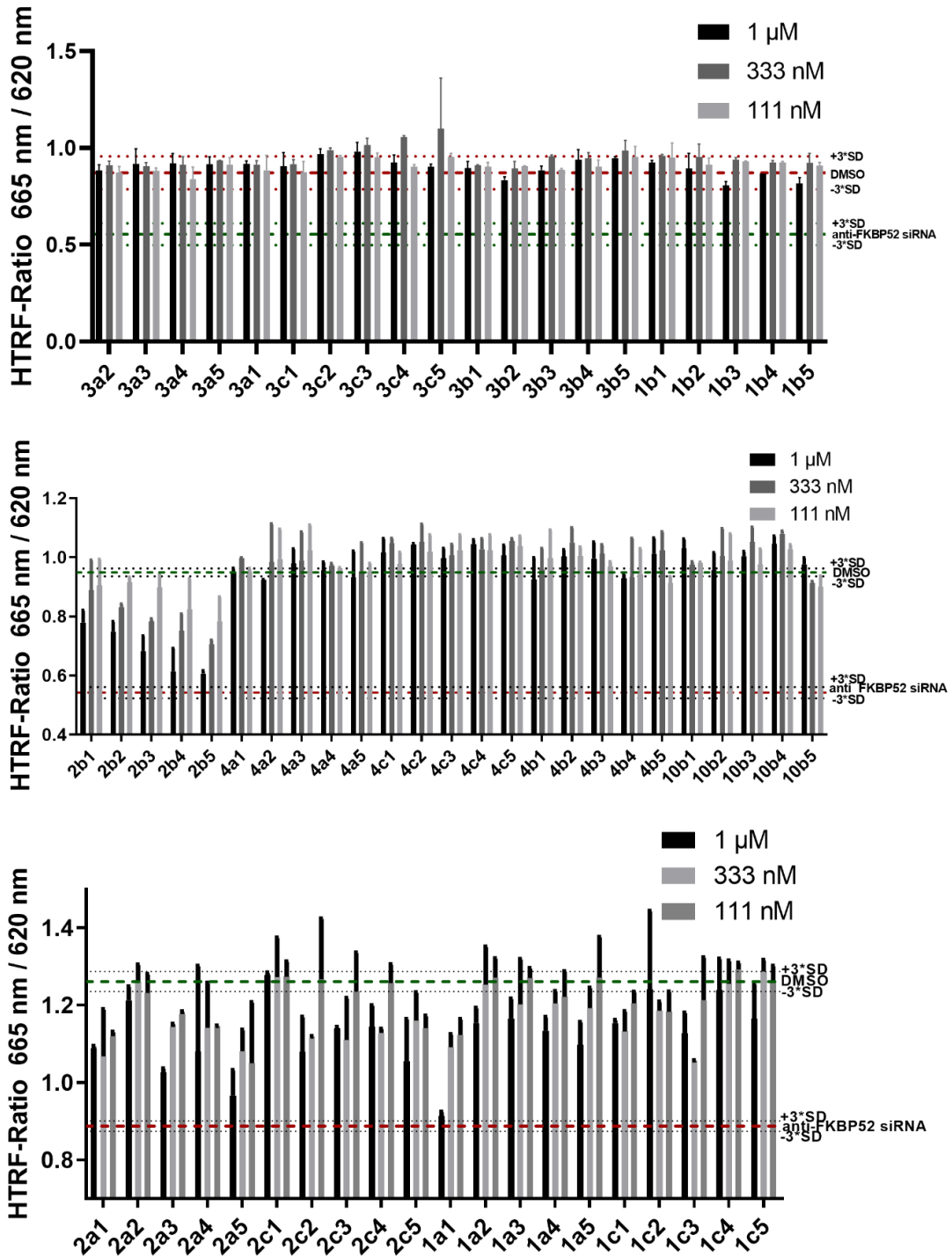
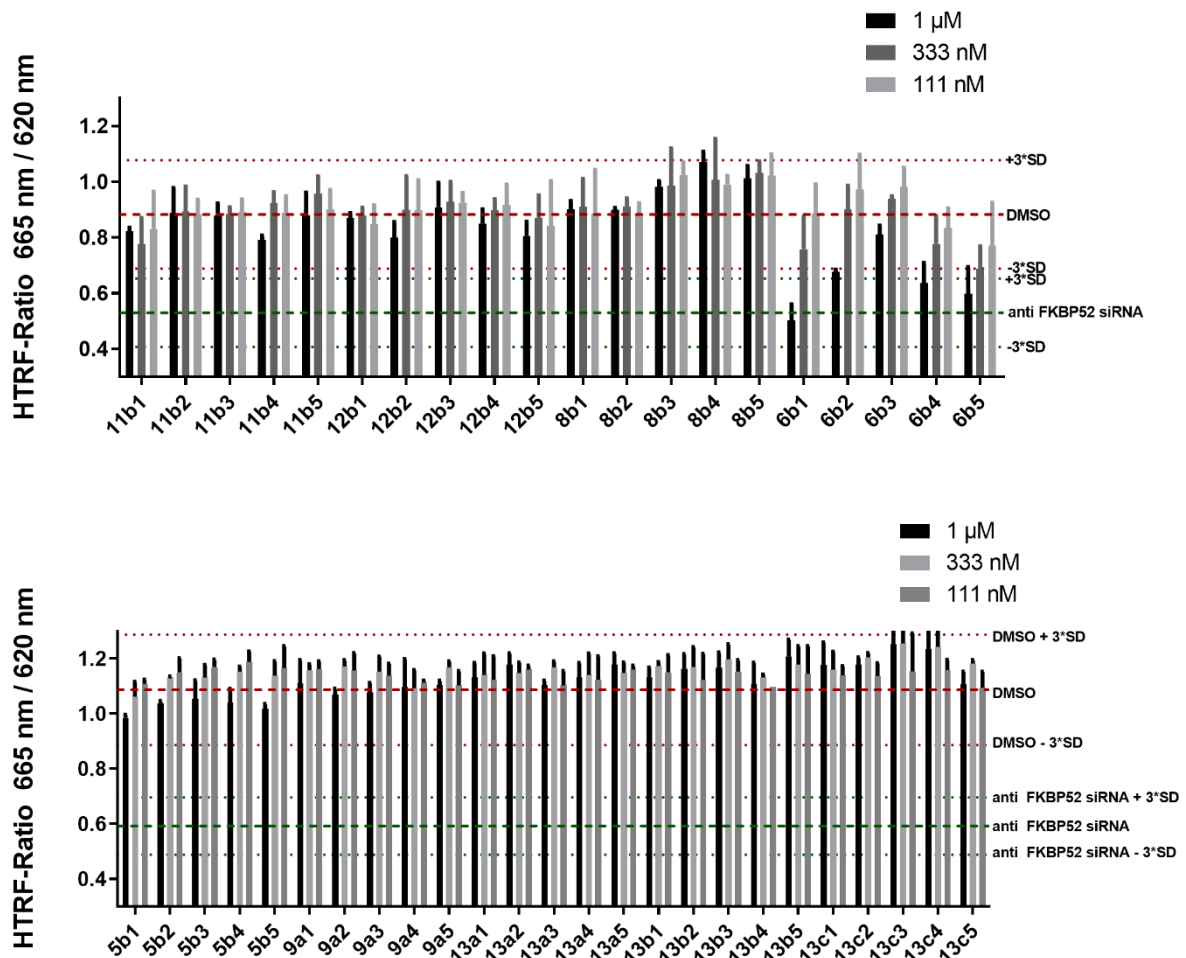


Figure 82 Part 5 of 5. PROTAC-mediated FKBP12 degradation in HEK293T cells after 24 h treatment.



**Figure 83 Part 1 of 2.** Relative HTRF-based quantification of endogenous FKBP52 levels after 24 h PROTAC treatment in HEK293T cell lysates. A homogeneous time-resolved FRET is observed between the fluorescent FKBP52-HTRF tracer MWa146 (120 nM) anti Rabbit IgG-Eu cryptate (1.2 nM) in combination with a primary anti FKBP52 antibody (1.25 nM) in the presence of FKBP52. HTRF ratios in range of siRNA positive control indicate lower FKBP52 samples in the treated samples compared to the DMSO control and are indicative of active PROTACs. Each bar represents mean and standard deviation of biological duplicates.



**Figure 83 Part 2 of 2.** Relative HTRF-based quantification of endogenous FKBP52 levels after 24 h PROTAC treatment in HEK293T cell lysates. A homogeneous time-resolved FRET is observed between the fluorescent FKBP52-HTRF tracer MWa146 (120 nM) anti Rabbit IgG-Eu cryptate (1.2 nM) in combination with a primary anti FKBP52 antibody (1.25 nM) in the presence of FKBP52. HTRF ratios in range of siRNA positive control indicate lower FKBP52 samples in the treated samples compared to the DMSO control and are indicative of active PROTACs. Each bar represents mean and standard deviation of biological duplicates.

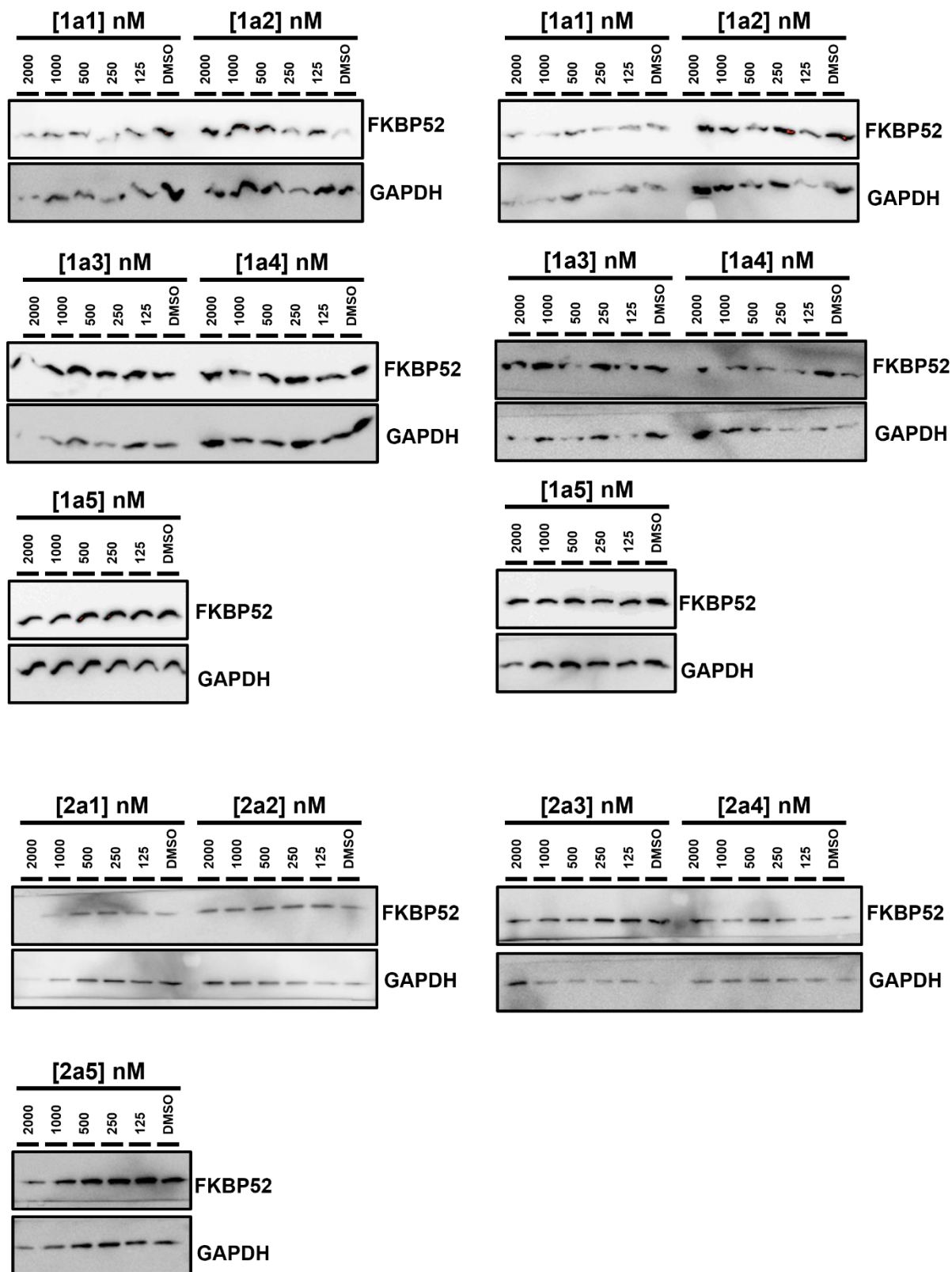


Figure 84 Part 1 of 4. PROTAC-mediated FKBP52 degradation in HEK293T cells after 24 h treatment.

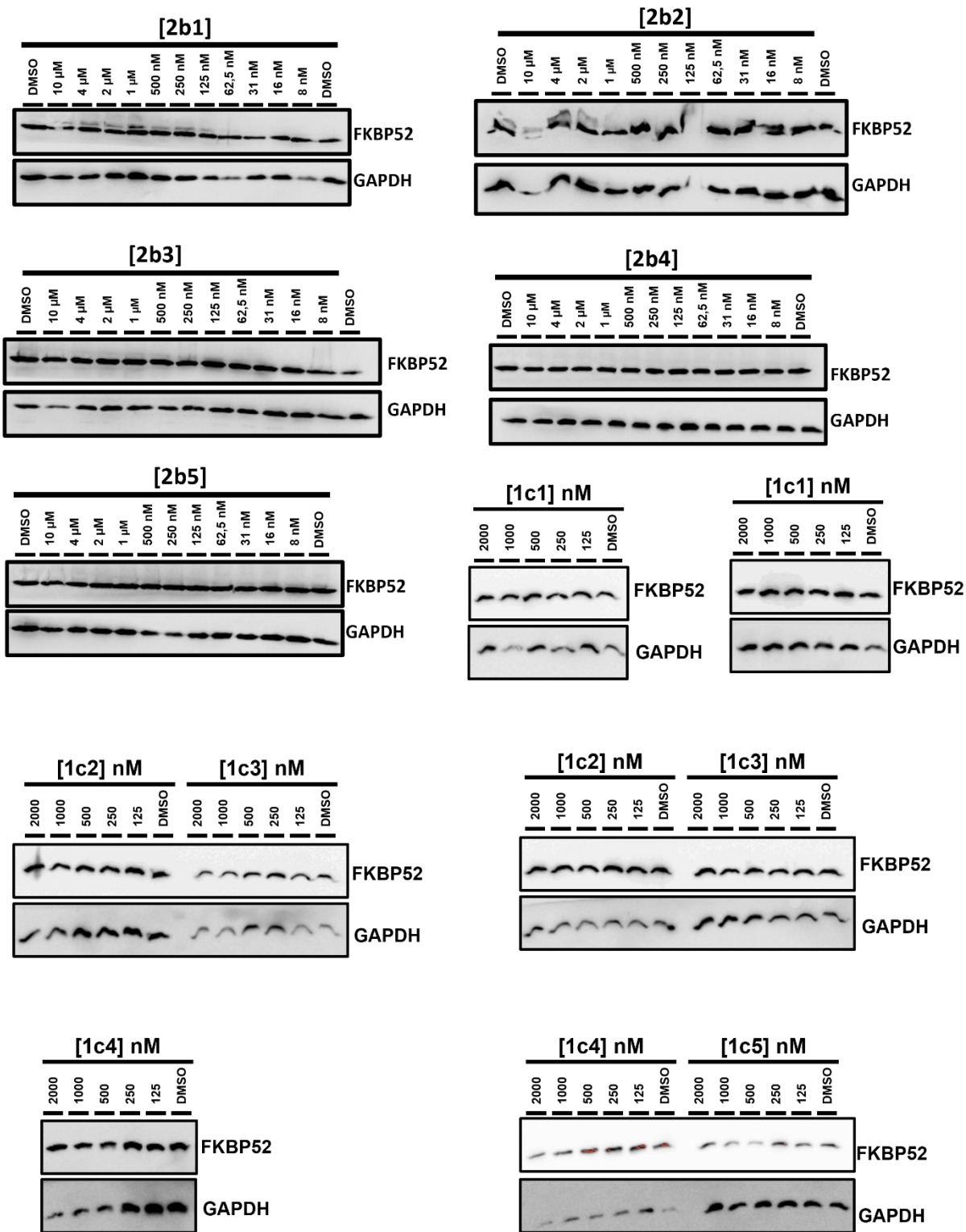


Figure 84 Part 2 of 4. PROTAC-mediated FKBP52 degradation in HEK293T cells after 24 h treatment

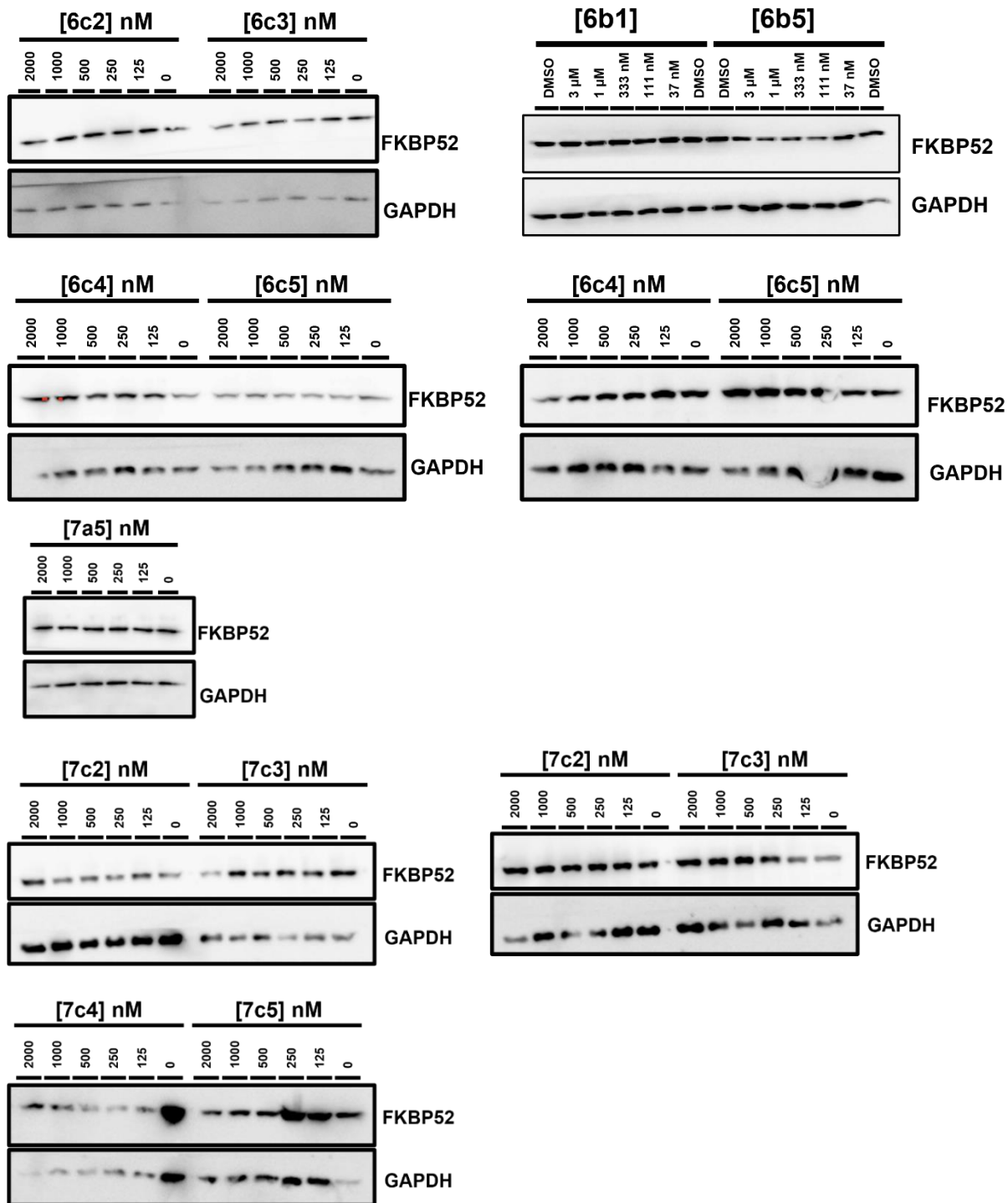
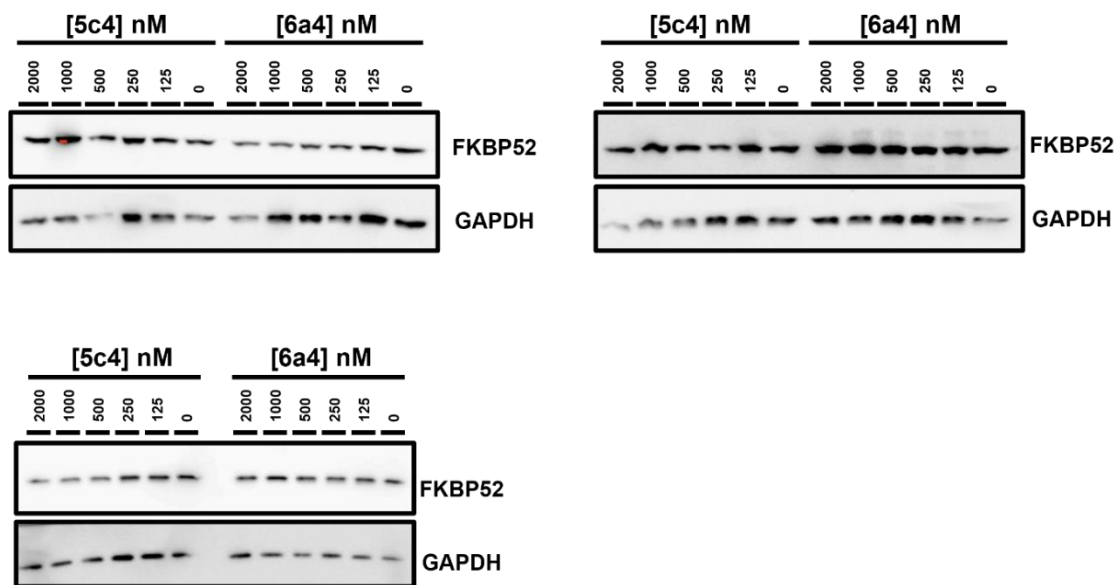
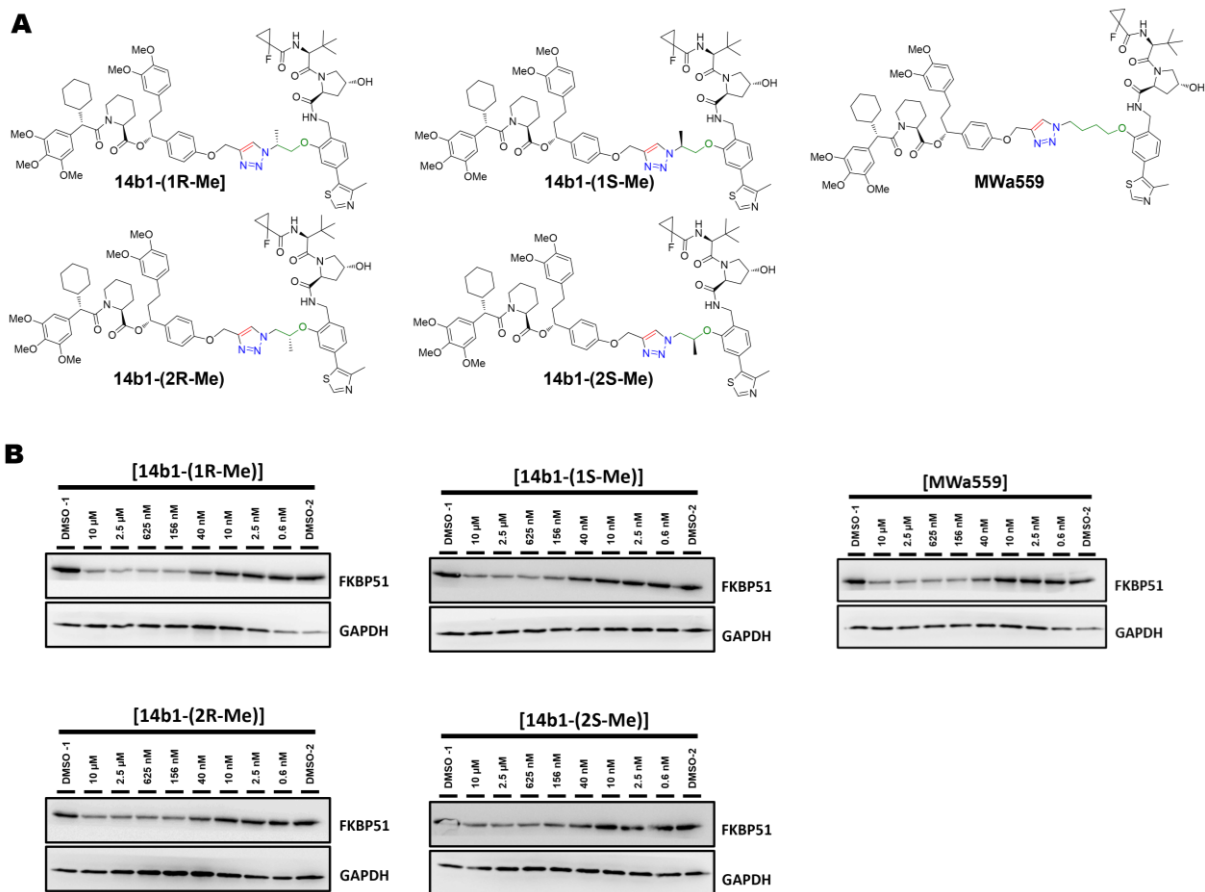


Figure 84 Part 3 of 4. PROTAC-mediated FKBP52 degradation in HEK293T cells after 24 h treatment



**Figure 84 Part 4 of 4.** PROTAC-mediated FKBP52 degradation in HEK293T cells after 24 h treatment.





**Figure 85** Cellular activity second generation FKBP51 PROTACs. **A** Chemical structure of PROTACs and western blots PROTAC-dependent FKBP51 degradation in HEK293T cells (24 h treatment).

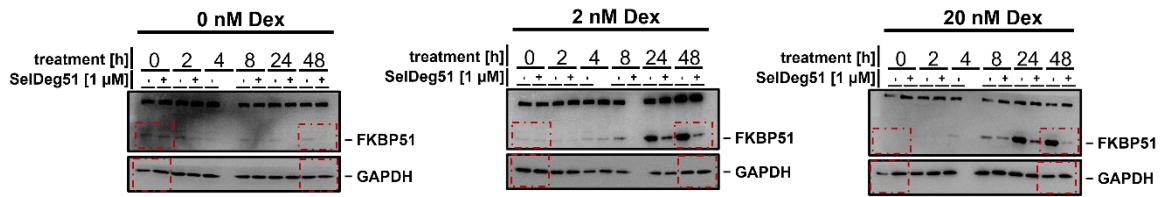


**Figure 86** FKBP51 levels are robustly increased by dexamethasone treatment (Dex) and are efficiently diminished by SelDeg51 co-treatment. Full blots to Figure 52A.

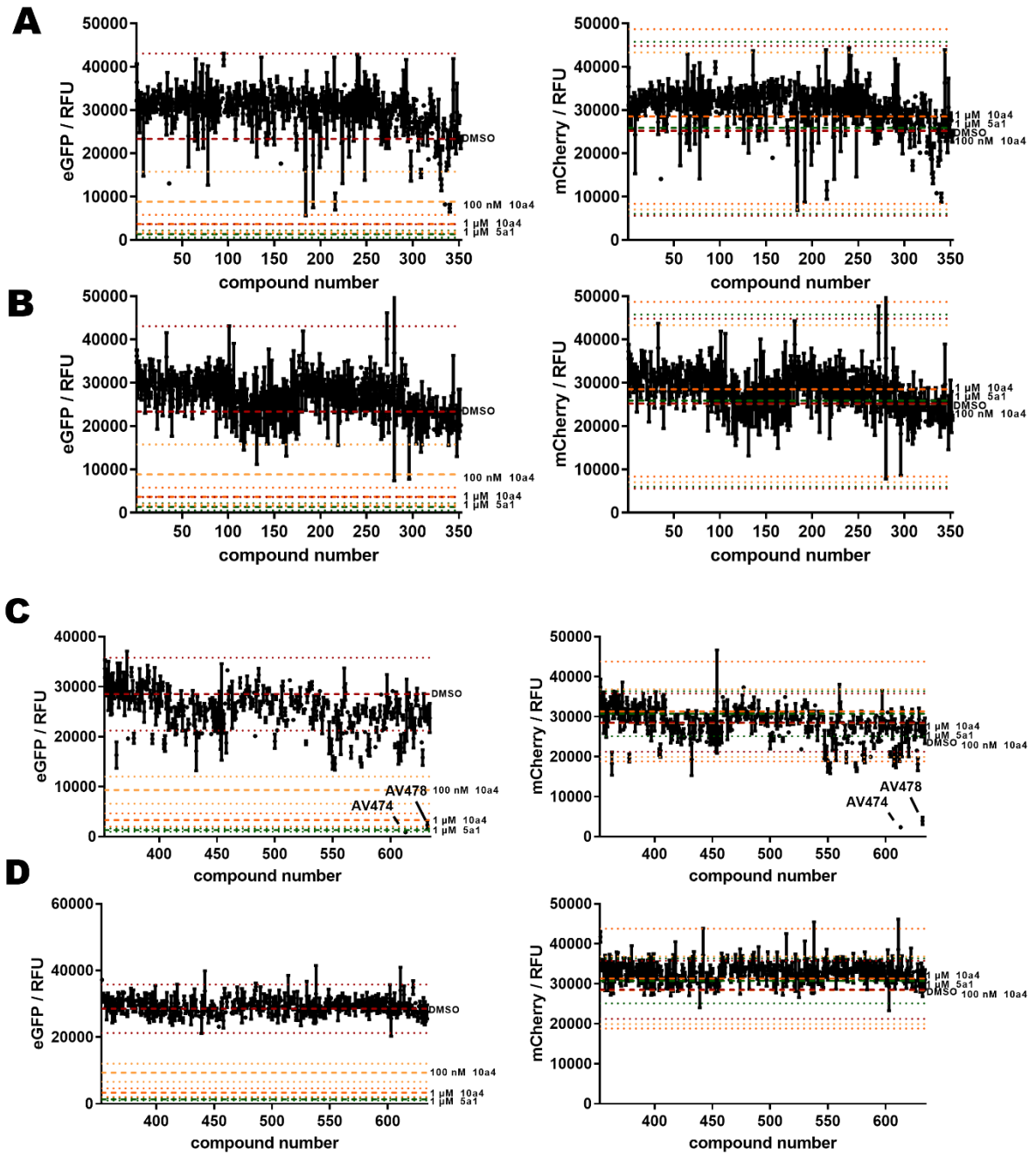


**Figure 87 Part 1 of 2** Cellular screening of FKBP-focused ligand library for FKBP12 degrading molecular glues. eGFP and mCherry fluorescence data after 48 h compound treatment at 10  $\mu$ M (A,C) or 0.5  $\mu$ M (B,D). Dashed line represent mean  $\pm$  3\*SD of the DMSO or PROTAC controls. Individual points and error bars represent the mean and standard deviation of independent biological duplicates.

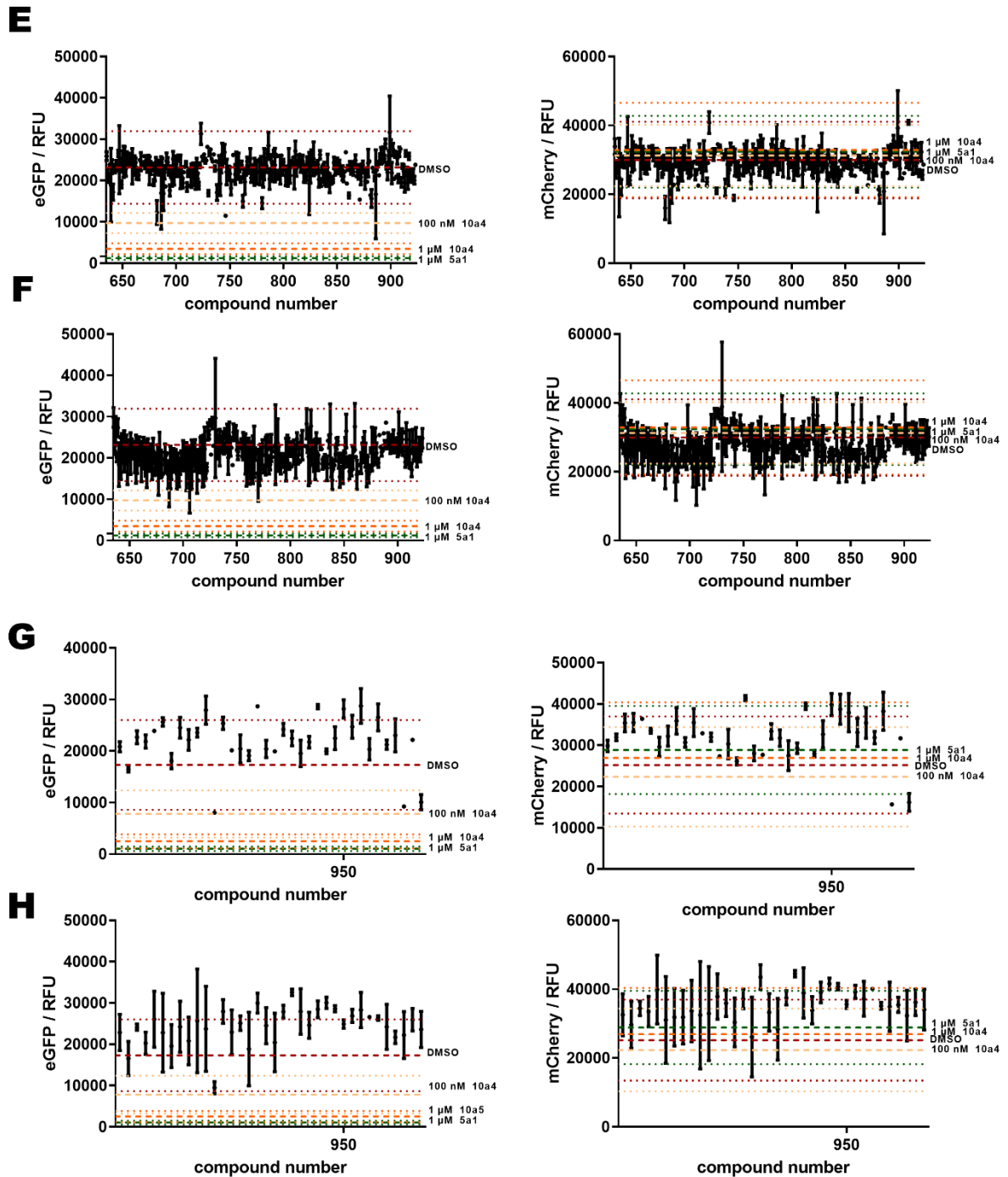


**Figure 87 Part 2 of 2** Cellular screening of FKBP-focused ligand library for FKBP12 degrading molecular glues. eGFP and mCherry fluorescence data after 48 h compound treatment at 10  $\mu\text{M}$  (E,G) or 0.5  $\mu\text{M}$  (F,H). Dashed line represent mean  $\pm$  3\*SD of the DMSO or PROTAC controls. Individual points and error bars represent the mean and standard deviation of independent biological duplicates.

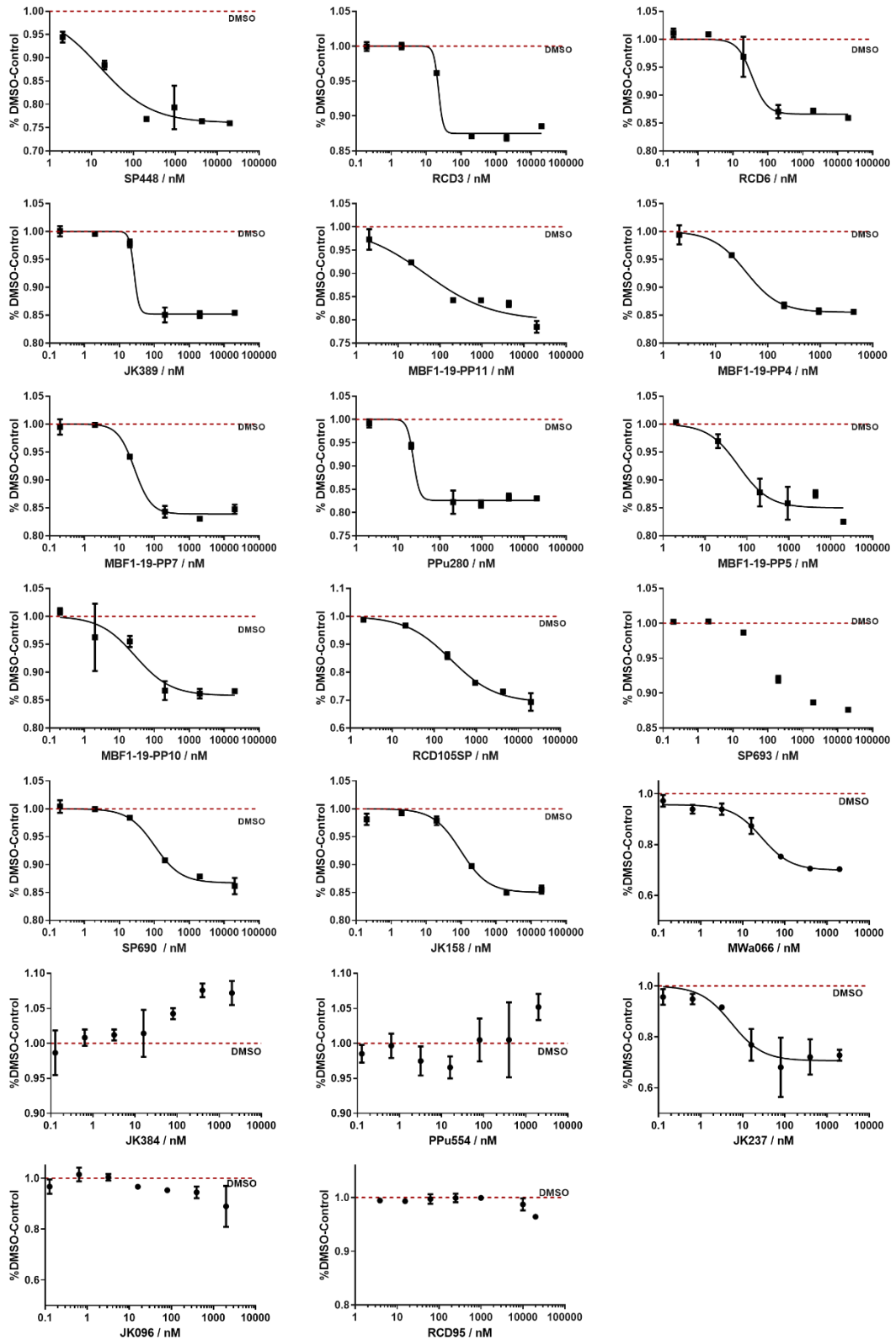


**Figure 88** Dose-response curves of initial hits for FKBP12-degrading molecular glues and close analogs thereof. FKBP12\_eGFP degradation was assessed in FKBP12\_eGFP reporter cells after 48 h treatment. Red dashed line represents mean of the DMSO control. Individual points and error bars represent mean and standard deviation of biological duplicates.

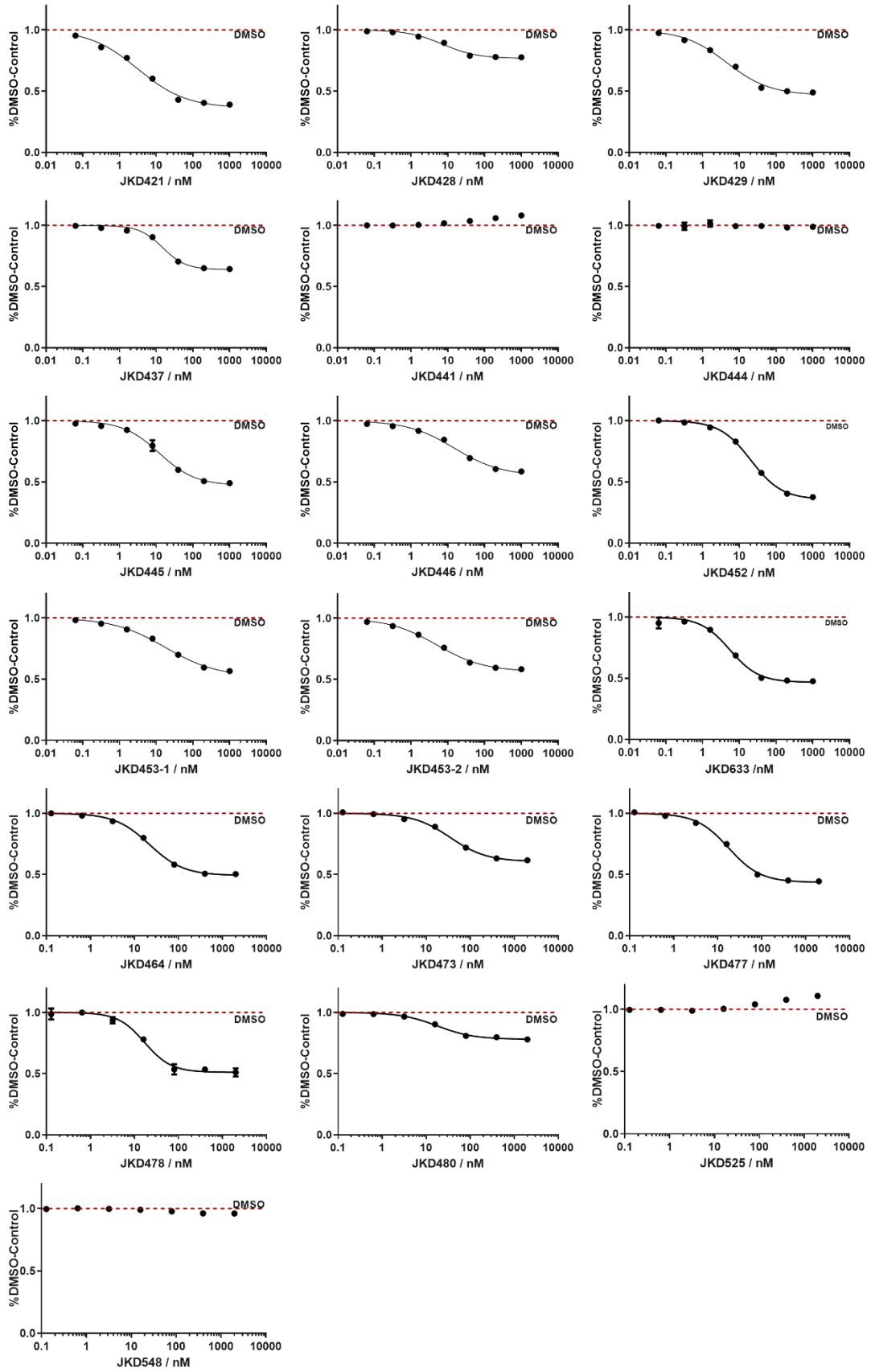


**Figure 89** Dose-response curves focused PPU670 analogs. FKBP12\_eGFP degradation was assessed in FKBP12\_eGFP reporter cells after 48 h treatment. Red dashed line represents mean of the DMSO control. Individual points and error bars represent mean and standard deviation of biological duplicates.

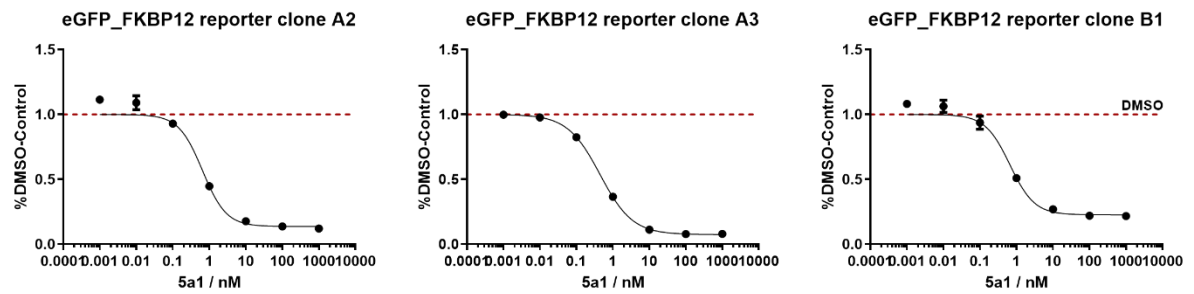


**Figure 90** Suitability of eGFP\_FKBP12 and mCherry expressing HEK293T clones as FKBP12 level reporter cell lines. Cells stably expressing eGFP\_FKBP12 and mCherry were treated for 48 hours with the active FKBP12-PROTAC 5a1 before cell lysis and eGFP (Ex.: 485 nm, Em.: 525 nm) and mCherry (Ex.: 580 nm, Em.: 620 nm) fluorescence quantification. Individual points represent mean and standard deviation of biological duplicates.

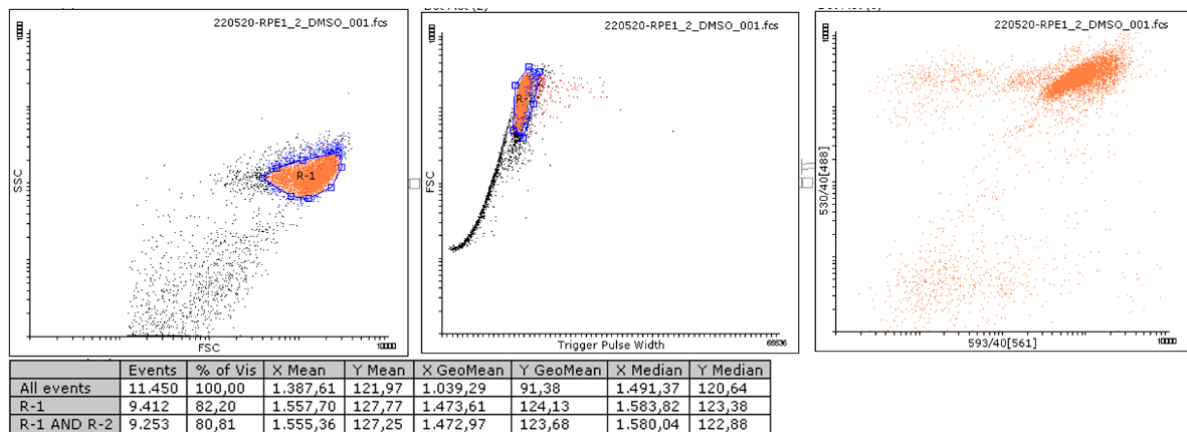


**Figure 91** Flowcytometry images and statistics of DMSO treated (48 hours) RPE1 FKBP12\_eGFP cells. FACS analysis was performed in the research group Kolmar (TU Darmstadt) under supervision and guidance of Dr. Andreas Christmann.

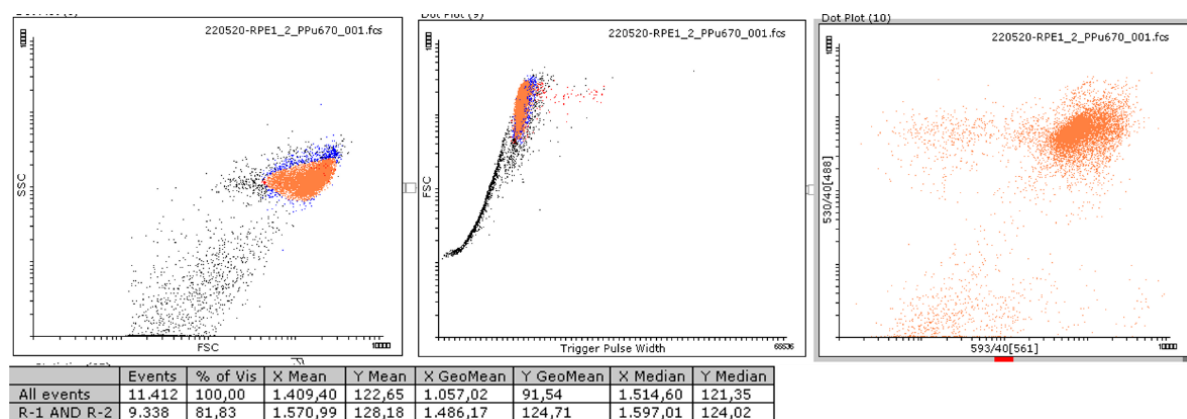


**Figure 92** Flowcytometry images and statistics of PPU670 (1 μM) treated (48 hours) RPE1 FKBP12\_eGFP cells. FACS analysis was performed in the research group Kolmar (TU Darmstadt) under supervision and guidance of Dr. Andreas Christmann.

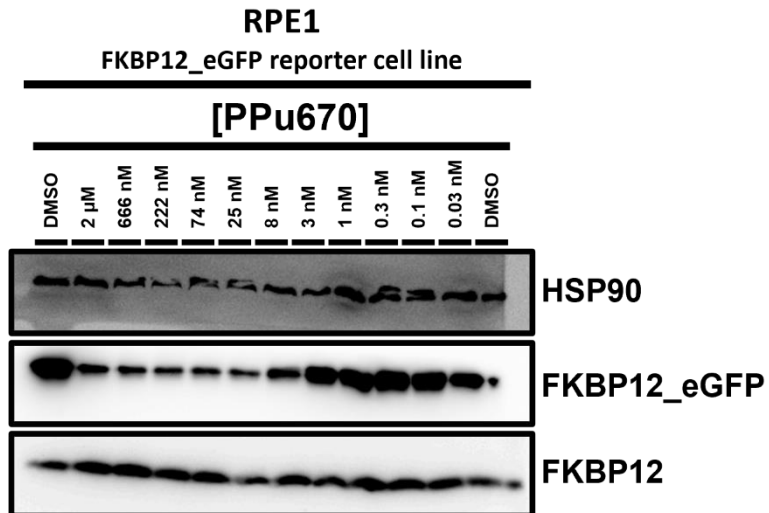


**Figure 93** Endogenous FKBP12 levels are not affected in the RPE1 FKBP12\_eGFP reporter cell line. PPU670 degrades FKBP12\_eGFP but not FKBP12 after 48 h treatment in the RPE1 FKBP12\_eGFP reporter cell line. The RPE1 FKBP12\_eGFP reporter cell line was generated by Dr. Yves Matthes.



---

## 9. Abbreviations

---

A647	AlexaFluor647
AP	accessory protein
approx.	approximately
APS	Ammonium persulfate
AR	androgen receptor
AST	Active site titrations
ATP	Adenosine triphosphate
AUTACs	autophagy-targeting chimeras
BCA	Bicinchoninic Acid
BCL-XL	B-cell lymphoma-extra large
BRD4	Bromodomain-containing protein 4
BRET	bioluminescence resonance energy transfer
CBRN	Cereblon
CDK12	cyclin-dependent kinase 12
CDK4	cyclin-dependent kinase 4
CELMoDs	Cereblon E3 ligase modulators
CN	serine–threonine protein phosphatase calcineurin
CRISPR	Clustered Regularly Interspaced Short Palindromic Repeats
CsA	Cyclosporin A
CSNK1A1	casein kinase 1 alpha
C-terminal	Carboxy-terminal
Cyp18	Cyclophilin 18
Cyp40	Peptidyl-prolyl cis-trans isomerase D
DC <sub>50</sub>	half-maximal degradation concentration
DCAF	DDB1 and CUL4 associated factor
DDB1	DNA damage-binding protein 1
Dex	dexamethasone
D <sub>max</sub>	maximal degradation
DMSO	Dimethyl sulfoxide
DTT	Dithiothreitol
EC <sub>50</sub>	Half maximal effective concentration
eGFP	Enhanced green fluorescent protein
ELISA	enzyme-linked immunosorbent assay

Em.	emission
ER	estrogen receptor
Eu	Europium
Ex.	excitation
FKBP	FK506-binding proteins
FKBP12	FK506-binding protein 12
FKBP12.6	FK506-binding proteins 12.6
FKBP51	FK506-binding protein 51
FKBP52	FK506-binding protein 52
FP	fluorescence polarization
FRB	FKBP-Rapamycin binding domain of mTOR
GAPDH	Glyceraldehyde 3-phosphate dehydrogenase
GR	glucocorticoid receptor
GRE	glucocorticoid responsive elements
GSPT1	Eukaryotic peptide chain release factor GTP-binding subunit ERF3A
HEK	Human embryonal kidney cells
HEMTACs	Hsp90-mediated targeting chimeras
HIF1 $\alpha$	hypoxia-inducible factor 1 subunit- $\alpha$
Hop	Hsp70-Hsp90 Organizing <i>Protein</i>
Hsp40	Heat shock protein 40
Hsp70	Heat shock protein 70
Hsp90	Heat shock protein 90
HTRF	Homogenous time-resolved fluorescence
i.p.	Intraperitoneal injection
IC <sub>50</sub>	Half maximal inhibitory concentration
IMAC	immobilized metal affinity chromatography
IMiDs	Immunomodulatory imide drugs
IPTG	Isopropyl $\beta$ -D-1-thiogalactopyranoside
IRES2	internal ribosome entry site 2
K <sub>D</sub>	dissociation constant
K <sub>i</sub>	Inhibitor dissociation constant
K <sub>m</sub>	Michaelis constant
lum	luminescence
LYTACs	lysosome-targeting chimeras
MDM2	mouse double minute 2

MG	Molecular glue
minP	minimal promotor
MMTV	Murine Mammary Tumor Virus
MR	mineralocorticoid receptor
mTORC1	mammalian target of rapamycin complex 1
N2a	Neuro-2a
NGS	next generation sequencing
Nluc	NanoLuc® Luciferase
norm.	normalized
NRF2	nuclear factor erythroid 2-related factor 2
N-terminal	Amino-terminal
pBpa	para-benzoyl phenyl alanine
PBS	Phosphate-buffered saline
PHLPP	PH domain and Leucine rich repeat Protein Phosphatase
PKB	protein kinase B
POI	protein-of-interest
PPI	protein-protein interaction
PPIase	peptidyl-prolyl-isomerase
PR	progesterone receptor
PROTAC	Proteolysis targeting chimeras
RBM23	RNA-Binding Motif Protein 23
RBM39	RNA-Binding Motif Protein 39
RBX1	RING-box protein 1
RPE	human retinal pigment epithelial
SAFit	selective antagonists of FKBP51 by induced-fit
SDS	Sodium dodecyl sulfate
SEC	Size exclusion chromatography
SelDeg51	Selective Degradar of FKBP51
SfA	Sanglifehrin A
sgRNA	single guide RNA
SHR	steroid hormone receptors
siRNA	Small interfering RNA
Tb	Terbium
TEMED	Tetramethylethylenediamine
TPD	targetd protein degradation

---

TPR	tetratricopeptide repeat
VHL	Von Hippel–Lindau tumor suppressor
ZFK1	Zinc finger transcription factors 1
ZFK3	Zinc finger transcription factors 3
ZFP91	Zinc finger protein 91

---

---

## 10. Curriculum Vitae

---

### Professional Experience:

Since 10/2019      PhD studies at the Technical University Darmstadt  
Research Group Prof. Dr. Hausch; Targeted protein degradation of FK506-binding proteins

### University Education and School:

09/2017 – 8/2019      Degree Master of Science  
Master studies Biomolecular Engineering at Technical University of Darmstadt

10/2014-08/2017      Degree Bachelor of Science  
Bachelor studies Biomolecular Engineering at Technical University of Darmstadt

2014                      A-Levels (Abitur)

---

## 11. Fellowships, Key Publications, Prizes, Conference contributions and Co-authorships

---

### 11.1. Fellowships

- 10/2017 – 10/2019 **Deutschlandstipendium**  
Two one-year fellowships for gifted and high-achieving students
- 12/2017 **Prize of the Dr.-Anton-Keller-Stiftung**  
Prize for excellent performance in the B.Sc. final exam

### 11.2. Key publications

Thomas M. Geiger<sup>[+]</sup>, Michael Walz<sup>[+]</sup>, Christian Meyners<sup>[+]</sup>, Wisely Oki Sugiarto, Edvaldo Maciel, Min Zheng, Frederik Lermyte, Felix Hausch. Discovery of a potent PROTAC enables targeting of FKBP51's scaffolding functions. (In Revision in *Angewandte Chemie International Edition*)

Geiger, T.M., Schäfer, S.C., Dreizler, J.K., Walz, M. and Hausch, F., 2022. Clues to molecular glues. *Current Research in Chemical Biology*, 2, p.100018. DOI: 10.1016/j.crchbi.2021.100018

Gnatzy, M.T. <sup>[+]</sup>, Geiger, T.M. <sup>[+]</sup>, Kuehn, A., Gutfreund, N., Walz, M., Kolos, J.M. and Hausch, F., 2021. Development of NanoBRET-binding assays for FKBP-ligand profiling in living cells. *ChemBioChem*, 22(13), pp.2257-2261. DOI: 10.1002/cbic.202100113

Geiger T.M., Dreizler J.K., Walz M., Meyners C., Sugiarto W.O., Hausch F., Development of a HTRF-binding assay for high affinity FKBP ligands.  
(In preparation)

---

### 11.3. Congress talks

Protein Degradation & Targetting Undruggables Congress: Europe 2023 (Basel, September 2023)

Title: Clues to molecular glues

3rd Annual TPD Europe Summit 2023 (London, March 2023)

Title: Linkerology as a Key Aspect in PROTAC Design & FKBP-degrading molecular glues

### 11.4. Conference and congress posters

Advances in Chemical Biology 2023 (Frankfurt, January 2023)

Title: Cellular identification of FKBP12-degrading molecular glues

Degradation & Targeting Undruggables Congress, (Basel, October 2022)

Title: Cellular identification of FKBP12-degrading molecular glues

### 11.5. Co-authorships

1. Baischew, A., Engel, S., Geiger, T.M. and Hausch, F., 2023. Large-scale in-cell photocrosslinking at single residue resolution reveals the molecular basis for glucocorticoid receptor regulation by immunophilins. *bioRxiv*, pp.2023-01 doi: 10.1101/2023.01.16.524346  
(In press at **Nature Structural and Molecular Biology**)
2. Deutscher, R. C.; Meyners, C.; Schäfer, S. C.; Repity, M. L.; Sugiarto, W. O.; Kolos, J.; Heymann, T.; Geiger, T. M.; Knapp, S.; Hausch, F. Discovery of fully synthetic FKBP12-mTOR molecular glues, 2023. DOI: 10.26434/chemrxiv-2023-4vb0m (**In preparation**)
3. Deutscher, R. C. E.; Safa Karagöz, M.; Purder, P. L.; Kolos, J. M.; Meyners, C.; Oki Sugiarto, W.; Krajczyk, P.; Tebbe, F.; Geiger, T. M.; Ünal, C.; Hellmich, U. A.; Steinert, M.; Hausch, F. 4.3.1Bicyclic FKBP Ligands Inhibit Legionella Pneumophila Infection by LpMip-Dependent and LpMip-Independent Mechanisms. **ChemBioChem** 2023, e202300442. DOI: 10.1002/cbic.202300442.
4. Knaup, F.H., Meyners, C., Sugiarto, W.O., Wedel, S., Springer, M., Walz, C., Geiger, T.M., Schmidt, M., Sisignano, M. and Hausch, F., 2023. Structure-based discovery of a new selectivity-enabling motif for the FK506-binding protein 51. **Journal of Medicinal Chemistry**, 66(8), pp.5965-5980. DOI: 10.1021/acs.jmedchem.3c00249
5. Baischew, A., Engel, S., Geiger, T.M., Taubert, M.C. and Hausch, F., 2023. Structural and biochemical insights into FKBP51 as a Hsp90 co-chaperone. **Journal of Cellular Biochemistry**. DOI: 10.1002/jcb.30384

- 
6. Kolos, J. M.; Pomplun, S.; Jung, S.; Rieß, B.; Purder, P. L.; Voll, A. M.; Merz, S.; Gnatzy, M.; Geiger, T. M.; Quist-Løkken, I.; Jatzlau, J.; Knaus, P.; Holien, T.; Bracher, A.; Meyners, C.; Czodrowski, P.; Krewald, V.; Hausch, F. Picomolar FKBP inhibitors enabled by a single water-displacing methyl group in bicyclic 4.3.1 aza-amides. **Chemical Science** 2021, 12 (44), 14758–14765. DOI: 10.1039/d1sc04638a.
  7. Martinelli, S.; Anderzhanova, E. A.; Bajaj, T.; Wiechmann, S.; Dethloff, F.; Weckmann, K.; Heinz, D. E.; Ebert, T.; Hartmann, J.; Geiger, T. M.; Döngi, M.; Hafner, K.; Pöhlmann, M. L.; Jollans, L.; Philipsen, A.; Schmidt, S. V.; Schmidt, U.; Maccarrone, G.; Stein, V.; Hausch, F.; Turck, C. W.; Schmidt, M. V.; Gellner, A.-K.; Kuster, B.; Gassen, N. C. Stress-primed secretory autophagy promotes extracellular BDNF maturation by enhancing MMP9 secretion. **Nature Communication** 2021, 12 (1), 4643. DOI: 10.1038/s41467-021-24810-5
  8. Voll, A. M.; Meyners, C.; Taubert, M. C.; Bajaj, T.; Heymann, T.; Merz, S.; Charalampidou, A.; Kolos, J.; Purder, P. L.; Geiger, T. M.; Wessig, P.; Gassen, N. C.; Bracher, A.; Hausch, F. Macrocyclic FKBP51 Ligands Define a Transient Binding Mode with Enhanced Selectivity. **Angewandte Chemie International Edition** 2021, 60 (24), 13257–13263. DOI: 10.1002/anie.202017352
  9. Hähle, A., Geiger, T.M., Merz, S., Meyners, C., Tianqi, M., Kolos, J. and Hausch, F., 2019. FKBP51 and FKBP12. 6—Novel and tight interactors of Glomulin. **PLoS One**, 14(9), p.e0221926. DOI: 10.1371/journal.pone.0221926
  10. Degreif, D., Kremenovic, M., Geiger, T. and Bertl, A., 2018. Preloading budding yeast with all-in-one CRISPR/Cas9 vectors for easy and high-efficient genome editing. **Journal of Biological Methods**, 5(3). DOI: 10.14440/jbm.2018.254



---

## 12. Acknowledgment

---

I am thankful for Prof. Dr. Felix Hausch for giving me the opportunity to work in his group and on such an exciting topic. I am grateful for the trust in my work, fruitful discussions, and the excellent guidance I received throughout my PhD studies.

I want to thank Prof. Dr. Harald Kolmar who agreed to be the second supervisor of this thesis.

Moreover, I want to thank Dr. Christian Meyners for teaching me in assay development and all the helpful discussions.

I want to thank my colleagues Michael Walz, Johannes Dreizler, Robin Deutscher, Tianqi Mao, Patrick Purder and Min Zheng for their synthetic work and always helping me with chemistry related topics. Additionally, I want to thank Prof. Dr. Manuel Kaulich, Dr. Yves Matthes and Dr. Martin Wegner for their commitment to and work on the elucidation of UBR3 as the relevant E3 ligase for FKBP12\_eGFP-degrading molecular glues.

Many thanks to my biochemistry colleagues: Asat Baischew, Sarah Engel, Martha Taubert, Monika Gnatzy, Anna Charalampidou, Stephanie Merz, Steffen Hartmann, Maximilian Repity, Sabine Schäfer, Angela Kühn, Wisely Oki Sugiarto and Christian Meyners. Thank you for your support, scientific discussions, the coffee breaks, motivation, and the nice working atmosphere.

Additionally, I want to thank the students who contributed to my projects, Monika Gnatzy, Angela Kühn, Thomas Stipp and Kevin Müller.

I want to thank all members of the Hausch lab for the nice working environment. Furthermore, I am thankful for all the chemists who established the FKBP-focused ligand library and thereby laid the foundation for the molecular glue project.

Last but not least, I want to thank my family and partner Mona Goebel for their continuous support during the last four years.